



**University of Liverpool**

**Doctoral Thesis**

---

***Mantle Serpentinisation,***

***carbon and life***

---

Thesis submitted in accordance with the requirements of the University of Liverpool  
for the degree of Doctor of Philosophy

By

**Tsvetomila Mateeva**

May 2018







# Declaration of Authorship

I declare that this thesis titled, “Mantle serpentinisation, carbon and life” and the work presented in it are my own work. The material contained in the thesis has not been presented, nor is currently being presented, either wholly or in part, for any other degree or qualification.

Signed:

Tsvetomila Mateeva

May 2018







# Abstract

Serpentinisation occurs at hydrothermal vents at slow-spreading ocean ridges and at magma-poor rifted continental margins. Serpentinisation and concomitant reduction of CO<sub>2</sub> to methane at modern hydrothermal vents supports hydrogen-driven microbial environments including methanotrophic biosystems. An important question is: "Are such bio-systems locally restricted to hydrothermal vents or are they more pervasive, being linked with the exhumation of serpentinised mantle at the seafloor?" Such a relationship is important for understanding the hidden sub-surface bio-systems and the fate of methane.

The ocean-continent transition (OCT) of magma-poor rifted continental margins provides an opportunity to investigate this. Serpentinite, intrusive magmatic rocks and the overlying sediments sampled in remnants of the fossil Tethyan OCTs exposed in the Alps or samples collected as part of the Ocean Drilling Program (ODP) from the OCT of the Iberian Newfoundland margins, were analysed for the presence or absence of methanotrophy within serpentinised exhumed mantle. Sampling of km scale exposures of exhumed serpentinised mantle in the Alps allows precise and extensive sampling which is not possible at ocean ridges. This provides an opportunity to investigate the organic matter in the ophiolite sequences relative to the seafloor. Samples from the Totalp unit, Tasna nappe and Platta unit of the Eastern Swiss Alps and Chenaillet in the Western Alps, all originating from the Alpine Tethyan magma-poor OCT, were selected for analysis. The fact that all these units were little affected by Alpine deformation and underwent only low-grade Alpine metamorphism makes them the world's best field analogue for magma-poor rifted margins.

All the Alpine Tethys lithologies sampled show the presence of hydrocarbons such as *n*-alkanes, low molecular weight polynuclear aromatic hydrocarbons (PAHs, indicating mixed petrogenic and pyrogenic sources), hopanes, steranes (indicating marine origin), and branched alkanes (pristane and phytane, non-specific marine origin). The identifiable biomarkers and the stable isotopic carbon data are consistent

with a marine origin and do not indicate a methanotrophic bio-system. The organic matter (OM) does not originate from the exhumed mantle rocks but corresponds to an autochthonous OM probably deriving from the sediment cover and overlying water. The OM indicates a depositional environment of marine organic matter dominated by planktonic algae and bacteria. It is noteworthy that mantle rocks in the Alpine Tethys OCT still contain marine organic matter 160 My after their exhumation, despite having experienced an Alpine reactivation.

The analysed ODP cores from the Iberia-Newfoundland margins show cyclic and branched alkanes in addition to the hydrocarbons present in the Alpine Tethyan OCT samples. The hydrocarbons detected in the Iberia-Newfoundland samples may originate from plankton and algae from a marine open-ocean source with no biological and isotopic evidence of a methanotrophic biosystem.

However, it should be noted that these observations are based on the analysis of a very small number of ODP core samples. The magmatic and metamorphic ODP core samples show evidence of contamination from drilling mud.

# Acknowledgement

*"I keep six honest serving men (they taught me all I knew);*

*Theirs names are What & Why & When & How & Where & Who"*

*Rudyard Kipling*

This project would not have been possible without the financial support from the Margin modelling program MM3. Therefore, thank you to support you gave to this project.

I would like to express my sincere gratitude to my supervisors – Nick Kuszniir, George Wolff, Gianreto Manatschal and John Wheeler for their continuous support of my PhD research. I would like to thank Nick Kuszniir for choosing me to be part of this project, which allowed to follow my scientific and academic vocation, communicate even further about my work and to have the chance to visit some magnificent places. Great thanks to George Wolff who initiated me into the life of organic geochemistry and without his great directions, patience and knowledge my research would not be a reality.

I would like to thank the people who gave me so much scientific and technical assistance, as well as inspirational conversations. Anu Thompson for initiating me to our geochemical lab, this research would not have been possible without your help and advices. To Steven Crowley for isotope analyses, Sabena Blackbird for carbon measurements, James Utley for XRD, Gareth Harriman and Elizabeth Fisher for giving me materials for the GC-MS.

My thanks to my colleagues and friends for making my PhD a pleasant journey by their day-to-day support and friendship - Nealy, Charli, Louise, Caroline, Suraya and so on. From ordinary days out, to a serious colleague help, I enjoyed and appreciated every bit of it.

I would like to thank my boyfriend Simeon Petev for his moral and emotional support and total understanding of the PhD life. My cats Poupou, Xonia and Popi with their fluffiness and zen attitude showed me that if the day goes bad a good sleep would rectify that.

Last but not the least, I would like to thank my whole family - my parents, for giving birth to me at the first place and for their constant support throughout all my life, and my sister, my small support.

# Dedication

This thesis is dedicated to my partner, Simeon Petev

You are my rock!







# Contents

Declaration of Authorship.....	i
Abstract.....	iii
Acknowledgement .....	v
Dedication .....	vii
List of figures.....	xiii
List of tables .....	xxiv
List of equations.....	xxviii
List of abbreviations.....	xxxii
1. Introduction .....	1
1.1. Aim and motivation.....	3
1.2. Significance of the study .....	4
1.3. Context of the study.....	5
1.4. Research strategy.....	5
1.5. Selection of field samples areas.....	7
1.6. Structure of thesis .....	8
2. Background .....	11
2.1. Serpentinisation .....	13
2.1.1. Serpentinisation process.....	13
2.1.2. Where? Serpentinite location.....	15
2.1.3. Serpentinisation and transfer of elements.....	17
2.1.4. Serpentinisation and Hydrogen (H <sub>2</sub> ).....	19
2.1.5. Importance of serpentinisation in the generation of abiotic gases.....	20
2.1.6. Microbial life and relation with the serpentinisation .....	22
2.1.7. Why study the serpentinisation.....	23
2.1.8. Importance of serpentinisation in geology.....	23
2.2. Geological context.....	27
2.2.1. Hyperextended rifted margins and Ocean continental transition (OCT)	27
2.2.2. Slow-spreading ridges.....	28
2.2.3. Hydrothermal system.....	29
2.2.4. Hydrothermal vents .....	31
2.3. Methanotrophic bacteria .....	42
2.3.1. What are methanotrophic bacteria? .....	42

2.3.1.	Biomarkers .....	46
2.3.2.	Biomarkers for methanotrophs.....	48
3.	Preserved organic matter in a fossil Ocean Continent Transition in the Alps: the example of Totalp, SE Switzerland .....	51
3.1.	Abstract.....	53
3.2.	Introduction .....	53
3.3.	Regional geological setting of the Totalp unit.....	55
3.3.1.	Pre-Alpine and Alpine geological and thermal history .....	56
3.3.2.	Lithologies .....	56
3.4.	Sample Collection, Preparation and Analysis .....	62
3.4.1.	Sample collection .....	62
3.4.2.	Sample preparation.....	63
3.4.3.	Mineralogical analyses .....	63
3.4.4.	Geochemical analyses .....	64
3.4.5.	Contaminant.....	66
3.5.	Carbon and hydrocarbon distributions in the analysed lithologies .....	69
3.5.1.	Serpentinite .....	73
3.5.2.	Ophicalcite.....	77
3.5.3.	Sediments.....	78
3.5.4.	Silica – rich carbonate (sulphide-rich outcrop) .....	80
3.6.	Interpretation and discussion.....	81
3.6.1.	Source of OM.....	81
3.6.2.	Thermal history of OM .....	86
3.6.3.	Origin of calcite veins .....	86
3.6.4.	OM in serpentinite – mechanism of emplacement .....	87
3.7.	Conclusions.....	89
4.	Preserved Organic Matter in the Fossil Alpine Tethyan Ocean Continental Transition.....	91
4.1.	Abstract.....	93
4.2.	Introduction .....	93
4.3.	Fossil Alpine OCT .....	96
4.3.1.	Tasna OCT.....	97
4.3.2.	Totalp unit .....	99
4.3.3.	Platta nappe .....	102
4.3.4.	The Chenaillet unit .....	105
4.4.	Sample Collection, Preparation and Analysis .....	106
4.4.1.	Sample collection .....	106
4.4.2.	Sample preparation.....	107
4.4.3.	Mineralogical analyses .....	108
4.4.4.	Geochemical analyses .....	109
4.5.	Results.....	111
4.5.1.	Mineralogy .....	111
4.5.2.	Hydrocarbon distributions in the analysed lithologies: Biomarkers..	115
4.5.3.	Carbon isotopes.....	131

4.5.4.	Fossil geological emplacement at the Tethys ocean .....	131
4.5.5.	Platta Sulphide mine .....	133
4.6.	Interpretation and discussion .....	135
4.6.1.	Source of OM .....	136
4.6.2.	Thermal history of OM .....	138
4.6.3.	Transport mechanism of OM .....	139
4.6.4.	Origin of calcite veins .....	140
4.6.5.	Platta Sulphide mine: Is the sulphide – serpentinite deposit a fossil hydrothermal vent? .....	143
4.7.	Summary.....	146
5.	Organic matter in Ocean Continent Transitions of present-day magma-poor rifted margin: the examples of Iberia and Newfoundland .....	149
5.1.	Abstract .....	151
5.2.	Introduction.....	152
5.3.	Iberia and Newfoundland continental margins, examples of a magma-poor rifted margins with serpentinitised exhumed mantle .....	154
5.3.1.	Iberia-Newfoundland margins and serpentinitisation .....	154
5.3.2.	Chosen ODP Sites for Analysis .....	156
5.3.3.	IODP cores and contamination .....	164
5.4.	Methods .....	166
5.4.1.	Sample preparation.....	167
5.4.2.	Geochemical analyses.....	167
5.5.	Results: carbon and hydrocarbon distributions .....	171
5.5.1.	Hydrocarbons in other lithologies .....	176
5.5.2.	Carbonate isotopes .....	177
5.6.	Discussion .....	177
5.6.1.	Origin of organic matter from biomarkers of sediment samples (149/897C/1A/63R1 91-95.5) .....	177
5.6.2.	GDGTs (Glycerol dibiphytanyl glycerol tetraethers) .....	180
5.6.3.	HCs in other lithologies .....	181
5.6.4.	Carbonate isotopes - source temperature.....	183
5.7.	Conclusion .....	184
6.	Discussion and Summary .....	187
A.1.	Abstract .....	189
6.1.	OM in the target samples.....	189
6.2.	Evidence of methanotrophic biosystem .....	194
6.3.	An upper bound on methanotrophic biomass associated with serpentinitised mantle? .....	195
6.4.	Recommendation .....	206
6.5.	Remaining questions .....	207
6.6.	Contribution .....	209
A.	Appendix A Organic geochemistry.....	213
A.1.	Serpentinitisation chemistry .....	215

A.2.	Ions used for single ion monitoring SIM in GC-MS analyses .....	218
A.3.	Hydrocarbons found in our samples .....	219
A.4.	Other contaminants.....	232
A.4.1.	<i>2,4-Di-tert-butylphenol</i> .....	232
A.4.2.	<i>Hopanoic acid</i> .....	234
A.4.3.	Dimethylpolysiloxane .....	234
A.4.4.	Linear alkylbenzene (LAB) $C_6H_5C_nH_{2n+1}$ .....	235
A.5.	Hydrocarbons biomarkers for anaerobic methanotrophs .....	236
B.	Appendix B: Methods.....	239
B.1.	Thin sections images.....	241
B.2.	Methods.....	243
C.	Appendix C : Mass spectrum and Gas chromatogram.....	245
C.1.	Sepiolite drilling mud.....	247
C.2.	Mass spectrum profiles .....	250
7.	Bibliography .....	257

# List of figures

Figure 2.1 - Phase diagram describing the possible MgO–SiO <sub>2</sub> –H <sub>2</sub> O System of serpentine by Evans et al. 2013. The grey bands represent H <sub>2</sub> O-conserved reactions. The lizardite is stable at 200 and 300 °C, antigorite grows from lizardite and chrysotile at the shown temperature.....	14
Figure 2.2. Conceptual sketch indicating the serpentinisation and carbonation into the footwall of the axial (asymmetric exhumational) normal fault modified from Picazo et al., 2013. The serpentinisation is observed no more than 3-4 km below the seafloor and along the footwall (Cannat et al. 2010). The most deformed rocks are the serpentinite gouges and cataclasites along the fault. Carbonation occurs after serpentinisation within 20 m of the paleo-seafloor (Picazo et al., 2013).....	16
Figure 2.3 Figure from Guillot and Hattori 2003 showing serpentinisation at ocean ridges and subduction zones with their fluid and mobile-elements transfer. ....	17
Figure 2.4 Figure from Evans et al. 2013 comparing the fluid-mobile elements of mantle-wedge serpentinite with those from volcanic-front magmas suggesting a genetic relationship between them.....	18
Figure 2.5. Serpentinisation relation with physical properties: Serpentinisation is a process related to the distance from the water contact (Cole et al. 2000, Skelton et al. 2005); Serpentinisation changes the density (Miller and Christensen 1997); Serpentinisation changes the velocity (Miller and Christensen 1997).....	26
Figure 2.6. a. Figure from Tugend et al. 2015 naming different parts of a magma-poor/starved margin depending of the type of study. B. Simplified figure of the hyper-extended magma starved margin by Mohn et al. 2012 with the different part as follows: from right to left proximal margin formed by thinned crustal domain about 30 km; necking zone (Mohn et al. 2012); distal margin less than 10km (Peron-Pinvidic, Manatschal, and Osmundsen 2013, Mohn et al. 2012) and ocean-continent transition (OCT) with exhumed mantle.....	28

Figure 2.7. A geological model of slow and fast spreading ridge showing the tectonic spreading and melt circulation from Carbotte et al. 2016. .... 30

Figure 2.8. Figure showing the chemical paths in a hydrothermal vent..... 32

Figure 2.9. Map from vents-data.interridge.org with the location of the confirmed hydrothermal vents September 2017 ..... 34

Figure 2.10. Different type of hydrothermal vents according to the mineral deposits and hydrothermal fluids depending on the distance from ridge, fault (Pinto 2014). The first line represents the mineral deposits and the second line the elements enriched in the fluids. The type 1 is a white smoker and the other two are black smokers. .... 34

Figure 2.11. Locations of the five hydrothermal vents (in bold) with serpentinisation on the northern Mid-Atlantic Ridge..... 36

Figure 2.12. Genealogical tree starting from LUCA (last universal common ancestor) showing the place of the aerobic and anaerobic methanotrophic in the two different branches – bacteria (prokaryotes, unicellular organism) and Euryarchaea (Archea, single-celled organism), respectively modified after Nitschke et Russell 2017. .... 43

Figure 2.13. Incomplete graph shows the type of hydrocarbons and the places of isoprenoid in the lipid’s sub-domain..... 47

Figure 2.14. Chemical structures of the hydrocarbon biomarkers for anaerobic methanotrophs..... 49

Figure 3.1. Maps showing location and geology of the Totalp area a) Location of the Totalp area in the tectonic map of the Alps (from(Schmid et al. 2004); modified by (Mohn et al. 2010)) b) Location of Totalp as a part of the South Penninic units in Grisons (Manatschal et al. 2003) c) Geological map of Totalp (modified from (Picazo et al. 2013)) showing location of the analyzed samples as well as the distribution of the major lithologies and samples described in this study (for description of samples see Table 3.1). .... 58

Figure 3.2. Sketch showing the lithologies and the stratigraphy of the Totalp area ((Weissert and Bernoulli 1985; Früh-Green et al. 1990; Manatschal et al. 2003; Picazo et al. 2013)).	59
Figure 3.3 Sample 26 ophticalcite from Totalp area showing late serpentinite – chrysotile only presented in vein and not observable in hand specimen in a mesh texture serpentinite.	61
Figure 3.4. The sulphide bearing outcrop in the Totalp area showing weathered lithology. Red circles are the sampling location in this outcrop. In the line-drawing on the right, light red identifies radiolarian cherts, dark red silicious shale and yellow sulphate rich carbonate, rich in silica a) Zoom of outcrop b) Sample 65 is composed by calcite 50%. 25% quartz and is highly weathered c) Sample shows visible hematite crystals and calcite as the major mineral d) Sample 60 shows a siliceous rock with 3 different colours composed by 83% quartz, 10% albite and pyrite, illite and chlorite.	62
Figure 3.5. Mass spectrum of a squalene.	66
Figure 3.6. Mass spectrum of a phthalate.	68
Figure 3.7. Mass spectrum of sulphur.	69
Figure 3.8. a) Global range of carbon isotopic composition of carbonates precipitated during early diagenetic processes (modified after Coleman et al. 1993;(Kiriakoulakis 1997); Heydari 1997) b) Carbon and oxygen isotopic composition of calcite veins in Totalp samples. c) Limestone (sample 19) showing two generation of calcite veins.	70
Figure 3.9. Representative mass chromatograms of the HCs of a typical sample of limestone (sample 10) a) <i>n</i> -alkanes (m/z 85) of sample 10 (limestone) b) Total Ion Chromatogram of sample 10	74
Figure 3.10. Representative mass chromatograms of the HCs of a typical sample of a siliceous rock from the sulphide rich outcrop of Totalp (sample 60). a) Total Ion	

Chromatogram of sample 60 b) sterane distribution (m/z 217, 218) of sample 60 c) PAH distribution (m/z 178, 192, 202, 228) of sample 60. For abbreviations see appendix..... 75

Figure 3.11. Thermal maturity parameters of C<sub>27</sub> steranes for Totalp samples. The classification is from Peters et al., 2005. The brown shaded area represents the range of complete isomerization for the 20S/(20S + 20R) aaa C<sub>27</sub> steranes (ca. 55%) and αββ/(ααα + αββ) C<sub>27</sub> steranes (ca. 68%). ..... 76

Figure 3.12. Plot of pristane/n-C<sub>17</sub> vs phytane/n-C<sub>18</sub> for Totalp samples used to identify depositional environment and OM type (after (Peters et al. 1999)). A gas chromatogram from each group is presented with retention time 20 to 35. .... 83

Figure 3.13. Sterane ternary distribution of the analyzed samples for the αββ steranes of Totalp samples. The interpretation of depositional environment is from Patrycja Wójcik-Tabol & Ślącza (2015). A gas chromatogram from each group is presented with retention time 50 to 60. .... 85

Figure 3.14. Conceptual model explaining origin and migration of OM from the seawater into different lithologies in the Totalp unit. a) The OM is represented by particulate and dissolved organic matter (POM and DOM, respectively). The OM infiltrates the basement rock by rock-fluid circulation. b) Some OM may be deposited within the carbonate veins (e.g. calcite veins). c) OM circulates with fluids through fractures and porosity of sediments to migrate into the basement rock. d) OM is preserved at the surfaces and in the interlayer surfaces of clay minerals in the sediments. (Schwarzenbach et al. 2013). ..... 88

Figure 3.15. Summary flow chart of chapter 3 ..... 90

Figure 4.1. a) Map showing the location of the studied areas (Tasna, Platta and Chenaillet as well as the location of Totalp studied in a previous study). b) Paleogeographic position of the studied unit modified after Manatschal and Müntener 2009. c) Reconstructed section across the Alpine Tethys modified after Manatschal and Müntener 2009..... 98

Figure 4.2. a, b) Panoramic photo and figure of Tasna unit (Manatschal et al. 2006) c -e) samples from Tasna unit f) Lithostratigraphic section of Tasna unit (Manatschal et al. 2006).....	100
Figure 4.3. a) Geological map of Totalp unit (Picazo et al. 2013) b) Lithological section of the Totalp unit (Mateeva et al. 2017) c-d) Outcrop showing neptunian dykes in serpentinised Iherzolite. ....	101
Figure 4.4. a) Geological map of Platta nappe (Schaltegger et al. 2002) b-c) Lithological and cross-section of the Platta unit (Epin et al. 2017) e) Samples from Platta unit. ....	103
Figure 4.5. Sulphide mines a, c) W of Marmorera lake represent oxidised serpentinite rich in polymetallic sulphides b) E of Marmorera lake d) opicalcite sample e) sample from sulphide mine W of Marmorera f) sample from sulphide mine E of Marmorera. ....	104
Figure 4.6 a) Geological map of Chenaillet (Manatschal et al. 2011). The locations of the analysed samples are shown with a red star. b) Lithological section of the Chenaillet (Manatschal et al. 2011) c-f) Samples from Chenaillet. ....	106
Figure 4.7. Thin sections from Chenaillet (a-d) and Totalp (e-h). a-d. serpentinite gouge and serpentinite cataclasite with foliated matrix and (table 1). e. opicalcite representing serpentine clast in a carbonate matrix. f. mesh structure of serpentinite g-h. serpentinite mesh structure with olivine completely serpentinised, rest of clinopyroxene, later chrysotile veins cross-cutted by carbonate vein (see B.1). ....	117
Figure 4.8. Representative mass chromatograms of the HCs of a serpentinite gouge C1 (Chenaillet). a) Total Ion Chromatogram b) <i>n</i> -alkanes distribution (m/z 85) c) sterane distribution (m/z 217, 218) d) PAH distribution (m/z 178, 192, 202, 228). For abbreviations see appendix. ....	119
Figure 4.9. Representative mass chromatograms of the HCs of sample C3 serpentinised Iherzolite from Chenaillet a) Total Ion Chromatogram b) <i>n</i> -alkanes	

distribution (m/z 85) c) sterane distribution (m/z 217, 218) d) PAH distribution (m/z 178, 192, 202, 228). For abbreviations see appendix. .... 121

Figure 4.10. Representative mass chromatograms of the HCs of serpentinite sample P\_1\_16 from sulphide mine. a) Total Ion Chromatogram b) *n*-alkanes distribution (m/z 85) c) sterane distribution (m/z 217, 218) d) PAH distribution (m/z 178, 192, 202, 228). For abbreviations see appendix. .... 123

Figure 4.11. Sterane ternary distribution of the analysed samples for the studied areas for the  $\alpha\beta\beta$  and  $\alpha\alpha\alpha$  steranes, modified after Mateeva et al. 2017. The interpretation of depositional environment is from Patrycja Wójcik-Tabol & Ślęczka (2015). A gas chromatogram from each group is presented with retention time 50 to 60. .... 124

Figure 4.12 Carbonate staining of sample 19, a limestone from Totalp. It is clearly seen in blue the limestone matrix and horizontal bigger calcite veins and in pink several veins almost perpendicular to the blue one. .... 125

Figure 4.13. Mass chromatograms (m/z 191) of sample P1 (serpentinised basalt) showing the distribution of hopanes (including gammacerane) ..... 127

Figure 4.14. Plot of pristane/*n*-C17 vs phytane/*n*-C18 for Platta, Tasna, Chenaillet and Totalp samples used to identify depositional environment and OM type (Peters et al. 1999, Mateeva et al.2017). A gas chromatogram from each group is presented with retention time 20 to 35. .... 130

Figure 4.15 Conceptual sketch visualising different lithology on the seafloor. For these sketches software Stretch was used to draw the detachment normal faults. .... 133

Figure 4.16. a) Carbon and oxygen isotopic composition of calcite veins in Tasna and Platta samples compared to Totalp samples and to in-situ sample from modern ocean seafloor (Mateeva et al. 2017). b) Summarized graph explaining the global range of carbon and oxygen isotopic composition in passive margin settings, modified after Kiriakoulakis (1997), Heydari (1997) c). calcite grain from one calcite veins sample 19

limestone, Totalp, showing twinning d) calcite grains from a calcite vein in sample 72 vein supported serpentinite breccia, Totalp unit. ....	141
Figure 4.17. Summary flow charts of chapter 4.....	147
Figure 5.1. Chemical structures of the hydrocarbon biomarkers for anaerobic methanotrophs. ....	153
Figure 5.2. Maps and figure showing the locality of the chosen ODP sites on the Iberian and Newfoundland margins. A- Simplified map showing the position of the four sites modified from Jagoutz et al. 2007. B – Figure showing the position and main lithology of the sites (Sutra et al. 2013).....	157
Figure 5.3. Images of the taken samples with their depth (mbsf – meters below seafloor), ODP number and lithology, TC, TOC and HC values with their analytical uncertainty (see Table 2). There is no apparent correlation between measured data and depth for the small number of sample. ....	164
Figure 5.4. Ion chromatogram profile of the clayey limestone sample for <i>n</i> -alkanes (m/z 85), PAHs and steranes (m/z 217, 218). ....	174
Figure 5.5. Ion chromatogram (m/z 85) of the <i>n</i> -alkanes of three samples. a. and b. serp. breccia from leg 173 Iberian margin b. gabbro from leg 210 Newfoundland showing similar distribution c. serpentinitised peridotite from leg 149 Iberian margin. ....	175
Figure 5.6. GDGTs results for sedimentary sample 897/63R1. Different ratios result from the GDGTs are given using formulas described in methodology section. ....	176
Figure 5.7. A star-plot diagram of alkane ratios from eight igneous and metamorphic samples from ODP Legs 173 and 210 from Iberian and Newfoundland margin showing similar distribution pattern. The peaks are shown in the GC-MS profile with their approximated RT and KI is shown in the table. We could propose that a contamination is realistically conceivable. The second star-plot diagram shows the distribution pattern of <i>n</i> -alkanes and isoprenoids for the two samples from ODP Leg 149 Site 897C	

(1A/63R1/91-95.5 clayey limestone and 63R2/92-97.5 serp. peridotite) using a different kind of drilling mud (bentonite) and showing different path from the samples from ODP Legs 173 and 210 and from each other. ....	182
Figure 5.8. Summary flow charts of chapter 5 .....	185
Figure 6.1 Plot of pristane/ <i>n</i> -C17 vs phytane/ <i>n</i> -C18 shows the depositional environment. Isoprenoids/ <i>n</i> -alkanes ratio (pristane/phytane) show consistency in the results with rather reducing environment. Only one sample, the clayey limestone from site 897C, Iberian margin shows very low maturation compare to the other samples. Modified after Mateeva et al. 2017. ....	191
Figure 6.2 Pristane/phytane ratios versus CPI ( <i>n</i> -alkanes) confirms the depositional environment conditions (Meyers and Snowdon 1993). ....	191
Figure 6.3 Sterane C27/(C27+C29) vs Pristane/phytane ratios showing depositional environment conditions and source input. Here, it indicates mostly a pelagic anoxic environment (Powell 1988).....	192
Figure 6.4 Sterane ternary distribution ( $\alpha\beta\beta$ steranes). Classification is after Patrycja Wójcik-Tabol & Ślęczka (2015). For the sediment sample from the Iberian margin (149/897C/63R1) both $\alpha\beta\beta$ (left side) and $\alpha\alpha\alpha$ (right side) type steranes are shown both displaying the input of terrestrial OM. Modified after Mateeva et al. 2017. .	192
Figure 6.5 Hopane/steranes versus pristane/phytane ratios differentiates between algal and bacterial source input, as well as depositional environment conditions anoxic or oxic (El Diasty and Moldowan 2012). ....	193
Figure 6.6 Mean, median and standard deviations of HC concentrations in the four studied Alpine areas.....	193
Figure 6.7 Scheme showing the calculation of maximum amount of methanotrophic biomass per unit rock sample. ....	198

Figure 6.8 Logarithmic plot showing the global mass of methanotrophs (in $y$ ) as a function of the thickness of serpentinised mantle that may host methanotrophs (in $x$ ). Here taken between 1 and 1000 m. The percentage of exhumed mantle on the ocean floor, $f$ , is shown for three values 0.05, 0.1 and 0.15%. It is compared with the present day global total bio-mass.....	201
Figure 6.9 Logarithmic plot comparing the annual rate of mass per year of the calculated methanotrophs with the oceanic biomass.....	203
Figure 6.10. Mass spectrum of hopanoic acid. ....	234
Figure 6.11. A chromatogram showing a column bleeding and the mass spectrum of Dimethylpolysiloxane.....	235
Figure 6.12 Gas chromatogram showing different LABs and the mass spectrum of a chosen molecule in RT =24.17 .....	236
Figure 6.13 An additional panel with thin section images from Totalp. Sample 5 is serpentinised lherzolite and sample 4 is ophicalcite. ....	241
Figure 6.14. Sketch summarising the serpentinisation based on sample 5 from Totalp. Pyroxene is still present in the serpentinite but not olivine. This could be due to the fact that in low fluid flux serpentinisation start with olivine and in later stage in more open fluid condition magnetite appeared (Bach et al. 2006). The oxydes are magnetite and spinel. Chrysotile and carbonate veins are observed in thin section but invisible to the naked eye. The samples represent also later fluid veins and fractures (coloured in baby blue). ....	242
Figure 6.15 Gas chromatogram profiles of a drilling mud (sepiolite). ....	247
Figure 6.16 Ion chromatogram ( $m/z$ 85) from two samples and sepiolite. The three ion chromatograms show a dominance of C18 $n$ -alkane. ....	248

Figure 6.17 A star-plot diagram of alkane ratios from eight igneous and metamorphic samples from Legs 173 and 210 from Iberian and Newfoundland margin from figure 5.7 compared to sepiolite. .... 249

Figure 6.18 Mas spectrum of the cyclic and branches alkanes used in figure 5.7... 255



# List of tables

Table 2.1 Table showing the different types of methane – abiogenic and biogenic from Etiope et Sherwood 2013. ....	21
Table 2.2. Table generalising the difference between black and white smokers type hydrothermal vents. The data used in this table is mentioned and referenced in the chapter. ....	33
Table 2.3. Showing the serpentinite driven hydrothermal vents (partially or not) with their characteristics. No data available or found explain the missing cells. References from Exomar(2006) and Serpentine(2007) cruise of Ifremer a- (Beltenev et al. 2005; Fouquet et al. 2008; Charlou et al. 2010). b - (Fouquet et al. 2008; Charlou et al. 2010). c- (Batuyev et al. 1994; Gebruk et al. 1997; Charlou et al. 1998; Charlou et al. 2010; Cherkashov et al. 2010). d- (Schmidt et al. 2007; Fouquet et al. 2008; Reed et al. 2009). e - (Devey et al. 2005; Koschinsky 2006; Melchert et al. 2008; Schrenk et al. 2013). f - (Charlou et al. 1998; German et al. 1998; Douville et al. 2002; Reed et al. 2009; Charlou et al. 2010). g - (German et al. 2002). h - (Kelley et al. 2001; Kelley et al. 2005; Brazelton et al. 2006; Ludwig et al. 2006; Charlou et al. 2010). i - (Barriga et al. 1998; German et al. 1998; Dias and Barriga 2006; Dias et al. 2010; Dias et al. 2011). j - (Connelly et al. 2012; Hodgkinson et al. 2015; McDermott et al. 2015; Reveillaud et al. 2016).....	38
Table 2.4. Table showing the anaerobic methanotroph (ANME) , their symbiot with SRB and their biomarkers.....	44
Table 3.1. Results by lithology including mineralogy and texture observed in hand specimens and the texture on the calcites used for the isotopic analyses ( $\delta^{13}\text{C}_{\text{VPDB}}$ , $\delta^{18}\text{O}_{\text{VPDB}}$ ). The vein generation is defined from the specific example and may not correlate across all samples. <sup>1</sup> Thin section of the lithology is observed. • All lithology are from the lower sub-unit with the exception of the massive serpentinite (samples 77, 78).....	70

Table 3.2. Results by lithology including TC, TOC in ppm (parts per million), total HC concentration in ppb (parts per billion) and organic carbon isotopic composition of bulk rock  $\delta^{13}\text{C}_{\text{Organic}}$ . For the n-alkanes: the carbon number range (*n*-alkane range), the maximum carbon number (Cmax), carbon preference index (CPI values) and mean carbon number (MC#) are shown. For the steranes, hopanes and PAHs the concentrations are in ppb and are represented in intervals by star symbol \*, where \* = [0 - 0.1), \*\* = [0.1 - 1) and \*\*\* = [1 - 10) and BDL = below detection limit. a: identified PAHs in the samples were: Phenanthrene, P; Fluoranthene, Fluo; Pyrene, Pyr; Chrysene, Chry; Benzo(a)anthracene, BaA; Benzo(b)fluoranthene, BbF; Benzo(a)pyrene, BaP; Indeno(1,2,3-cd)pyrene, IndPy; Benzo(ghi)perylene, BghiP; Dibenzothiophene (DBT) , methylP (3,2,1 and 9 MPs) and 2-methyl naphthalene ; not all were present in every sample. 1 All lithology are from lower sub-unit except the massive serpentinite (samples 77, 78) which is from upper sub-unit..... 79

Table 4.1 Results by lithology including mineralogy and texture observed in hand specimens..... 112

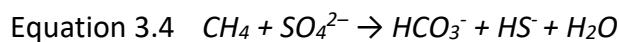
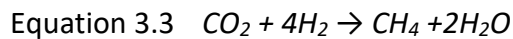
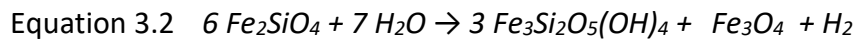
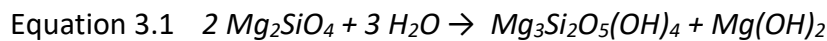
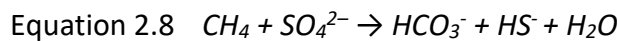
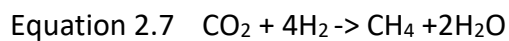
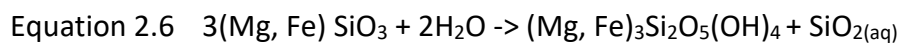
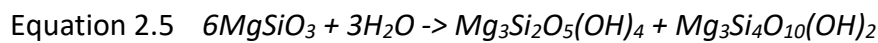
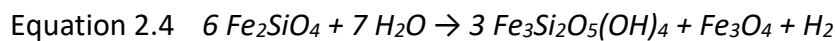
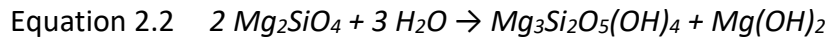
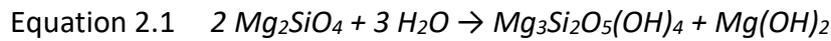
Table 4.2 TOC and TC in ppm (parts per million), total HC concentration in ppb (parts per billion) and organic carbon isotopic composition of bulk rock  $\delta^{13}\text{C}_{\text{Organic}}$ . For the n-alkanes: the carbon number range (*n*-alkane range), the maximum carbon number (Cmax), carbon preference index (CPI values) and mean carbon number (MC#) are shown. For the steranes, hopanes and PAHs the concentrations are in ppb and are represented in intervals by star symbol \*, where \* = [0 - 0.1), \*\* = [0.1 - 1) and \*\*\* = [1 - 10) and BDL = below detection limit. .... 113

Table 4.3 PAHs ratios for the samples from Cheanillet, Platta and Tasna. The ratios show the rapport between PAHs as an indication of the HT source origin. Identified PAHs in the samples used for the ratios were: Phenanthrene,P; Fluoranthene, Flui; Pyrene, Pyr; Chrysene, Chry; Benzo (a) anthracene, BaA; methyl (3,2,1 and 9 MPs) naphthalene ..... 114

Table 4.4. Table showing the result from carbonate straining. Where the staining shows blue colour, it is interpreted as reducing environment, where the colour is pink is interpreted as oxidizing environment. ....	126
Table 4.5 Table showing the carbon and oxygen isotopic results of the carbonate texture on samples from Tasna and Platta. ....	133
Table 4.6. Table showing results from XRF for the samples from Platta sulphide mine .....	134
Table 4.7. Table showing mineralogical composition of sulphide mine's samples from XRD analyses. ....	134
Table 5.1. Results by samples IODP sites including mineralogy and texture observed in hand specimens and the texture on the calcites used for the isotopic analyses ( $\delta^{13}C_{VPDB}$ and $\delta^{18}O_{VPDB}$ ).....	165
Table 5.2 Results by IODP sites including TC (%), TOC (ppm) and total HC concentration ppb. For the <i>n</i> -alkanes: the carbon number range ( <i>n</i> -alkanes range), the maximum carbon number (C <sub>max</sub> ), carbon preference index (CPI values) and mean carbon number (MC#) are shown.....	171
Table 5.3 Table showing the identified <i>n</i> -alkanes, PAHs, steranes and hopanes in the samples. For the abbreviations of the names see glossary. Where Phenanthrene, P; Fluoranthene, Fluo; Chrysene, Chry; Benzo(a)anthracene, BaA; Benzo(b)fluoranthene, BbF; Benzo (k) fluoranthene BFs; Benzo(a)pyrene, Benz; Dibenzothiophene (DBT), methyl DBT (MDBT) and methylP (3,2,1 and 9 MPs). ....	172
Table 5.4. Biomarkers ratios used to indicate the source input and thermal maturity. ....	179
Table 6.1. Table showing the organic carbon data for 6 analysed samples from the Alpine Tethys OCT. ....	195

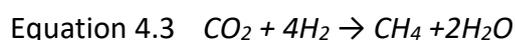
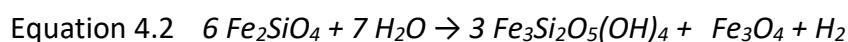
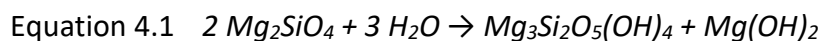
Table A.1 Table showing the ions used for single ion monitoring (SIM) during GC-MS analyses.....	218
--------------------------------------------------------------------------------------------------	-----

# List of equations



Equation 3.5  $MC\# = \sum ([C_i] \times C_i) / \sum [C_i]$

Equation 3.6  $CPI = 0.5 \times \sum ([\text{odd } C_{21} - C_{35}] / \sum ([\text{even } C_{20} - C_{34}] + \sum [\text{odd } C_{23} - C_{37}] / \sum [\text{even } C_{22} - C_{36}]))$



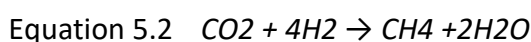
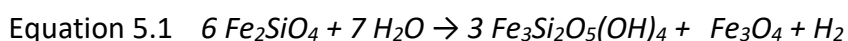
$$\text{Equation 4.5 } MC\# = \sum ([C_i] \times C_i) / \sum [C_i]$$

$$\text{Equation 4.6 } CPI = 0.5 \times \sum ([\text{odd } C_{21} - C_{35}] / \sum ([\text{even } C_{20} - C_{34}] + \sum [\text{odd } C_{23} - C_{37}] / \sum [\text{even } C_{22} - C_{36}]))$$

$$\text{Equation 4.7 } MP/P = 1.89 \times (3MP + 2MP) / (P + 1.26(9MP + 1MP))$$

$$\text{Equation 4.8 } MPI = (2MP + 3MP) / (2MP + 3MP + 1MP + 9MP)$$

$$\text{Equation 4.9 } \sum TOC f_0 + \delta i = \delta a$$



$$\text{Equation 5.4 } 1000 \ln \alpha = 2.78 (106 \times T - 2) - 3.39$$

$$\text{Equation 5.5 } \alpha_{A-B} = (1000 + \delta_A) / (1000 + \delta_B)$$

$$\text{Equation 5.6 } MC\# = \sum ([C_i] \times C_i) / \sum [C_i]$$

$$\text{Equation 5.7 } CPI = \sum (\text{odd } C_{17} - C_{21}) / \sum (\text{even } C_{16} - C_{20})$$

$$\text{Equation 5.8 } KI = 100 \times ((n + RT_{\text{unknown}} - RT_n) / RT_n - RT_n)$$

$$\text{Equation 5.9 } BIT = ( (GDGT -1) + (GDGT -2) + (GDGT -3) ) / ( (GDGT -1) + (GDGT -2) + (GDGT -3) + (Cren) )$$

$$\text{Equation 5.10 } MI = ( (GDGT -1) + (GDGT -2) + (GDGT -3) ) / ( (GDGT -1) + (GDGT -2) + (GDGT -3) + (Cren) + (Cren. Isomer) )$$

$$\text{Equation 5.11 } TEX_{86} = ( (GDGT -2) + (GDGT -3) + (Cren. Isomer) ) / ( (GDGT -1) + (GDGT -2) + (GDGT -3) + (Cren. Isomer) )$$

$$\text{Equation 5.12 } RI = ( 1 \times (GDGT -1) + 2 \times (GDGT -2) + 3 \times (GDGT -3) + 4 \times (GDGT -4) ) / ( (GDGT -1) + (GDGT -2) + (GDGT -3) + (GDGT -4) )$$

Equation 6.1  $\chi = \lambda \cdot \theta$

Equation 6.2  $\sigma = \kappa / \chi$

Equation 6.3  $M_{sp} = V_{sp} \cdot \rho_{sp}$

Equation 6.4  $V_{sp} = A_{exm} \cdot t_{sp}$

Equation 6.5  $M_{sp} = V_{sp} \cdot \rho_{sp}$

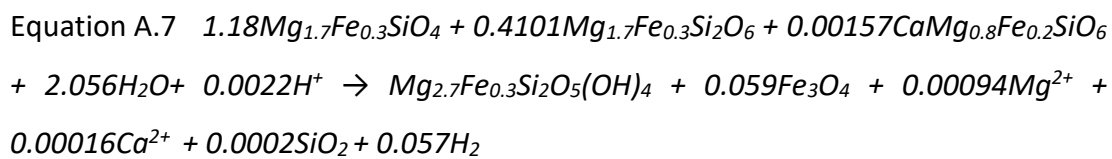
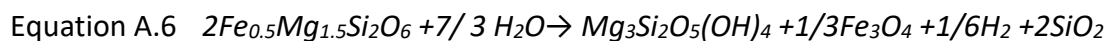
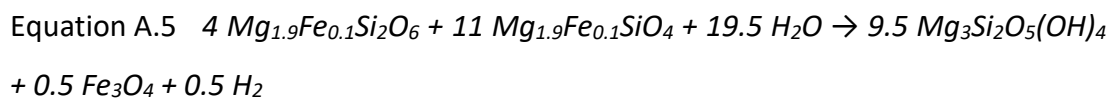
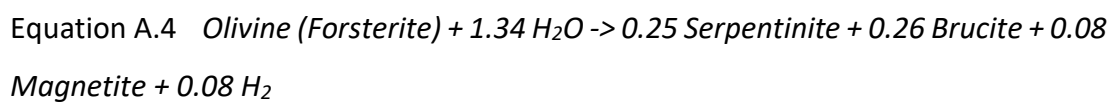
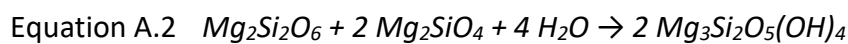
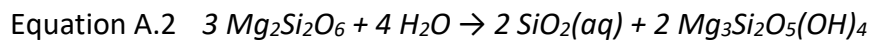
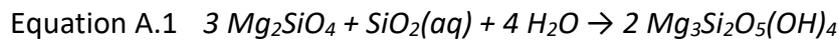
Equation 6.6  $M_{gmt} = (M_{sp} \cdot \mathcal{K})$

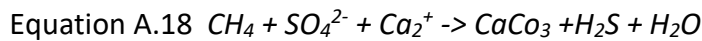
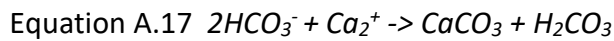
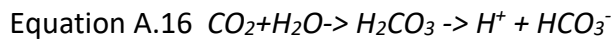
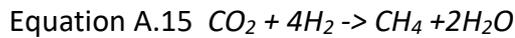
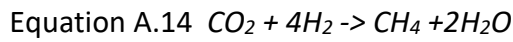
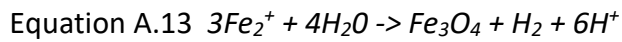
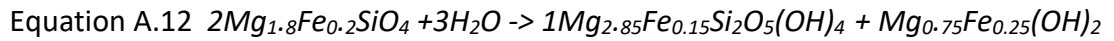
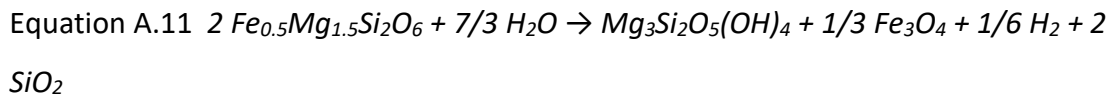
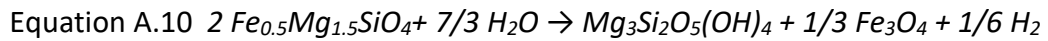
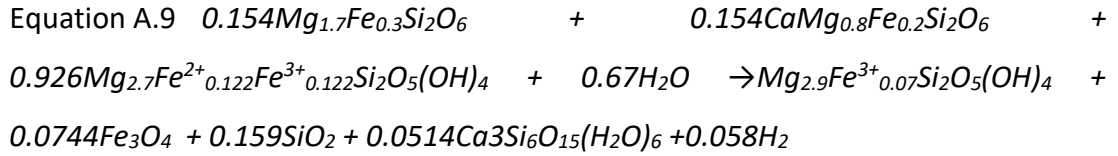
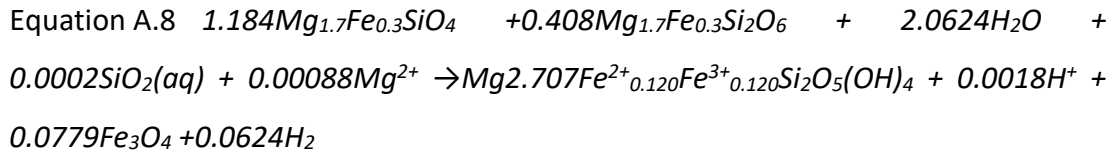
Equation 6.7  $R_{gmt} = M_{gmt} / 180 \text{ Myr}$

Equation 6.8  $R_{ocbm} = 10 \times 10^{12} / 10 \text{ kg/yr}$

Equation 6.9  $M_{sp} / 180 \text{ Ma} = S_{rate}$

Equation 6.10  $S_{CH4} = CH4 \text{ rate} \cdot S_{rate}$

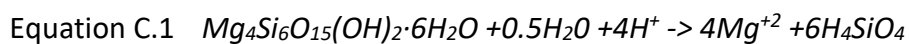




Equation B.1  $\delta^{18}\text{O}_{\text{SMOW}} = 1.03092 * \delta^{18}\text{O}_{\text{VPDB}} + 30.92$

Equation B.2  $1000 \ln \alpha = 2.78 (106 \times T - 2) - 3.39$

Equation B.3  $\alpha_{A-B} = (1000 + \delta_A) / (1000 + \delta_B)$



# List of abbreviations

149/897C/1A/63R1 91-95.5

149 – leg

897 – Site

C – hole

1A – acoustic formation on west Iberia margin (Located by drilling and multichannel seismic reflection profiles e.g. (Mauffret and Montadert 1988; Sawyer et al. 1994))

63 – core number

R – rotary drilling (rotary core barrel, core type)

91-95.5 – sample taken between this interval

ANME – ANaerobic Methanotroph

AOM – anaerobic oxidizing methane

Biomarkers – molecular remains of former living organisms

DOM – Dissolved organic matter

GC – Gas chromatography

GC – MS – gas chromatography mass spectrometry

GDGT – Glycerol dialkyl glycerol tetraether, a main constituent of the archaeal core membrane lipids

HC – Hydrocarbon

HCL – Hydrochloric acid

Hopane

29 $\alpha$  $\beta$  17 $\alpha$ (H), 21 $\beta$ (H)-Norhopane

30 $\alpha$  $\beta$  17 $\alpha$ (H), 21 $\beta$ (H)-Hopane

31 $\alpha$  $\beta$  S 17 $\alpha$ (H), 21 $\beta$ (H)-22S-Homohopane

31 $\alpha$  $\beta$  R 17 $\alpha$ (H), 21 $\beta$ (H)-22R-Homohopane

30 $\beta$  $\beta$  17  $\beta$ (H), 21 $\beta$ (H)-hopane

32 $\alpha$  $\beta$  S 17 $\alpha$ (H), 21 $\beta$ (H)- 22S- Homohopane

32 $\alpha$  $\beta$  R 17 $\alpha$ (H), 21 $\beta$ (H)- 22R- Homohopane

34 $\alpha$  $\beta$  R 17 $\alpha$ (H), 21 $\beta$ (H)-22R- Homohopane

34 $\alpha$  $\beta$  S 17 $\alpha$ (H), 21 $\beta$ (H)-22R- Homohopane

Margin – (from latin: margo, margin meaning edge) transition between continental and oceanic lithosphere

MAR – mid-Atlantic ridge

Mbsf – metre below seafloor

MOR – mid ocean ridge

Ocean Ridge – (from old engl: hrycg meaning spine, crest) an elevation of land created by the forming plate obtained by the plate extension

OCT – Ocean-continent transition

OM – Organic matter

PAH – Polynuclear aromatic hydrocarbons

A – Anthracene

P – Phenanthrene

2N – 2-phenyl Naphthalene

Fluo – Fluoranthene

Pyr – Pyrene

Chry – Chrysene

BaA – Benzo(a)anthracene

BbF – Benzo(b)fluoranthene

BaP – Benzo(a)pyrene

BFs – Benzo (k) fluoranthene

Benz – Benzo(a)pyrene

IndPy – Indeno(1,2,3-cd)pyrene

BghiP – Benzo(ghi)perylene

DBT – Dibenzothiophene

MDBT – methalDBT

3,2,1 and 9 MPs – 3-,2-,1- and 9-methylphenanthrene

Passive margin – continental-oceanic transition which not lie on the end of an active plate (Dewey and Bird 1970)

POM – Particle organic matter (1 ppm = 1 mg/l; 1 mg/kg)

POC – Particle organic carbon, organic carbon fraction with particle sizes  $\leq 0.45 \mu\text{m}$

PPM – Parts per million in terms of mass (1 ppm = 1 mg/l; 1 mg/kg)

SRB – Sulphide Reducing Bacteria

SSR – Slow spreading ridge

Steranes

C27ba20S 20S 13b(H),17a(H)-diacholestane

C27ba20R 20R 13b(H),17a(H)-diacholestane

C27ab20S 20S 13b(H),17a(H)-diacholestane

C27ab20R 20S 13b(H),17a(H)-diacholestane

C28ba20S 20S 24-methyl-13b(H),17a(H)- diacholestane

C28ba20R 20R 24-methyl-13b(H),17a(H)- diacholestane

C27aaa20S 20S 5a(H), 14a(H), 17a(H)-cholestane

C27abb20R 20R 5a(H), 14a(H), 17a(H)-cholestane

C27abb20S 20S 5a(H), 14a(H), 17a(H)-cholestane

C27aaa20R 20R 5a(H), 14a(H), 17a(H)-cholestane

C28aaa20S 20S 24-methyl-5a(H), 14a(H), 17a(H)- cholestane

C28abb20R 20R 24-methyl-5a(H), 14a(H), 17a(H)- cholestane

C28abb20S 20S 24-methyl-5a(H), 14a(H), 17a(H)- cholestane

C28aaa20R 20R 24-methyl-5a(H), 14a(H), 17a(H)- cholestane

C29aaa20S 20S 24-ethyl-5a(H), 14a(H), 17a(H)- cholestane

C29abb20R 20R 24-ethyl-5a(H), 14a(H), 17a(H)- cholestane

C29abb20S 20S 24-ethyl-5a(H), 14a(H), 17a(H)- cholestane

C29aaa20R 20R 24-ethyl-5a(H), 14a(H), 17a(H)- cholestane

TOC – Total organic matter

TC – Total carbon

XRD – X-ray diffraction

‰ – Per mille symbol

Units:

1 ppm = 1 mg/l; 1 mg/kg

1mol = 1000 mmol

1g = 10<sup>3</sup>mg = 10<sup>6</sup>µg = 10<sup>12</sup>pg

1 Tg =  $10^{12}$  g

1 g CH<sub>4</sub> = 0.0623 mol CH<sub>4</sub>

wt % - percentage by weight





# Chapter 1

## 1. Introduction

*What do we mean – it is a common term of praise – when we say that a book is “original”? Not, usually that the writer has invented something without precedent, but that she has made us ‘perceive’ what we already, in a conceptual sense, ‘know’, by deviating from the conventional, habituated ways of representing reality. Defamiliarisation, in short, is another word for “originality”.*

*David Lodge, The Art of Fiction: Illustrated from Classic and Modern Texts 1992, p 55)*



## 1.1. Aim and motivation

*“Every problem has a gift for you in its hands”*

*Richard Bach*

My thesis titled “Mantle serpentinisation, carbon and life?” investigates the relationship between mantle serpentinisation and the deep biosphere at ocean continent transition (OCT) in magma-poor rifted margins. This project is part of a collaboration between the University of Liverpool and the University of Strasbourg related to the study of rifted continental margins and mantle exhumation.

The primary aim of this research is to establish whether methanotrophic biosystems are localised and only flourish in the conditions generated by hydrothermal vents at ocean ridges or are pervasive within oceanic regions of exhumed mantle and active serpentinisation. While methanotrophic activity has been investigated in hydrothermal vents at mid ocean ridges (MOR), similar studies have not been carried out for the OCT of magma-poor rifted margin.

If a methanotrophic bio-system was pervasive within serpentinised exhumed mantle at slow spreading ocean ridges then this would have important implications for our understanding of the global biomass of the deep biosphere, and the methane and carbon cycle.

To address the main aims of my PhD, I carried out the following observations and analyses:

- (i) I investigate whether organic matter can be found in the serpentinised mantle and overlying lithologies of the fossil Alpine Tethys OCT. I then determined if there is molecular evidence of methanotrophic bacteria within this organic matter.
- (ii) I also investigate whether organic matter can be found in the serpentinised mantle of the OCT of the present-day Iberian and

Newfoundland margins, and whether it contains molecular evidence of methanotrophic bacteria.

Using the results of my analyses, I attempted to answer the following questions:

- (i) Are there methanotrophic biosystems related to serpentinisation at deep water magma-poor rifted continental margins?
- (ii) Is there evidence of methanotrophic biosystems in the serpentinised mantle unrelated to hydrothermal vents?
- (iii) Can evidence be found for the presence of methanotrophic bacteria or other organic matter in serpentinised mantle in the fossil OCT of Alpine Tethys and what would that mean?
- (iv) Is there a difference in the organic matter in the exhumed serpentinised mantle and in the overlying sediments?

## **1.2. Significance of the study**

*“You must have faith. In reason. In discovery.  
And in the endurance of the logical mind.”*

*Baleth, The Orville series*

The key question of my PhD research is whether methanotrophic bio-systems are generally pervasive in their association with serpentinised mantle in the subsurface. The answer to this question would have important global implications for the importance of the hidden sub-surface bio-systems, the fate of methane and the carbon cycle. Studying the link between serpentinisation and methanotrophic community could help us better understand the methane cycle, a cycle which is governed primary by methanogenic and methanotrophic bacteria. Methane is a more powerful greenhouse effect compared to CO<sub>2</sub> and is the fourth most present gas in the atmosphere (500 Tg with increase of 0.8% per year) (Etiope and Klusman 2002). Evidence of a relationship between methanotrophs and serpentinisation away from the prolific condition of the hydrothermal vents could have significant importance in the search for life on other silicate planets such as Mars or Enceladus (Saturn’s moon) (Etiope 2015; Glein et al. 2015).

### **1.3. Context of the study**

The discovery of hydrothermal vents in 1977 showed that these environments are linked with deposits of rare earth elements and unique biological communities. Some of these hydrothermal vents and their biosystems are partially supported by energy from serpentinisation. It has been suggested that serpentinisation and hydrothermal vents played a central role in the emergence of life (Russell et al. 2010). The first discovery of a white smoker (the Lost city) was in 2001 near the Atlantic ridge (Kelley et al. 2001). This type of hydrothermal system has fluids with high concentrations of hydrogen and methane (and other low-molecular-weight hydrocarbons) and is supported by low-temperature serpentinisation, which serves as an important energy sources for anaerobic microorganisms such as the methanotrophic bacteria (Hinrichs et al. 2000; Kelley et al. 2001; Orphan et al. 2001; Kelley et al. 2005).

Evidence based on drilling and dredging at mid ocean ridges and direct sampling of the OCT of the Tethyan margin in the Alps supports the hypothesis that mantle serpentinisation is a common process that results from the interaction of mantle rock and water. It occurs at slow-spreading mid ocean ridges and magma-poor rifted margins. Observations at hydrothermal systems in modern slow-spreading ridges suggest that methane produced by serpentinisation can support methanotrophic bio-systems. The serpentinisation process produces free hydrogen, which can react at high pressure and temperature with CO<sub>2</sub> via Fisher-Tropsch-like reactions to form methane. This methane forms the source of carbon and energy for methanotrophs (Archaea, Eukaryote). This sequence of abiotic anaerobic chemical reactions produced by the serpentinisation may have supplied chemical energy for some of the first organisms living on Earth and could possibly provide chemical energy for extra-terrestrial life.

### **1.4. Research strategy**

Several strategies have been employed to achieve the main objectives of this study. Kilometre scale exposures of exhumed serpentinised mantle of the Tethyan magma-poor rifted continental margin in the eastern Swiss Alps allow 3D mantle sampling

which has the potential to answer the question of whether sub-surface methanotrophic biosystems are localized or pervasive. In addition, ODP (Ocean Drilling Program) core samples from the OCT of the present-day Iberia and Newfoundland magma-poor rifted continental margins are also analysed. The analysis of OCT samples from both ODP cores and the fossils Alpine Tethyan margin will allow a comparison of their organic matter.

The OCT is the only part of the passive margin where the exhumed serpentinized mantle is observable and sampled. Considering the aim of this project, to find if the methanotroph biosystem is pervasive within the serpentinization, the field for this research is restricted to the OCT.

In order to identify specific biomarkers (i.e. lipids) in the collected samples, several bio-geochemical analytical methods have been used (e.g. measurement of the Total Carbon (TC) and Total Organic Carbon (TOC), GC – gas chromatography and GCMS-gas chromatography mass spectrometry, isotopic analysis of organic carbon). At the same time several geological/petrological/mineralogical methods have been used to understand the mineralogy/petrology and the geological context of the samples taken (e.g. optical analysis, XRD- X-ray diffraction analysis, oxygen and calcite isotopic analysis on calcite veins).

I use an organic geochemical approach to quantify OM in the fossil (Alpine Tethys) and modern OCT (Iberian and Newfoundland margins) exhumed mantle domains to better understand the relationship between OM and mantle serpentinisation. We look for specific biomarkers which are the molecular remains of former living organisms and especially hydrocarbons with an origin consistent with anaerobic methane oxidation (e.g. crocetane; (Peters and Moldowan 1993; Blumenberg et al. 2004)).

Biomarkers have been used to determine source rock OM type (i.e. open marine, restricted marine, or terrestrial environments), thermal maturity of preserved OM, and the geological age and lithology of the source rock (Peters and Moldowan 1993). Specific biomarkers can show the presence of methanotrophic bacteria (e.g.

crocetane) as well as to describe the relationship between microorganism, serpentinisation and hydrothermal vents (Pancost et al. 2000).

Recent studies have focussed on the relationship between serpentinisation and organic compounds (mainly methane) in the laboratory (*e.g.* (McCollom and Seewald 2013; Etiope and Ionescu 2014)), at present-day serpentinite-hosted hydrothermal vents (*e.g.* (Kelley et al. 2005; Delacour et al. 2008c; Proskurowski et al. 2008)), mud volcanoes (*e.g.* (Mottl et al. 2003; Holm et al. 2006)), and exhumed serpentinite mantle domains with high hydrogen concentrations and high pH (*e.g.* (Cardace et al. 2013)). At present, however, there are insufficient studies which examine biomarkers in serpentinised peridotite of fossil OCT with low concentration of H<sub>2</sub>. This research project is aimed to fill exactly this gap.

### **1.5. Selection of field samples areas**

Samples from the OCT of Alpine Tethys and the Newfoundland and Iberia rifted margins were selected to highlight the relationship between organic matter and serpentinisation of exhumed serpentinised mantle. The studied areas in the Alps include ophiolitic units in the Platta, Totalp and Tasna areas of the SE Swiss Alps, as well as Chenaillet in the Western Alps. ODP (Ocean drilling program) cores from the OCT of the Iberian and Newfoundland hyper-extended magma-starved rifted margins were taken from the MARUM repository in Bremen to examine in-situ OCT samples. Samples from the Iberia-Newfoundland rifted margins have been chosen for analysis because these margins are the most well studied hyper-extended rifted margins and their tectonic and sedimentary evolution have been successfully compared with that of the Alpine Tethys OCT (Manatschal et al. 2007).

The fossil Alpine Tethyan OCT has several advantages over the present-day Iberia-Newfoundland margin in terms of sample collection. The Alpine sampling is less spatially restrictive and also drilling and sampling has not introduced contamination or alteration (*e.g.* hand sampling, hand drilling using only water). The chosen Alpine Tethyan sampling locations (Totalp, Tasna, Platta and Chenaillet) were selected because they provide the best opportunity to investigate the presence or absence of

methanotrophic biosystems within serpentinised exhumed mantle in the Alpine Tethyan OCT. Sampling of the OCT of magma poor rifted margin has been focussed on where there is diversity of rock types. The locations contain serpentinised mantle, ophicalcites and syn to post-tectonic sediments and are among the best locations which have little Alpine deformation and only a low-grade metamorphic overprint (mostly <200 °C, from prehnite-pumpellyite to greenschist facies). The samples were chosen so that they were close to the seafloor and in contact with the serpentinised mantle to look for evidence of methanotroph into the serpentinite or originated by it but upward it into the overlain lithologies. Sampling is taken at each outcrop. Sampling precision is reached by taking three sample from the same lithology of an outcrop. Pragmatic reasons such as physical attainability are also considered.

Samples from serpentinised peridotite and overlying or intrusive lithologies were analysed from 3 sites on the Iberian margin and one site on the Newfoundland margin (leg 149 site 897C, leg 173 sites 1068A and 1070A and leg 210 site 1277A).

The geological background of the studied areas is explained in detail in the appropriate chapters (III, IV and V).

## **1.6. Structure of thesis**

The author believes the work presented in this PhD thesis is original and results from my own PhD research studies. This thesis consists of an introduction, a background chapter, three main chapters (chapters 3, 4 and 5) that report the results study and form the core of the thesis, and discussion and summary chapters that draw together the thesis observations to provide an overall conclusion. This thesis includes the complete versions of 3 manuscripts prepared for publication in international journals (chapters 3,4 and 5). Some repetition of aims and methodology is therefore necessary in each chapter.

One manuscript is already published (chapter 3) and one is submitted for publication and is under review (chapter 4).

Chapter 1 (this chapter) introduces the aims, background and relevance of this PhD study.

Chapter 2 describes the framework of my research and includes three main parts. The first describes the tectonic background of serpentinised mantle exhumed at magma poor rifted margins (OCT) and slow-spreading ridges. The second part is a review of hydrothermal vents and its biosphere and the last part describes the methanotroph biosystem.

Chapter 3 describes the Totalp study explaining the sampling and analysis methodologies, and the biomarkers found there. This chapter is published Mateeva et al. 2017 in the *Swiss Journal of Geoscience*.

Chapter 4 corresponds to a full manuscript entitled "Preserved organic matter in the fossil Alpine Tethyan Ocean Continental Transition" prepared for publication for the journal *Chemical Geology*. This chapter describes the sampling and analysis of the Platta, Tasna and Chenaillet localities of the Alpine Tethyan OCT. The organic matter found in these 3 localities is presented and discussed together with that found in the Totalp area (chapter 3).

Chapter 5 corresponds to a manuscript entitled "Organic matter in a present-day margin: the example of Iberia and Newfoundland margin ". This chapter presents the organic geochemical results from samples collected from IODP drilling of the OCT of the Iberia-Newfoundland passive continental margin.

Chapter 6 is a discussion summarizing the results presented in the previous chapters and focuses on the questions identified in Chapter 1. In this chapter, I discuss the significance of my PhD results, the contribution of this thesis to this research field and its limitations, as well as the scientific questions raised by this study.



## Chapter 2

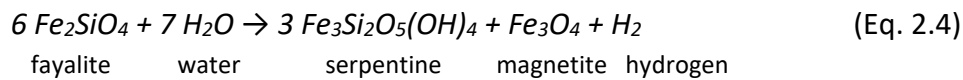
# 2. Background

This background section has been organised to provide understanding of the serpentinisation process and the geological background for this study (OCT in a hyperextended magma poor rifted margin) as well as for the hydrothermal vents, a geological place where the serpentinisation is believed already to be supporting the methanotroph biosystem. It also presents the base to comprehend this methanotrophic biosystem.





The Fe component of olivine may form serpentinite as follows:



Where the enstatite (Mg- pyroxene) may form serpentinite as follows:

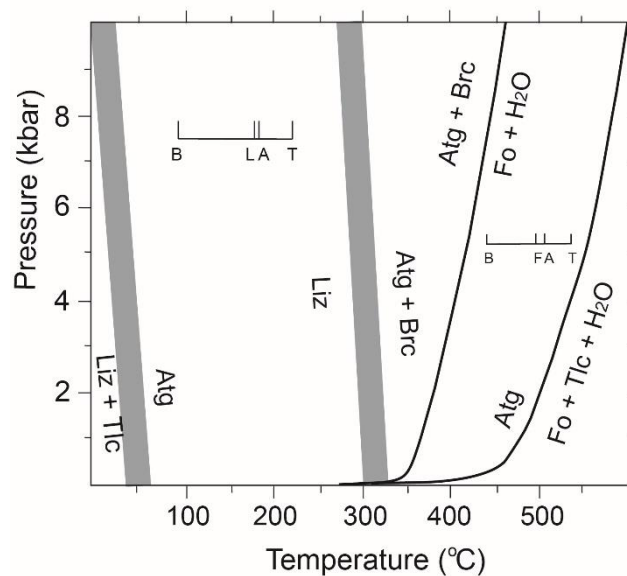
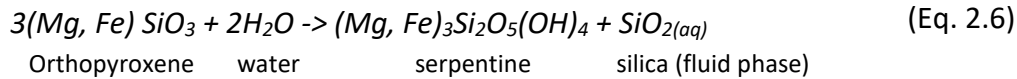
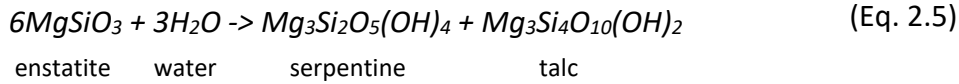


Figure 2.1 - Phase diagram describing the possible MgO–SiO<sub>2</sub>–H<sub>2</sub>O System of serpentinite by Evans et al. 2013. The grey bands represent H<sub>2</sub>O-conserved reactions. The lizardite is stable at 200 and 300 °C, antigorite grows from lizardite and chrysotile at the shown temperature.

Three main structural types of serpentinite exist - lizardite, chrysotile and antigorite, and their formation depends on the temperature and fluid (fault-controlled flow) where antigorite is the only one stable at 650 °C (O'hanley 1991; Ulmer and Trommsdorff 1995). Lizardite is the most common occurring serpentine mineral, being stable at low temperature and is favoured by low rock to fluid ratio, low permeability and porosity as physical condition (Fig. 2.1) (Evans 2004; Roehrig et al. 2015). Chrysotile is the metastable phase with asbestos-form habits; it is favoured by

low fluid to rock ratio supersaturation and abundant porosity it has three polytypes and is the least abundant serpentine mineral (Wicks and O'Hanley 1988; Roehrig et al. 2015). Chrysotile occurs in tectonically active environments, typically in veins, cracks and voids created after initial hydration and is formed from lizardite rather than olivine (O'hanley 1991; Roehrig et al. 2015). Antigorite is the high temperature phase serpentine (~ 650 °C ) and occurs at high-grade metamorphic phase when the serpentinite is recrystallized (Fig. 2.1) (Roehrig et al. 2015). Low-temperature serpentinisation occurs a long way from the ocean ridge where cold seawater circulates through fractures heated by the cooling of the mantle and the exothermic serpentinisation reactions (Agrinier and Cannat 1997; Kelley et al. 2001; Früh-Green et al. 2003; Allen and Seyfried Jr 2004; Alt et al. 2007; Schwarzenbach 2011; Schwarzenbach et al. 2012).

Several experiments have shown that serpentinisation occurs at 200 °C to 400 -450 °C depending on the pressure (McCollom and Bach 2009; Marcaillou et al. 2011) and parameters like - temperature, water-rock ratio and the nature of the fluid (e.g. salinity) (Marcaillou et al. 2011; Evans et al. 2013; Lamadrid et al. 2017). The water-rock ratio influences the alteration the mineralogy and fluid composition and is dependent on the temperature (McCollom and Bach 2009). The proportion of element incorporation Si, Mg, Fe into different minerals and its dissolved concentration also depend on temperature (McCollom and Bach 2009). The rate of serpentinisation, olivine hydration, decrease as salinity increase and fluid activity decreases (Lamadrid et al. 2017)

### **2.1.2. Where? Serpentinite location**

Serpentinisation occurs in dry gas seeps, mud volcanoes (e.g. Mariana), along strike-slip faults, but mainly in the ocean seafloor - ocean ridges, OCT, subduction zone and the OCT parts of a magma poor rifted margin (Fig. 2.2, 2.3) (Boillot et al. 1989; Beslier et al. 1990; Whitmarsh et al. 2001b; Kahl et al. 2015).

At ocean ridges, serpentinisation occurs till 3-4 km depth in the footwall of the offset normal faults during extensional spreading and near axial valleys (Fig. 2.2) (Cannat et

al. 2010; Reston and Manatschal 2011). New detachment faults are initiated inward the old individual inactive detachment faults which became inactive after few to tens of kilometres of displacements due to higher bending stress caused by footwall unroofing (Lavie et al. 1999; Cannat et al. 2010). Serpentinisation could be observed on the both ridge flanks of the fault due to flip polarity of the axial detachment as is observed in axial discontinuities with very small offset (<20 km), MAR 15°N and SWIR 61-69°E (Cannat et al. 2010). However, at given time and location the serpentinisation happens only on one ridge because the mantle exhumation occurs by asymmetric detachment faulting (Cannat et al. 2010). The mantle exhumation in ocean floor is said to be about 14660 km of the present -day ridge system with 11.4 mm/yr average exhumation rate, which made the serpentinisation widespread (Cannat et al. 2010).

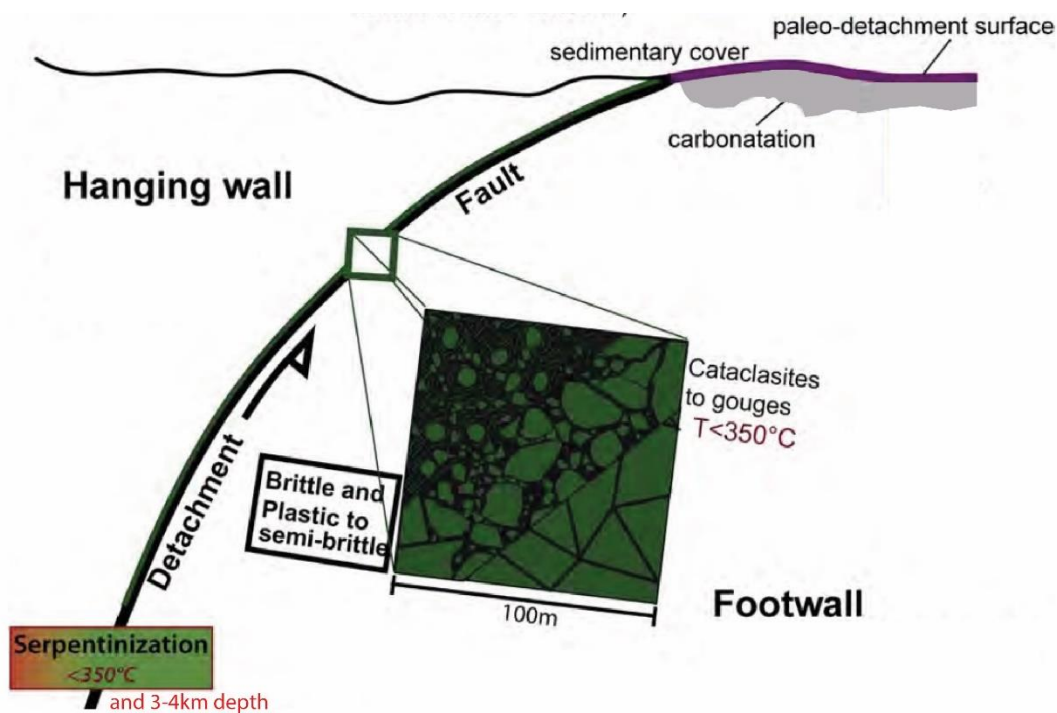


Figure 2.2. Conceptual sketch indicating the serpentinisation and carbonation into the footwall of the axial (asymmetric exhumational) normal fault modified from Picazo et al., 2013. The serpentinisation is observed no more than 3-4 km below the seafloor and along the footwall (Cannat et al. 2010). The most deformed rocks are the serpentinite gouges and cataclasites along the fault. Carbonation occurs after serpentinisation within 20 m of the paleo-seafloor (Picazo et al., 2013).

By volume percentage most of the serpentinite at the seafloor is produced during high temperature ( $<600^\circ\text{C}$ , 82.3-99.2% at a rate of  $0.47\text{-}0.77\text{ k m}^3\text{y}^{-1}$ ) along shear

zones with detachment faults , low- temperature (<200 °C, 0.8-16.7%) by cooling lithosphere and exothermic serpentinite reaction and mid temperature (350-400 °C) in hydrothermal vents (Alt et al. 2012). At slow-spreading ridges e.g. Atlantic ocean, serpentinitisation is estimated to be around 0.18 km<sup>3</sup>/year (Cannat et al. 2010).

The serpentinitisation occurs also at subduction zones near the base of the mantle wedge (Fig. 2.3) (Evans et al. 2013). Evidence of low and anisotropic seismic velocities suggest this emplacement of serpentinite having for origin the fluids from the subducted dehydrated slab and shallow mantle rocks range of 300 – 500 °C (Hirth and Guillot 2013).

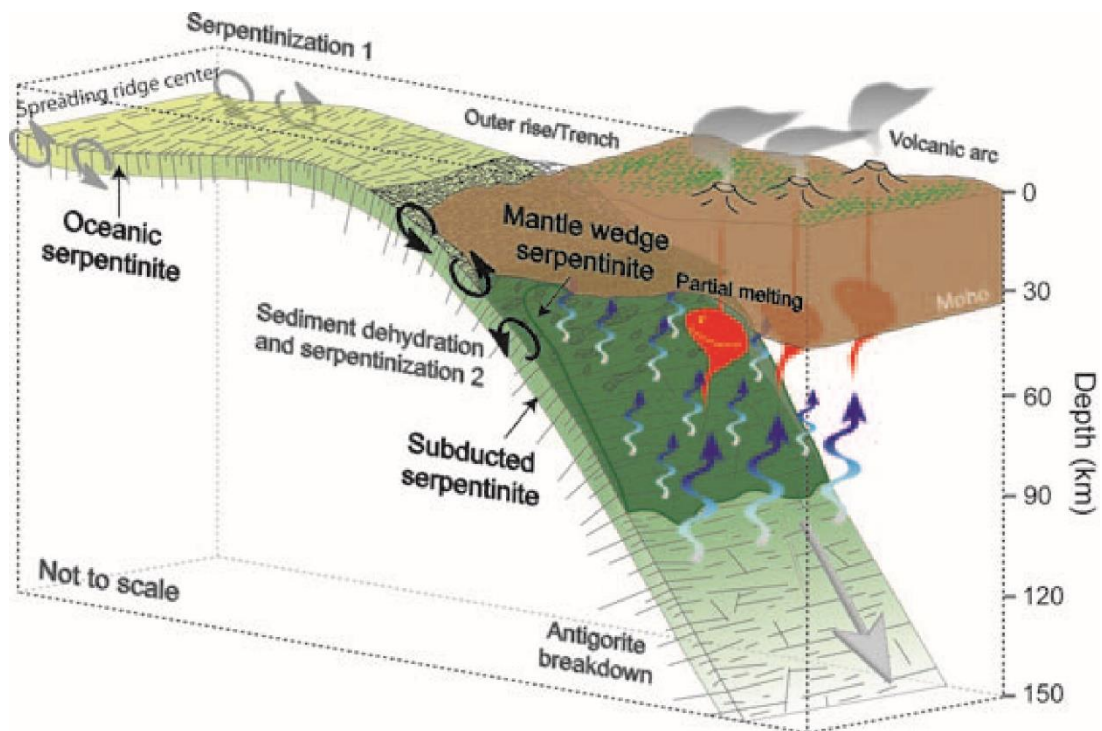


Figure 2.3 Figure from Guillot and Hattori 2003 showing serpentinitisation at ocean ridges and subduction zones with their fluid and mobile-elements transfer.

### 2.1.3. Serpentinisation and transfer of elements

Serpentinisation is an important process for the recycling of elements in the lithosphere by fluid-mobile element transmission (Vils et al. 2008; Deschamps et al. 2012; Evans et al. 2013). It is important sink for water and trace elements as carbon, sulphur, chlorine, arsenic, boron, uranium (e.g. In MARK area (MAR 23°N) - B (up to 136 ppm) and U( up to 7 ppm)), calcium, nitrogen and traces of acetate, molybdenum

and tungsten and increases solutions in  $\text{Ca}^{2+}$  and  $\text{OH}^-$  (Bonatti et al. 1984; Alt and Shanks 1998; Alt and Shanks 2003; Bach et al. 2004; Fruh-Green et al. 2004; Scambelluri et al. 2004; Barnes and Sharp 2006; Boschi et al. 2006; Paulick et al. 2006; Alt et al. 2007; Boschi et al. 2008; Delacour et al. 2008a; Delacour et al. 2008b; Delacour et al. 2008d; Vils et al. 2008; Deschamps et al. 2010; Lang et al. 2010; Harrison and Rajakaruna 2011; Kendrick et al. 2011; Schwarzenbach 2011; Vils et al. 2011; Schwarzenbach et al. 2012; Alt et al. 2013; Evans et al. 2013; Halama et al. 2014).

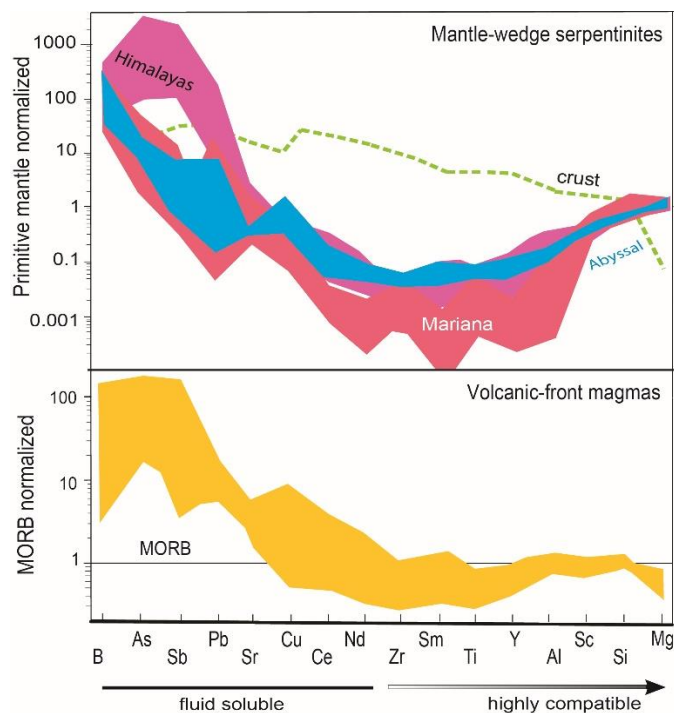


Figure 2.4 Figure from Evans et al. 2013 comparing the fluid-mobile elements of mantle-wedge serpentinite with those from volcanic-front magmas suggesting a genetic relationship between them.

Carbon in the serpentinite is originating from organic carbon and seawater derived carbonate (Alt et al. 2013). Sulphur is from the sulphate from seawater and oxidation of sulphide mineral due to the extensive circulation of seawater (Alt et al. 2013). Boron and uranium are also present in high concentration as sulphate (Evans et al. 2013). It has been estimated that serpentinisation in mid-ocean ridges is a sink for  $0.35\text{-}0.64 \times 10^{11}$  mol.C.y<sup>-1</sup> of carbon and  $0.13\text{-}1.46 \times 10^{11}$  mol.S.y<sup>-1</sup> of sulphur (Alt et al. 2013).

Serpentinisation of peridotite will incorporate soluble elements dissolved in the water and thus consumed during hydration (Fig. 2.4) (Evans et al. 2013). That enrichment of incompatible elements in the fluids occurs in a system with low fluid to rock ratio in the ocean ridges. The serpentinite transported this fluids to the subduction zone where the serpentine of the mantle wedge would have low concentration of these immobile, incompatible elements (Fig. 2.4) (Hattori and Guillot 2007; Evans et al. 2013).

The serpentinisation in the subduction zone is important for the global chemical cycle (Alt and Shanks 2006; Deschamps et al. 2013) and has implications for the occurrence of earthquakes (Moore et al. 1996), carbon dioxide sequestration (Power et al. 2013), plate boundary deformation (Hirth and Guillot 2013) and in the formation of arc volcanism (Guillot and Hattori 2013).

#### **2.1.4. Serpentinisation and Hydrogen (H<sub>2</sub>)**

Large amounts of hydrogen are produced during serpentinisation in the deep ocean (Charlou et al. 2002). Its production in the ridge axes having been estimated to be between 0.33 to  $4.1 \times 10^7$  mol  $y^{-1}$  km<sup>-1</sup> (Cannat et al. 2010), on the basis that serpentinisation produces around 15mmol kg<sup>-1</sup> of H<sub>2</sub> in the hydrothermal fluids (Russell et al. 2010). The only reaction which produces H<sub>2</sub> in the serpentinisation process is the oxidation of Fe<sup>2+</sup> from olivine to Fe<sup>3+</sup> in magnetite (Eq. 2.1 - 2.6). The production of hydrogen depends on the temperature of serpentinisation; for instance, lab experimental thermodynamic data show that very low amounts of hydrogen are produced below 250 °C with maximum production at 350 °C of H<sub>2</sub> ( $2.6 \times 10^{-3}$  mols after 190 alteration days; at 300 °C 1kg lherzolite produces 0.1 mole of H<sub>2</sub>) (Marcaillou et al. 2011; Marcaillou 2012). All the experimental data to produce H<sub>2</sub>, during the process of serpentinisation, are done at one constant pressure value – 35 MPa for maximum production of H<sub>2</sub> between 200-315 °C for that of McCollom and Bach 2008 and 300bar for those of Marcaillou et al. 2011.

Hydrogen gas can also form by a high temperature reaction between water and pulverized rock through tectonic stressed (degassing) (Giardini et al. 1976; Sugisaki et al. 1983), or by H<sub>2</sub>O radiolysis (Onstott et al. 2006).

Hydrogen is a very important source of energy to the carbon cycle, as it will interact with CO<sub>2</sub> at high temperature and pressure via the Fisher-Tropsch (FT) or Sabatier type reaction and to form abiotic methane CH<sub>4</sub> (eq. 2.6, (Bradley and Summons 2010)). The serpentinisation relationship with the abiotic methane and later the methane uses of methanotrophs that are the central for this research and will be discussed in more detail later in this chapter and in the backgrounds of chapter 3 to 5.

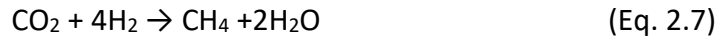
The FT reaction could be catalysed by iron, chromium, iron-nickel alloys and cobalt below 200 °C and ruthenium for temperature below 100 °C for land-based serpentinisation (Horita 1999; Etiope and Ionescu 2014).

#### **2.1.5. Importance of serpentinisation in the generation of abiotic gases**

*"The capital fact to note is that petroleum was born in the depths of the earth, and it is only there that we must seek its origin."*

*--Dmitri Ivanovitch Mendeléeiev, 1877*

Serpentinisation generates hydrogen, methane, minor amounts of formate, ammonia, calcium and traces of acetate (Lang et al. 2010). Furthermore, it leads to the abiotic reduction of CO<sub>2</sub> by creating H<sub>2</sub>. These two molecules react at high temperature and pressure via the Fisher-Tropsch or Sabatier type exothermic reaction to form methane (eq.2.7, (Bradley and Summons 2010)). This interaction could also lead to other hydrocarbons such as ethane and propane, as well as amorphous carbonaceous phases. Carbon dioxide CO<sub>2</sub> derives from the mantle itself or its reaction with downward flow of ocean water (Seewald et al. 2006; Etiope and Ionescu 2014). Methanogens could also produce CH<sub>4</sub> from CO<sub>2</sub> competing with the abiotic FT reaction (Zehnder and Brock 1979; Hoehler et al. 1994; Harder 1997; Larson et al. 2015).



This reduction of CO<sub>2</sub> could be sustained by serpentinisation produced hydrogen for more than 100 000 years in hydrothermal vent environments (Russell et al. 2010).

Methane can have a biogenic, thermogenic or bacterial source depending on temperature (Table 2.1). At low temperature (<80 °C) bacterial degradation of organic matter produces methane in anoxic, shallow water environments (Rice and Claypool, 1981).

Table 2.1 Table showing the different types of methane – abiogenic and biogenic from Etiope et Sherwood 2013.

CH <sub>4</sub> type	origin	conditions	δ <sup>13</sup> C <sub>CH<sub>4</sub></sub> (‰)
biogenic	bacterial decomposition (e.g. methanogens)	organic rich sediments	-55 to -110
	thermal decomposition	<100°C	-25 to -55
abiogenic	inorganic synthesis (FT reaction)		-30 to -24
	mantle outgassing	>700	-15 to -20

Methane is an important greenhouse gas and as a source of geothermal reservoirs (Etiope and Klusman 2002). Geological methane emissions are estimated to be between 30-70 Mty<sup>-1</sup> compared to the total methane emission of 559 (540-568 Tg y<sup>-1</sup> for 2003-2012 period and the methanotrophic consumption (aerobic) in soils (15-45 Mty<sup>-1</sup>) (Etiope and Klusman 2002; Saunio et al. 2016). Methane anomalies are observed in the water column above the serpentinised peridotite (Charlou and Donval 1993; Charlou et al. 1998; Charlou et al. 2002), however abiogenic CH<sub>4</sub> is not thought to be an important carbon source (Birgel et al. 2006).

The first direct evidence by hydrothermal exhalations of abiotic methane production comes from the Lost city hydrothermal system (Proskurowski et al. 2006; Konn et al. 2009; Lang et al. 2010). Methods to differentiate the different kind of methane involve molecular composition of associated gases, noble gas isotopes (He, Ne, Ar, Kr, Xe (Etiope and Sherwood Lollar 2013), δ<sup>13</sup>C and δD signal (Whiticar et al., 1986).

### **2.1.6. Microbial life and relation with the serpentinisation**

Serpentinisation is seen as a primary process for the emergence of life in the early Earth (Russell et al. 1989; Russell et al. 1994; Fruh-Green et al. 2004; Holm et al. 2006; Schulte et al. 2006; Russell et al. 2010). In the primitive metal-rich carbonic Hadean ocean (4.4 Ga, pH 5.1 to 6), high temperature hydrothermal springs (ca. 400 °C) with locally lower pH were favourable for the emergence of life (Russell et al. 2010).

The environment of the early Earth was different to today, having an atmosphere with elevated CO<sub>2</sub> between 0.03 and 5 bar (Owen et al. 1979; Grotzinger and Knoll 1999) and a seawater with higher amounts of dissolved inorganic carbon (DIC) (Bristow and Grotzinger 2013). The pH of the Archean ocean would have been lower than today, around 6.9 (Grotzinger and Kasting 1993; Halevy et al. 2010). Serpentinisation would have occurred in the oceanic crust by fracture convection of komatiitic flows (basalt with a chemistry of peridotite) (Russell et al. 2010). This lithology was typical of the Archean and would have been rich in magnesium and poor in silica.

The hydrothermal system provides a stable closed biological system, being active for 100 ky or more dependent on thermal output, where organic molecules could have been synthesised and developed from the mantle serpentinisation (Baaske et al. 2007; Budin et al. 2009; Russell et al. 2010) and likely occurred 4 billion years ago (Holm and Andersson 1998). Serpentinisation provides ions which are used as a primary source of energy for microbial organisms (Wolin 1982; Morita 1999; Shock et al. 2002; Takai et al. 2004; Spear et al. 2005; Amend and McCollom 2009). Mud volcanoes have been suggested to be better environments for the early life than hydrothermal vents, since they form a source of phosphorus and were likely more abundant during Hadean times than serpentinisation in the ridge zone (Pons 2011; Pons et al. 2011). More recently a hypothesis for the synthesis of the first nucleotides and polymerization into RNA emerge in one to few wet-dry cycles in a warm little ponds bombarded by meteorites (Pearce et al. 2017).

Serpentinisation is suggested to sustain life on other planets (e.g. Mars) where life in relation to the process will be easier to detect because of the “limited recent aqueous activity” (Greenberger et al. 2015).

Even if serpentinisation was the central process involved in the emergence of life from abiotic source, the convincing evidence found in is the alkaline hydrothermal vents (Russell et al. 2010). It is assumed that serpentinisation is the mechanism fuelling to the FTT reaction to reduce CO<sub>2</sub> by producing H<sub>2</sub>.

#### **2.1.7. Why study the serpentinisation**

Serpentinisation is so important that it may have been the first stable layer floating in the Hadean magmatic ocean thus being the first lithospheric layer due to a high Sm/Nd reservoir and the source of the processes of plate tectonics (Boyet et al. 2003; Swan et al. 2010). It could possibly be important for other silicate planets like Mars and Europa (Ehlmann et al. 2010; Webster et al. 2011; Greenberger et al. 2015). The main reason to be interested in the serpentinisation is its relationship with the biosystems. Serpentinisation provides a sustainable source of metabolic energy (electrons) necessary for the microorganisms and synthesized organic molecules in the prolific environments such as the hydrothermal vents (e.g. (Russell et al. 2010). It is used to understand the early chemical evolution of the Earth’s crust and the possible life on silicate aqueous planets. Serpentinisation at moderate temperature with alkaline pH on off-ridge could favour other molecules necessary for life (amines, thiolates and phosphate) which could react with the Hadean ocean water (CO<sub>2</sub>-rich, mildly acidic) and be the source of the origin of life (Russell et al. 2010).

#### **2.1.8. Importance of serpentinisation in geology**

Serpentinisation transforms mantle peridotite and changes its physical properties such as volume, rheology, density, seismic properties, electrical conductivity, magnetic properties and porosity (Fig. 2.5) e.g. (Hirth and Guillot 2013). Serpentinisation is associated with a net total volume and solid volume increase of nearly 50% according to lab experiments (Bogolepov 1970; Coleman and Keith 1971; Evans 2004). The calcium is the most mobilize of the major elements during

serpentinisation which could lead to this volume increase by vein formation accommodated by tectonic activity in the extensional environment (Coleman and Keith 1971; Mével 2003). This volume increase is often related to increase in surface elevation and erosion (Kelemen and Hirth 2012).

Serpentinisation is a long process that decrease gradually the porosity by volumetric expansion from the olivine serpentinisation filling the microcrack pore space or by a latent volumetric expansion (Miller and Christensen 1997). The porosity lower also into the serpentinised peridotite samples due to swelling of the serpentine veins filling the microcrack pore space (Miller and Christensen 1997). The serpentinisation decreases also the permeability by blocking flow paths and obstruct fluid circulation by mineral precipitation in the oceanic crust in a short time, meaning that the ultramafic-hosted hydrothermal vents need a regular initiation of permeable pathways using tectonic activity and crystallisation pressure (Farough et al. 2016). Where the permeability is continuous for a longer period is likely to produce 100% serpentinisation or carbonation depending on the temperature 260 and 180 °C, respectively (Kelemen and Hirth 2012).

The density of the peridotite~ 3.3 g/cm<sup>3</sup> decreases to~ 2.5 g/cm<sup>3</sup> for serpentinite (Fig. 2.5) (Miller and Christensen 1997). With increasing degree of serpentinisation, seismic velocity decreases, being related also to density (Fig. 2.5) (Christensen 1972; Miller and Christensen 1997). Seismic velocity also depends of other parameters such as mineralogy, porosity, preferred mineral orientation, degree of alteration and chemical composition. The antigorite has the highest velocity from the three serpentine types, depending of the orientation of the grain 8.4 km/s and 6.6 km/s for parallel and perpendicular to the b-axis of the grain respectively, but is the rarest in the oceanic floor (Phillips et al. 1969; Miller and Christensen 1997; Watanabe et al. 2007). It is difficult to differentiate the physical properties between partially serpentinized peridotite and lower crustal gabbro based only on remote seismic data. However of serpentinised peridotite with 30 -35% serpentinisation, the Vp and Vs – seismic velocity as well as density are easily distinguish from crustal gabbro (Miller and Christensen 1997). There is a strong negative correlation between seismic

velocity ( $V_p$  and  $V_s$ ) and the degree of serpentinisation but restricted to the resolution of remote geophysical velocity data (Miller and Christensen 1997). This seismic velocity front could be indication of the hydration of the peridotite from the fresh peridotite, a thermal boundary of around 500 °C rather than gabbro serpentinite limit (Mével 2003).

Magnetic susceptibility increases in relation to the amount of magnetite formed during the serpentinisation (Coleman 1971; Dunlop and Prévot 1982; Toft et al. 1990; Oufi et al. 2002). However, magnetite production does not increase linearly with the percentage of serpentinisation, since  $Fe^{3+}$  is not entirely incorporate into magnetite (Marcaillou et al. 2011). Positive magnetic anomalies observed along fracture zones and ocean ridges are attributed to serpentinite (Raleigh and Paterson 1965; Dymant and Arkani-Hamed 1995; Dymant et al. 1997; Russell and Whitmarsh 2003). The magnetite in the serpentinite is in his highest when the peridotite are serpentinised of more than 60-70% (Bach et al. 2006). In seismic section, the bright mantle reflectivity is interpreted on being due to serpentinisation (Ranero et al. 2003).

The thermal conductivity of the serpentinisation is  $2.84 \text{ Wm}^{-1}\text{K}^{-1}$  (Diment 1964) and could provide an explanation for heat flow anomalies observed in oceanic basins.

Serpentinisation also changes rheology by hydrating mantle peridotite (Raleigh and Paterson 1965; Reinen et al. 1991; Ulmer and Trommsdorff 1995; Hirth and Guillot 2013); the serpentinite rock is weaker and is deformed during brittle/frictional deformation (Escartin et al. 1997b,a,2001; Hilairet and Reynard 2009). Serpentinite has a low internal friction coefficient ( $\mu_i = -0.3$ ) which would decrease the optimal fault angle of large-displacements faults and increase the displacement along low detachment faults and strain localization (Escartin et al. 1997b,2001). It was believed that is the serpentinisation that promote the formation of the fault structures and theirs strain localisation. However serpentinisation is the consequence rather than the cause of the extensional environment (Manatschal et al. 2006) but contributes to these forces by increasing the percentage of hydrothermal minerals (Ranero et al. 2003; Skelton et al. 2005).

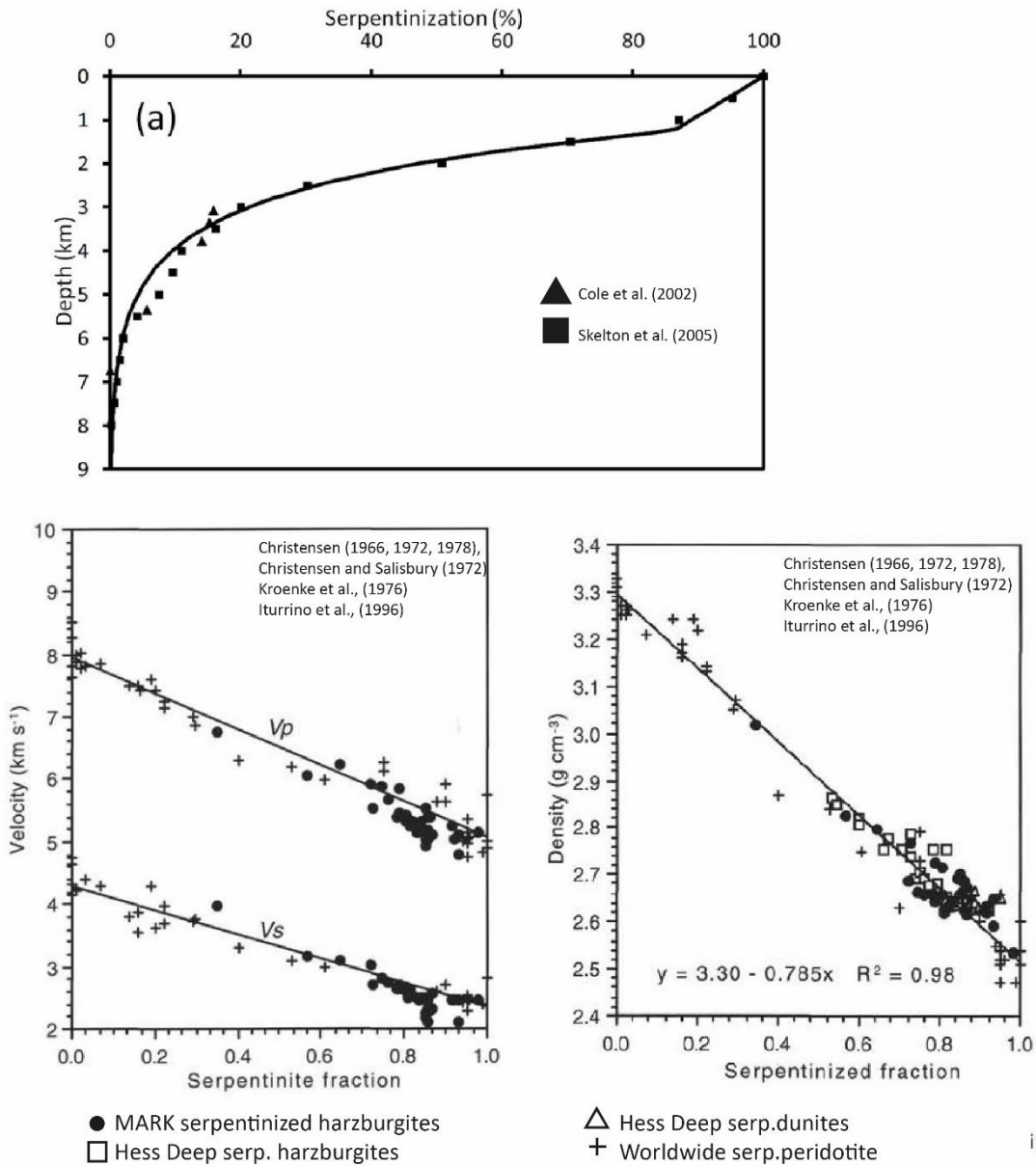


Figure 2.5. Serpentinisation relation with physical properties: Serpentinisation is a process related to the distance from the water contact (Cole et al. 2000, Skelton et al. 2005); Serpentinisation changes the density (Miller and Christensen 1997); Serpentinisation changes the velocity (Miller and Christensen 1997).

## **2.2. Geological context**

### **2.2.1. Hyperextended rifted margins and Ocean continental transition (OCT)**

Ocean-continent transitions of rifted magma-poor margins are characterized by thinned, hyper-extended and locally also exhumed continental crust and mantle with variable amounts of magmatic additions (Fig. 2.6) (Pérez-Gussinyé and Reston 2001; Mohn et al. 2012; Masini et al. 2013; Peron-Pinvidic et al. 2013). It is now well understood that some rifted margins are magma poor or even magma starved. Magma starved rifted margins show a zone of exhumed mantle separating hyper-extended continental crust from oceanic crust.

Hyper-extension is observed in today's rifted margins (i.e. western Iberia-Newfoundland margin (Péron-Pinvidic and Manatschal 2008); Angolan (Unternehr et al. 2010); mid-Norwegian (Osmundsen and Ebbing 2008)) and in fossilised margins exposed in collisional orogens (i.e. Alps (Manatschal 2004); Western Pyrenees (Masini et al. 2014)). One of the most studied margins in the world is the Iberia-Newfoundland hyper-extended magma starved rifted margin (Manatschal et al. 2009; Sutra et al. 2013).

At magma starved margin the transition from continental to oceanic crust occurs where serpentinitised mantle can be observed on the seafloor surface (Fig. 2.6). The Iberian margin was the first where the occurrence of serpentinitised mantle in the OCT domain has been confirmed by drilling and corroborated by geophysical data (Boillot et al. 1980; Boillot 1986). The mantle is exhumed by extensional detachment faults on the ocean floor; these faults are the result of the localization of deformation during rifting (Manatschal et al. 2006).

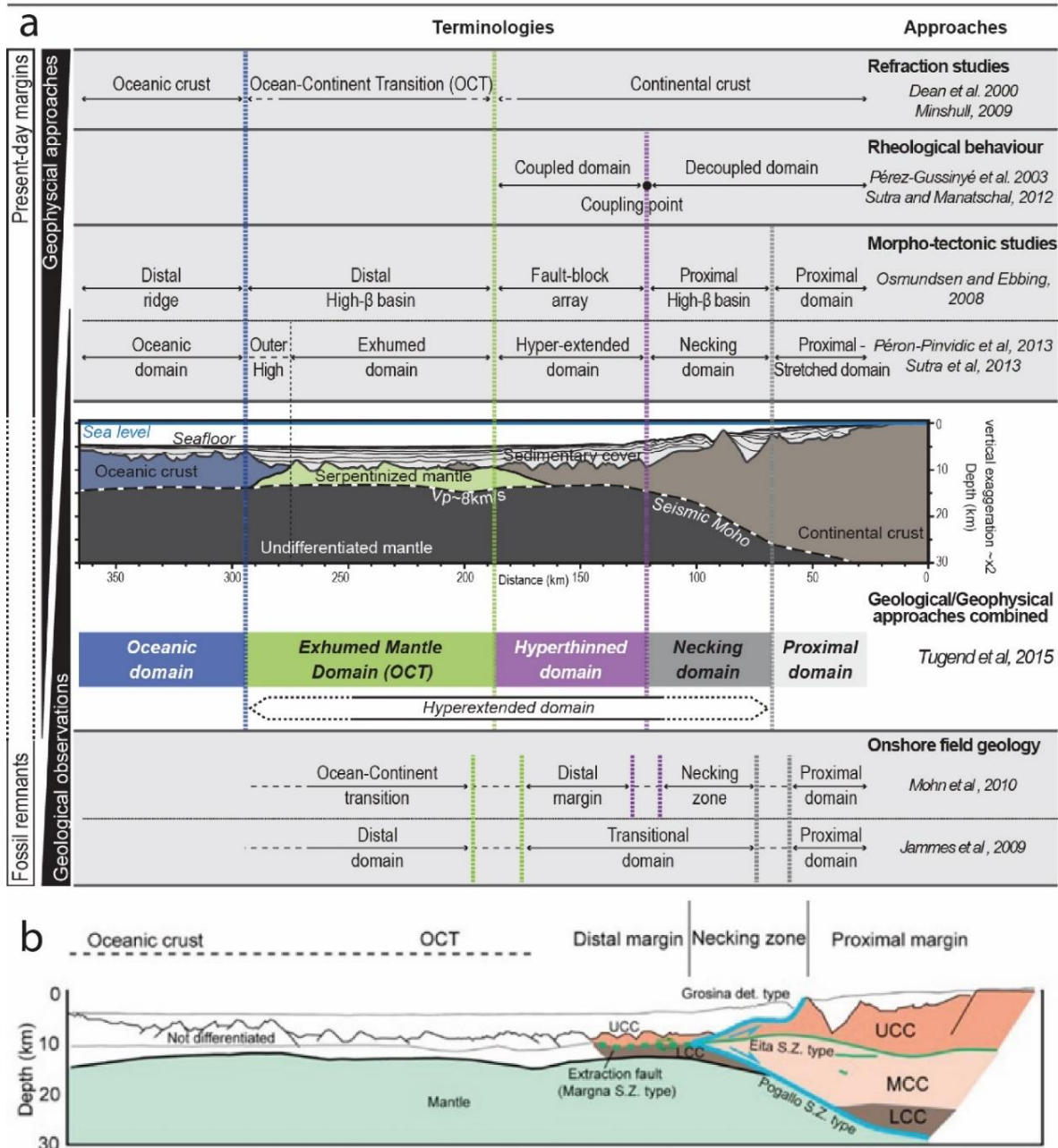


Figure 2.6. a. Figure from Tugend et al. 2015 naming different parts of a magma-poor/starved margin depending of the type of study. B. Simplified figure of the hyper-extended magma starved margin by Mohn et al. 2012 with the different part as follows: from right to left proximal margin formed by thinned crustal domain about 30 km; necking zone (Mohn et al. 2012); distal margin less than 10km (Peron-Pinvidic, Manatschal, and Osmundsen 2013, Mohn et al. 2012) and ocean-continent transition (OCT) with exhumed mantle.

## 2.2.2. Slow-spreading ridges

An ocean spreading ridge is a fracture zone along the ocean seafloor where new crust is being created through igneous activity. The rate of divergence of a ridge defines the type, either as an ultra-slow with rate less than  $20 \text{ mm y}^{-1}$ , slow from  $20 \text{ mm y}^{-1}$  to  $50 \text{ mm y}^{-1}$ , intermediate ( $50 \text{ mm y}^{-1}$  to  $90 \text{ mm y}^{-1}$ ) or rapid ( $> 90 \text{ mm y}^{-1}$ ) (Fig. 2.6).

The main physical characteristics of slow spreading ridges are usually narrower lateral extension, deep rift valley, often rougher transversal profiles and smaller amounts of magma than fast spreading ridges and average spreading rates of less than 40 mm y<sup>-1</sup> (22 mm/y) (Fig. 2.7) (Cannat et al. 2010).

50% of mid-ocean ridges are slow-spreading ridges and ultraslow spreading ridges represent more than 35% of all ridges (Dick et al. 2003). Considering that 20–25% of the ocean floor is occupied by mantle-derived ultramafic rocks (Cannat et al. 2010), the proximity of peridotite and seawater means that the serpentinisation process is likely to be pervasive. Slow spreading ridges create “incomplete ophiolite” sequences as is the case in the Alps (e.g. Platta) (Bernoulli 2001).

Rapid spreading ocean ridges (Southeast Indian ridge, Central Indian ridge, Pacific-Atlantic ridge, Juan de Fuca, Gorda, Gal ridge) are not considered here as they have shown no evidence of serpentinisation. Slow-spreading ridges (e.g. slow: mid-Atlantic ridge MAR, ultraslow: Southwest Indian ridge, Gakkel ridge, Cayman ridge, Mohn ridge) on the other hand are where serpentinisation is most likely to occur. Lizardite is the main product of serpentinisation in slow-spreading mid-ocean ridges (Wicks and Whittaker 1977; Caruso and Chernosky 1979).

### **2.2.3. Hydrothermal system**

*“ geochemical template upon which biological chemiosmotic harnessing evolved “*

*(Russell et al. 2010)*

*“the chain of life is ... a continuous one, from the mineral at one end to the most complicated organism at the other”. Leduc (1911, p.XV)*

A general definition of a hydrothermal system is one where fluid supply (e.g. water) changes the thermal gradient of a system (Fig. 2.8). There are several types of

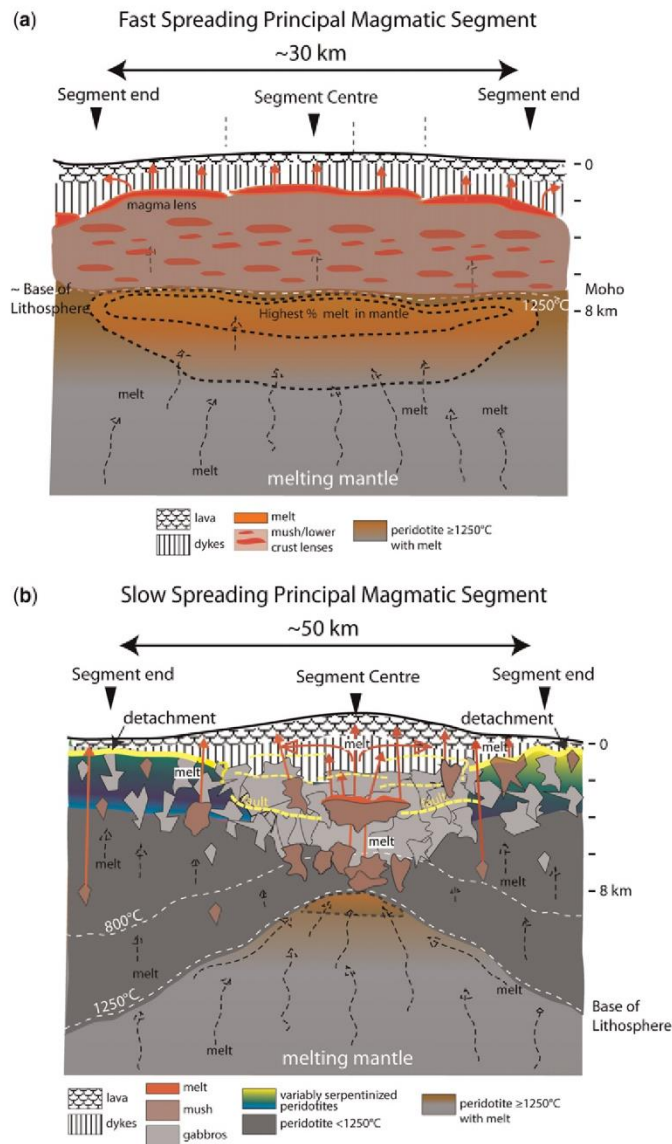


Figure 2.7. A geological model of slow and fast spreading ridge showing the tectonic spreading and melt circulation from Carbotte et al. 2016.

geological hydrothermal processes, but the most important involve the upper part of the mantle or the top of the oceanic crust as in the case during subduction. Hydrothermal processes are divided in two main types "sediments free on axis systems on plate tectonic spreading centres and off axis systems on the flanks of the spreading centres"(Holm and Andersson 1998). According to Holm and Andersson (1998) the on-axis systems is due to the steep temperature gradients and is driven by the magma chamber (600-1300 °C) underneath the axis called a forced convection, instead of free convection used in the off-axis systems due to oceanic crust cooling with average temperature 150 °C. An on-axis system could be hydrothermal vent

heated from magma or magma intrusion, whereas the off-axis could be during serpentinisation process.

In the hydrothermal vents cold seawater interacts with heat produced by lithospheric cooling, serpentinisation exothermic reaction and mainly by magmatic heat source. The hydrothermal fluids produced involved in the hydrothermal process could reach above the seawater critical point ( $T_c = 374\text{ }^\circ\text{C}$ ,  $P_c = 22.1\text{ MPa}$ ) (Deguchi and Tsujii 2007), thus becoming a supercritical water (SCRIW). SCRIW, due to its high pressure does not evaporate, has a higher degree of alteration and dissolves and decompose various organic matter. Hydrothermal waters above this critical point with  $T = 407\text{ }^\circ\text{C}$ ,  $P_c = 29.8\text{ MPa}$  were first observed in hot black smokers (Turtle Pits and Sister Peak) near the Atlantic ridge (Koschinsky et al. 2008). Fluids penetrate the oceanic crust also far from ridges hot spots and hydrothermal systems still participating in alteration of rocks, precipitation of minerals, serpentinisation, formation of abiotic hydrocarbons and affecting the life in deep bio-systems (Fig. 2.7) e.g. (Baross and Hoffman 1985).

#### **2.2.4. Hydrothermal vents**

The first hydrothermal vent was discovered by a group of Scripps Institution of Oceanography scientists in 1977 and was a black smoker in the Galapagos Spreading Centre. This discovery led the scientific community to propose new hypothesis for the origin of life (Macdonald et al. 1980). Since then, more than 689 hydrothermal vent fields worldwide have been visually confirmed (Fig. 2.8) (Vents 07.2017). Hydrothermal chimneys vary mineralogically, chemically and texturally depending on their geographical emplacement, lithological base, and different fluid temperatures that result in the precipitation of different minerals and suspended particles in the water column (Fig. 2.8, 2.10, Table 2.2) (Haymon 1983). The differing chemistry also influence the vent fauna.

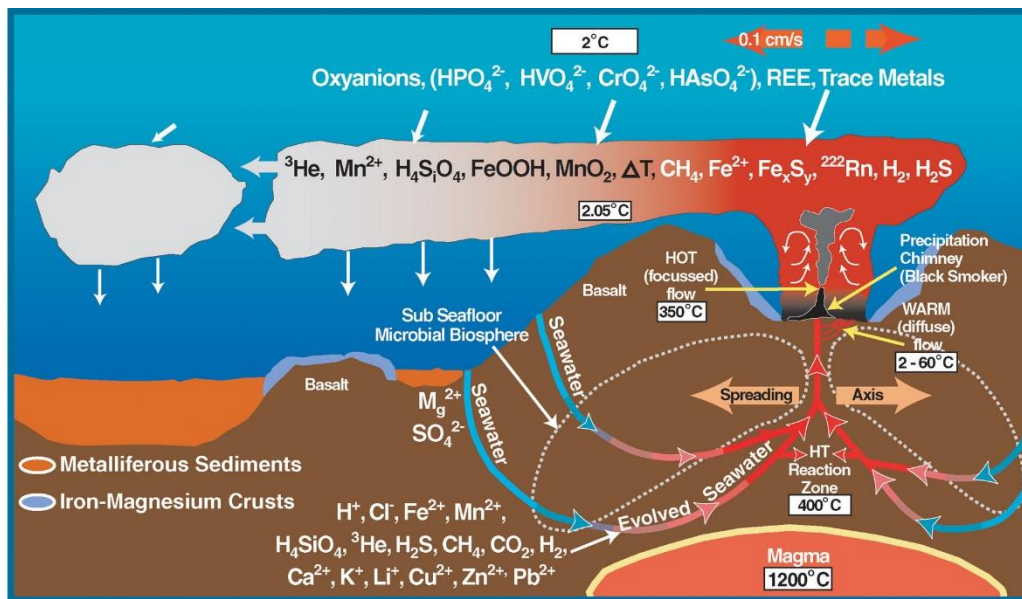


Figure 2.8. Figure showing the chemical paths in a hydrothermal vent.

Hydrothermal vents are formed by the reaction of heated oceanic water by magma, magmatic intrusion or serpentinisation with the thinned lithosphere (Fig. 2.8). They occur on the exhumed footwall of axial detachment faults near spreading ridges (fast to ultra-slow Arctic Mid-Ocean ridge (Pedersen et al. 2010), MAR, Southwest Indian ridge (German et al. 1998)), hotspots (e.g. Lucky strike) and subduction zones e.g. (de Ronde et al. 2001; Allen and Seyfried Jr 2004). To recognize a hydrothermal system a set of seismic, thermal, petrological, structural, gravitational, geochemical, electrical, acoustic and magnetic criteria are used (Rona 1978). However, the most usual way to discover hydrothermal vents is using different manned or unmanned submersibles equipped of camera (e.g. Nautile for Logatchev, Saldanha, Autosub6000 for Von Damm vent field VDVF, Alvin for Lost city, remotely operated vehicle ROV Quest for Lilliput). The vents can be visually detected by the presence of emitted material; most analyses are directly carried out at the vents e.g. (Desbruyères et al. 2001).

Table 2.2. Table generalising the difference between black and white smokers type hydrothermal vents. The data used in this table is mentioned and referenced in the chapter.

Site name	White smoker	Black smoker
host rock	ultramafic rock	magma chambers (gabbro, basalt) 1-3km below seafloor ± ultramafic rock
distance from ridge	of-axis	on ridge axis
fluid Temp (°C)	<100	<405
pH	9-11	2-3
fluid composition	rich in alkaline earth minerals	rich in dissolved transition metals
Chimney	carbonate	sulfide
H <sub>2</sub> (mM/kg)	0.5 - 14.4	0.1-16
CH <sub>4</sub> (mM)	1 to 2mmol/kg greater to classic black smoker or similar to bl.smoker with ultramafic rock	0.05-4.5
CO <sub>2</sub> (mM/kg)	0.0001 to 0.1	4 to 60

Depending on the fluid temperature, main rock source of heat (magmatic intrusion, serpentinisation) and tectonic emplacement (distance from ridge, distance from fault) different types of vents have been described in the literature, namely black and white smoker (high and low temperature, respectively) (Fig. 2.10, Table 2.2). Depending on the spreading rates, the vents can retain the heat source beneath them for a different period. At a fast spreading ridge such as in the Pacific ocean, black smokers type vents tend to cool after a year or so (Koschinsky et al. 2008), this could also be an indication of a crust becoming more "water -logged". The life of a hydrothermal system on slow to ultra-slow spreading ridges depends on the heat source and also on detachment fault and the stability of the chimney conduits (Pedersen et al. 2010). Haymon (1983) describes the evolution of a vent from a black smoker to an inactive white smoker. Initially, the temperature of the black smoker decreases, worm tubes start to appear and the fluid bearing changes from sulphide, pyrrhotite and iron-rich sphalerite to amorphous silica, barite and pyrite (Haymon 1983). The white smoker created later, was infilled with sulphide until it became inactive and reduced to rubble. Some minerals like anhydrite and caminite are completely absent in inactive vents while others will form from the low temperature alteration of the sulphide minerals (oxyhydroxides, chlorides and hydrous sulphates) (Haymon 1983). Thus physical evidence of hydrothermal vents on the surface disappears completely after a few thousand years (Haymon 1983).



Figure 2.9. Map from vents-data.interridge.org with the location of the confirmed hydrothermal vents September 2017

The hydrothermal vents provide a closed system with formed ambient pH and redox gradients and restrict the diffusion of the hydrothermal fluids (Russell et al. 2010). They are seen as environment for beginning of life from both conceptual and experimental models (Russell et al. 2010).

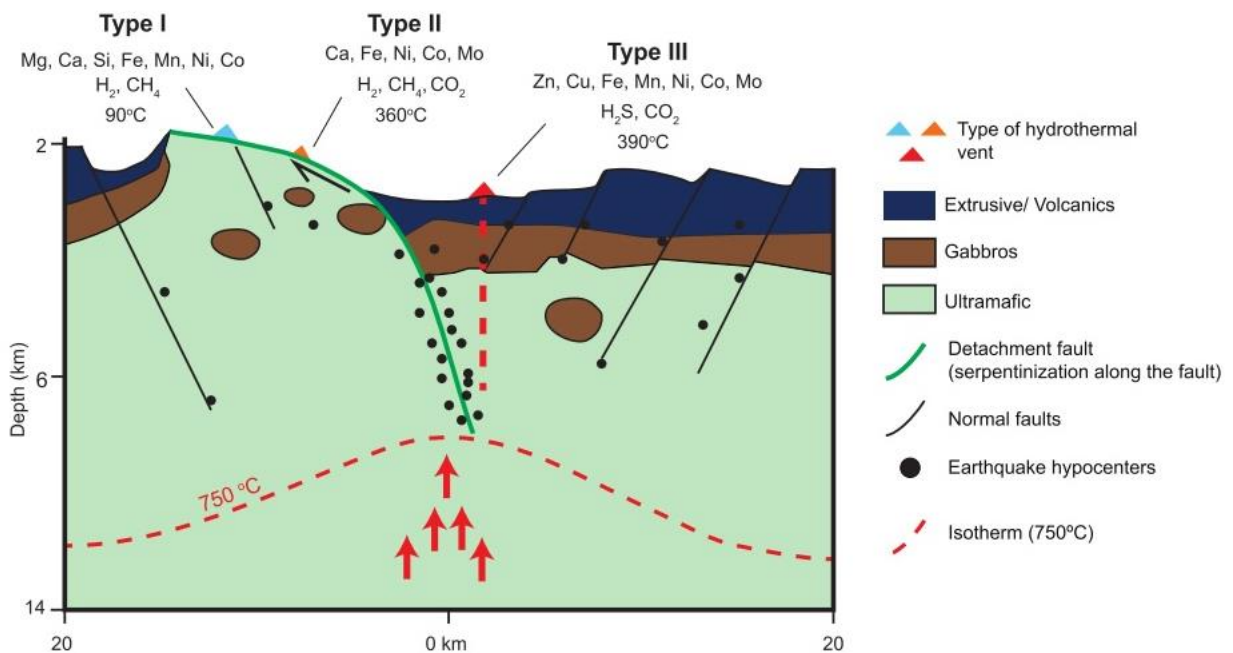


Figure 2.10. Different type of hydrothermal vents according to the mineral deposits and hydrothermal fluids depending on the distance from ridge, fault (Pinto 2014). The first line represents the mineral deposits and the second line the elements enriched in the fluids. The type 1 is a white smoker and the other two are black smokers.

Hydrothermal vents are present at all type of ridges from ultra-slow to fast spreading ridges, but they are related to serpentinisation only at the slow and ultra-slow

spreading mid-ocean ridge environments. Hydrothermal vents (e.g. Rainbow, Logatchev) related to serpentinisation, and magmatic rocks are also situated into the exhumed footwall of axial detachment faults (Cannat et al. 2009).

Of the worldwide studied hydrothermal vents, few are hosted by serpentinite; only Mount Saldanha on MAR (mid-Atlantic ridge) was believed to be entirely driven by the heat produced from serpentinisation due to its low fluid temperature (Table 2.3) (Dias and Barriga 2006). The hydrothermal vents supported by serpentinisation are found in the mid-ocean settings, mainly along the MAR (Fig. 2.11). However, this could be explained by the focus of scientific research on the Atlantic Ocean, and that the majority of the visually confirmed hydrothermal vents have not been studied in detail. The only exception is the VDVF system, which is found at another slow spreading ridge, the mid-Cayman spreading centre in the Caribbean sea (Connelly et al. 2012).

These vents are partially on serpentinisation produced energy and heat source, as well as lithospheric cooling, but mainly is the mafic rock (crystallized magmatic bodies, magma chamber), which produce the heat necessary for the hydrothermal vents (Bach and Früh-Green 2010). Hydrothermal vents with lower fluid temperature (e.g. white smoker types) and Ni and Co enrichment in the mineral deposit are described as resulting from energy from ultramafic rock aka serpentinisation reaction (Fouquet et al. 2010).

The hydrothermal vents hosted by serpentinite on the MAR with low temperature are Lost city, Mount Saldanha and with high temperature - Aschandze, Drachenschlund (Nibelungen), Lilliput, Logatchev and Rainbow (Fig. 2.11, Table 2.3). Only the Von Damm field is situated on the ultra-slow ridge in the mid-Cayman rise (Table 2.3).

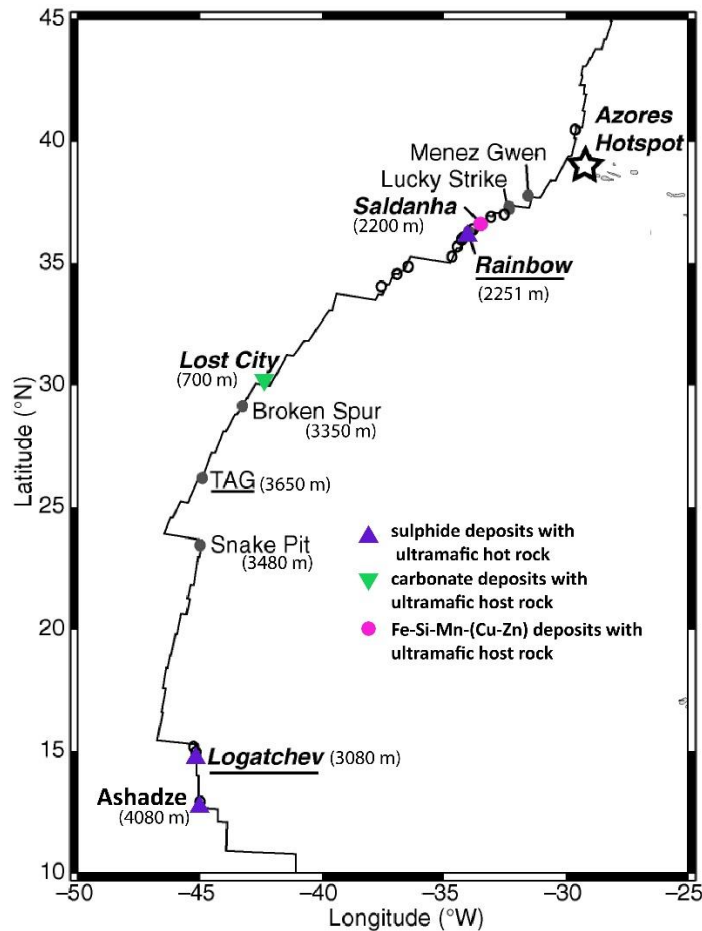


Figure 2.11. Locations of the five hydrothermal vents (in bold) with serpentinisation on the northern Mid-Atlantic Ridge.

#### 2.2.4.1. Black smokers

Black smokers are characterized by high venting temperatures (<405 °C), sulphide rich fluid composition and high concentrations of H<sub>2</sub> and CH<sub>4</sub>, attributed to seawater and hydrothermal fluids interaction at depth of 2-8km within the oceanic crust close to a volcanically active place (Table 2.2) (Von Damm 1990; Kelley 2001). The sulphide chimneys have fluids rich in transition metals such as iron, manganese, hydrogen, nickel, copper and zinc (e.g. (Allen and Seyfried Jr 2003; Martin et al. 2008). Black smokers lie directly on the magmatic basement (basalt) with deposits of the minerals sphalerite, wurtzite, iron-sulphides (pyrite, marcasite, melnikovite, rare pyrrhotite) and rare copper – sulphides (chalcopyrite, cubanite, covellite, digenite), and other minor minerals such as amorphous silica, barite, talc, native sulphur, iron oxyhydroxides, jarosite, gypsum and caminite (Haymon 1983). The elements

associated with these types of deposits are zinc, iron, copper, sulphur, calcium, magnesium, silicon and barium with the trace elements arsenic, cadmium, manganese, antimony, vanadium, silver and lead (Haymon 1983).

Despite the hostile environment, with no sunlight, black smokers are also complete ecosystems fueled by chemosynthetic energy. Hydrogen and CO<sub>2</sub> using metal sulphides catalysts synthesize to an abiotic CH<sub>4</sub> and release necessary energy for life for the macro- and microorganisms. The abiogenic CH<sub>4</sub> and acetate leads to a pathway for the formation of acetyl-CoA, central for the microbial metabolism (Martin et al. 2008). Macroorganisms in these vents including arthropods (shrimps, crab), annelids (giant tube-worm) and molluscs (bivalvia) are common (e.g. (Juniper 2004)).

The first 'off-axis' black smoker with increased talc precipitation (85-90% of the volume) was found in the VDVF, N Atlantic (Table 2.3) (Connelly et al. 2012; Hodgkinson et al. 2015). It was found in 2010 from the National Oceanography Center, Southampton, using deep-sea cameras and was confirmed later in 2013 by analysis of fluids, rocks and fauna samples. It is located about 13 km from the axis of the ocean ridge, on the flanks of the Mid-Cayman spreading center and emit fluids at 215 °C, which is intermediate temperature between white and black smoker fluids (Connelly et al. 2012; Hodgkinson et al. 2015) . The VDVF field is constituted of a 3m high sulphide mound lying on 2 My old crust formed of gabbro and peridotite (Hodgkinson et al. 2015). The fluids are of intermediate pH (5.8), hot, pale in color, with gases consisting mainly of methane and hydrogen, free from metal particles and having a high concentration of chloride (667 mmol.kg<sup>-1</sup>). The hydrothermal vent chimney is 90-95% talc with a small quantity of amorphous silica, heights of 3 m and 1 m in diameter (Connelly et al. 2012).

Table 2.3. Showing the serpentinite driven hydrothermal vents (partially or not) with their characteristics. No data available or found explain the missing cells. References from Exomar(2006) and Serpentine(2007) cruise of Ifremer a- (Beltenev et al. 2005; Fouquet et al. 2008; Charlou et al. 2010). b - (Fouquet et al. 2008; Charlou et al. 2010). c- (Batuyev et al. 1994; Gebruk et al. 1997; Charlou et al. 1998; Charlou et al. 2010; Cherkashov et al. 2010). d- (Schmidt et al. 2007; Fouquet et al. 2008; Reed et al. 2009). e - (Devey et al. 2005; Koschinsky 2006; Melchert et al. 2008; Schrenk et al. 2013). f - (Charlou et al. 1998; German et al. 1998; Douville et al. 2002; Reed et al. 2009; Charlou et al. 2010). g - (German et al. 2002). h - (Kelley et al. 2001; Kelley et al. 2005; Brazelton et al. 2006; Ludwig et al. 2010). i - (Barriga et al. 1998; German et al. 1998; Dias and Barriga 2006; Dias et al. 2010; Dias et al. 2011). j - (Connelly et al. 2012; Hodgkinson et al. 2015; McDermott et al. 2015; Reveillaud et al. 2016).

Site name	Ashadze 1 <sup>a</sup>	Ashadze 2,3 <sup>b</sup>	Logatchev 2 <sup>c</sup>	Logatchev 5 <sup>d</sup>	Nibelungen <sup>e</sup>	Rainbow <sup>f</sup>	Lilliput field <sup>g</sup>	Lost City <sup>h</sup>	Mount Saldanha <sup>i</sup>	Von Damn Vent Field (VDVF) <sup>j</sup>
Latitude (DD)	12.9733	12.9917	14.7200	14.7500	-8.3000	36.23	-9.33	30.125	36.5667	18.3777
Longitude (DD)	-44.8633	-44.9067	-44.9380	-44.9700	-13.5200	-33.902	-13.5	-42.11833333	-33.4333	-81.7972
depth (m)	3300	4530	2650	2900	2915	2300	1500	700-800	2200	2372
fluid Temp (°C)	353	>296	320	353?	153 to 371	324-365	17	90-93	9	215
Active/Inactive	A	A	A	I	A	A	A	A	A	A
pH	3.1	4.1-4.2	4.2		2.9	2.8-3	6.4	12.1		5.8
H <sub>2</sub> (mM)	8, 19	26.5	11-19		11.4	12.9 -16	16mM	0.5 to 14.4		18.2
CH <sub>4</sub> (mM)	0.5, 1.2	0.8	1.2-3.5		1.4	1.65, 2.5	0.0026	0.9-14.4		2.81
CO <sub>2</sub> (mM)	3.7	n.d.	2.1-3.5, 6.2			16-17		1-2		2.8
δ <sup>13</sup> CH <sub>4</sub>	-12.3 to -14.1	-8.7	-6.1			-15.8	-32.6	-11.9	-16 (-13 to -18.2)	-15.4
ANME			ANME-2e	ANME-2e		non ANME		ANME-1		ANME-1b, ANME-2

These vents are also a source of sulphides and methane. In contrast to typical black smokers, they draw their heat from the interaction between ultramafic and mafic basement rocks. The heat flux measured at the VDVF field is  $487 \pm 101$  MW which is higher than systems delivering their heat by the exothermic processes of serpentinisation. This type of vent is important in the understanding of the ocean crust heating flux circulation which is a long distance away from slow and ultra-slow spreading ridge (Hodgkinson et al. 2015).

The Ashadze fields are high-temperature (black smoker) systems (between 300- 400 °C), in which sulfides are deposited from low-pH and Fe-rich fluids (Table 2.3). In the Ashadze field there are four vents, three of which are active (Ashadze 4 (2007) is inactive). Ashadze (1 (2003) and 3 (2005)) are the deepest hydrothermal vents hosted by serpentinite rocks (Charlou et al. 2010). The Ashadze 2 (2007) has very low salinity phase therefore low precipitation of metals (Charlou et al. 2010).

Drachenschlund (Nibelungen) is an ultramafic-hosted vent situated on the eastern scarp of a fault-block (Table 2.3) (Melchert et al. 2008). The Nibelungen field has a crater resembling Logatchev but without fauna around it and several extinct chimneys. This ultramafic-hosted vent has a thermal output estimated to be  $60 \pm 15$  MW based on plume rise-height information (Melchert et al. 2008).

Lilliput contains only low temperature vents due to the thickened crust at this location (Table 2.3) (Perner et al. 2007). The pH of venting fluids is low and sulphide is the most abundant inorganic energy source associated with diverse bacteria (Perner et al. 2007).

The Logatchev field contains five vents (Logatchev, -2,3,4,5) of which Logatchev 2 and 5 are ultramafic-hosted but only Logatchev 2 is still active (Fig. 2.11, Table 2.3) (Fouquet et al. 2008). Its deposit types are polymetallic massive sulphide, chalcopyrite, sphalerite and chalcocite (Fouquet et al. 2008). Methanotrophs of type ANME-2 have been identified at Logatchev by analysis of 16S ribosomal ribonucleic acid (16s rRNA) (Perner et al. 2007).

The Rainbow hydrothermal vent is situated on the western flank of a non-volcanic ridge between the South AMAR and AMAR segments of the Mid-Atlantic Ridge (Fig. 2.11, Table 2.3). The host rock is made up of serpentinised mantle with gabbroic and basaltic intrusions (Charlou et al. 2002). Hydrogen gas dissolves the iron and the calcium which leads to low pH conditions; on the other hand pyroxene, from the mantle rock alters to talc-tremolite assemblages, which lead to increases in dissolved SiO<sub>2</sub>% (Allen and Seyfried Jr 2003). The hydrogen is used for energy source by lithotrophic bacteria and used in the abiotic FT reaction at high temperature to produce organic compounds such as linear saturated carbon C<sub>16</sub>-C<sub>29</sub> and *n*-alkanes C<sub>10</sub>-C<sub>40</sub> with C<sub>25</sub> dominant (Holm and Charlou 2001). The Rainbow system supports methanotroph of type ANME-2 as found by analysis of 16s rRNA (Roussel et al. 2011).

#### 2.2.4.2. White smokers

The first white smokers (Lost city) were discovered in 2001 near the mid-Atlantic ridge (Fig. 2.11, Table 2.3) (Kelley et al. 2001). The white coloured chimneys are constituted of carbonate, unlike black smokers which are usually sulphide rich (Table 2). The fluids have a moderate temperature (< 300 °C), and when less than 110 °C with a basic pH represent optimal conditions for microbial life (Ménez et al. 2012). The white smokers are at a longer distance from the heating source (spreading ridge, magma chamber) compare to black smokers thus their different characteristics like fluid temperature (Connelly et al. 2012).

The vents of the white smokers release cooler water than those of the black smokers, containing more barium, calcium sulfate and silica. These fluids interact with seawater causing white color, hence the name "white smoker". Compare of to the black smokers, the fluids here are depleted in metals and CO<sub>2</sub>, but they have high concentrations of H<sub>2</sub> 0.5 to 14.4 mmol/kg and CH<sub>4</sub> (and other low-molecular-weight hydrocarbons), which serve as important energy sources for anaerobic microorganisms within the porous chimney walls (Table 2.2) (Kelley et al. 2005; Proskurowski et al. 2006; Proskurowski et al. 2008). The white smokers are characterized by worm tubes and fluids of amorphous silica, barite and pyrite

(Haymon 1983). The chimneys are made from carbonate -brucite and some of them are up to 60 metres high (Früh-Green et al. 2003). The brucite is a product of the serpentinisation of ocean peridotites. In the hydrothermal events the alkaline condition produces formate, bicarbonate and carbonate and decrease the concentration of CO, CO<sub>2</sub> and formate acid (Seewald et al. 2006).

The Lost City hydrothermal vents are Ca-enriched with fluids of pH 9-11 and with temperatures of between 40-90 °C (Fig. 2.11, Table 2.3) (Kelley et al. 2005). The biology and chemistry were described in 2005 and are characterised by a small biomass of chemosynthetic organisms (Kelley et al. 2005). The biosystem is the first described fully working hydrothermal vent biosystem and is also the most studied (Boetius 2005). Even methanotrophs of type ANME-1 have been identified at Lost City using 16S rRNA genetic sequencing (Brazelton et al. 2006). Radiocarbon aging and strontium, carbon and oxygen data shows at least 30 000 years of hydrothermal activity related at Lost City to serpentinisation (Früh-Green et al. 2003). Radiocarbon and hydrogen isotopic evidence suggest that abiotic synthesis of low molecular weight (C<sub>1</sub> to C<sub>4</sub>) hydrocarbons is possible having for origin mantle-derived inorganic carbon, ultramafic rock and sea water interaction at moderate heat (<150 to 250 °C), occurs in the Lost City hydrothermal field (Proskurowski et al. 2008). Lost City was the first hydrothermal vent with biological local system discovered to be supported by serpentinisation (Kelley et al. 2001), however the system is also hosted by gabbroic rock. It is also the first hydrothermal vent with evidence for methane associated biology (Kelley et al. 2001).

Mount Saldanha (1998) is a low temperature hydrothermal vent located on the top of a serpentinised massif (Fig. 2.11, Table 2.3). It was believed to be the only one to be hosted solely by serpentinite as suggested by its low temperature of 25-105 °C, typical for serpentinisation (Dias and Barriga 2006). However samples collected in particularly a core containing serpentine, talc and other minerals precipitation characteristic for hydrothermal vents (e.g. chalcopyrite, pyrrhotite, metal enrichments, REE) are indicative of high temperature from 260 to 330 °C due to magmatic heat source (Dias et al. 2011).

## **2.3. Methanotrophic bacteria**

### **2.3.1. What are methanotrophic bacteria?**

Methanotrophic bacteria oxidize a compound with a single carbon atom - methane and use it as their only source of energy and electrons. Methanotrophic bio-systems are found in dry lands, volcanic geothermal soils, methane seeps, microseepage, marine sediments and hydrothermal vents, where the aerobic MOB (methane oxidizing bacteria) are ubiquitous in water and sediments/soils (Hinrichs et al. 2000; Etiope and Klusman 2002; Gagliano et al. 2014). Study about methanotrophs are important for understanding the methane cycle and variations in the cycle due to climate change.

Methanotrophs can oxidize methane aerobically or anaerobically (Fig. 2.13) e.g.(Nitschke and Russell 2013). The aerobic methanotrophic microorganisms are prokaryotes, bacteria typically having sterols in their membrane (Brock and Madigan 1991) and the anaerobic ones are in the Euryarchaea family (Fig. 2.13) (Nitschke and Russell 2013). Aerobic methanotrophs are divided into three different groups depending on their metabolism (group 1:  $\gamma$  Gammaproteobacteria; group 2:  $\alpha$  Alphaproteobacteria and group 3:  $\beta$  Verrucomicrobia) (Fig. 2.10) (Kalyuzhnaya et al. 2015). The anaerobic methanotrophs ANME (ANaerobic Methanotroph) are ANME-1, ANME-2 and -3 (Fig. 2.13, Table 2.4). In this research is the anaerobic methanotroph that are studied, as they are the one present at the ocean floor and related to hydrothermal vent and anaerobic environment.

The consumption of methane by methanotrophs is estimated to be around  $38 \text{ Tgy}^{-1}$  (Ridgwell et al. 1999). ANME are found in marine sediments and play a significant role removing ca. 90% of all the methane produced in anoxic environments, of which only 2% is released into the atmosphere (Reeburgh et al. 1996; Hinrichs et al. 2000). Methane is produced by methanogens in deep sediments down to 800m below the

seafloor, upwards through a sulphate-deplete sediment (mm to 200m from seafloor) where is consumed by ANME.

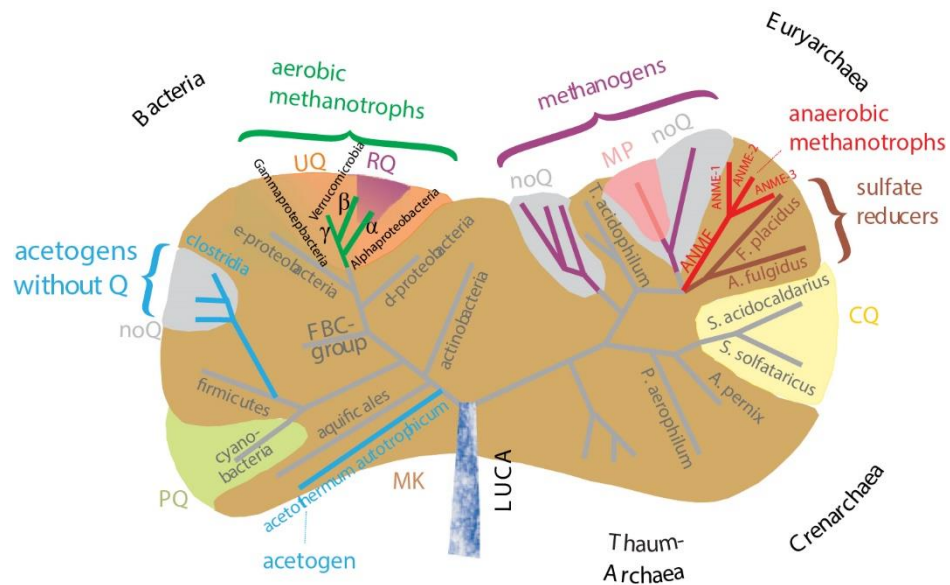
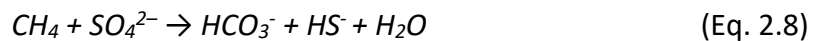


Figure 2.12. Genealogical tree starting from LUCA (last universal common ancestor) showing the place of the aerobic and anaerobic methanotrophic in the two different branches – bacteria (prokaryotes, unicellular organism) and Euryarchaea (Archea, single-celled organism), respectively modified after Nitschke et Russell 2017.

Anaerobic oxidation of methane (AOM) is typically carried out by a consortium of at least two different types of organisms; methanotrophs and another organism accepting electrons such as psychrophilic sulphate-reducers, mesophilic sulphate-reducers, hydrogen-oxidizing bacteria, archaeal relatives of methanogens or sulphate-reducing  $\delta$ -proteobacteria (Hinrichs et al. 2000; Kalyuzhnaya et al. 2015) (Eq. 2.8).



Methane interacts with sulphate to produce hydrogen sulphide which is used by chemosynthetic microorganisms to fix carbon (eq. 2.8). The consortium between methanotrophic bacteria and sulphide reducing bacteria (SRB) is very common and has the advantage of having a good transfer of intermediates by molecular diffusion (Table 2.4) (Boone et al. 1989). Sulphate reducers are one of the dominant bacterial populations at hydrothermal vents (McCollom and Shock 1997), and sulphate is used for methane oxidation instead of participating in remineralization (Hinrichs et al. 2000).

Table 2.4. Table showing the anaerobic methanotroph (ANME), their symbiot with SRB and their biomarkers (Wegener et al. 2017, Rossel et al. 2008, Nauhaus et al. 2007, Blumenberg et al. 2004, Hinrichs et al. 2000).

	ANME-1	ANME-2	ANME-3
Methanogens association	non-direct association, Methanosarcinales, Methanomicrobiales	<i>Methanosarcinales</i> , <i>Methanomicrobiales</i>	<i>Methanococcoides</i> , <i>Methanlobus</i>
SRB (sulfate reducing consortia) consortia	<i>Desulfosarcina</i> , <i>Desulfococcus group</i> , mono specific aggregats, single cells	<i>Desulfosarcina</i> , <i>Desulfococcus group</i>	<i>Desulfobulbus spp.</i>
Biomarkers ANME	mainly diglyceiodic GDGT derivatives, cyclized tetraether lipids typical for thermophiles	lipids phosphate-based derivatives of archaeol & hydroxyarchaeol dominance (e.g. Anme-2: sn-2-hydroxyarchaeol, archaeol, crocetane, pentamethylcosatriene, 2,6,10,15,19-pentamethylcosenes with four and five double bonds (PMI:4, PMI:5)), glycerol ether lipid archaeol (2,3-di-O-phytanyl-sn-glycerol) (Elvert et al 2000).	
Biomarkers SRB	monioprenoides glyceroles diethers	sn-2-hydroxyarchaeol, archaaole crocotane, hexadecenoic-11 acid (16:1 $\omega$ 5c), 11,12-methylene-hexadecanoic acid (cy17:0 $\omega$ 5,6), sn-1-mono alkyl glycerol ethers (MAGE 14:0, 16:1 $\omega$ 5c and 16:0)	

The maximum methane consumption occurs at the sulphate-methane transition zones SMTZ in the 20-200 cm below seafloor sediments, where SRB+AOM consortium is at its maximum (Niemann et al. 2006). SRB are found to exist in deep methanogenic sediments for more than 20 Ma (Glombitza et al. 2016).

Anaerobic methanotrophic bacteria are discovered in several hydrothermal vents. Methanotrophic bacteria are discovered in the hydrothermal sediments of the Guaymas basin hydrothermal vents with methane content of 12 to 16 mM (270 to 360ml kg<sup>-1</sup>) (Teske et al. 2002). 16S rRNA gene sequences, special biomarkers and isotopic analyses are used to detect methanotrophic biosystems in these environments (e.g. (Hinrichs et al. 1999; Bian et al. 2001; Teske et al. 2002).

Methanotrophic bacteria have been found in symbiosis with deep-sea bivalves in the Gulf of Mexico (Cavanaugh et al. 1987) associated with sulphur – oxidizing chemolithoautrophic bacteria and in the MAR hydrothermal vents (Menez Gwen) as

endosymbiont (Pond et al. 1998). The bacteria could be detected in the mussels tissue i.e. gills by their monounsaturated (n-8) fatty acids and heavy carbon isotopic values ( -24.9 to -34‰ Menez Gwen in the range for methanotrophic nutrition; -51 to -57‰ Gulf of Mexico (Childress et al. 1986; Pond et al. 1998)).

During the Deepwater Horizon oil spill (2010), a bloom of methanotrophic bacteria occurred near the plume for several months and disappeared before the methane source was exhausted (Kessler et al. 2011; Shiller and Joung 2012). After the event the seawater was depleted in oxygen and nutrients (nitrate, phosphate) which could be one of the reasons for the early retrieving of this bio-community, the other being depletion of trace minerals or consumption by other microorganisms (Crespo-Medina et al. 2014).

The presence and distribution of specific phylogenetic groups of Archaea and Bacteria from which methanotrophic bacteria of type ANME-1 In the Lost city demonstrate the biogeochemical link between serpentinisation and microbial metabolism (Brazelton et al. 2006). The Lost city is dominant by serpentinisation derived fluids enriched in  $^{13}\text{C}$  and free  $\text{H}_2$  with absence of DIC (dissolved inorganic carbon) as well as biomarkers as squalane (irregular acyclic isoprenoid) and analyses of 16S rRNA gene indicating the ANME-1 (Brazelton et al. 2006; Delacour et al. 2008b).

ANME-1 are the dominant ANME in hydrothermal vents due to their possible relation with  $\delta$ -proteobacteria (Table 2.4) (Webster et al. 2011). Methanotrophic bacterias (AOM) have been studied in *invitro* experiments in sediments samples enriched in methanotrophic community but not in pure culture (Wegener et al. 2008). It is difficult to culture the ANME in the laboratory, in contrast to the MOB (methane oxidizing bacteria) due to their difficult and extremely slow growth rates as well as obligate symbiotic relationships with other bacteria (e.g. sulphate reducing) and low  $\text{CH}_4$  incorporation (Turetsky et al. 2014).

### 2.3.1. Biomarkers

Biomarkers or biological markers are molecular fossils, derived from formally living organism (Peters et al. 2005b). They are made up of carbon, hydrogen and other elements and are structurally similar to their parent organic molecules in living organisms (Peters et al. 2005b).

Biomarkers are used to indicate source, depositional environment, process and age of the organic matter (OM). Because biomarkers could occur only in certain types of living organisms and under specific condition make the organic geochemistry method using them accurate.

One of the most important class of biomarkers are the lipids (Fig. 2.12). They include fats, waxes, steroids, hydrocarbons, isoprenoids, phospholipids, combinations of samples molecules (e.g. alcohols, aliphatic carboxylic acids) and others (Fig. 2.12) (Peters et al. 2005b). In this study, we studied hydrocarbons consisting entirely of hydrogen and carbon, for example alkanes and isoprenoids (Fig. 2.12). Although methane is a hydrocarbon it is not a valuable biomarker, because every living organism could produce it when heated ; nevertheless it could reflect its geological history and origin (Peters et al. 2005b). In the analysed samples in this study the majority of hydrocarbons were *n*-alkanes, isoprenoids, steranes, hopanes and PAHs.

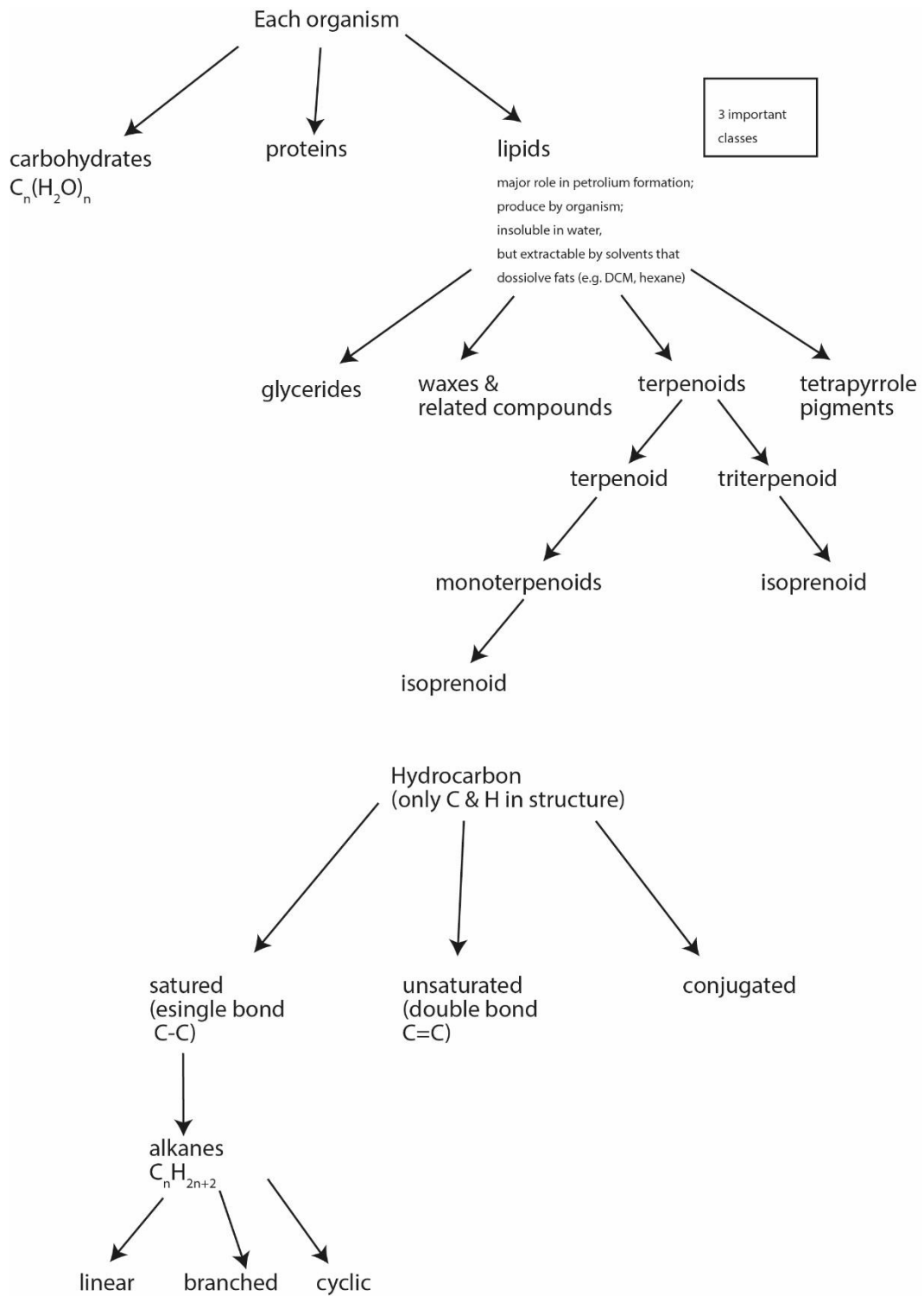
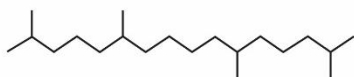


Figure 2.13. Incomplete graph shows the type of hydrocarbons and the places of isoprenoid in the lipid's sub-domain.

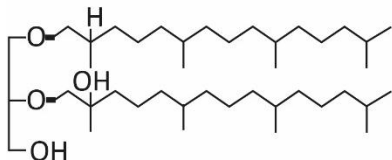
### 2.3.2. Biomarkers for methanotrophs

Methanotrophic biosystem can be recognised by their unusually depleted  $\delta^{13}\text{C}$  isotopic composition and by biomarkers such as crocetane (Thiel et al. 1999; Bian et al. 2001), sn-2-hydroxyarchaeol (Hinrichs et al. 1999), archaeol (Hinrichs et al. 1999), biphytanic diacids (Birgel et al. 2008), glycerolethers (Hinrichs et al. 1999) and  $\text{C}_{20}$ ,  $\text{C}_{25}$  sn-2 hydroxy isoprenoid glycerol diether for ANME-2 (Stadnitskaia et al. 2008), as well as characteristic sulphur isotopic composition related to anaerobic oxidation of methane (AOM) (Boetius et al. 2000) (Fig.2.14, Table 2.4). Methanotrophic communities are also dominated by specific intact polar lipids (IPLs) biomarkers phosphatidylethanolamine and phosphatidyl-(N,N)-dimethylethanolamine Species) (Table 2.4) (Rossel et al. 2008). The methanotrophic communities having one of the three archaea dominant populations (Euryarchaeota) (show different dominant biomarkers ANME-1: polar dialkylglycerolethers; ANME-2 and ANME-3: mixed acyl/ether glycerol derivatives (Table 2.4) (Niemann et al. 2006; Rossel et al. 2008). Other biomarkers associated with AOM are pentamethylcosane (PMI), archaeol, hydroxyarchaeol and glycerol dibiphytanyl glycerol tetraethers (GDGTs) (Table 2.4) (Birgel et al. 2008).  $\text{C}_{16}$  and  $\text{C}_{18}$  cyclic fatty acids could have also be used as biomarkers because of their dominance in free-living sulphide-oxidizing bacterium (*Thermothix thiopara*) ( ~ 57%), 17% in the sulphur-oxidizing bacteria and 8% in some endosymbiotic methanotrophic bacteria (Pancost et al. 2001). A high Pr/Phy (>1.5) ratio could be seen as a result of the large contribution of methanogens but this ratio must be taken with caution and used in conjunction with other biomarkers (Rowland 1990).

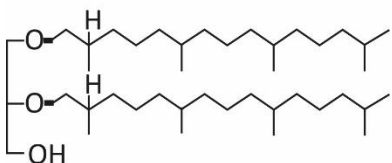
**Crocetane**  $C_{20}H_{42}$



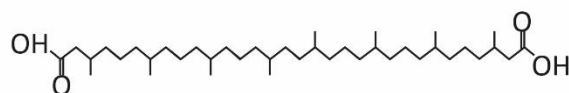
**Sn-2-hydroxyarchaeol**  $C_{43}H_{88}O_4$



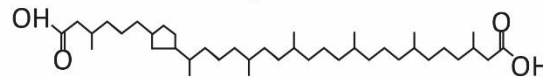
**Archaeol**  $C_{43}H_{88}O_3$



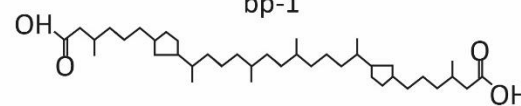
**Biphytanic diacids**



bp-0



bp-1



bp-2

**$C_{20,25}$  sn-2 hydroxy isoprenoid glycerol diether**  $C_{38}H_{76}O_4$

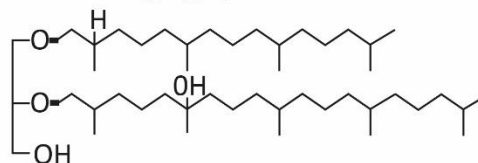


Figure 2.14. Chemical structures of the hydrocarbon biomarkers for anaerobic methanotrophs.

Anaerobic methanotrophy-sulfate reduction is suggested to occur in the anoxic environment at 2.7 Ga (Hinrichs 2002), however even if they show depleted  $\delta^{13}C$  values (~45 to -60‰), methanotrophy is difficult to detect (Slotznick and Fischer 2016). Many of these compounds are labile and unlikely to survive over geological time but their breakdown products as hydrocarbons might (Brocks et al. 1999).

The sequence of methods leading to find a methanotrophic biosystem normally could be summarised as follows: depleted  $\delta^{13}C$  isotopic composition on the total organic carbon are found in systems (e.g. hydrothermal vents); then a search of specific biomarkers related to methanotroph are put in evidence (e.g. crocetane); at the end  $\delta^{13}C$  isotopic composition on each molecular compound related specifically or not to the methanotroph is undertaken.



## Chapter 3

# **3. Preserved organic matter in a fossil Ocean Continent Transition in the Alps: the example of Totalp, SE Switzerland**

This chapter is derived from a paper published in *Swiss Journal of Geosciences*, accepted for publication on 3 November 2015 and first published online on 2 March 2017. Authors of the manuscript are Tsvetomila Mateeva (main author), George A. Wolff, Gianreto Manatschal, Suzanne Picazo, Nick J. Kusznir and John Wheeler. The aim of this study was look for biological evidences consistent with anaerobic methane oxidation in the Totalp area, a fossil Alpine OCT. All authors helped draft the manuscript, read and approved the final manuscript.



### **3.1. Abstract**

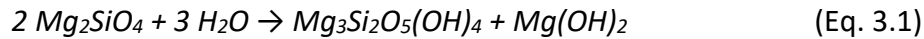
Evidence from ultraslow spreading mid-ocean ridges and both fossil and present-day Ocean-Continent Transitions (OCT) demonstrates that mantle serpentinisation resulting from the interaction of mantle rock and water during tectonic exhumation is widespread. Observations at white smokers in modern ocean settings suggest that methane produced by serpentinisation can support methanotrophic bio-systems, which use methane as the only source of carbon. An important question is whether such bio-systems are more generally pervasive in their association with serpentinised mantle in the subsurface. In this study, we examined whether there is evidence for such a methanotrophic system in exhumed serpentinised mantle at a magma-poor rifted continental margin, by probing for characteristic biological markers in these and associated sedimentary rocks in the Totalp unit of SE Switzerland. This represents a remnant of the former OCT of the southern Alpine Tethyan margin and was chosen because of its mild Alpine tectonic and low-grade metamorphic overprint during the Alpine orogeny, hence giving potential for the preservation of indigenous organic matter (OM).

Totalp samples are characterized by low organic carbon contents of 11 to 647 ppm. The majority of the samples contain hydrocarbons in the form of *n*-alkanes in the range C<sub>17</sub> - C<sub>36</sub>. Some sediments contain isoprenoids, for example pristane and phytane and a suite of steranes that are consistent with a marine origin for the OM preserved in the rocks. Traces of marine planktonic and bacterial OM are preserved in the serpentinised mantle and overlying sediments of this ancient Tethyan OCT, but there is no evidence that the OM has been generated from methanotrophic bio-systems.

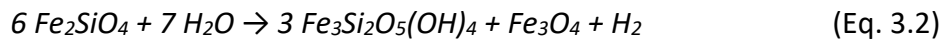
### **3.2. Introduction**

Serpentinisation is an important metamorphic exothermic hydration process potentially contributing chemical energy for anaerobic life, as well as thermal energy at oceanic hydrothermal vents (*e.g.* (Shock et al. 2002; Jamtveit and Hammer 2012a)). Serpentinisation converts olivine and pyroxene to serpentine, other Fe-Mg minerals

(magnetite, brucite, talc) and free molecular hydrogen (Eq. 3.1). Typically the hydration of the end-member is shown in literature; the Mg component of olivine may hydrate as follows:



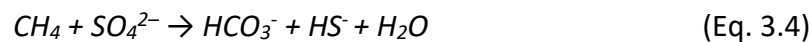
The Fe component of olivine contributes to forming Fe-Mg serpentine by an analogous reaction and/or by reducing water



It has been proposed (*e.g.* (McCollom 2013)) that molecular hydrogen can then reduce CO<sub>2</sub> derived from carbonate and hydrogen carbonate in sea-derived pore waters to methane (CH<sub>4</sub>) at high pressure and temperature, *via* a Fischer-Tropsch-like reaction (Eq. 3.3).



Serpentinised mantle rocks exposed along slow to ultraslow-spreading Mid-Ocean Ridges (MOR) show positive anomalies of methane and hydrogen in the overlying water column above active tectonic zones (Rona et al. 1987; Charlou et al. 1988; Rona et al. 1992; Bougault et al. 1993; Charlou and Donval 1993; Charlou et al. 1998; Gràcia et al. 2000; Kelley and Shank 2010). The abiotically produced methane can be anaerobically oxidised by methanotrophic bacteria using sulphate as the electron acceptor (Eq. 3.4).



Sulphate reducers are one of the dominant bacterial populations at hydrothermal vents (McCollom and Shock 1997). Furthermore, methanotrophic bacteria have been identified at Lost City (mid-Atlantic Ocean), a low-temperature alkaline hydrothermal vent supported by energy derived from the formation of serpentinite (Hinrichs et al. 2000; Kelley et al. 2001; Orphan et al. 2001; Kelley et al. 2005). Recently, bacterial anaerobic nitrate oxidation of methane has been demonstrated in the laboratory ((Haroon et al. 2013; Arshad et al. 2015), using two different microorganisms (Raghoebarsing et al. 2006)); this may also occur at the MOR methane sources, but is

likely to be a minor pathway as nitrate concentrations in seawater are significantly lower than sulphate ( $\mu\text{M}$  vs.  $\text{mM}$ , respectively).

Recent studies have focussed on the relationship between serpentinisation and organic compounds, mainly methane in the laboratory (*e.g.* (McCollom and Seewald 2013; Etiope and Ionescu 2014)), at present-day serpentinite-hosted hydrothermal vents (*e.g.* (Kelley et al. 2005; Delacour et al. 2008c; Proskurowski et al. 2008)), mud volcanoes (*e.g.* (Mottl et al. 2003; Holm et al. 2006)), and exhumed serpentinite mantle domains with high  $\text{H}_2$  concentrations and high pH (*e.g.* (Cardace et al. 2013)). High concentrations of OM found at the Mid-Atlantic Ridge (MAR; 4-6°N) were associated with serpentinised peridotite rather than with the hydrothermal vents ((Ménez et al. 2012)).

Hence, the present study uses an organic geochemical approach to quantify OM in the exhumed mantle from an OCT in order to better understand the relationship between OM and mantle serpentinisation. We selected the Totalp unit exposed in the Eastern Swiss Alps, which represents a remnant of the fossil Tethyan OCT emplaced during the Alpine orogeny (Fig. 3.1a) (Bernoulli et al. 1985, Manatschal et al. 2003, Picazo et al. 2013). We searched for biomarkers or molecular remains of former living organisms, specifically hydrocarbons with an origin consistent with anaerobic methane oxidation (*e.g.* crocetane; (Blumenberg et al. 2004)). A wider suite of biomarkers was used to determine source and thermal maturity of OM preserved in the rocks.

### **3.3. Regional geological setting of the Totalp unit**

The Totalp unit is located north of Davos in SE Switzerland. It is part of the Tethyan OCT (Fig. 3.1b). The peculiarity of the Totalp unit is that it experienced little Alpine deformation and only a low grade Alpine metamorphic overprint, not exceeding 100-150 °C, *i.e.* prehnite-pumpellyite grade (Peters 1968; Früh-Green et al. 1990). The Totalp unit consists of two Alpine tectonic units namely the Upper and Lower Ultramafic Totalp sub-units (*e.g.* Picazo et al. 2013). These are mainly composed of serpentinised peridotite exhumed at the seafloor during Jurassic times and

ophicalcites that occur at the top basement and which can be found re-worked into the overlying Jurassic marine sediments (Fig. 3.1c). In addition, the primary contacts between the exhumed serpentinitised mantle, the ophicalcites and the oceanic sediments are well-preserved (Weissert and Bernoulli 1985).

### **3.3.1. Pre-Alpine and Alpine geological and thermal history**

The serpentinitised peridotites of the Totalp unit were exhumed to the Jurassic seafloor during final late Middle Jurassic rifting (Peters and Stettler 1987; Bernoulli et al. 2003). Later, during the Alpine orogeny, the exhumed mantle rocks were first tectonically emplaced within a Late Cretaceous E-W directed nappe stack before being positioned during the Tertiary collision over the European units forming the present-day Alpine orogen (Weissert and Bernoulli 1985; Früh-Green et al. 1990; Manatschal et al. 2003). The serpentinitised peridotites in Totalp are interpreted to be fertile subcontinental lithospheric mantle (Manatschal et al. 2001; Müntener et al. 2010; van Acken et al. 2010), similar to other described remnants of fossil OCTs from the Alps (*e.g.* Platta, (Desmurs et al. 2002); Malenco in the Italian Alps, (Müntener et al. 2004)). Extensional faults and unroofing of their footwalls are responsible for the mantle exposure at the seafloor (Picazo et al. 2013).

### **3.3.2. Lithologies**

The Totalp unit consists mainly of serpentinitised peridotites, ophicalcites and post-rift sediments (Figs. 3.1, 3.2; Table 3.1). This association is typical of an OCT across magma-poor margins where magmatic rocks are often either very rare or absent. Three types of serpentinitised mantle rocks were identified:

Massive serpentinitised peridotites, which preserve mantle textures and mainly consist of serpentinitised spinel-lherzolite. Locally these rocks also contain pyroxenite and amphibole- and chlorite-rich layers (Picazo et al. 2013).

During exhumation, the serpentinitised peridotites are affected by localization of the deformation and intensive fluid circulation leading to complete serpentinitisation of fault-rocks, including serpentinite gouges, serpentinite cataclasites and foliated

cataclasites (Picazo et al. 2013). These rocks are best exposed in the Obersasställi area and they occur in the uppermost 150 m of the exhumed mantle in the footwall

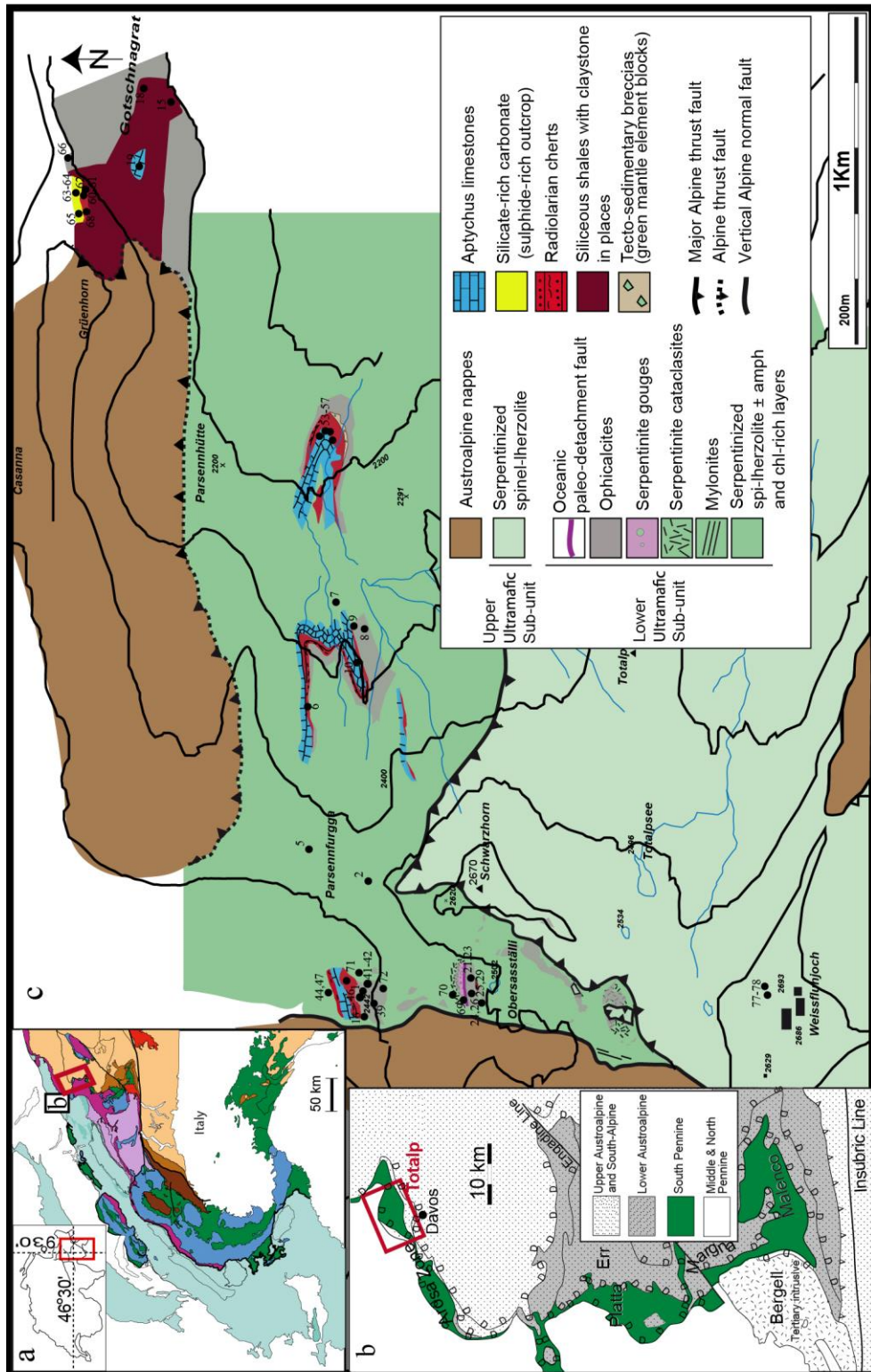


Figure 3.1. Maps showing location and geology of the Totalp area a) Location of the Totalp area in the tectonic map of the Alps (from (Schmid et al. 2004); modified by (Mohn et al. 2010)) b) Location of Totalp as a part of the South Penninic units in Grisons (Manatschal et al. 2003) c) Geological map of Totalp (modified from (Picazo et al. 2013)) showing location of the analyzed samples as well as the distribution of the major lithologies and samples described in this study (for description of samples see Table 3.1).

of a Jurassic extensional detachment fault (Figs. 3.1, 3.2) (Picazo et al. 2013)).

Veins of serpentine that have been interpreted to result from later serpentinisation during low-grade Alpine metamorphism, as suggested by the oxygen isotopes (Früh-Green et al. 1990). Sample 26, an ophicalcite with clasts of serpentine in a carbonate matrix show these late veins of serpentine - chrysotile (Fig.3.3). The chrysotile is forming cross fibre veinlets in the thin section visually looking as “spaghetti” (Fig.3.3).

Some serpentine veins may result from the percolation of meteoric water associated with regional metamorphism (Burkhard and O'Neil 1988).

Ophicalcites are complex rocks that are made of serpentinite and calcite and represent the result of different processes (Bernoulli and Weissert 1985; Lemoine et al. 1987). They either result from the total to partial *in-situ* replacement of serpentine by carbonate, tectonic processes related to exhumation and hydrothermal systems, and/or cementation and filling of fractures by sediments (*e.g.* neptunian dykes of (Bernoulli and Jenkyns 2009)). These processes occur at or near the seafloor and are often associated with hydrothermal fluid circulation at temperatures of 100-150 °C ((Früh-Green et al. 1990; Picazo et al. 2013)). Most ophicalcites are formed under static (non tectonic) conditions within 20 m of the paleo-seafloor (Picazo et al. 2013).

Sedimentary ophicalcites at Totalp include neptunian dykes and debris-flows (Fig. 3.2). The neptunian dykes are carbonate veins filled with pink or grey carbonate (pelagic sediments or mechanically reworked cements), filling fractures in the exhumed mantle. These dykes are typically located in the tectonized, serpentinised peridotites forming the uppermost few meters of the exhumed mantle (Bernoulli and Weissert 1985; Picazo et al. 2013).

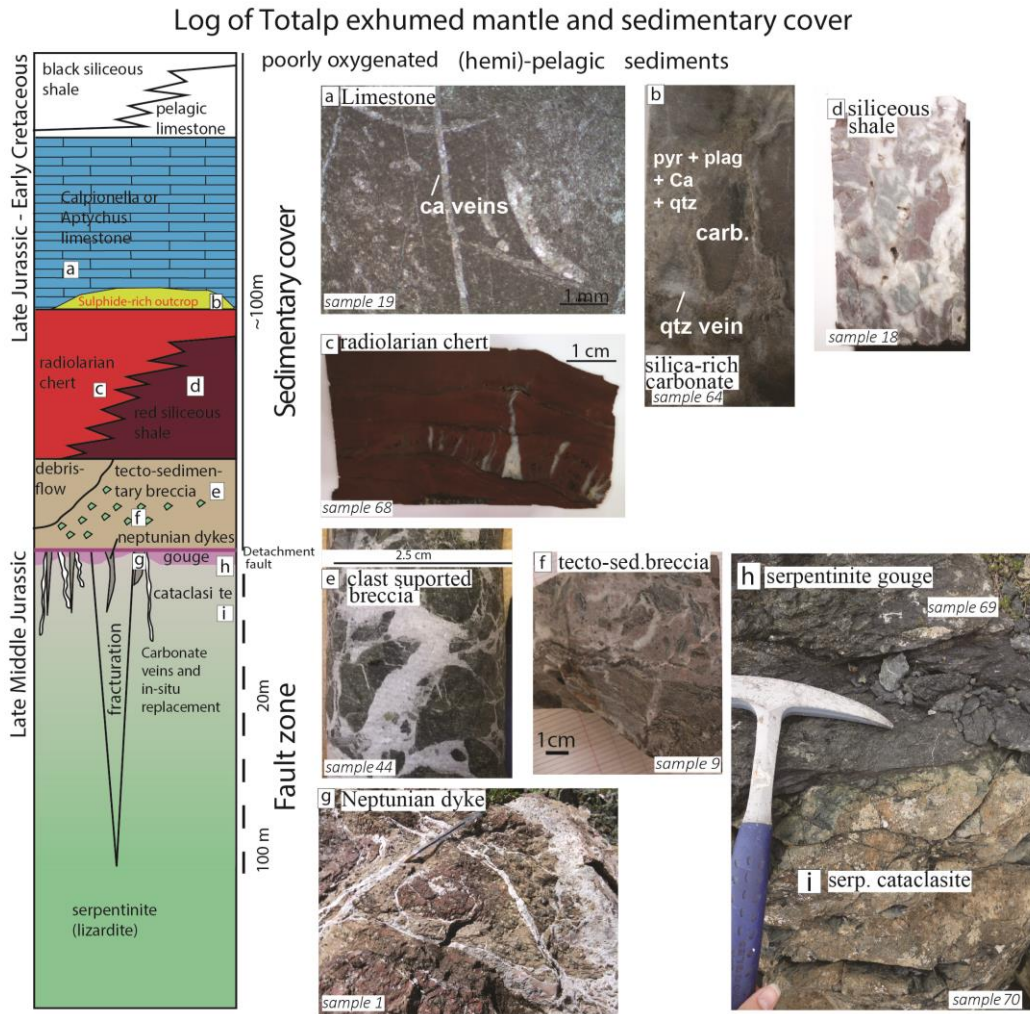


Figure 3.2. Sketch showing the lithologies and the stratigraphy of the Totalp area ((Weissert and Bernoulli 1985; Früh-Green et al. 1990; Manatschal et al. 2003; Picazo et al. 2013)).

The second main type, the tectono-sedimentary ophiolites, include cemented clasts of serpentinite, gabbro and continental basement (Manatschal and Bernoulli 1999; Bernoulli et al. 2003; Picazo et al. 2013).

The sediments overlying the ophiolite are mainly pelagic deposits of Late Jurassic to Early Cretaceous age, some of which have been reworked (most likely by ocean bottom currents) (Weissert and Bernoulli 1985). Red shales are overlain by radiolarian cherts and grey micritic limestones intercalated with claystones (e.g. Radiolarite Formation and *Calpionella* or *Aptychus* limestone Formation of Weissert and Bernoulli 1985). The top of the sequence is formed by black siliceous shales that

are characteristic of poorly oxygenated bottom waters during the Early Cretaceous (Weissert et al. 1985; Weissert and Bernoulli 1985).

In the north east of Totalp, on a topographic cliff near Gotschnagrat (Figs. 3.1, 3.4), there is a weathered outcrop with visible pyrite on the top of the radiolarian cherts and siliceous claystones (Fig. 3.4; (Weissert and Bernoulli 1985)). The outcrop has been described by Früh-Green et al. (1990) as a zone of pyrite mineralization associated with radiolarian cherts. The radiolarites contain quartz, illite, hematite and chlorite (Weissert and Bernoulli 1985). The sulphidized outcrop has a bulk chemistry different from its surrounding and could have been formed during early diagenesis or metasomatism of amorphous silica or limestone (Berner 1984; Williams et al. 1985). Alternatively, the sulphide could be related to a fossil hydrothermal system (e.g. (Styrt et al. 1981), (Beard and Hopkinson 2000; Zeng et al. 2015)). Early diagenetic reactions producing pyrite depend *inter alia* on a source of OM as electron donor (Fig. 3.3b); the high present-day porosity of the rock (Fig. 3.3c) could be produced by weathering of calcite (Berner 1984). Hydrothermal vent systems are characterized by pelagic sediment accumulation alongside ferrous oxides (*i.e.* radiolarian chert) of hydrothermal origin which can potentially be preserved (Haymon 1989; Montgomery and Kerr 2009). The second most common mineral in the sulphide bearing samples is quartz and may have originated from amorphous silica or opal, which are common in hydrothermal vents (e.g. MAR- mount Saldanha 36.30N (Dias and Barriga 2006); 25°48'N (Rona 1984), 24°21'N (Rona 1984) ; Kane 23°35'N Fracture zone (Kelley and Delaney 1987)) reflecting a large input of hydrothermal silica (Dias and Barriga 2006). There is no evidence of fossilized worm tubes associated with the zone of pyrite mineralization; these are characteristic of inactive white smokers (Haymon 1983) and so the origin of this formation remains unclear.

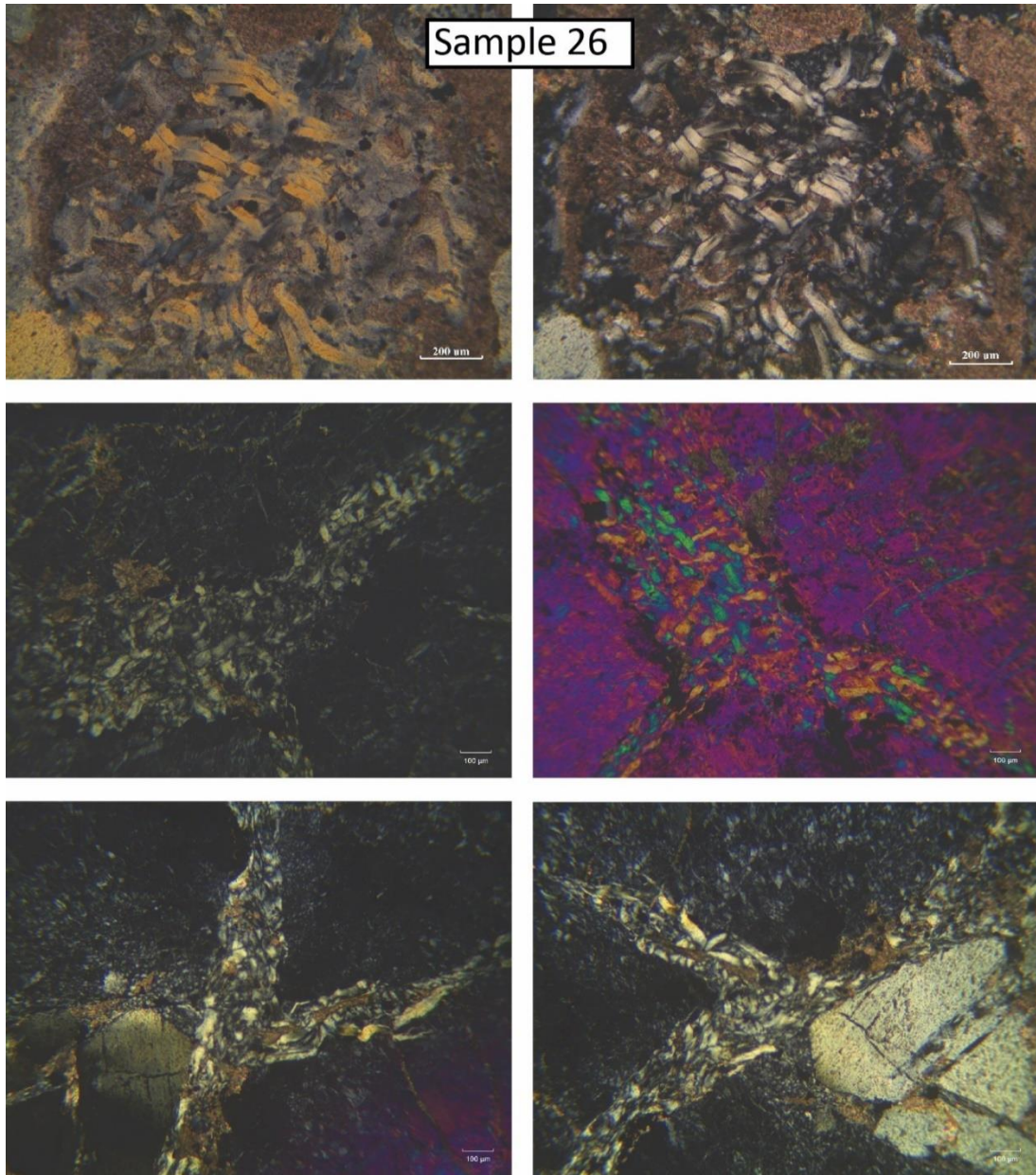


Figure 3.3 Sample 26 opicalcite from Totalp area showing late serpentinite – chrysotile only presented in vein and not observable in hand specimen in a mesh texture serpentinite.

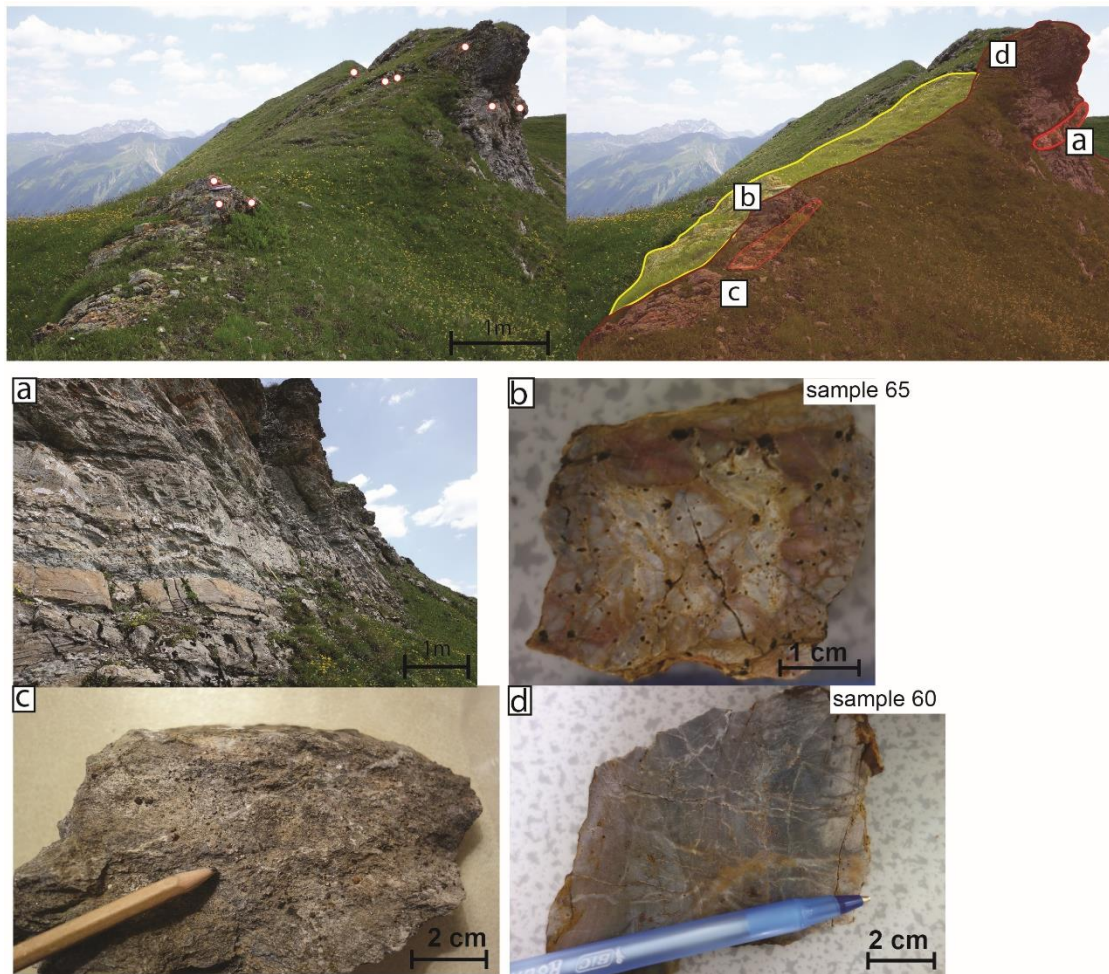


Figure 3.4. The sulphide bearing outcrop in the Totalp area showing weathered lithology. Red circles are the sampling location in this outcrop. In the line-drawing on the right, light red identifies radiolarian cherts, dark red silicious shale and yellow sulphate rich carbonate, rich in silica a) Zoom of outcrop b) Sample 65 is composed by calcite 50%. 25% quartz and is highly weathered c) Sample shows visible hematite crystals and calcite as the major mineral d) Sample 60 shows a siliceous rock with 3 different colours composed by 83% quartz, 10% albite and pyrite, illite and chlorite.

### 3.4. Sample Collection, Preparation and Analysis

#### 3.4.1. Sample collection

A total of 47 samples were selected from the Totalp unit for geological and organic geochemical studies (Table 3.1). We collected samples from the three main lithologies: serpentinised mantle rock (lizardite, serpentinite gouge and cataclasite), both type of ophicalcites (neptunian dykes and tectono-sedimentary breccias) and associated sediments (Figs. 3.1, 3.2; Table 3.1). Sampling is taken at each outcrop. For

relevant characteristic for each lithology a minimum of three representative sample are required. Samples were oriented, geo-referenced and collected using a geological hammer or a hand drill using water as lubricant. The sample's accuracy is expressed with a Global Positioning System (GPS) using the Garmin eTrex 30x GPS with Western Europe Maps is used. The required sample size is bigger for the organic geochemistry analyses, allowing that the outer part would be removed from the sample. On collection the samples were wrapped in pre-combusted foil (400 °C) for return to the laboratory.

### **3.4.2. Sample preparation**

In order to avoid contamination with modern material the samples were cleaned with de-ionised water (18 MΩ cm<sup>-1</sup> resistivity; Milli-Q) and rinsed with re-distilled dichloromethane (DCM). The outer edges were removed from each sample, which was then cut into smaller pieces using a small rock saw lubricated with water. The aim was to get fresh, unweathered samples for laboratory analysis. These were then used for preparing thin sections and for stable isotope analyses of carbonate veins, with 90 - 110 µg of calcite being extracted using a small electrical hand drill. For organic geochemistry selected pieces were washed with Milli-Q water and DCM, then crushed (to particles <50 µm) using a tungsten Tema Mill, which was previously thoroughly cleaned (Decon-90 solution 2% v/v, milli-Q water, methanol and finally DCM). In order to assess lab contamination, blanks composed of pre-combusted silica gel (600 °C) were subjected to the same procedures as the samples.

Lipid analyses do not allow the description of the entire microbial diversity, however due to the amount and variety of biomarkers in the studied lipids analyses might provide the best way forward for this type of research (Rossel et al. 2008).

### **3.4.3. Mineralogical analyses**

Optical microscopy, cathodoluminescence microscopy (CL; CITL Mk5-2) and X-Ray Diffraction (XRD) were used to identify the mineralogy, chemistry, texture and textural relations within the samples and to associate the mineralogy with the OM.

A Panalytical X'Pert PRO XRD system (CuK<sup>α</sup> radiation, 45 kV, 40 mA) was used to identify the volume proportions of the minerals associated with serpentinisation and the polytypes of the serpentine minerals.

#### **3.4.4. Geochemical analyses**

Analyses of total carbon (TC) and total organic carbon (TOC) were performed before and after decarbonation (10% HCL, 25 °C), respectively, using a Carlo Erba Instrument NC2500 elemental analyser.

Stable isotopic analyses of organic carbon were carried out on five samples of four different lithologies, prepared using a “sealed tube” method and injecting the resulting CO<sub>2</sub> into a VG Sira 10 dual-inlet mass spectrometer (Craig 1957; Frazer and Crawford 1963; Sofer 1980). The standard error for analysis is ± 0.1‰. The isotope data was normalized to IAEA-CH7 calibration material and reported using the VPDB scale. Carbon and oxygen isotope measurements on calcite were performed on material extracted from veins by conversion to CO<sub>2</sub> using a VG SIRA 10 MS Isocarb (common acid bath). The carbon and the oxygen isotope analyses are referenced to the VPDB standard with a standard error for each analysis of ± 0.1‰ (McCrea 1950; Craig 1957; Friedman and O'Neil 1977; Swart et al. 1991).

Soxhlet extraction was used to extract the bitumen from the powdered rocks using DCM: methanol (24 h) (modified after (Wolff et al. 1995)). Full blank extractions were conducted in parallel to identify any possible contamination. After evaporation of the solvent, the extracts were re-dissolved and passed through short columns of alumina and sodium sulphate using hexane as solvent to isolate the hydrocarbons. The eluent from the alumina column was re-dissolved in hexane (50 µL) and analysed by gas chromatography (GC) and GC- mass spectrometry (GC-MS).

For GC-MS we used a GC Trace 1300 and Thermoquest ISQMS single quadrupole fitted with a split-splitless injector, GC column (DB-5MS non-polar 5% phenyl and 95% methyl silicone stationary phase, 60m x 0.25 mm i.d., film thickness 0.1 µm) using helium as a carrier gas (2mL min<sup>-1</sup>). The GC oven temperature was programmed from

60 °C to 170 °C after 1 min at 6 °C min<sup>-1</sup>, then from 170 °C to 315 °C at 2.5 °C min<sup>-1</sup> and finally held at 315 °C for 15 min. GC-MS was carried out in full data acquisition mode, providing mass spectra of compounds eluting from 20 to 90 minutes; these were identified by comparison with the literature and with authentic standards where available (PAHs - polynuclear aromatic hydrocarbons). 5 $\alpha$ (H)-Cholestane was used as an external standard for quantification; response factors were assumed to be 1, hence data are semi-quantitative. Data were processed using XCalibur 1.2 software (ThermoScientific).

The mean carbon numbers, MC# (Peltzer and Gagosian 1989) and the carbon preference index (CPI) of *n*-alkanes (Peters et al. 2005a) were calculated over the carbon number range C<sub>16</sub>- C<sub>40</sub> (Eq. 3.5 and 3.6; Table 3.2).

$$MC\# = \frac{\sum ([C_i] \times C_i)}{\sum [C_i]} \quad (\text{Eq. 3.5})$$

Where [C<sub>i</sub>] = concentration of the *n*-alkane with C<sub>i</sub> carbon number

$$CPI = 0.5 \times \frac{\sum ([\text{odd } C_{21} - C_{35}])}{\sum ([\text{even } C_{20} - C_{34}] + \sum [\text{odd } C_{23} - C_{37}] / \sum [\text{even } C_{22} - C_{36}])} \quad (\text{Eq. 3.6})$$

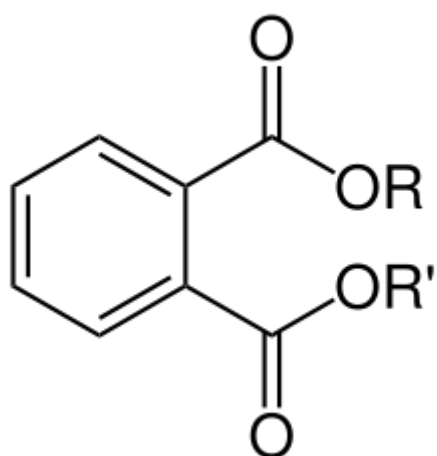


The squalene could be observed in the chromatogram in figure 4.8 c and 4.9 c.

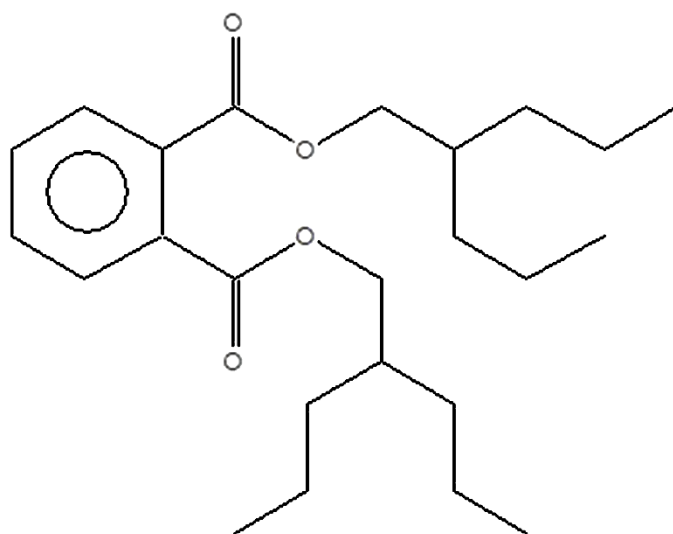
### Phthalate

RT  $\approx$  47

Source : Plastic, vinyl gloves



Phthalic acid, di(2-propylpentyl) ester  
Formula C<sub>24</sub>H<sub>38</sub>O<sub>4</sub>, MW 390, CAS# NA, Entry# 138707  
§:28KIYUVQCUDDMZRE-UHFFFAOYSA-N



56seds\_mm114 #8031 RT: 47.31 AV: 1 SB: 149 51.75-51.95 45.29-45.58 NI: 4.21F7  
T: + c EI Full ms [50.00-600.00]

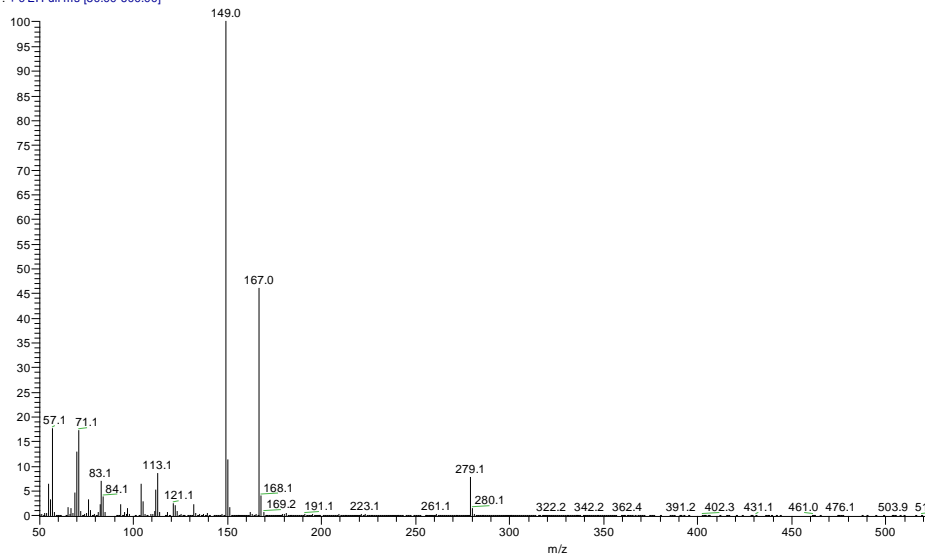


Figure 3.6. Mass spectrum of a phthalate.

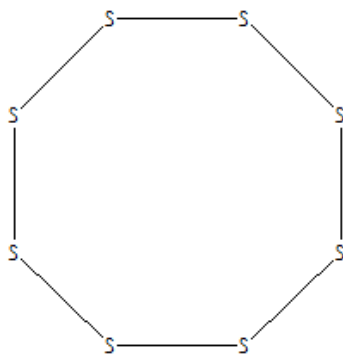
The phthalic acid could be observed in the chromatogram in figure 3.9 b, 3.10 a and 4.9 a.

### Elemental sulphur

RT  $\approx$  32

Ions (m/z) = 256

Cyclic octatomic sulfur  
Formula S<sub>8</sub>, MW 256, CAS# 10544-50-0, Entry# 31817  
Sulfur (S<sub>8</sub>)



Even if the elemental sulphur is not a contaminant in *senso stricto*, its present could decrease the readability of the other molecules present.

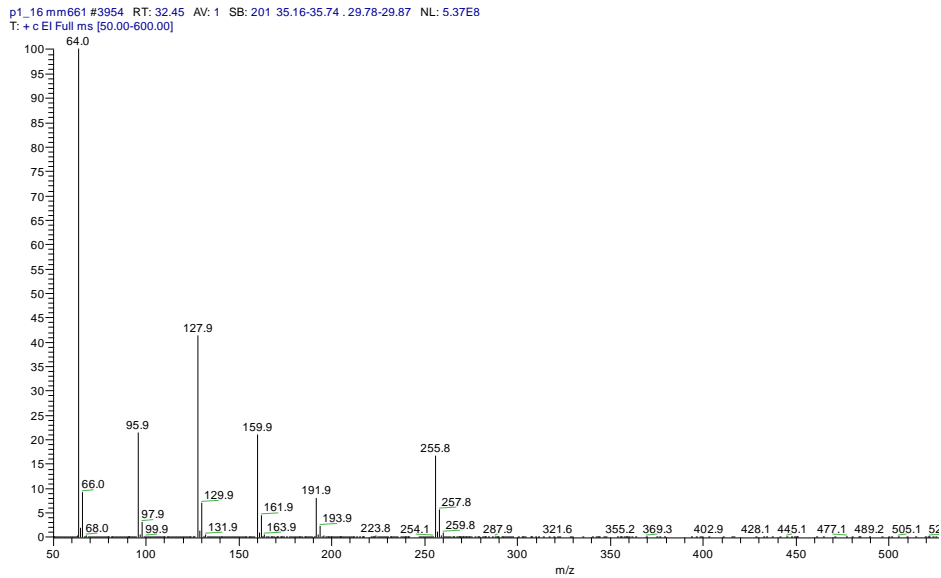


Figure 3.7. Mass spectrum of sulphur.

The elemental sulphur could be observed in the total chromatogram in figure 4.10 a.

### 3.5. Carbon and hydrocarbon distributions in the analysed lithologies

The TOC and TC results are summarized in Table 2 and vary considerably. The TOC values are low, while TC reflect carbonate contents. The stable isotopic composition of carbonate varied from -0.78 to 1.86‰ VPDB and -11.7 to -6.2‰ VPDB for  $\delta^{13}\text{C}$  and  $\delta^{18}\text{O}$ , respectively (Fig. 3.8, Table 3.1). Five decarbonated samples (sample 1 - neptunian dyke, samples 9 and 39 -reworked tectono-sedimentary opicalcite, sample 19 - limestone and sample 69 from the sulphide- rich outcrop) have similar values for  $\delta^{13}\text{C}_{\text{VPDB organic}}$  of between -27.4 and -26.2 ‰ (Table 3.2).

Hydrocarbons (HCs) identified in Totalp samples include *n*-alkanes, steranes, polynuclear aromatic hydrocarbons (PAHs), hopanes and isoprenoids, namely

pristane and phytane. Results from organic geochemical analyses do not show the presence of any specific methanotrophic biomarkers, so it is assumed that if these biomarkers exist, they are below the analytical detection limit. Samples of the same lithology do not necessarily have similar distributions of HCs (Table 3.2). This may reflect the heterogeneity of the samples collected, for example in the relative amount of carbonate, calcite veins and serpentinite clasts.

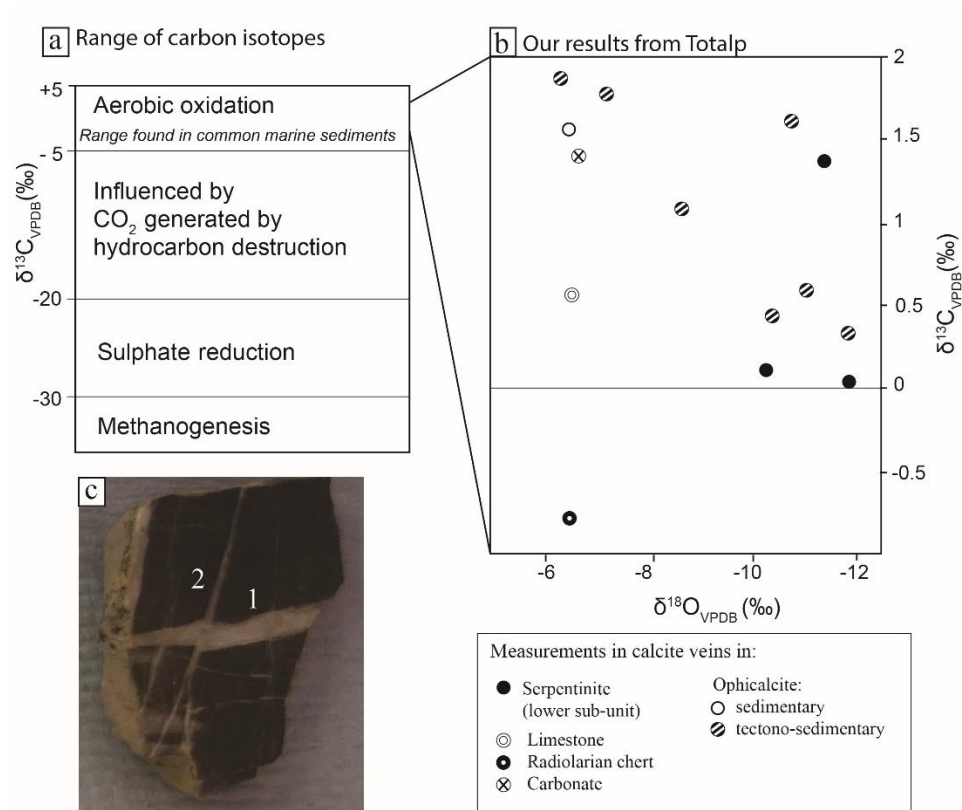


Figure 3.8. a) Global range of carbon isotopic composition of carbonates precipitated during early diagenetic processes (modified after Coleman et al. 1993;(Kiriakoulakis 1997); Heydari 1997) b) Carbon and oxygen isotopic composition of calcite veins in Totalp samples. c) Limestone (sample 19) showing two generation of calcite veins.

Table 3.1. Results by lithology including mineralogy and texture observed in hand specimens and the texture on the calcites used for the isotopic analyses ( $\delta^{13}\text{C}_{\text{VPDB}}$ ,  $\delta^{18}\text{O}_{\text{VPDB}}$ ). The vein generation is defined from the specific example and may not correlate across all samples. <sup>1</sup> Thin section of the lithology is observed. • All lithology are from the lower sub-unit with the exception of the massive serpentinite (samples 77, 78).

rock type	sample number	coordinates (UTM)		locality	macroscopic description	mineralogical description	texture	Carbonate texture	$\delta^{13}\text{C}_{\text{VPOB}}$ (‰) Ca veins	$\delta^{18}\text{O}_{\text{VPOB}}$ (‰) Ca veins	
		X (m)	Y (m)								
<b>Serpentinite</b>											
Massive serpentinite	5	561895	5188662	Parsennfurugga	massive black serpentinite with white Olivine completely replace by angular borders defining the ex-serpentine minerals, phantoms of peridotite minerals, small green pyroxene, magnetite, later chrysotile veinlets and white carbonate carbonate vein; calcite veins with veinlets	Broken serpentinite clasts from a first mainly mesh texture with rare generation of greyish deformed calcite ribbon texture; randomly supported breccia <sup>1</sup> by a second generation of white calcite grain; later veins of chrysotile veins	mesh <sup>1</sup>	calcite vein, 1 <sup>st</sup> generation	0.11	-10.2	
Serpentinite with numerous calcite veins	16	561522	5188399	2442m. Obersasställi Parsennfurugga							
	24	561514	5188009	Obersasställi							
	26	561504	5188010								
	44	561518	5188415	2442m. Obersasställi							
	47	561540	5188427	Parsennfurugga							
Red serpentinite	71	561588	5188095	2442m. Obersasställi Parsennfurugga	red matrix with dark-black deformed the serpentinite is lizardite clasts/veins with numerous calcite containing also talc and calcite; veins, also contain dark green the red colour is due to hematite serpentinite.	red serpentinite breccia	red	calcite vein, 2 <sup>nd</sup> generation	1.37	-11.3	
Serpentinite gouge	69	561929	5187152	Obersasställi	black fine-grained deformed serpentinite with equant grain following and distributed systematically and fine short veinlets (chrysotile; calcite)	fine grained					
Serpentinite catadasite	70	561929	5187152	Obersasställi	black serpentinite with subangular serpentine clasts showing no preferred orientation	fine grained					
Massive serpentinite *	77	561482	5187004	Weissfluhjoch	black serpentinite with sub-rounded anhydral white-grayish peridotite mineral (pyroxene) and small chrysotile veins	mesh					
	78	561482	5187004								
<b>Sedimentary ophicalcite</b>											
Limestone (Neptunian dykes)	1	561543	5188408	2442m. Obersasställi Parsennfurugga	fine micritic pink and red pelagic three types of carbonate crystal limestone; serpentine minerals as clasts growing; the matrix composed of and veins	paraphro-clastic <sup>1</sup>		calcite vein, 2 <sup>nd</sup> generation	1.56	-6.4	
	23	561514	5188009	Obersasställi							
<b>Tectono-sedimentary ophicalcite</b>											
Tectono-sedimentary ophicalcite	21	561520	5188015	Obersasställi	red fine carbonate matrix with black serpentinite clasts broken by fine grained anhydral serpentinite broken clasts several generation of carbonate veins; several stage of crystal growing for the carbonate;			calcite vein, 1 <sup>st</sup> generation	0.32	-11.7	
	25	561511	5188009					calcite vein, 1 <sup>st</sup> generation	0.58	-10.9	
	39	561515	5188439	2442m. Obersasställi Parsennfurugga				calcite vein, 2 <sup>nd</sup> gener.	1.78	-7.1	
	41	561572	5188406					calcite vein, 1 <sup>st</sup> and 2 <sup>nd</sup> gener.	0.42; 1.07	-10.3; -8.6	
	42	561572	5188406								
	46	561540	5188418								
	66	564260	5190402	near Grüenhorn				calcite vein, undetermined generation	1.86	-6.2	

rock type	sample number	coordinates (UTM)		locality	macroscopic description	mineralogical description	texture	Carbonate texture	$\delta^{13}\text{C}_{\text{VPDB}}$ (‰) Ca veins	$\delta^{18}\text{O}_{\text{VPDB}}$ (‰) Ca veins
		X (m)	Y (m)							
Reworked tec-sed. ophicalcite	9	562586	5188578	Parsennfurga-Parsennhütte	pink carbonate with randomly orientated elongated clast of ophicalcite (serpentine+carbonate); numerous calcite veins	no thin section or XRD	<i>reworked<sup>1</sup></i>			
	72	561929	5187152	2442m. Obersasställi Parsennfurga	centimetric angular clasts of green serpentine tectonically broken by calcite veins	no thin section or XRD	<i>vein supported breccia</i>	calcite vein, undetermined generation	1.60	-10.6
<b>Sediments</b>										
Radiolarite	62	564212	5190386	near Grünhorn from sulphide rich outcrop	hard fine grained red siliceous rock ; post deposition quartz vein perpendicular to the geometry of deposition	no thin section or XRD	<i>fine grained</i>	post-deposit calcite vein	- 0.79	-6.4
	68	564252	5190393							
Siliceous shale	60	564212	5190386	near Grünhorn from sulphide rich outcrop	greyish - reddish fine grained siliceous rock, great porosity and numerous fractures	composed mainly by quartz (46%), plagioclase(30%), chlorite, muscovite and hematite	<i>fine grained</i>			
	61	564212	5190386							
Limestone	15	564049	5189517	Gotschnagrat	red and grey fine grained intercalated siliceous shale with deformed quartz veins	dominated by quartz (89%) with plagioclase, muscovite, chlorite and trace of hematite	<i>fine grained</i>			
	18	564213	5189544							
Limestone	10	562494	5188558	Parsennfurga-Parsennhütte	grey limestone with numerous calcite veins of two generation almost perpendicular to each other	pelagic limestone, evidence of fossil organisms filled by sparry calcite	<i>fine grained</i>			
	19	563790	5189694	Gotschnagrat				calcite vein, 1 <sup>st</sup> generation	0.56	-6.5
Limestone	53	563144	5188716	south from Parsennhütte	grey limestone with fine veinlets and rare short calcite veins with places	no thin section or XRD	<i>fine grained</i>			
	54	563140	5188707							
	56	563140	5188707							
	57	563144	5188716							
	58	563144	5188716							
Carbonate (Sulphide rich outcrop)	63	564212	5190386	near Grünhorn	carbonate rock with deformed quartz veins; microscopic grain everywhere except in the quartz and calcite veins	dominated by calcite (53%) with quartz, chlorite (12%) and pyrite.	<i>porphyro-clastic</i>			
	64	564212	5190386					calcite vein, 2 <sup>nd</sup> generation	1.4	-6.6
	65	564252	5190393		very fractured sample with greater porosity					

Aliphatic compounds (> C15), mainly in the form of *n*-alkanes dominate (Fig. 3.9 a). The CPI (carbon preference index) for the *n*-alkanes are in the range  $1 \pm 0.3$ , except for two samples that were visibly weathered, having CPI = 2.6 - 2.87, i.e. an odd over even ratio for the *n*-alkanes confirming contamination from modern material, such as soil (e.g. (Villanueva et al. 1997)). Steranes included 20R and 20S  $\alpha\beta\beta$  isomers from C<sub>27</sub> to C<sub>29</sub>, as well as 20 R and S diacholestane and pseudohomologues (Fig. 3.10 b). The steranes were dominated by C<sub>27</sub> compounds with a lower abundance of C<sub>28</sub> and C<sub>29</sub> pseudo-homologues (Fig. 3.10 b). The ranges of values for the thermal maturity parameters of the C<sub>27</sub> steranes are between 0.41 and 0.69 for ST1 =  $\alpha\alpha\alpha$  20S/ $\alpha\alpha\alpha$ 20S+  $\alpha\alpha\alpha$  20R and 0.37 and 0.59 for ST2 =  $\alpha\beta\beta$ / $\alpha\alpha\alpha$ + $\alpha\beta\beta$  (Fig. 6; (Seifert and Moldowan 1980; Peters et al. 2005b)). PAHs having molecular masses  $\leq 276$  were identified in some of the bitumen extracts (Table 3.2; Fig. 3.10 c)

### 3.5.1. Serpentinite

All serpentinite samples contain *n*-alkanes, and several PAHs in the form of phenanthrene (P) and fluoranthene (Fluo); steranes and hopanes were largely absent (Table 3.2).

#### 3.5.1.1. Upper ultramafic sub-unit

##### *Massive serpentinite*

The massive serpentinites collected from the Weissfluhjoch (samples 77, 78; Fig. 3.1c; Table 3.1) area have HC concentrations between 0.05 to 4 ppb while the C<sub>29</sub> *n*-alkane dominates their distribution (C<sub>max</sub>=29; Table 3.2). Total carbon (454 ppm) and total organic carbon (TOC) ( $\approx 180$  ppm) concentrations are both very low.

#### 3.5.1.2. Lower ultramafic sub-unit

##### *Massive serpentinite*

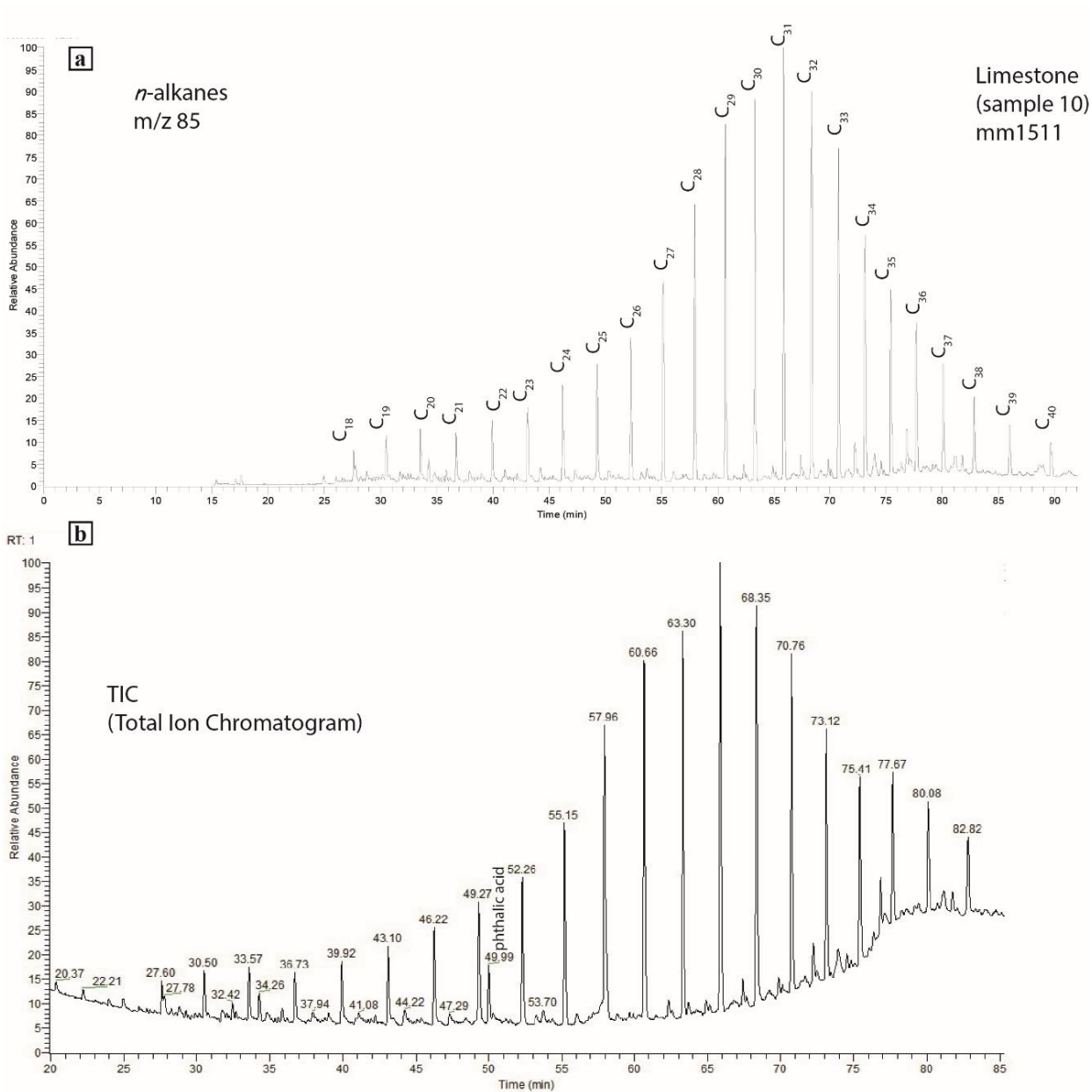


Figure 3.9. Representative mass chromatograms of the HCs of a typical sample of limestone (sample 10) a) *n*-alkanes (m/z 85) of sample 10 (limestone) b) Total Ion Chromatogram of sample 10

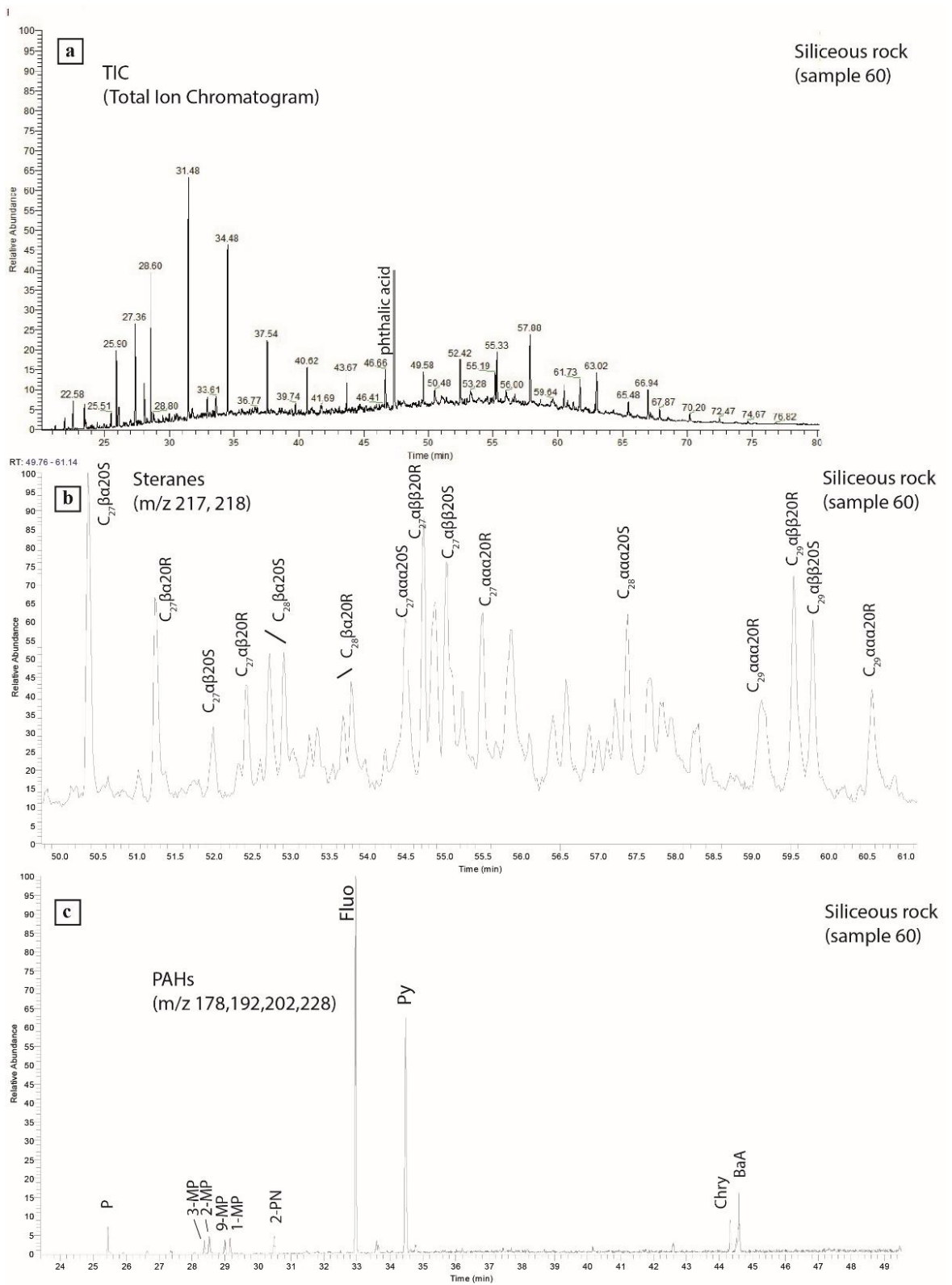


Figure 3.10. Representative mass chromatograms of the HCs of a typical sample of a siliceous rock from the sulphide rich outcrop of Totalp (sample 60). a) Total Ion Chromatogram of sample 60 b) sterane distribution (m/z 217, 218) of sample 60 c) PAH distribution (m/z 178, 192, 202, 228) of sample 60. For abbreviations see appendix.

XRD analysis shows a lizardite polytype 1 (Bailey 1969) (87%), garnet (andradite) (7%) and pyroxene (clinopyroxene) (5%). In thin section olivine is completely replaced by serpentine minerals, with phantoms of pyroxene, euhedral magnetite, spinel and several calcite and carbonate veins not visible to the naked eye (Table 3.1).

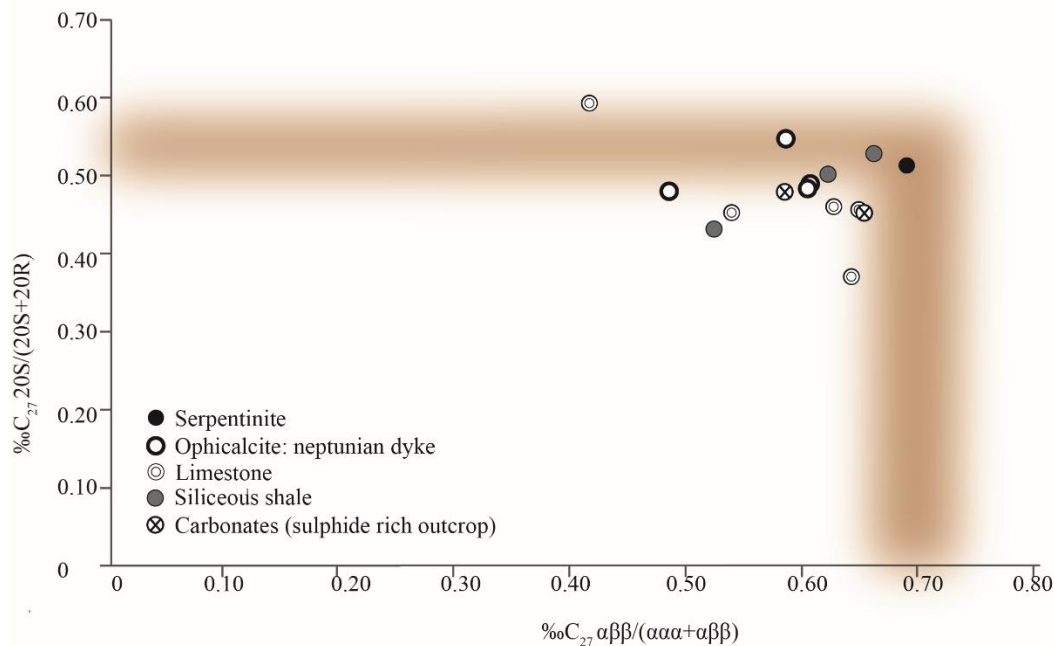


Figure 3.11. Thermal maturity parameters of C<sub>27</sub> steranes for Totalp samples. The classification is from Peters et al., 2005. The brown shaded area represents the range of complete isomerization for the 20S/(20S + 20R)  $\alpha\alpha$  C<sub>27</sub> steranes (ca. 55%) and  $\alpha\beta/(\alpha\alpha + \alpha\beta)$  C<sub>27</sub> steranes (ca. 68%).

HC concentrations vary from 23 ppb for the serpentinite from Parsenfurrga (sample 5) to 900 ppb from an outcrop with ophicalcite in Obersasställi (sample 16; Fig. 3.1c; Table 3.2). The TOC values range from 102-176 ppm and TC from 395-3134 ppm; steranes and hopanes are below detection limits (BDL) (Table 3.2). Serpentinite samples showing numerous calcite veins (sample 24, 26, 44 and 47) have higher amounts of TC (20400 to 42500 ppm). They show variable TOC (19 to 135 ppm) and low HC concentrations (1- 124 ppb). In the lower ultramafic sub-unit a red colored serpentinite was identified by XRD to contain hematite (4%) (Table 3.1). The serpentine mineral is a lizardite polytype 1 (59%), also containing talc (18%) and

calcite (19%). The isotopic composition of the calcite in the veins is 0.03‰ and -11.75‰ for  $\delta^{13}\text{C}_{\text{VPDB}}$  and  $\delta^{18}\text{O}_{\text{VPDB}}$ , respectively (Fig. 3.8).

### *Serpentine cataclasite and gouges*

The serpentine cataclasites and gouges have TC of 540-875 ppm, *n*-alkanes with a carbon number range of C<sub>17</sub>-C<sub>36</sub> and no detectable steranes or hopanes (Tables 3.1, 3.2). The serpentine cataclasites (sample 70), which are less deformed than the serpentine gouge (sample 69), contain more hydrocarbons (46 ppb and 3 ppb, respectively Table 3.2) but similar TOC contents (284 and 269 ppm, respectively).

## **3.5.2. Opicalcite**

The opicalcites from the Totalp unit all contain *n*-alkanes and the PAHs (P, Fluo and Pyr, see glossary; Table 3.2). Steranes and hopanes are also present in the majority of samples.

### 3.5.2.1. Neptunian dykes

The neptunian dykes samples have a red micritic limestone matrix with millimeter-scale serpentinite clasts and calcite veins (samples 1, 23) (Fig. 3.1c, Table 3.1). The  $\delta^{13}\text{C}_{\text{VPDB organic}}$  of one of the samples (sample 1) was -27.1‰ (Table 3.2). There are high amounts of TC with variable TOC (15 to 103 ppm) and HC concentrations (0.3 – 121 ppb) (Table 3.2).

### 3.5.2.2. Tectono-sedimentary opicalcites

The tectono-sedimentary opicalcite has various sub-lithologies from a reworked tectono-sedimentary breccia with folded serpentinised and carbonate clasts in a red carbonate matrix cross-cut by calcite veins (sample 9) to centimeter scale serpentinite clasts in a carbonate vein (sample 72) (Fig. 3.1c) (Table 3.1). The stable isotopic composition  $\delta^{13}\text{C}_{\text{VPDB organic}}$  of one of the samples was -26.1‰ (sample 9) (Table 3.2). A second type of opicalcite, a serpentinite breccia composed only of serpentinite clasts fragmented by calcite veins has low TOC (30 ppm) and HCs concentrations (124 ppb) including only *n*-alkanes (sample 72) (Table 3.2). The

isotopic compositions of the calcite veins surrounding the serpentinite clast are 1.60‰ and -10.6‰VPDB for  $\delta^{13}\text{C}$  and  $\delta^{18}\text{O}$ , respectively. The third most common ophicalcite is composed of anhedral serpentinite clasts, carbonate veins, calcite veinlets in a reddish pelagic matrix and has a low amount of TOC (11-116 ppm), but high concentrations of HCs (2-2470 ppb) (samples 21, 25, 39, 41, 42, 44, 66; Fig. 3.1c; Tables 3.1, 3.2). The isotopic composition of the samples varies from  $\delta^{13}\text{C}_{\text{VPDB}} = 0.32\text{‰}$ ,  $0.42\text{‰}$  and  $0.58\text{‰}$  with  $\delta^{18}\text{O}_{\text{VPDB}} = -11.75\text{‰}$ ,  $-10.28\text{‰}$  and  $-10.9\text{‰}$  (for samples 25, 42 and 39 respectively) to  $\delta^{13}\text{C}_{\text{VPDB}} = 1.07$  and  $1.78\text{‰}$  with  $\delta^{18}\text{O}_{\text{VPDB}} = -11.7$  to  $-7 \text{‰}$  for samples 42 (second generation calcite vein) and 41 (Fig. 3.8, Table 3.1). Isotopic analysis of organic carbon (sample 39) gave  $\delta^{13}\text{C}_{\text{VPDB organic}} = -27.4\text{‰}$  (Table 2). The ophicalcite outcrop near the Gotschnagrat NE Totalp has isotopic values for calcite veins of  $1.86\text{‰}$  for  $\delta^{13}\text{C}_{\text{VPDB}}$  and  $-6.2\text{‰}$  for  $\delta^{18}\text{O}_{\text{VPDB}}$  (sample 66).

### 3.5.3. Sediments

Limestones are, together with radiolarian cherts, the most common sediments in the Totalp unit. All of the sediment samples contain detectable levels of HCs including PAHs.

#### 3.5.3.1. Radiolarian cherts

The radiolarian cherts are situated mostly around the Gotschnagrat NE Totalp (samples 62, 68) and along small distributed outcrops some of which are 1-2 m in length and located between Parsennfurgga and Parsenhütte (sample 6; Fig. 3.1c). Except for the weathered sample, they have very low concentrations of HCs (1 -17 ppb) and low TOC values (66-187 ppm) (Table 3.2). The radiolarian cherts are hard, fine grained siliceous sediments that are transected by post-depositional quartz and calcite veins, the latter having isotopic compositions of  $\delta^{13}\text{C}_{\text{VPDB}} = -0.79\text{‰}$  and  $\delta^{18}\text{O}_{\text{VPDB}} = -6.4\text{‰}$  (Sample 62; Table 3.1; Fig. 3.8).

Table 3.2. Results by lithology including TC, TOC in ppm (parts per million), total HC concentration in ppb (parts per billion) and organic carbon isotopic composition of bulk rock  $\delta^{13}C_{\text{organic}}$ . For the n-alkanes: the carbon number range (n-alkane range), the maximum carbon number (Cmax), carbon preference index (CPI values) and mean carbon number (MC#) are shown. For the steranes, hopanes and PAHs the concentrations are in ppb and are represented in intervals by star symbol \*, where \* = [0 - 0.1), \*\* = [0.1 - 1) and \*\*\* = [1 - 10) and BDL = below detection limit. a: identified PAHs in the samples were: Phenanthrene, P; Fluoranthene, Flu; Pyrene, Pyr; Chrysene, Chry; Benzo(a)anthracene, BaA; Benzo(b)fluoranthene, BbF; Benzo(a)pyrene, BaP; Indeno(1,2,3-cd)pyrene, IndPy; Benzo(ghi)perylene, BghiP; Dibenzothiophene (DBT), methylP (3,2,1 and 9 MPs) and 2-methyl naphthalene; not all were present in every sample. 1 All lithology are from lower sub-unit except the massive serpentinite (samples 77, 78) which is from upper sub-unit

	sample number	Total Carbon ppm	Total C <sub>organic</sub> ppm	Hydrocarbons (HC) ppm	n-alkanes			$\delta^{13}C_{\text{VPDB}}$ (‰) on TOC	Steranes	Hopanes	PAH*
					Range	C <sub>max</sub>	CPI				
<b>Serpentinite</b>											
Massive serpentinite	5, 16	395- 3135	102 - 176	23-900	16-39	C <sub>20</sub> , C <sub>29</sub>	0.76 - 1.29	20 - 28	BDL	BDL	*
Serpentinite with numerous Ca veins	24, 26, 44, 47	20400-42500	19 - 135	1 - 124	16 - 35	C <sub>20</sub> , C <sub>26</sub>	0.8 - 1.05	22 - 28	BDL	BDL	*
Red serpentinite (with hematite)	71	88205	268	1	17-35	C <sub>26</sub>	1.17	22.3	BDL	BDL	**
Serpentinite gouge	69	539	284	3	17-33	C <sub>29</sub>	0.94	26.0	BDL	BDL	*
Serpentinite cataclasis	70	876	269	46	17-36	C <sub>20</sub>	0.94	24.1	BDL	BDL	**
Massive serpentinite <sup>1</sup>	77, 78	454	≈ 190	0.05-4	17-40	C <sub>29</sub>	0.84 - 0.97	29 - 30	BDL	BDL	*
<b>Ophicalcite</b>											
<i>Sedimentary ophicalcite</i>											
Neptunian dykes	1, 23	95600 - 107500	15 - 103	0.03 - 121	17 - 35	C <sub>29</sub>	1.05	27 - 29	**	**	**
<i>Tectono- sedimentary ophicalcite</i>											
Red matrix, serp. claste and Ca veins	21, 25, 39, 41, 42, 46, 66	33360 - 101700	11 - 116	2 - 2470	17-38	C <sub>18</sub> to C <sub>28</sub>	0.81 - 1.42	23 - 31	**	**	**
Reworked tec-sed. Ophicalcite	9	106000	86	50	16-36	C <sub>22</sub>	0.65	24	BDL	*	**
Serp.clasts in Ca veins	72	69600	30	124	20-36	C <sub>29</sub>	0.90	28	BDL	BDL	BDL
<b>Sediments</b>											
Radiolarite from sulphide rich outcrop	62, 68	671 - 13200	66-187	1 - 17	17 - 34	C <sub>20</sub> C <sub>31</sub>	1.19-2.87	24 - 28	BDL	**	*
Siliceous shale from sulphide rich outcrop	60, 61	384 - 672	194 - 433	22-144	16 - 37	C <sub>20</sub> C <sub>27</sub>	1.05 - 1.52	23 - 25	**	**	**
Siliceous shale near sulphide rich outcrop	15, 18	285 - 318	136 - 145	13 - 27	16-33	C <sub>18</sub> , C <sub>20</sub>	0.95 - 1.19	23 - 24	*	*	BDL
Limestones	10,19	98200 - 129000	74 - 82	79 - 171	16-35	C <sub>22</sub> , C <sub>27</sub>	0.92 - 0.94	23 - 27	BDL	BDL	***
Limestone from Pارسننھتے	53, 54, 56, 57, 58	46500 - 94500	14 - 92	3 - 238	16 - 37	C <sub>23</sub> , C <sub>29</sub>	0.82 - 1.10	22 - 23	*	*	**
Sulphide rich outcrop	63, 64, 65	442 - 90400	153 - 647	1 - 24	17-33	C <sub>20</sub> C <sub>27</sub>	0.93 - 1.55	23 - 26	**	**	**

#### 3.5.3.2. Siliceous shales

The siliceous shales are situated mostly above Parsennhütte and around the Gotschnagrat (samples 15, 18, 60, 61; Fig. 3.1c). XRD analysis of the siliceous shales (sample 61) above the pyrite rich area have mineralogy of quartz (83%), albite (10%), pyrite (2%), illite/muscovite (4%), chlorite and hematite. This composition is similar to the siliceous shale (samples 15, 18) found nearby, which consists of quartz (89%), plagioclases (6%), illite/muscovite (4%), chlorite and trace of hematite (Fig. 3.1c; Table 3.1). They have low concentrations of HCs (13 – 144 ppb) and variable amounts of TOC (194-433 ppm) (Table 3.2).

#### 3.5.3.3. Limestone

Samples (53 -57) are pelagic grey limestones that contain visible calcite veinlets and fine greyish veinlets (serpentinite) from the syncline in the Parsennhütte (Fig. 3.1c) (Table 3.1). They contain a low amount of TOC (14-92 ppm) and variable concentrations of HCs (Table 3.2).

The pelagic limestones with higher amount of calcite veins (samples 10, 19) are also poor in TOC (74- 82 ppm) and contain HCs from 79 to 171 ppb (Fig. 3.1c; Tables 3.1, 3.2). Isotopic analyses of the first generation of calcite veins in sample 19 show  $\delta^{13}\text{C}_{\text{VPDB}} = 0.56\text{‰}$  and  $\delta^{18}\text{O}_{\text{VPDB}} = -6.5\text{‰}$  and  $\delta^{13}\text{C}_{\text{VPDB organic}} = -26.6\text{‰}$  (Fig. 3.8; Table 3.1).

#### 3.5.4. Silica – rich carbonate (sulphide-rich outcrop)

The mineralogy of the pyrite rich rocks is dominated by calcite (53%) with quartz (24%), chlorite (12%) and pyrite (6%) being the other main minerals (sample 63, 64, 65; Figs. 3.1c, 3.4; Table 3.1). The samples were on the top of the radiolarian chert and red shale sequences where the contact between these rocks are weathered and not affected by deformation (Fig. 3.4). Isotopic composition of organic carbon is  $\delta^{13}\text{C}_{\text{VPDB organic}} = -26.02\text{‰}$  (sample 64) and of the calcite veins in the same sample 1.4‰ for  $\delta^{13}\text{C}_{\text{VPDB}}$  and -6.6‰ for  $\delta^{18}\text{O}_{\text{VPDB}}$  (Table 3.1). The samples are characterized by a TOC contents from 153 to 647 ppm and low HC concentrations (1 – 24 ppb)

(Table 3.2); bitumen extracts are dominated by elemental sulphur, but HCs include *n*-alkanes, PAHs (P, Fluo, MPs) and steranes (Table 3.2).

### **3.6. Interpretation and discussion**

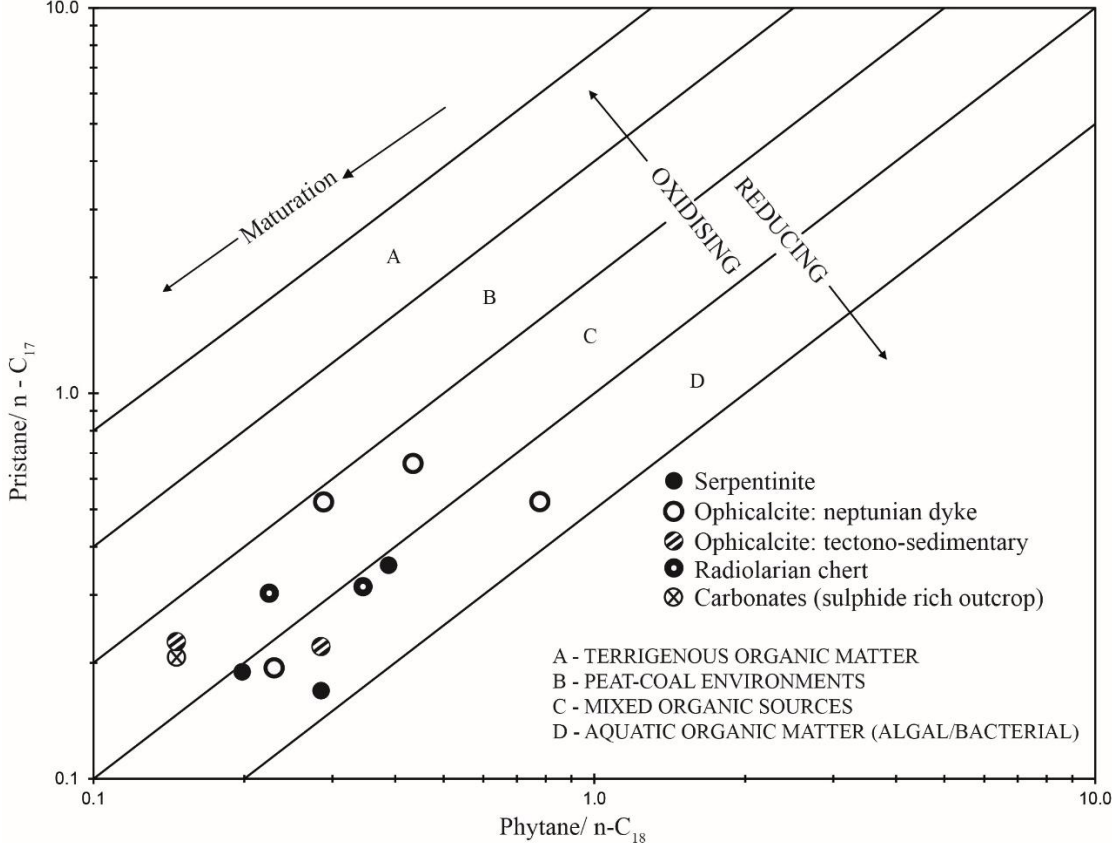
We found traces of OM in the serpentinised exhumed mantle with a composition consistent with a marine origin. The generally low and variable amounts of TOC reflect the large lithological diversity of the Totalp area, and the distributions of hydrocarbons are consistent with the temperature history of the Totalp unit (*i.e.* no metamorphic overprint) (Table 3.2; Fig. 3.9 – 3.11).

#### **3.6.1. Source of OM**

A cross-plot of Pristane (Pr) to *n*-C<sub>17</sub> versus phytane (Ph) to *n*-C<sub>18</sub> is commonly used to determine the depositional environment of OM in sedimentary rocks (Peters et al. 2005b). For the Totalp samples (Fig. 3.12), this cross-plot implies a reducing (anoxic) depositional environment for the OM, with a marine source of planktonic algal/bacterial OM consistent with a marine mixed transitional environment that might be expected at this fossil OCT. Sterane ternary diagrams are also commonly used to provide information on the source of OM in sedimentary rocks (Peters et al. 2005a). Comparison of Totalp steranes with predicted distributions of source materials (Fig. 3.13) are consistent with a mixed marine source of planktonic algal and bacterial OM (Gonçalves et al. 2013; Wójcik-Tabol and Ślącza 2015) and are similar to OM deposited in marine settings during and since the Jurassic (Grantham and Wakefield 1988; Wójcik-Tabol and Ślącza 2015). Such a source for OM in the radiolarian cherts reflects the dominant planktonic signature of coccoliths and nanoconids (Manatschal et al. 2003). The variability in the sterane distributions most likely reflects spatial and temporal variability in environmental conditions during OM deposition.

In five samples (ophicalcite, limestone and samples from the sulphide bearing outcrop) with enough TOC to allow measurement of its stable isotopic composition, the determined values of  $\delta^{13}\text{C}_{\text{VPDB organic}}$  of *ca.* -26.2 to -27.4‰ (Table 3.2) are again

consistent with an origin from marine OM ( $-26\text{‰} \pm 7\text{‰}$ ) ((Schidlowski 1988; Hayes et al. 1990)) and are similar to those found in hydrothermal systems from the Galapagos ( $\delta^{13}\text{C} = -27.4\text{‰}$ ) and the Guaymas Basin ( $\delta^{13}\text{C} = -25\text{‰}$  to  $-21\text{‰}$ ) ((Orem et al. 1990)). Orem et al. (1990) argued that the OM in these hydrothermal systems derived from chemoautolithotrophic bacterial production. The carbon isotopic composition of methane in modern hydrothermal vents ranges from  $-8.8$  to  $-19.6\text{‰}$  ( e.g. TAG  $26^\circ\text{N}$   $-8/-9.5\text{‰}$ , Rainbow  $36^\circ14'\text{N}$   $-15.8\text{‰}$ , see (Charlou et al. 2002); Lost City  $30^\circ\text{N}$   $-13.6$  to  $-8.8\text{‰}$ , (Kelley et al. 2005; Bradley and Summons 2010)). Fixation of hydrothermal methane by methanotrophs would be expected to lead to OM more depleted in  $^{13}\text{C}$



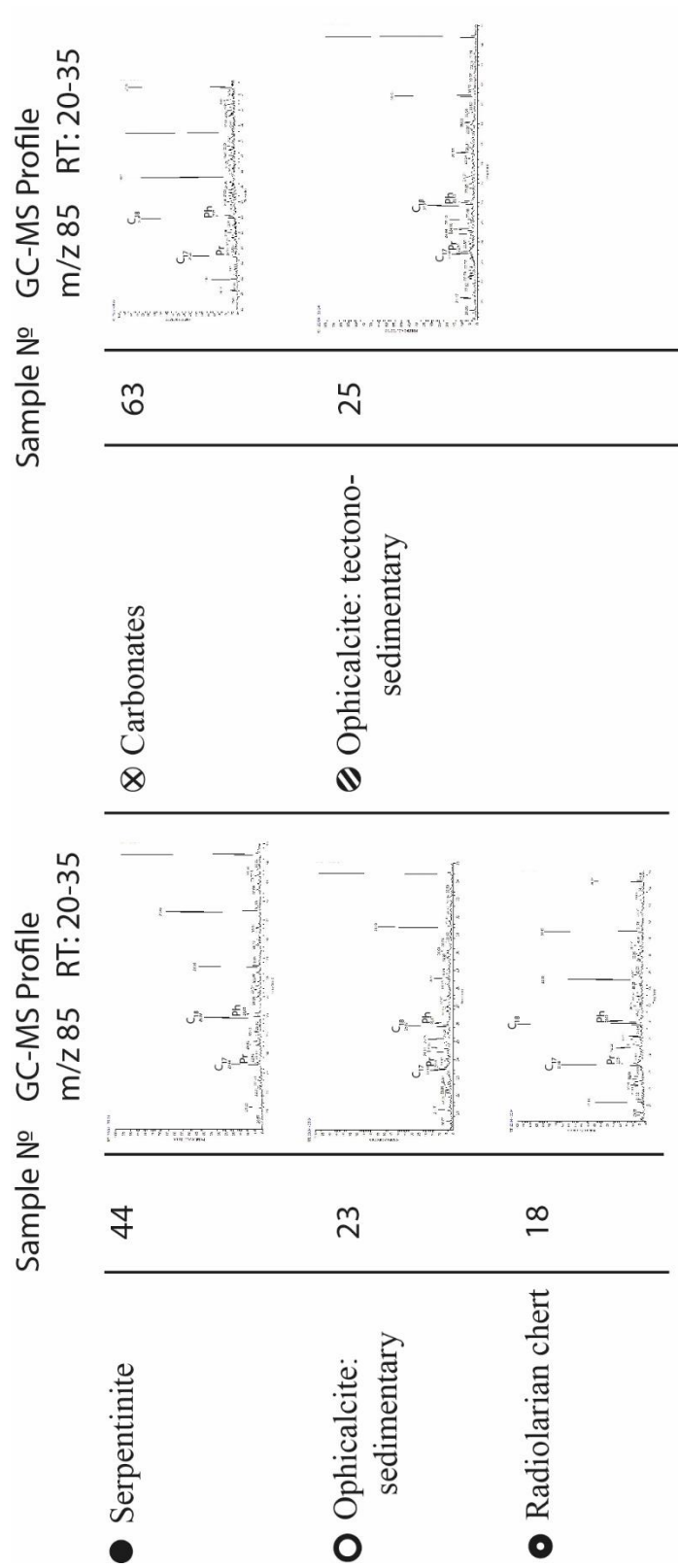
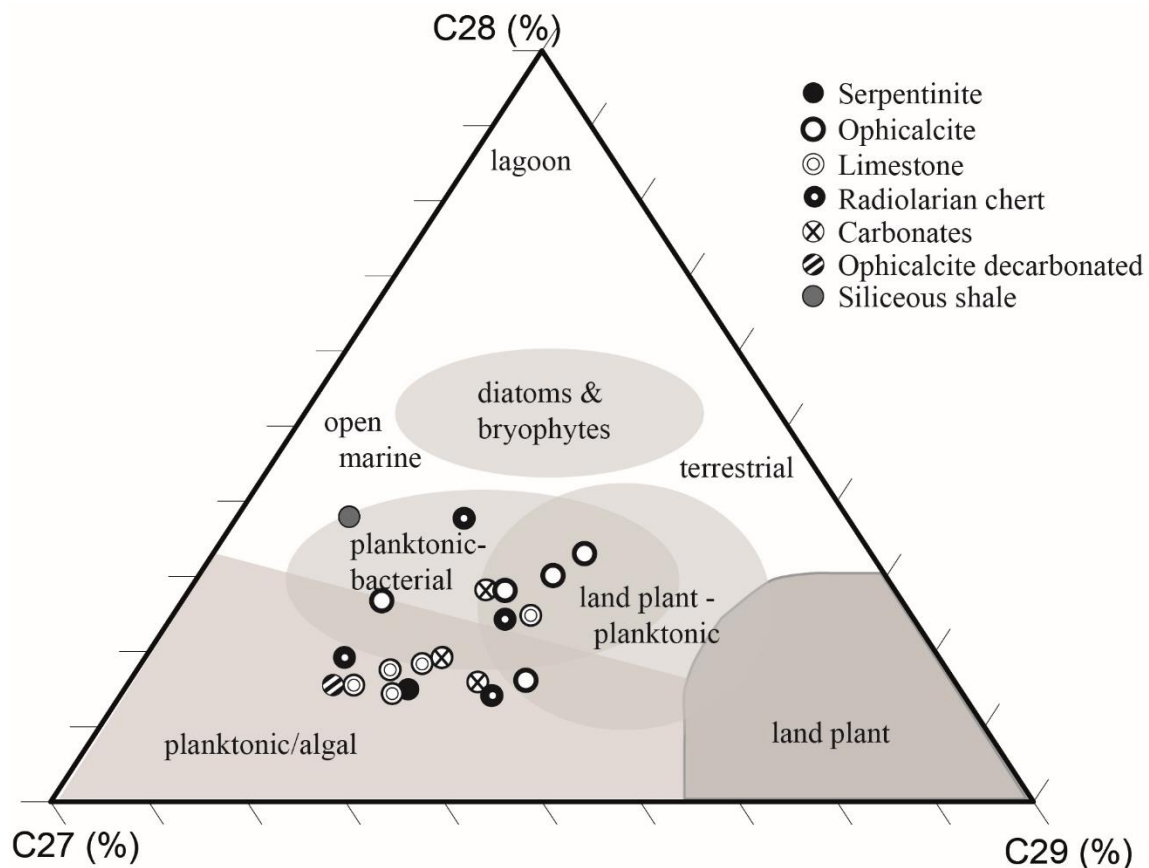


Figure 3.12. Plot of pristane/n-C<sub>17</sub> vs phytane/n-C<sub>18</sub> for Totalp samples used to identify depositional environment and OM type (after (Peters et al. 1999)). A gas chromatogram from each group is presented with retention time 20 to 35.

by 15 - 30‰ (Summons et al. 1994; Schidlowski 2001; Templeton et al. 2006), i.e. in the range -23.8 to -34.6‰ assuming the most conservative fractionation.

The isotopic composition ( $\delta^{13}\text{C}_{org}$ ) of OM at Lost City is -28.9‰ to -21.5‰ i.e. typically marine, yet methanotrophy is established there using biomarkers e.g. squalene (Delacour et al. 2008b). It is difficult to find isotopic evidence of methanotroph, because of the dominance of marine OM. Therefore, the  $\delta^{13}\text{C}_{VPDB\ organic}$  could be used only as an additional method due to its limitation.

Hence, isotopic data from the Totalp samples suggests that there could be a contribution from methanotrophic biomass, however the values are also consistent with marine-derived OM. Taken together with the molecular data and in the absence of specific methanotrophic biomarkers (e.g. crocetane), we consider that the Totalp hydrocarbons derive from marine OM.



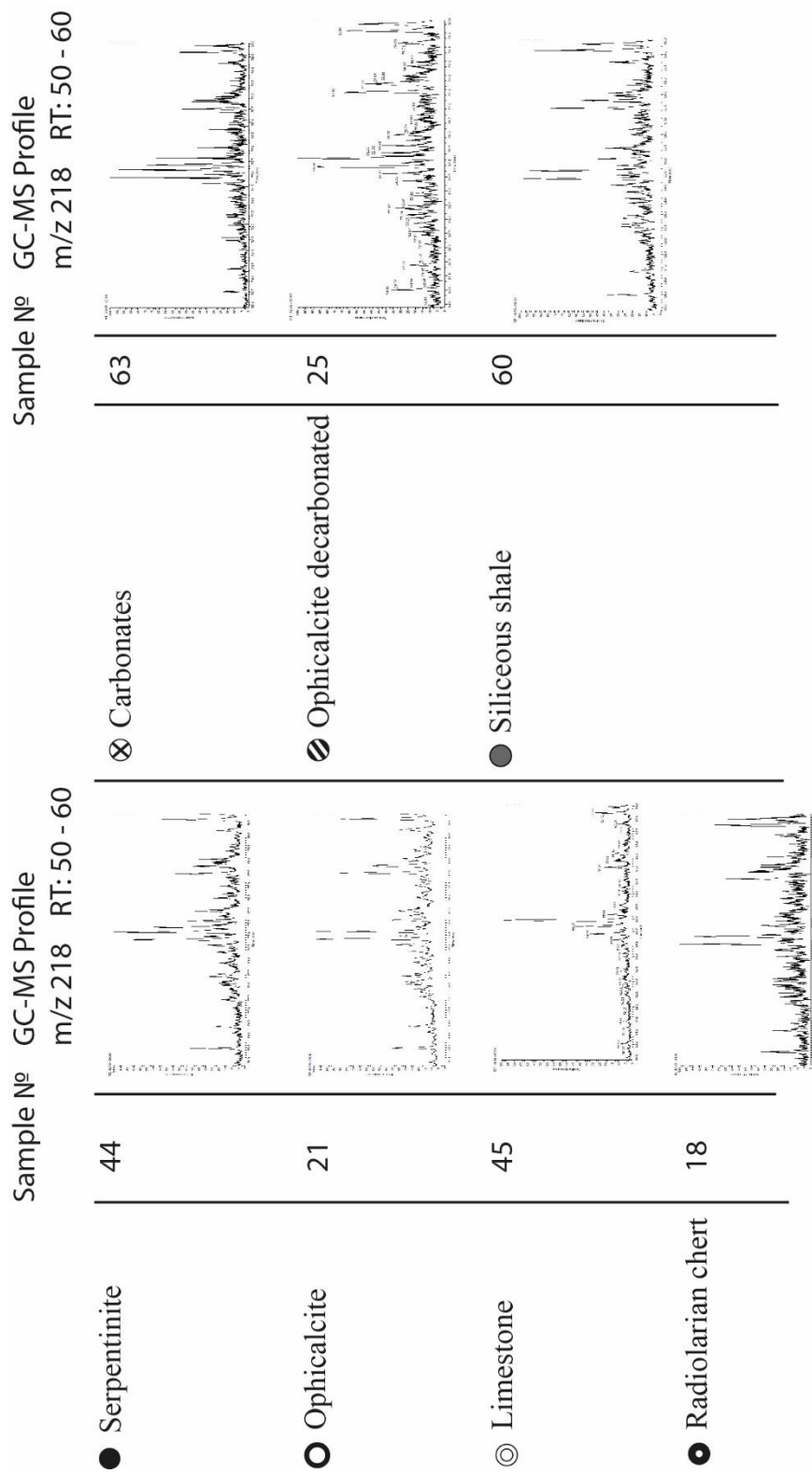


Figure 3.13. Sterane ternary distribution of the analyzed samples for the  $\alpha\beta$  steranes of Totalp samples. The interpretation of depositional environment is from Patrycja Wójcik-Tabol & Ślącza (2015). A gas chromatogram from each group is presented with retention time 50 to 60.

### 3.6.2. Thermal history of OM

The distributions of PAHs are in part consistent with a high temperature origin - pyrolytic source of PAHs (*e.g.* (Killops and Massoud 1992)), for example with pyrolytic residues (*e.g.* (Geissman et al. 1967)) arising from OM alteration by hydrothermal activity (Kawka and Simoneit 1990a) or low-grade metamorphism (Heymann et al. 2003). Hence, the methyl-PAH/PAH ratios of  $\leq 0.8$  observed in our samples are consistent with a pyrogenic source (Saha et al. 2009). However, the Fluo/Pyr ratio  $< 0.6$  of all the samples is lower than what would be expected of an exclusively pyrolytic source and indicates that lower temperature pathways of PAH formation also contribute to the HCs (Fabiańska et al. 2016).

The biomarker maturation parameters of  $C_{27}$  steranes fall within values that might be expected within a temperature envelope consistent with a moderate thermal history (Fig. 6; *ca.* 80 – 150 °C; (Mackenzie et al. 1980; Peters et al. 2005a)) and are therefore consistent with the temperature history of the basin (Früh-Green et al. 1990; Peters et al. 2005b). This suggests that where steranes are present, their degree of isomerisation reflects gradual maturation over time, rather than the pyrogenic process that may have yielded PAHs at the contact of hot rock with seawater OM.

### 3.6.3. Origin of calcite veins

The measured carbon and oxygen isotopic composition of carbonates are 0 to 2‰ and - 11.7 to - 6.2‰, for  $\delta^{13}C_{VPDB}$  and  $\delta^{18}O_{VPDB}$ , respectively and are similar to values previously reported for calcite veins in ophicalcite and late calcite veins collected in the Davos-Parsenn and Arosa areas (Fig. 3.4; (Früh-Green et al. 1990)). The  $\delta^{13}C_{VPDB}$  values are consistent with seawater-derived early diagenetic calcite (Fig. 3.8 a) (Hudson 1977; Coleman et al. 1993; Heydari 1997). The  $\delta^{18}O_{VPDB}$  values of the calcite veins for the majority of samples vary between -11.7 to -6.2‰ and indicate calcite precipitation during shallow burial (<250 m), not influenced by organic carbon derived  $CO_2$  but typical of Cretaceous calcite (Dix and Mullins 1992; Heydari 1997).

One sample (radiolarian chert) has a negative calcite carbon isotope value perhaps indicating the influence of CO<sub>2</sub> delivered from diagenesis of OM (Heydari 1997).

#### **3.6.4. OM in serpentinite – mechanism of emplacement**

The occurrence of HCs in the serpentinite rocks of Totalp is at first sight surprising. Schwarzenbach et al. (2013) listed the five main sources of organic carbon (OC) that can be preserved in basement rocks, namely from seawater, mantle, Fischer-Tropsch-like reactions (F-T), *in-situ* production from microbial activity in the basement rock or thermogenic decomposition of OM. The hydrocarbons recovered from the Totalp serpentinites and the OC isotopic composition are consistent with an origin from marine OM *i.e.* a seawater source rather than *in-situ* production or abiotic F-T reactions. Therefore, the probable origin of the OC preserved in the rocks is from dissolved and particulate organic carbon (DOC and POC) derived from seawater or thermal alteration of OM in sediments that then migrated to the basement rock within fluids (Fig. 3.14 a). However, there could be different pathways of emplacement of OM in the serpentinites.

The OM could have been deposited within the two types of precipitated carbonate found in the serpentinite, namely the mechanically deposited carbonate that fills fractures, or *via* pore fluids fuelling the formation of calcite veins (Fig. 3.14 b) (Bernoulli and Weissert 1985; Früh-Green et al. 1990)). The latter has an isotopic composition consistent with seawater carbonate and any DOM transported with the pore fluids would be trapped within the calcite matrix on precipitation (Figs. 3.8, 3.14). The presence of ophicalcite and the numerous calcite veins from the time of exhumation indicates a high supply of dissolved inorganic carbon (Ménez et al. 2012). As the OM clearly has a marine origin, it could have been emplaced by the first main phase of fluid-rock interactions at the ocean floor and the tectono-sedimentary and hydrothermal processes described by Früh-Green et al. (1990). The OM may have migrated with seawater through fractures in the sediment into the basement rock (Fig. 3.14 c; (Delacour et al. 2008c)). These fractures are formed by tectonic and crystallization stresses, which are not reliant on matrix permeability (Farough et al.

2016). Where initial contact between DOM-containing fluid and rock was at relatively high temperature, this could have led to the formation of the pyrolytic PAHs.

With respect to the sedimentary facies, organic carbon preservation is linked to grain size (or mineral surface area) and oxygen exposure after deposition (Fig. 3.14 d) (Hartnett et al. 1998; Kennedy et al. 2002)). Clay minerals, one of the constituents of shale sediments found in the Totalp unit, strongly retain DOM both on the external surfaces and interlayer spaces of clay particles (Kennedy et al. 2002). However, the Totalp sediments have low TOC values and could be highly oxidised during deposition or diagenesis. During deposition of shales, OM is also deposited as discrete biogenic particles, but largely these are not preserved; rather clays, particularly smectites, facilitate the absorption of DOM and POM from seawater and pore-fluids, and preserve it during burial (Kennedy et al. 2002).

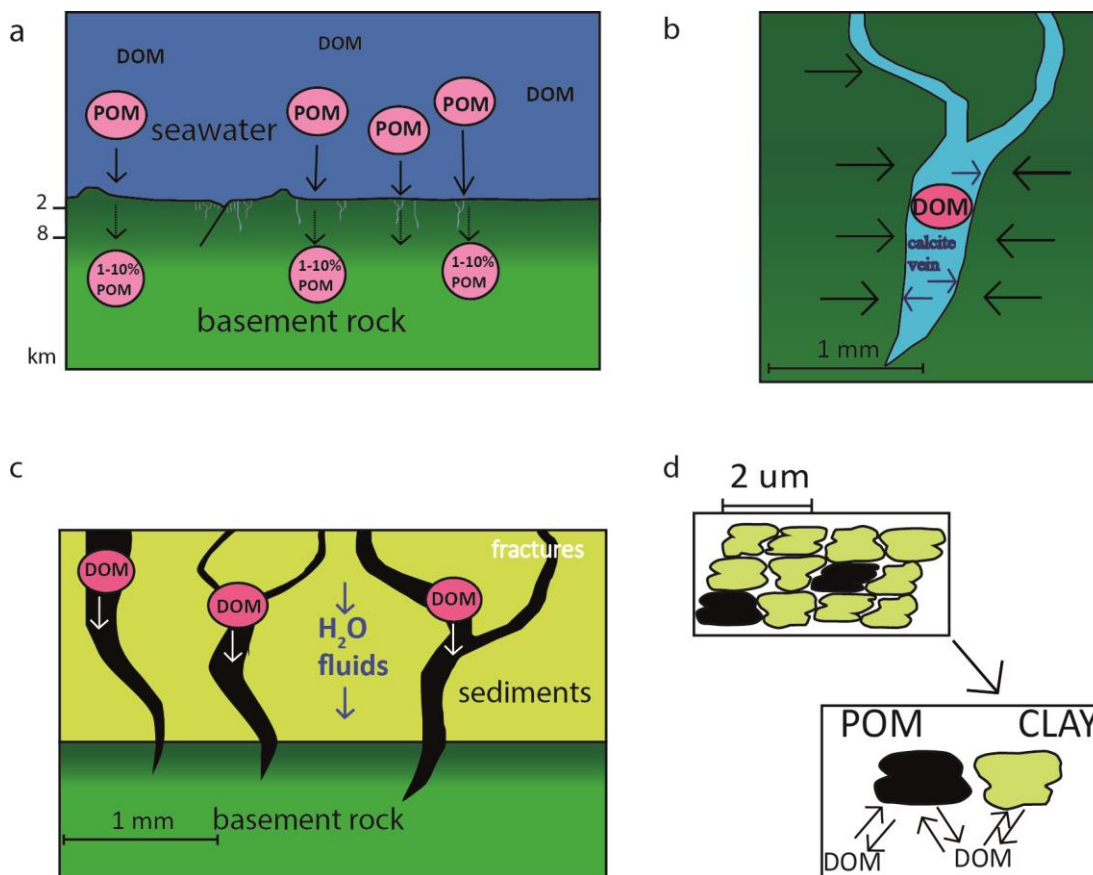


Figure 3.14. Conceptual model explaining origin and migration of OM from the seawater into different lithologies in the Totalp unit. a) The OM is represented by particulate and dissolved organic matter (POM and DOM,

respectively). The OM infiltrates the basement rock by rock-fluid circulation. b) Some OM may be deposited within the carbonate veins (*e.g.* calcite veins). c) OM circulates with fluids through fractures and porosity of sediments to migrate into the basement rock. d) OM is preserved at the surfaces and in the interlayer surfaces of clay minerals in the sediments. (Schwarzenbach et al. 2013).

We conclude that OM in the exhumed mantle rocks at Totalp is of marine origin that migrated into the serpentinite most likely from the overlying seawater or sediment cover (Simoneit et al. 1978; Simoneit and Philp 1982). Our results are consistent with previous studies that show a lack of, or only minor formation of the CH<sub>4</sub> and H<sub>2</sub> needed for the production of OM involving serpentinisation at low-temperature (McCollom and Donaldson 2016) and that the molecules necessary for life at hydrothermal systems are formed during the abiotic degradation of existing OM at low temperatures on the ocean floor (Reeves et al. 2014).

### **3.7. Conclusions**

*“Conclusion by no means give new knowledge”*

*Arthur Schopenhauer, 1788-1860*

We provide evidence for the preservation of traces of OM originally deposited in a reducing marine environment in serpentinised mantle rocks and overlying sediments, but with no indication that the OM was generated from methanotrophic bio-systems. The OM was not created due to serpentinisation process so distinction between different type of serpentine is unnecessary. The presence of OM within serpentinised mantle is attributed only to migrated OM from the seawater. However, this presence raises two questions; how much is there and how is this OM distributed in depth? Drilling to recover rock cores from the Totalp area would allow sampling of serpentinised mantle deeper than surface outcrops and would shed light on the depth distribution of OM and its composition.

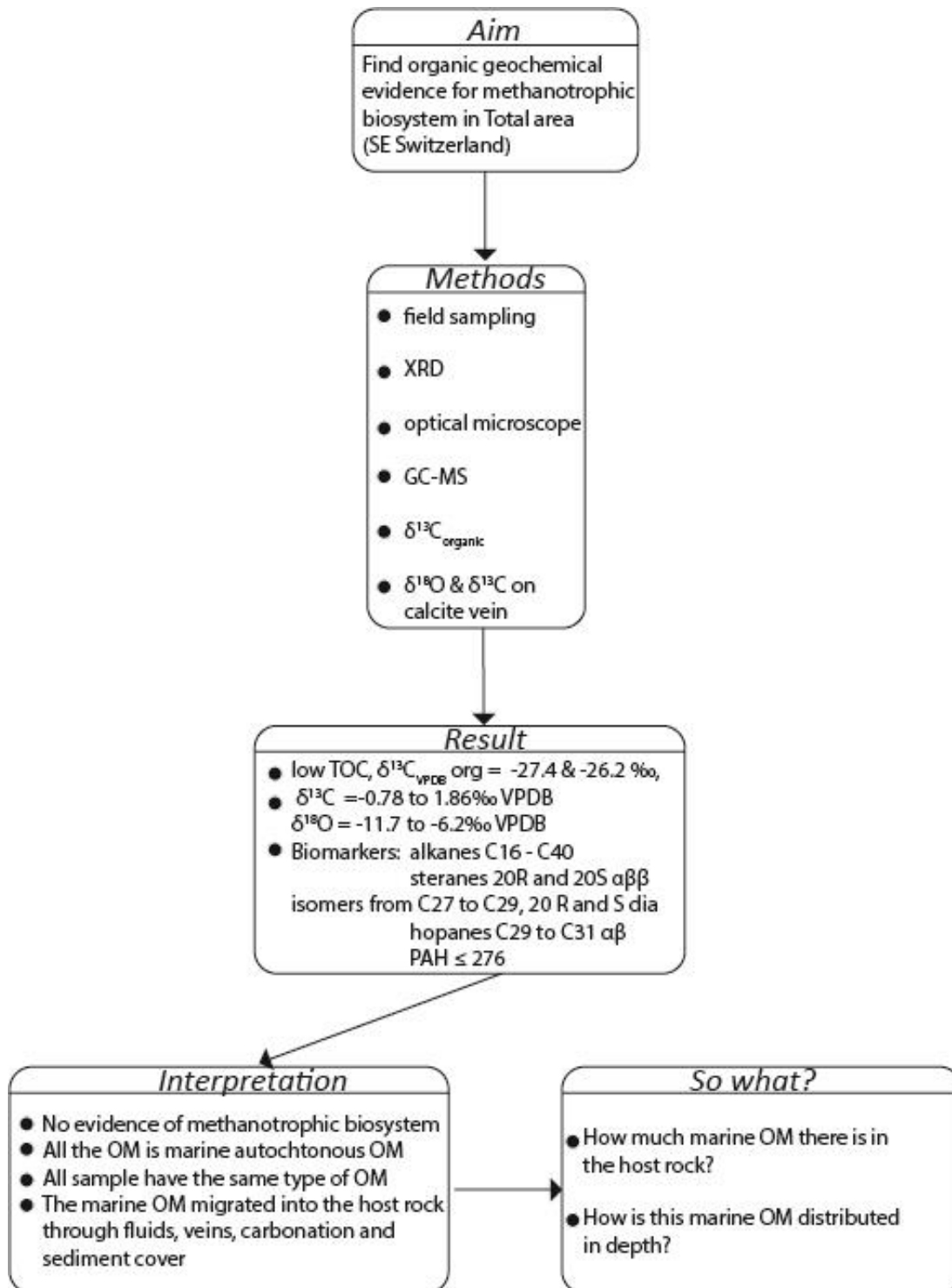


Figure 3.15. Summary flow chart of chapter 3

## Chapter 4

# **4. Preserved Organic Matter in the Fossil Alpine Tethyan Ocean Continental Transition**

This chapter is prepared for publication for the journal *Chemical Geology*. Authors of the manuscript are Tsvetomila Mateeva (main author), George A. Wolff, Nick J. Kusznir, Gianreto Manatschal and John Wheeler. The aim of this study was to look for biological evidences consistent with anaerobic methane oxidation in Platta, Tasna and Chenaillet localities of the fossil Alpine Tethyan OCT. It is a supplementary work to the work already done in Totalp (Chapter 3) but covers more study field area.



#### **4.1. Abstract**

Serpentinisation in modern hydrothermal vents can support hydrogen-driven microbial environments including methanotrophic biosystems. An important question is “Are such bio-systems locally restricted to hydrothermal vents or are they more pervasive, being linked with the occurrence of serpentinised mantle at the seafloor”. If the latter, then this would have important implications for sub-surface bio-systems and the fate of methane.

The ocean-continent transition (OCT) of magma-poor rifted continental margins provides an opportunity to investigate this question. Samples from the fossil Alpine Tethys OCT were examined for biomarkers (e.g. crocetane, sn-2-hydroxyarchaeol) and isotopic signals of methanotrophy within serpentinised exhumed mantle. The presence of various types of hydrocarbons can be confirmed in all the studied sample locations - Chenaillet (Western Alps) and Totalp, Tasna and Platta units (Central Alps).

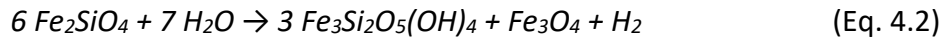
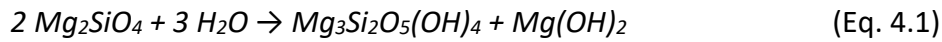
The main hydrocarbon types found in the Tethyan OCT rocks are *n*-alkanes, from C<sub>16</sub> to C<sub>32</sub>, low molecular weight polynuclear hydrocarbons (PAHs), hopanes, steranes, including 20R and 20S αββ isomers from C<sub>27</sub> to C<sub>29</sub>, as well as 20 R and 20 S diacholestanes and branched alkanes in the form of pristane and phytane.

The identified biomarkers and the isotopic data for bulk TOC are consistent with a marine origin but do not indicate a methanotrophic bio-system. Biomarkers related to methanotrophic bacteria may not be preserved, or, they may not be pervasive with the zone of serpentinisation except under special environmental conditions (e.g. hydrothermal vents).

#### **4.2. Introduction**

Serpentinisation is considered to be the most important metamorphic hydration process for transfer of elements between the hydrosphere and lithosphere. It also contributes to thermal energy at oceanic hydrothermal vents and potentially chemical energy for anaerobic life in the early Earth’s history (e.g. (Shock et al. 2002; Deschamps et al. 2012; Jamtveit and Hammer 2012a)). Serpentinisation converts

olivine and pyroxene to serpentine, other Fe-Mg minerals (magnetite, brucite, talc) and free molecular hydrogen (Eq. 4.1, 4.2). The Mg and Fe components of olivine (forsterite, enstatite) may hydrate to form serpentine as follows:

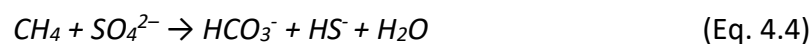


The relationship of serpentinisation to organic molecules (e.g. methane, CH<sub>4</sub>) at high pressure and temperature, *via* a Fischer-Tropsch-type (FTT) reaction, has been widely investigated (Eq. 4.3) e.g. (McCollom and Seewald 2013). Hence, molecular hydrogen can reduce CO<sub>2</sub> derived from abiotic source (mantle outgassing) or biogenic source (dissolved limestone) to methane e.g.(Seewald et al. 2006):



FTT was previously reported to also produce unbranched alkane (*n*-alkane > *n*-alkenes > *n*-alkan-1-ols) under hydrothermal conditions (McCollom and Seewald 2006). Previous studies have reported positive anomalies of methane and hydrogen in the water column above active serpentinisation zones along slow to ultraslow-spreading Mid-Ocean Ridges (MOR) (Rona et al. 1987; Charlou et al. 1988; Rona et al. 1992; Bougault et al. 1993; Charlou and Donval 1993; Charlou et al. 1998; Gràcia et al. 2000; Kelley and Shank 2010).

The abiotic methane can be anaerobically oxidised by methanotrophic bacteria together with sulphate reducing bacteria, which act as an electron acceptor to produce hydrogen sulphide (Eq. 4.4) e.g. (Michaelis et al. 2002).



Anaerobic oxidation of methane (AOM) is achieved by a consortium of at least two different organisms: methanotrophic archaea and sulphate reducers (e.g. community psychrophiles sulphate-reducing, mesophilic sulphate-reducing) (Hinrichs et al. 2000). Sulphate reducers are one of the dominant bacterial populations at

hydrothermal vents (McCollom and Shock 1997) and in anoxic marine sediments (Jørgensen 1982; Canfield et al. 1993).

Methanotrophic bacteria (ANME-1) together with a sulphur-oxidizing symbiont have been identified in the LCHF (MAR) (Hinrichs et al. 2000; Kelley et al. 2001; Orphan et al. 2001; Kelley et al. 2005; Martin et al. 2008), in deep-sea bivalves in the Gulf of Mexico (Cavanaugh et al. 1987) and in the MAR hydrothermal vents (Menez Gwen) as endosymbiont in hydrothermal vent mussels (Pond et al. 1998). It has been suggested that AOM coupled with sulphate reduction occurred in the anoxic environments as early as 2.7 Ga (Hinrichs 2002). In the oxygenated environment, methanotrophic bacteria can also associate with iron ( $\text{FeCl}_2$ ,  $\text{FeCl}_3$ ) and manganese ( $\text{MnO}_2$ ) reduction, and have the potential to oxidise all the produced  $\text{CH}_4$  flux in the early Earth history (Beal et al. 2009). Another association demonstrated in the laboratory is nitrate-AOM (ANME-2d) (Haroon et al. 2013; Arshad et al. 2015), but is likely to be a minor pathway due to the lower nitrate concentrations in seawater compared to sulphate ( $\mu\text{M}$  vs.  $\text{mM}$ , respectively). Ultimately, methanotrophs are highly significant in mediating  $\text{CH}_4$  in the atmosphere by removing up to 90% of the  $\text{CH}_4$  (Reeburgh 2007) produced in the ocean by methanogenic bacteria (300Tg/year) (Knittel and Boetius 2009). Hence, methanotrophic bacteria are involved in the biogeochemical cycles of carbon as well as iron, manganese and sulphur.

Previous studies have focussed on the relationship between serpentinisation and organic compounds at present-day serpentinite-hosted hydrothermal vents (e.g. (Teske et al. 2002; Delacour et al. 2008c; Reeves et al. 2014), mud volcanoes (e.g. (Mottl et al. 2003)), and surface ophiolite domains characterized by high  $\text{H}_2$  concentrations and high pH (Oman ophiolite, California ophiolite) (e.g. (Neal and Stanger 1983; Cardace et al. 2013; Rajendran and Nasir 2014)) or even in the astrophysical domain (e.g. (Holm et al. 2015)). Preserved biomarkers derived from methanotrophic bacteria and carbon isotopes enable well establish methods to detect the presence of the volatile  $\text{CH}_4$  in these fossil serpentinised environment (e.g. (Childress et al. 1986; Pond et al. 1998)).

High concentrations of OM found at the Mid-Atlantic Ridge (MAR; 4-6°N) were associated with serpentinised peridotite rather than with the hydrothermal vents (Ménez et al. 2012) raising the question of whether the OM could be associated with the serpentinisation process. Understanding the relationship between the serpentinisation (geological abiotic process) and the methanotrophs organisms (eukaryotes, living thing) has great importance for the carbon cycles on a geological timescale.

The present study, representing three additional locations, adds to the work presented for the Totalp area (Mateeva et al. 2017), which used an organic geochemical approach to quantify OM in the serpentinised mantle and overlying lithologies from a fossil OCT to better understand the relationship between OM and mantle serpentinization.

OM extracted and analysed from the sampled Alpine Tethys OCT areas would provide biomarkers that serve to determine its source and thermal maturity, as well as evidence consistent with AOM origin (*e.g.* crocetane (Thiel et al. 1999; Blumenberg et al. 2004)).

### **4.3. Fossil Alpine OCT**

The distal OCT of the Tethyan Ocean continental margin is preserved in the Alps. Remnants of this fossil OCT have been reconstructed in the Platta and Err units in the Central Alps (SE Switzerland) and elsewhere. Although the fossil OCTs have been deformed during the Alpine orogeny the metamorphic overprint is very low (< 300 °C) (Froitzheim and Manatschal 1996; Manatschal and Nievergelt 1997; Manatschal and Bernoulli 1999; Mohn et al. 2012) (Fig. 4.1).

The Tasna, Platta, Chenaillet and Totalp sites represent different fossil parts of the Piemonte-Liguria OCT, an embryonic sediment starved ocean basin, originating from the exhumation of subcontinental mantle (Fig. 4.1) (Müntener et al. 2004; Manatschal et al. 2006; Manatschal and Müntener 2009). Although the paleogeographic positions are difficult to locate with precision, the paleo location of these units has been proposed based on field observation and U-Pb zircon data (Fig.

4.1 b) (Manatschal and Müntener 2009). Tasna has been suggested to be on the continental edge of the European/ Briançonnais margin, Chenaillet near the oceanic ridge, Platta on the oceanic crust near the Adriatic margin (Fig. 4.1 b) (Manatschal and Müntener 2009). While the Tasna, Platta and Totalp represent parts of the fossil OCT, Chenaillet more likely corresponds to a fossil oceanic core complex (Manatschal et al. 2011) (Fig. 4.1 c). The Totalp OCT, whose organic geochemistry has previously been investigated and is described in Mateeva et al. (2017), is located in exhumed mantle on the Adriatic margin.

A brief description of the Tasna, Platta, Chenaillet and Totalp OCTs is given below. The order of presentation is from proximal to distal.

#### **4.3.1. Tasna OCT**

The Tasna OCT is located in southeastern Switzerland, north of Scoul. It is the only exhumed Alpine OCT that includes parts of the thinned continental margin and the exhumed mantle derived from the Piemont-Ligurian basin (Manatschal et al. 2006) (Fig. 4.1 a). In the Tasna OCT, a system of extensional detachment faults is exposed and preserved over 5 km (Florineth and Froitzheim 1994; Manatschal et al. 2006) (Fig. 4.2 a). The temperature of serpentinisation has been calculated to be  $T=67-109\text{ }^{\circ}\text{C}$  and carbonate precipitation occurred between the seafloor and depth of 120 m at  $T=54-100\text{ }^{\circ}\text{C}$  using  $\delta^{18}\text{O}$  on unaltered mantle peridotite and calcite respectively (Engström et al. 2007).

Tasna is considered to be an analogue of the OCT at the present-day Iberian margin, where extensional detachment faults and exhumed mantle are revealed by seismic imaging and drill core samples (Manatschal et al. 2006). At Tasna the regional Alpine metamorphism did not exceed greenschist facies ( $<350\text{ }^{\circ}\text{C}$ ) for the transition between continental and exhumed mantle rocks, making Tasna the best worldwide analogue of an OCT (Fig. 4.2 a, c) (Florineth and Froitzheim 1994; Manatschal et al. 2006).

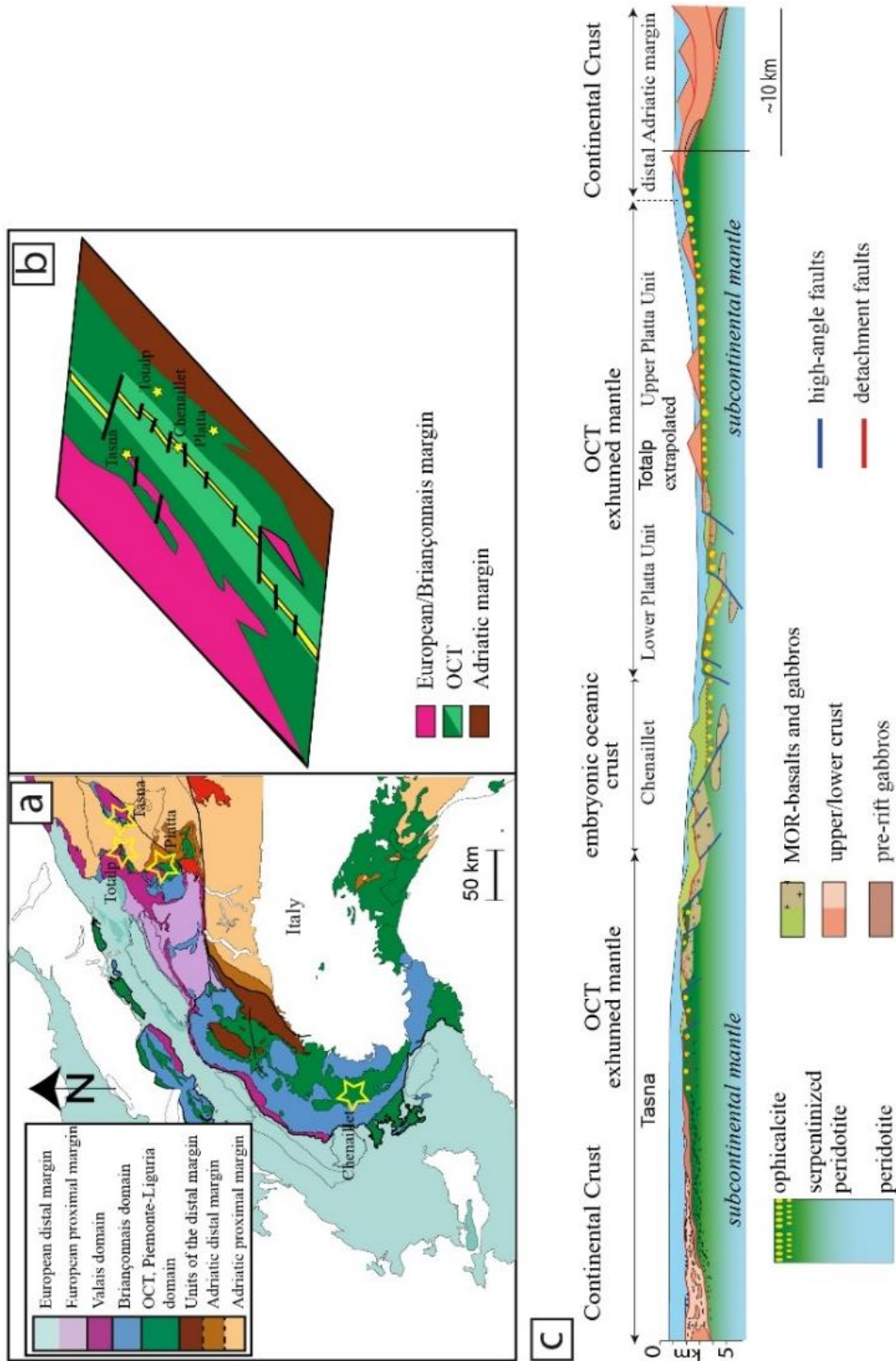


Figure 4.1. a) Map showing the location of the studied areas (Tasna, Platta and Chenaillet as well as the location of Totalp studied in a previous study). b) Paleogeographic position of the studied unit modified after Manatschal and Müntener 2009. c) Reconstructed section across the Alpine Tethys modified after Manatschal and Müntener 2009.

The Tasna OCT contains spinel –lherzolite, continental basement and sediments limited by extensional detachment faults referred to as the Lower and Upper Tasna Detachment (LTD, UTD) respectively (Manatschal et al. 2006) (Fig. 4.2 b, d). The mantle rocks are strongly serpentinised (>90%) lherzolites with spinel websterite layers. The top of the mantle is formed by foliated serpentinites, defined by serpentine minerals, talc and Fe-oxides, serpentinite cataclasites and serpentinite gouges (Manatschal et al. 2006). The olivine is completely serpentinised while the other ultramafic minerals (pyroxene, rare Ti-hornblende) and phlogopite are occasionally preserved or pseudomorphosed in bastite and the oxides (spinel) are rimmed by magnetite (Manatschal et al. 2006).

Sediments are deposited over the exhumed mantle and the continental basement (Tonschiefer formation) (Engström et al. 2007). The pre-rift sediments are Triassic dolomites, quartzite, gypsum, arkose, shale and cargneule (Gurler 1995). The syn–rift sediments are Jurassic and limestones (Froitzheim and Rubatto 1998) and polymictic breccias which overlie the Tasna basement (Manatschal et al. 2006). The post-rift sediments are from bottom to top constituted by the Tonschiefer Formation formed by dark shale (Florineth and Froitzheim (1994)); the Tristel formation of grey shales, calciturbidites and breccias (Schwizer, 1983), sandstones (Gault Fm), followed by Couches rouges of megabreccias and marly limestones; and finally, the Tasna flysh. The pre– and syn-rift sediments are not in direct contact with the exhumed mantle (Manatschal et al. 2006) (fig. 4.2 a).

#### **4.3.2. Totalp unit**

The Totalp unit is situated north of Davos in SE Switzerland (Fig. 4.1). It experienced little Alpine deformation and only a low grade Alpine metamorphic overprint, not exceeding 100-150 °C, *i.e.* prehnite-pumpellyite facies (Peters 1968; Früh-Green et al. 1990).

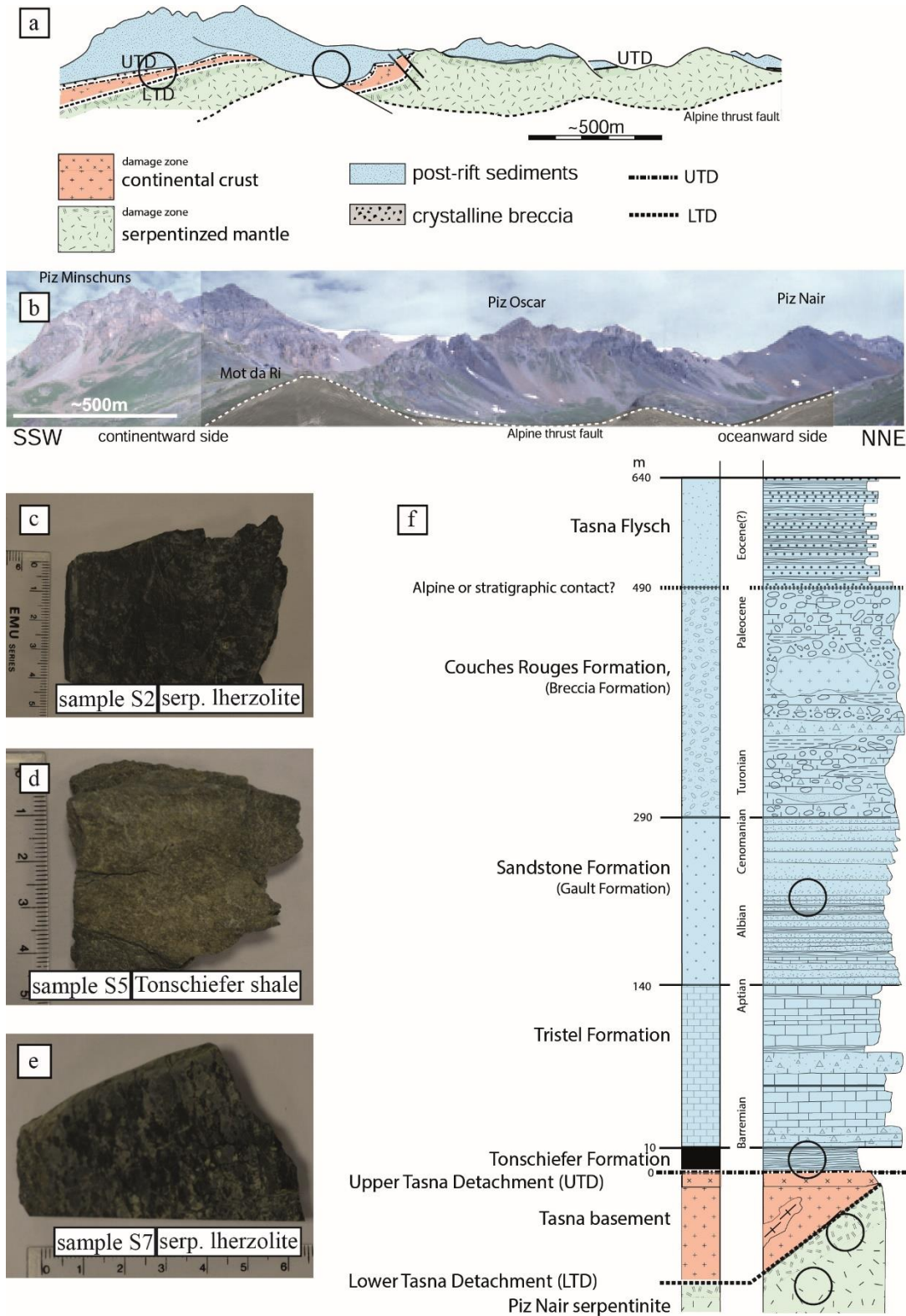


Figure 4.2. a, b) Panoramic photo and figure of Tasna unit (Manatschal et al. 2006) c -e) samples from Tasna unit f) Lithostratigraphic section of Tasna unit (Manatschal et al. 2006).

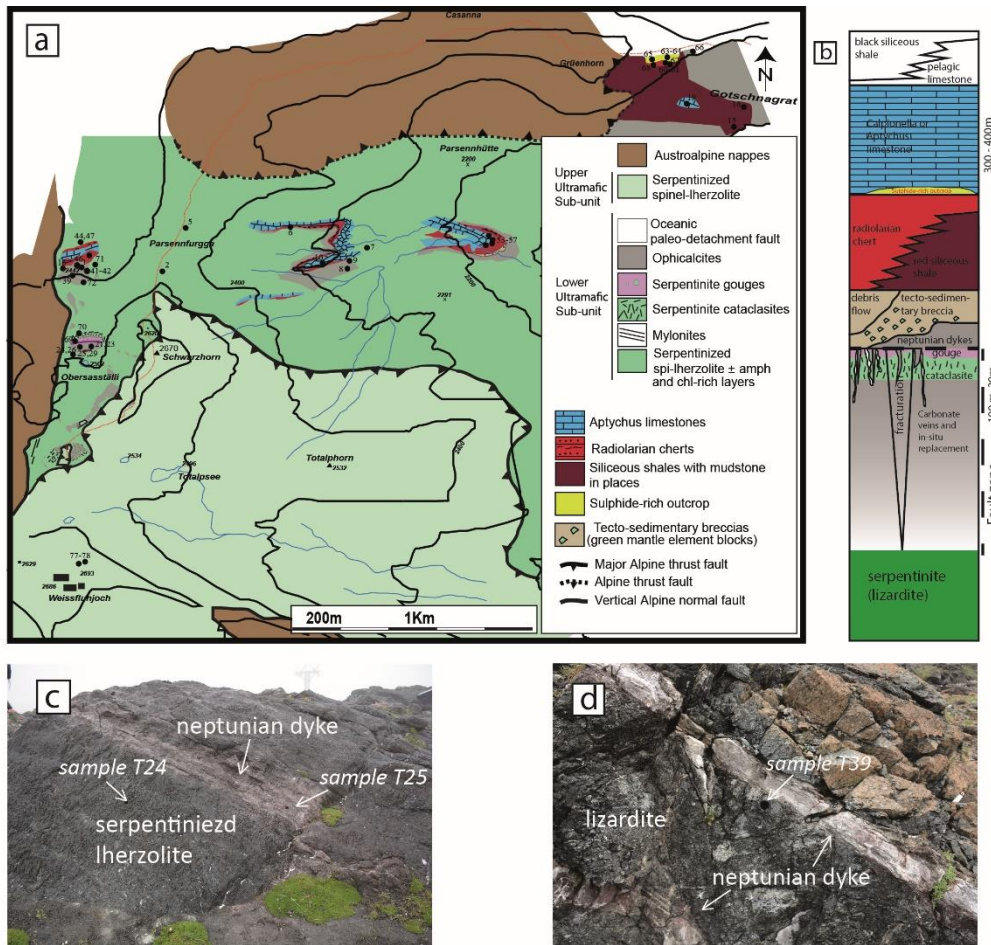


Figure 4.3. a) Geological map of Totalp unit (Picazo et al. 2013) b) Lithological section of the Totalp unit (Mateeva et al. 2017) c-d) Outcrop showing neptunian dykes in serpentinitised lherzolite.

The Totalp unit consists of serpentinitised peridotites that were exhumed at the seafloor during Jurassic time. At the top of the exhumed mantle there are ophicalcites of tectono-sedimentary and sedimentary origin that are overlain by post-rift deep marine Jurassic sediments (Fig. 4.3). The mantle rocks are serpentinitised lherzolite with mesh texture, gouges, cataclasites and serpentine veins. The sediments are mainly pelagic deposits of Late Jurassic to Early Cretaceous age and consist from bottom to top of red siliceous shale, radiolarian cherts, *Calpionella* or *Aptychus* limestones, pelagic limestones and black siliceous shales (Fig. 4.3 b, c). In addition, the primary contacts between the exhumed serpentinitised mantle, the ophicalcites and the oceanic sediments are well-preserved (Weissert and Bernoulli 1985).

### 4.3.3. Platta nappe

The Platta nappe in the eastern Swiss Alps corresponds to the southern prolongation of the south Pennine Arosa zone (Fig. 4.1 a). The Platta nappe preserves parts of the southeastern margin of the Liguria-Piedmont segment that correspond to the distal Adriatic margin in the Alpine Tethys. It preserves remnants of an OCT *senso stricto*, known as the Steinman trinity, consisting in serpentinites, basalts and radiolarian cherts (Steinmann 1905; Desmurs et al. 2001) (Fig. 4.4 a, b). The lithological sequence observed in the Platta nappe corresponds to that observed in magma-poor rifted margin (Manatschal and Bernoulli 1999). Subcontinental mantle rocks were exhumed at 165Ma along extensional detachment faults that are overlain by extensional allochthons of continental crust (Lemoine et al. 1987; Froitzheim and Manatschal 1996; Manatschal and Nievergelt 1997).

The Alpine metamorphic overprint increases from north (less than 250 °C) to south (>350 °C) across the Platta nappe and passes from lizardite-chrysotile serpentinite north of Bivio to antigorite-lizardite-chrysotile south of Bivio (Trommsdorff and Evans 1974; Trommsdorff 1983). The Alpine deformation in the Platta nappe can be subdivided in three main phases of Late Cretaceous to Oligocene age (Trommsdorff and Evans 1974; Manatschal and Nievergelt 1997). The lithologies forming the Platta nappe consist of serpentinitised lherzolite and harzburgite, ophicalcite including tectono-sedimentary breccias (Bernoulli and Weissert 1985), minor sill-like gabbroic

intrusions, overlain by basaltic rocks and sediments (Desmurs et al. 2001) (Fig. 4.4 c, d). Two Alpine tectonic units, the Upper and Lower Serpentinite units can be mapped,

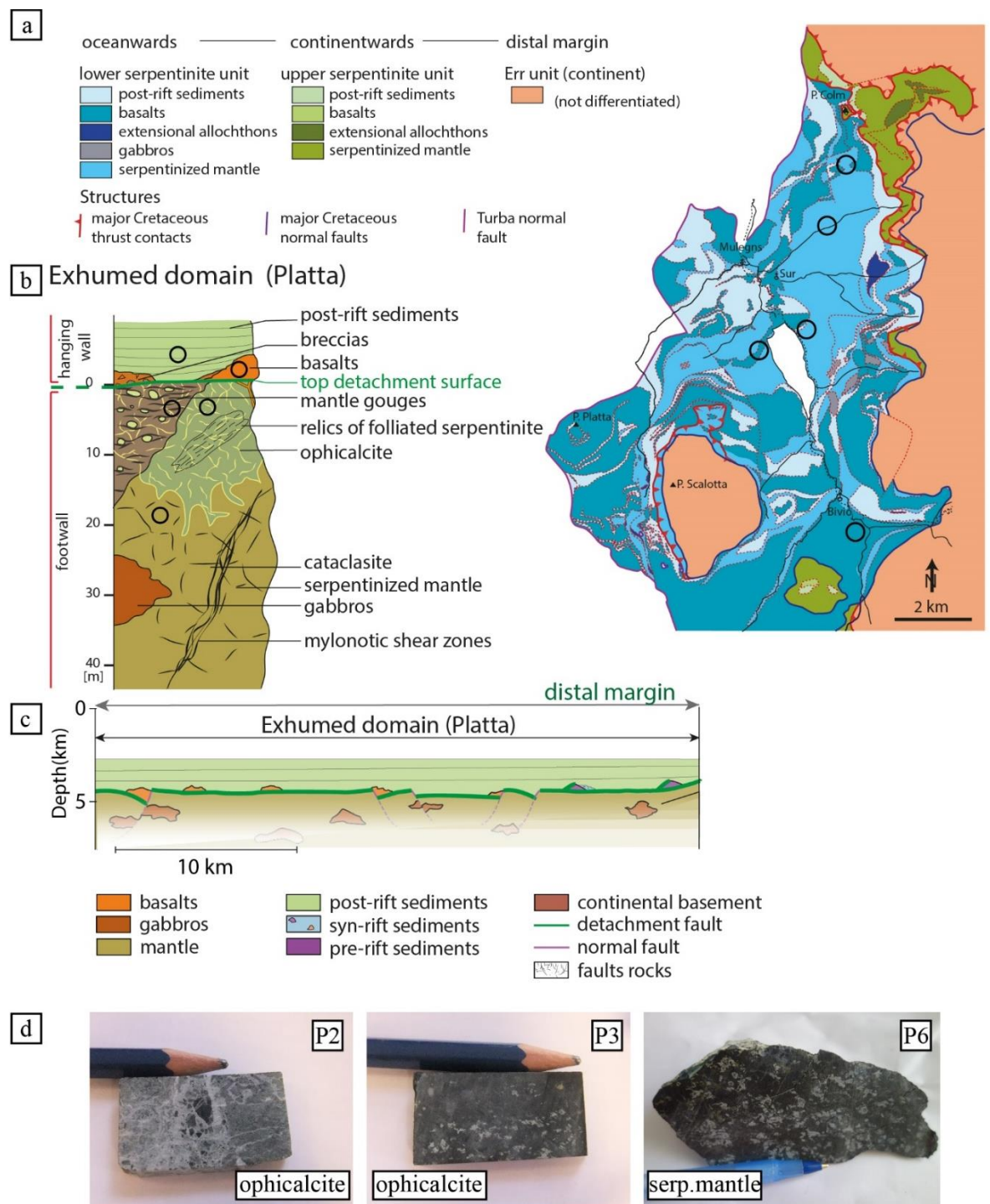


Figure 4.4. a) Geological map of Platta nappe (Schaltegger et al. 2002) b-c) Lithological and cross-section of the Platta unit (Epin et al. 2017) e) Samples from Platta unit.

made of different types of mantle rocks (Manatschal et al. 2003). Syn- to post tectonic sediments are composed of sedimentary and tectono-sedimentary breccias, turbidites and hemipelagic limestones (Manatschal et al. 2003). The deepwater sediments are constituted of siliceous shales and radiolarian cherts that are Callovian and younger. The Calpionella limestone, and the Palombini are dark siliceous shales and marlstones interbedded with sandstones that are Upper Jurassic to Lower Cretaceous (Dietrich 1970; Weissert and Bernoulli 1985; Pinto 2014).

In the Platta unit several sulphide rich mineralisation exist that were mined for iron and copper (Dietrich 1972) (Fig. 4.5). The deposits are rich in sulphide



Figure 4.5. Sulphide mines a, c) W of Marmorera lake represent oxidised serpentinite rich in polymetallic sulphides b) E of Marmorera lake d) ophicalcite sample e) sample from sulphide mine W of Marmorera f) sample from sulphide mine E of Marmorera.

mineralization and oxides surrounded to massive serpentinite to highly tectonized serpentinite (marble-like habit with colour change from black and dark green to light green zones) (Dietrich 1972). The sulphide deposits around Marmorera lake belong to mineralisation, described by Dietrich (1972), showing associations of paragenetic oxides and sulphide. In the field they are recognised by a strong red colour due to weathering.

#### 4.3.4. The Chenaillet unit

The Chenaillet unit is the best-preserved ophiolite sequence from the Piemonte-Ligurian basin exposed in the Western Alps. It represents an area of 25 km<sup>2</sup> and is situated south of Mongenèvre (France) near the French-Italian border (Fig. 4.1 a). It represents a fossil oceanic core complex derived from an ultraslow or slow spreading ridge, or an “embryonic” oceanic crust (Manatschal and Müntener 2009; Manatschal et al. 2011). The magmatic rocks formed from a depleted MORB-source (Li et al. 2013) (Fig. 4.6 a).

The Chenaillet unit was chosen because of its weak Alpine metamorphic overprint (prehnite-pumpellyite facies <200 °C, defined by prehnite, epidote, pumpellyite, albite and actinolite) and because it was not strongly overprinted by Alpine deformation (Pusztaszeri 1966; Mevel et al. 1978; Lewis and Smewing 1980; Manatschal et al. 2011). U-Pb dating of zircon from troctolites and albitites indicate a crystallisation age for the ophiolitic gabbros of around 165Ma (Li et al. 2013).

The Chenaillet unit consists of sediments and MOR basalt (mainly pillow lavas) overlying the tectonically exhumed serpentinised mantle including mafic intrusions (gabbros, dolerites and troctolites) (Manatschal et al. 2011) (Fig. 4.6 b, c, d). The serpentine is made of lizardite and chrysotile (Manatschal et al. 2011). An “oceanic extensional detachment fault” has been described between the exhumed mantle and the overlying volcanic sequences. The detachment surface is made of characteristic serpentinite gouges and calcified serpentinite breccias (E Chenaillet) (Manatschal et

al.

2011).

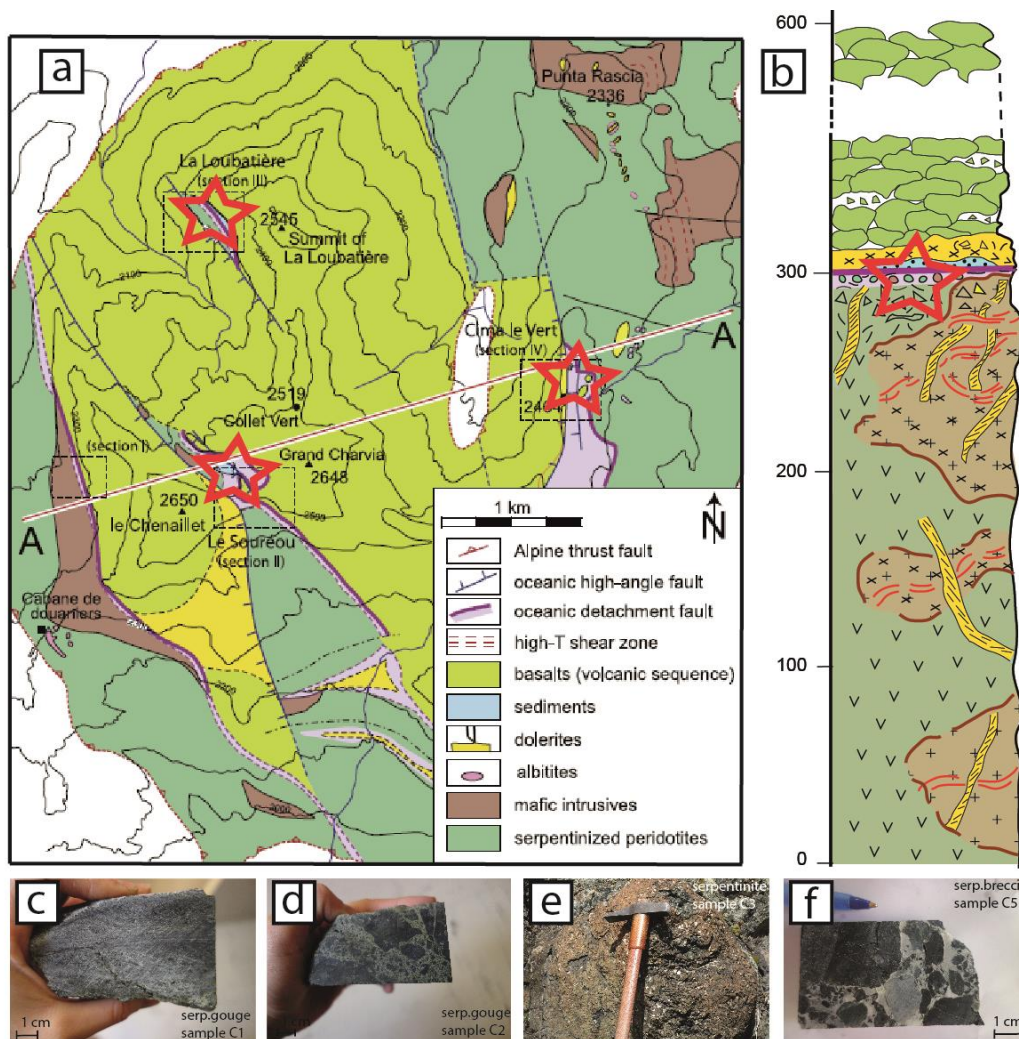


Figure 4.6 a) Geological map of Chenaillet (Manatschal et al. 2011). The locations of the analysed samples are shown with a red star. b) Lithological section of the Chenaillet (Manatschal et al. 2011) c-f) Samples from Chenaillet.

## 4.4. Sample Collection, Preparation and Analysis

### 4.4.1. Sample collection

Samples collection and analysis for the Tasna, Platte and Chenaillet localities of the Tethyan Ocean OCT (Fig. 4.1) are described below. Previous work detailing sample collection and analysis for the Totalp location is presented in Mateeva et al. (2017). A total of 40 samples were collected and prepared from the three areas, of which 25 samples are from the Platta unit, 10 from the Tasna unit and 5 from Chenaillet, for both mineralogical and organic geochemical studies (Table 4.1). Samples were

collected from the main lithologies: serpentinitised mantle rock (lizardite, serpentinitised basalt, serpentinite gouge and cataclasite), ophicalcites (neptunian dykes and tectono-sedimentary breccias), syn to post-rift sediments (radiolarian chert, limestone), as well as samples from the Platta sulphide mines associated with basalt and serpentinite around Marmorera lake (Fig. 4.4, 4.5). Ophicalcites were also analysed because of their long exposure ( $>10^6$  y) at the Jurassic seafloor, their overlying relationship with serpentinite and their high permeability (Manatschal et al. 2006).

Our Platta samples originated all from the Lower Serpentinite unit in the central and northern part of Platta including the area around the Marmorera lake and the Flix-Fallota area (northern Platta) (Table 4.1). Sampling in the Platta area also focused on the outcrops of oxide and sulphide mineralisation; sulphides in the oceanic domain could relate to sulphur reducing microorganism and thus could possibly be related to methanotrophic biosystems.

The Chenaillet samples represent exhumed mantle and reworked mantle rocks near the extensional detachment fault in the area of Collet Vert (2522 m.a.s.), west of la Loubatière (2545 m.a.s.) and Cima le Vert (2404 m.a.s) (Table 4.1). The serpentinitised samples from the Tasna unit are taken from the southern part of the exhumed mantle and in Mot de Ri where the samples lie exactly underneath the contact with the continental basement (Table 4.1). The ophicalcites and syn- and post-rift sediments samples are taken from the northern Tasna area and directly overlie the mantle. Samples were collected using a geological hammer and then wrapped in pre-combusted foil (400 °C) for return to the laboratory. Samples containing visible chrysotile veins were intentionally not crushed and used for further analyses for reason of health and safety.

#### **4.4.2. Sample preparation**

In order to avoid contamination with modern material, the samples were cleaned with hot tap water then rinsed with de-ionised water (18 M $\Omega$  cm<sup>-1</sup> resistivity; Milli-Q) followed by re-distilled dichloromethane (DCM). The outer edges were removed from

each sample using a small rock saw lubricated with tap water. The inner fresh, unweathered rock was then used for our laboratory analysis. Slices from this inner part were used for thin sections and for stable isotope analyses of carbonate veins, with 90 - 110 µg of calcite being extracted using a small electrical hand drill. Selected sub-samples were chosen for organic geochemistry analysis and washed thoroughly with Milli-Q water and DCM, then ground to a powder of particle size <50 µm using a tungsten Tema Mill, which was previously thoroughly cleaned using Decon-90 solution 2% v/v, milli-Q water, methanol and finally DCM.

#### **4.4.3. Mineralogical analyses**

A Panalytical X'Pert PRO X-ray diffractometer (XRD) system (CuK<sup>α</sup> radiation, 45 kV, 40 mA) was used to identify the volume proportions of the minerals associated with serpentinisation and the polytypes of the serpentine minerals. Data were collected between 3° and 70°2θ (diffracted beam) and mineral quantification (weight percent) was carried out using Panalytical HighScore Plus software, and the relative intensity ratio method. Because no antigorite and chrysotile were chosen, due to high temperature and safety reason, respectively, the XRD method was to distinguish the polytype of the main serpentinite. The method was also used to identify the volume proportions of the minerals in the small amount of sample analysed.

To distinguish between a condition with ferrous iron, therefore reducing and an oxidizing environment where the ferrous iron is not stable, we use the method of carbonate staining and acetate peels. This method is largely used to distinguish between ferroan and non-ferroan carbonate minerals (Dickson 1965). The carbon staining is the best method to differentiate ferroan calcite cements originating normally from deep burial reducing conditions in the pH 7-8 (Flügel 2013). However, a supplementary data OM origin could indicate for sure a reducing condition and its absence could derive from local oxidizing condition creating ferrous-iron-free cement (Evamy 1969).

This method consist of staining a flat surface of carbonate or containing carbonate sample using staining solutions alizarin red S and potassium ferricyanide in a 2%

hydrochloric acid solution (Dickson 1965). At the end of the staining, the non-ferroan calcite will be coloured in pale pink, red and the ferroan calcite in mauve to royal blue. The coloured rock sample is then copied using acetone and acetate piece. The imprint produced could be observed also under microscope to help the identification of carbonate structure.

Fourteen samples were chosen for carbonate staining samples - 9 from Totalp, 2 from Tasna and 1 from Platta. Some of them were already analysed for origin of OM, as well as calcite and oxygen isotopic analysis from the carbonate veins.

#### **4.4.4. Geochemical analyses**

Analyses of total carbon (TC) and total organic carbon (TOC) were performed before and after decarbonation (10% HCL, 25 °C, 24h), respectively, using a Carlo Erba Instrument NC2500 elemental analyser.

Stable isotopic analyses of organic carbon were carried out on one sample, a post-rift sediment from the Tasna unit which was the only one to have sufficient organic carbon for analysis. A “sealed tube” method was used where the resulting CO<sub>2</sub> is injected into a VG Sira 10 dual-inlet mass spectrometer (Craig 1957; Frazer and Crawford 1963; Sofer 1980). The standard measurement uncertainty for analysis was ± 0.1‰. The isotope data was normalized to IAEA-CH7 calibration material, the blank contribution was taken into account and the result reported using the VPDB scale.

Carbon and oxygen isotope measurements on calcite veins were performed by conversion to CO<sub>2</sub> using a VG SIRA 10 MS Isocarb (common acid bath). The carbon isotope data are referenced to the VPDB reference material with a standard measurement uncertainty for each analysis of ± 0.1‰ and the oxygen isotope are converted to the SMOW scale using equation 4.5 (McCrea 1950; Craig 1957; Friedman and O'Neil 1977; Swart et al. 1991).

$$\delta^{18}\text{O}_{\text{SMOW}} = 1.03092 * \delta^{18}\text{O}_{\text{VPDB}} + 30.92 \quad (\text{Eq. B.1})$$

Soxhlet extraction was used to extract the OM from the powdered rocks using DCM and methanol (9:1 ratio) (24 h) (Mateeva et al., 2017). Blank extractions containing

only the two solvents were conducted in parallel to identify any possible contamination. After evaporation of the solvent, the extracts were re-dissolved in hexane and passed through short columns of alumina and sodium sulphate using hexane as solvent to isolate the hydrocarbons. The samples rich in sulphide (e.g. Platta sulphide mine) were treated with activated copper prior to the alumina column to remove elemental sulphur (Blumer 1957). The eluent from the alumina column was re-dissolved in hexane (typically 50  $\mu\text{L}$ ) and analysed by gas chromatography - mass spectrometry (GC-MS).

GCMS was carried out using a split-splitless injector, GC column (DB-5MS non-polar 5% phenyl and 95% methyl silicone stationary phase, 60m x 0.25mm i.d., film thickness 0.1  $\mu\text{m}$ ) with helium as a carrier gas (2mL  $\text{min}^{-1}$ ). Samples were injected using an autoinjector and the oven temperature programmed from 60  $^{\circ}\text{C}$  to 170  $^{\circ}\text{C}$  after 1 min at 6  $^{\circ}\text{C min}^{-1}$ , then from 170  $^{\circ}\text{C}$  to 315  $^{\circ}\text{C}$  at 2.5  $^{\circ}\text{C min}^{-1}$  and finally held at 315  $^{\circ}\text{C}$  for 15 min. GC-MS ISQ LT with trace GC 1300 connected auto-sampler TriPlusRSH was carried out in full data acquisition mode, providing mass spectra of compounds eluting from 20 to 90 minutes. Compounds were identified by comparison with the literature, NIST library, Kovats indices and with authentic reference materials where available (PAHs - polynuclear aromatic hydrocarbons). 5 $\alpha$ (H)-Cholestane was used as an external reference material for quantification with response factors assumed to be 1, hence data are semi-quantitative. Data were processed using XCalibur 1.2 software (ThermoScientific).

The mean carbon number, MC# (Peltzer and Gagosian 1989) and the carbon preference index (CPI) of *n*-alkanes (Peters et al. 2005a) were calculated over the carbon number range C<sub>16</sub>- C<sub>40</sub> (Eq. 4.6, 4.7; Table 4.2).

$$MC\# = \frac{\sum ([C_i] \times C_i)}{\sum [C_i]} \quad (\text{Eq. 4.5})$$

Where [C<sub>*i*</sub>] = concentration of the *n*-alkane with C<sub>*i*</sub> carbon number

$$CPI = \frac{0.5 \times \sum ([\text{odd } C_{21} - C_{35}])}{\sum ([\text{even } C_{20} - C_{34}]) + \sum ([\text{odd } C_{23} - C_{37}])} \quad (\text{Eq. 4.6})$$

PAH ratios were also calculated to distinguish the HT origin in the OM. The methyl-phenanthrene to phenanthrene ration (MP/P) was corrected with the MS:

$$MP/P = 1.89 \times (3MP + 2MP) / (P+1.26(9MP+1MP)) \quad (\text{Eq. 4.7})$$

(Cassani et al. 1988)

$$MPI = (2MP+3MP)/(2MP+3MP+1MP+9MP) \quad (\text{Eq. 4.8})$$

## 4.5. Results

### 4.5.1. Mineralogy

The mineralogical and geographical description of the samples from Tasna, Platta and Chenaillet are presented in Table 4.1. The serpentinites are lizardite with a mesh texture. The chrysotile is present only in veins texture from pseudomorphic replacement of a fertile subcontinental lithospheric magma which is mostly lherzolite (Fig. 4.7) (Wicks and Whittaker 1977; Manatschal et al. 2001; Müntener et al. 2010). Olivine was replaced during the initial stage of serpentinisation, but pyroxene is still present, but pyroxene is still present. The chrysotile is present only in veins and antigorite is present only in the southern Platta area and has not been sampled because of the high temperature characteristic of this serpentine mineral. All the samples obtained from the sulphide rich deposits of Platta were serpentinites with visible shiny sulphides and without any calcite (veinlets or other) (Fig. 4.4). This sulphide deposit is situated on the top of what is interpreted as an extensional detachment fault surrounded only by serpentinite. The main mineralogy of the Platta sulphide mines is 80 to 90% lizardite according to XRD. Samples from the sulphide mines west of Marmorera lake have very zonal sulphides present with traces of ilvaite ( $\text{CaFe}^{3+}\text{Fe}_2^{2+}\text{O}(\text{Si}_2\text{O}_7)(\text{OH})$ ) and chlorite in samples P\_1\_16 and P\_3\_16 but no ilvaite in sample P\_2\_16 (Table 4.1). Sample P15 is characterised by other primary polymetallic sulphides such as pyrrhotite 6%, marcasite 6%, magnetite 5% and chalcocopyrite 1% and sample P\_2\_16 contain garnet and pyroxene showing an erratic mineral zonation within the outcrop (Table 4.1). Samples from the sulphide mines east of Marmorera lake contain only lizardite and ilvaite (samples P\_12\_16 to P\_18\_16) (Table 1).

Table 4.1 Results by lithology including mineralogy and texture observed in hand specimens

rock type	sample number	coordinates (°)		macroscopic description	mineralogical description
		Lat	Long		
<i>Chenaillet</i>					
Serp.gouge	C1	44.9108	6.7781	grey fine-grained deformed serpentinite with green serpentinite clastes following a direction	foliated matrix supported rounded claste of serpentinite and euhedral-subhedral magnetite (fig. 2 a,b)
Serp.cataclasite	C2	44.9222	6.7416	cataclasite serp. with sub-rounded serpentinite clastes in a serpentinite green matrix	foliated matrix with sub-angular serpentinite clastes (fig.2 c,d)
serp. lherzolite	C3	44.9212	6.7419	massive black serpentinite with white ultramafic minerals (pyroxene)	
ophicalcite	C5	45.9879	6.7438	white carbonate matrix with dark sub-rounded serpentinite clastes with finer chrysotile veins and gray clastes probably continental	deformed serpentinites clasts in carbonate matrix
Serp.breccia	C7	45.9879	6.7438	dark serpentinitate with several calcite veins and green veinlets, deformed, friable	no XRD or thin section
<i>Tasna</i>					
	S1	46.8409	10.2293	massive black serpentinite	lizardite, amphibole, replacement of olivine, pyroxene, spinel and magnetite; by serpentinite ± brucite ± talc ± magnetite
	S7	46.8263	10.2513	massive black greenish serpentinite	
serp.lherzolite	S8	46.8264	10.2510	black serpentinite with calcite veinlets and rest of ultramafic dark anhedral minerals and white-grayish peridotite minerals (px) and small chrysotile veinlets	
	S9	46.8298	10.2449		
	S10	46.8388	10.2574	till 1cm thickness neptunian dykes (calcite and pink limestone veins), previous chrysotile veins till 4mm tickness, black serpentinite with white sub-rounded mineral (px) and calcite veinlets	
	S2	46.8401	10.2613		
ophicalcite	S3	46.8391	10.2589	Carbonate with white crystallise calcite and rare serpentinite clasts	fine carbonate matrix with deformed serpetninite claste and later calcite veins
	S6	46.8398	10.2602	calcite veins with angular serpentinite clasts with chrysotile veinlets	
sandstone (Albian - Cenomamian)	S4	46.8401	10.2613	Cone in cone, gray siliclastic sandstones	
Tonschiefer shale	S5	46.8389	10.2589	dark gray fine shale with shistosity	
<i>Platta</i>					
serp.lherzolite	P6	46.3043	9.3864	sp very black wt rests of cpx mnl	no XRD or thin section
	P13	46.5083	9.6455	black serpentinite with anhedral gray serpentinitized ultramafic mineral	
serp.basalt	P1	46.5055	9.6280	iloclastic basalt forme like pillow lava	
serp.gouge	P3	46.5453	9.6587	massive black serpentinite with anhedral green serpentinite and outside dark olive colour platy showing foliation (Alpine deformation)	foliated fine grained matrix
	P5	46.4384	9.6448	High metamorphism serp.gouge in green schist, several serpentinitized veins cutting black clasts	
	P7	46.4994	9.6213	dark serpentine with grayish veins crossing smaller copper coloured & shiny white veins	90% serpentinite with ilvaite, chlorite and chalcopyrite (by XRD)
	P9	46.4998	9.6252		
	P10	46.5000	9.6238	white matt veins and clasts (>1cm) of pyroxen, broken serpentinite clastes ≈1mm or less	lizardite, pyroxene, chlorite and ilvaite (by XRD)
	P11	46.5003	9.6253	a lot of calcite veins, gray clair	
lizardite rich in sulphide	P12	46.5001	9.6250	dark serpentinite with several veins (white shiny; fine green ex-chrysotile), small equant oxides visible with gray serpentine claste and several generation of deformed veins	no XRD or thin section
	P18	46.4998	9.6166		
	P19	46.4986	9.6224	black serpentinite full of small equant oxides grains and thin serpetinized veinlets	
	P15	46.4986	9.6163	dark serpentinite sulphur smeeling and leaving black trace	lizardite 80%, 6% marcassite, 6% pyrrhotite, 5% magnetite and chalcopyrite (by XRD)
	P8	46.4998	9.6252	basaltic protolith, light green-grayish colour, chloritised -	lizardite, chlorite, garnet and pyroxene (XRD)
basalt	P17	46.5002	9.6172	> Low grade metamorphic basalt, greenschist -facies condition ?	
	P20	46.5000	9.6175		no XRD or thin section
	P21	46.5135	9.6436	dark serpentinite with white shiny coloured veins with black anhedral mineral following direction	lizardite and ilvaite (by XRD)
	P22	46.5135	9.6436	fine dark serpentinite with oxidised copper couleur veins and small fracture, anhedral black serpentine max 1mm	
lizardite	P23	46.5135	9.6436	dark serpentinite with deformed chrysotile veins and oxydised aound small fractures	more than 95% serpentinite (lizardite) and ilvaite (by XRD)
	P24	46.5135	9.6434	dark serpentinite with copper coloured veinlets and subhedral grains	
ophicalcite	P2	46.5460	9.6584	carbonate with calcite veins and serpentinite clasts (mm-cm), 306/45	fine carbonate matrix with deformed serpentinite clasts and carbonate clasts in calcite matrix
	P14	46.5458	9.6581	carbonate with calcite veins and rare serpentinite clasts	
post-rift sediment radiol.chert schist	P4	46.5451	9.6516	radiolarian mudstone	silica polymorphs
	P16	46.4998	9.6113	green fine matrix with angulars serpentinite clasts and calcite veins, protolite mudstone	pumpellyte 73%, plg 15%, calcite 10%, chl 2% by XRD

Table 4.2 TOC and TC in ppm (parts per million), total HC concentration in ppb (parts per billion) and organic carbon isotopic composition of bulk rock  $\delta^{13}\text{C}_{\text{organic}}$ . For the n-alkanes: the carbon number range (n-alkane range), the maximum carbon number (Cmax), carbon preference index (CPI values) and mean carbon number (MC#) are shown. For the steranes, hopanes and PAHs the concentrations are in ppb and are represented in intervals by star symbol \*, where \* = [0 - 0.1), \*\* = [0.1 - 1) and \*\*\* = [1 - 10) and BDL = below detection limit.

rock type	sample number	Total Carbon ppm	Total C <sub>organic</sub> ppm	Hydrocarbons (HC) ppb	n-alkanes				Steranes	Hopanes	PAHs
					Range	C <sub>max</sub>	CPI	Mean C#			
<i>Chenaillet</i>											
Serp.gouge	C1	566	134	1939	16-36	C16	0.68	19.63	*	*	**
Serp.cataclasite	C2	603	189	2580	16-38	C16	0.68	20	BDL	*	***
serp.lherzolite	C3	450	113	230	16-39	C22	0.86	23.9	*	*	**
ophicalcite	C5	23166	170	658	17-38	C29	1.12	29.56	*	*	*
Serp.breccia	C7	10379	111	140	16-38	C29	3.12	23.17	BDL	*	*
<i>Tasna</i>											
	S1	392	158	0.96	16-37	C20	1.33	26.11	*	BDL	*
	S2	1737	123	0.38	16-37	C29	0.97	26.19	BDL	*	*
serp.lherzolite	S8	1360	203	-	-	-	-	-	-	-	-
	S9	3098	171	0.57	16-33	C20	0.86	24.35	BDL	BDL	*
	S10	50529	52	0.18	16-33	C20	0.91	27.72	BDL	BDL	BDL
ophicalcite	S3	117533	16500	0.46	22-35	C29	1.15	28.94	BDL	BDL	BDL
	S6	73353	23000	0.93	16-37	C18	0.81	23.5	BDL	BDL	*
sandstone (Albian - Cenomamian)	S4	70832	49	55	16-36	C22	0.81	22.87	BDL	BDL	BDL
Tonschiefer shale	S5	692	700	29	16-37	C16	0.88	20.03	BDL	BDL	BDL
<i>Platta</i>											
serp.lherzolite	P6	232	230	0.40	18-37	C29	1.1	27	BDL	BDL	*
	P13	3156	252	1	18-36	C20	0.9	24	BDL	BDL	*
serp.basalt	P1	2971	141	36.50	17-41	C20	1.0	27	*	*	*
serp.gouge	P3	375	105	24	17-35	C21	1.0	25	*	*	*
	P5	491	268	1046	16-38	C16	0.9	28	*	*	**
sulphide mine	P7	337	235	0.09	18-40	C27	1.1	28	BDL	BDL	*
serpentinite	P9	401	189	37	20-38	C29	1.1	28	BDL	BDL	*
Cotschens	P10	294	179	339	20-33	C22	0.9	24	BDL	BDL	*
W of Marmorera lake	P11	1046	670	8.10	16-32	C22	1.0	24	BDL	BDL	*
	P12	296	339	0.07	17-33	C27	1.1	26	BDL	BDL	*
	P18	310	135	1.70	19-35	C22	0.9	24	BDL	BDL	*
	P19	414	180	7.30	17-35	C20	1.0	26	BDL	BDL	*
	P15	436	365	0.01	22-32	C22	0.8	26	BDL	BDL	BDL
sulphide mine	P8	330	200	0.20	18-31	C22	0.9	24	BDL	BDL	*
basalt E of	P17	279	245	0.04	17-24	C17	0.8	24	BDL	BDL	*
Marmore lake	P20	395	236	0.20	16-34	C27	1.3	26	BDL	BDL	*
sulphide mine	P21	291	181	29	20-42	C23	1.0	26	BDL	BDL	*
serpentinite	P22	270	288	2.10	19-35	C19	0.9	25	BDL	BDL	*
Mottas	P23	263	255	0.20	17-34	e28	1.0	26	BDL	BDL	*
E of Marmore lake	P24	267	150	6.80	19-30	C24	0.9	23	BDL	BDL	*
ophicalcites	P2	89798	13	66	16-37	C21	0.9	25	**	*	***
	P14	92828	82	1	16-36	C17	0.8	22	BDL	BDL	BDL
radiol.chert	P4	1113	650	1	21-38	C29	1.0	29	BDL	BDL	*
(post-rift)											
metamorphic mudstone	P16	3839	235	0.03	17-38	C29	0.9	27	BDL	BDL	*

Table 4.3 PAHs ratios for the samples from Cheanillet, Platta and Tasna. The ratios show the rapport between PAHs as an indication of the HT source origin. Identified PAHs in the samples used for the ratios were: Phenanthrene,P; Fluoranthene, Flui; Pyrene, Pyr; Chrysene, Chry; Benzo (a) anthracene, BaA; methyl (3,2,1 and 9 MPs) naphthalene

	MP/P ≤0.5	(3+2-MP)/(3+2+9+1-MP)	Fluoranthene/Pyrene >1	BaA/BaA+Chry > 0.35	MPAHs/PAHs ≤ 0.3
Petrogenic source	MP/P >3.5		Fluoranthene/Pyrene <1	BaA/BaA+Chry <0.2	MPAHs/PAHs ≥2.2
Mixed	MP/P >0.5 & <3.5			BaA/BaA+Chry >0.2 & <0.35	MPAHs/PAHs > 0.3 & <2.2
references	(Saha et al. 2012)		Motelay-Massei et al. 2007	(Yunker et al. 2012)	(Saha et al.2012)
Samples					
C1	0.4	0.5			
C2	0.4	0.6			0.5
C3	0.6	0.5		0.6	0.3
C7	0.1	0.5			
S1	1.2	0.6	5.7	0.5	0.1
S9			0.4		
P1	1.0	0.5			0.1
P2	0.9	0.5	0.6		0.1
P5	0.6	0.5			0.8
P_1_16			1.1	0.7	
P_2_16			0.0		
P_3_16			0.7		
P_4_16	0.9	0.5	0.4		0.1
P_7_16	0.2	0.2	0.4	0.3	0.5
P_8_16	1.0	0.4	0.4		0.1
P_9_16					
P_10_16					0.0
P_11_16	0.9	0.5	0.8		0.2
P_12_16	0.7	0.5	0.0		0.3
P_13_16	0.7	0.4	0.3		0.1
P_14_16	1.0	0.5	1.1		0.2
P_17_16	0.9	0.5	0.6		0.2

#### 4.5.2. Hydrocarbon distributions in the analysed lithologies: Biomarkers

The TC reflects the carbonate contents of the various lithologies, for example the ophicalcite contain more carbon than the serpentinites. The TOC values are low and do not show a positive correlation with the TC or HC values (Table 4.2).

Hydrocarbons in samples from the three areas are characterized mainly by aliphatic compounds ( $>C_{16}$ , *n*-alkanes) and PAHs with 3-5 benzene rings (Table 4.2) (Fig. 4.8 - 4.10). The CPI (carbon preference index) for the *n*-alkanes are in the range  $1\pm 0.3$ , except for one deformed serpentinite breccia in the Chenaillet (C7) which had a CPI of 3.1 and was clearly contaminated with modern OM (Table 4.2).

The present PAHs are P, MPs, Fluo, Pyr and rarely Chry and BaA, their ratios are used to calculate their source (Fig. 4.8 d, 4.9 d, 4.10 d, Table 4.3). The PAHs ratios are shown in Table 4.3, however due to their low concentrations, the ratios must be treated with some caution and are used only as supportive data. Among polycyclic biomarkers, steranes and hopanes were present in some of the samples (Table 4.2).

Hopanes include mainly  $C_{29}$  to  $C_{31}$   $\alpha\beta$  with  $C_{29}$  dominant.

The steranes present in the samples consist of 20S, R  $\alpha\alpha\alpha$  and  $\alpha\beta\beta$  isomers from  $C_{27}$  to  $C_{29}$ , as well as diasteranes 20S, R  $C_{27}$  to  $C_{29}$  with  $C_{27}$  dominance (Table 4.2) (Fig. 4.8- 4.10 c). The ternary diagram of  $C_{27}$ ,  $C_{28}$ ,  $C_{29}$  steranes (Fig. 4.11) is plotted to infer the source of OM, where  $C_{27}$  is associated with zooplankton,  $C_{28}$  with phytoplankton and  $C_{29}$  to higher lands plants or major input of algal OM (Huang and Meinschein 1979; Peters et al. 2005b; Volkman 2005; Wójcik-Tabol and Ślęczka 2015). The  $C_{27}$  is dominant (27 to 68%),  $C_{29}$  is intermediate (11.3 to 45%) and  $C_{28}$  is minor (13 to 38%) (Fig. 4.11).

The only isoprenoids present in the samples are pristane and phytane. The isoprenoids (pristane, phytane)/*n*-alkanes ratio plot is used to distinguish the

depositional conditions of the OM (Fig. 4.10). The isoprenoids/*n*-alkane ratios range for all the areas are 0.17 to 0.66 for Pr/*n*-C<sub>17</sub> and in the range of 0.14 to 0.77 for Ph/*n*-C<sub>18</sub> (Fig. 4.14).

Samples from the three OCT areas plotted on a ternary plot of regular steranes and the isoprenoid/*n*-alkane ratios plot are added to the data already published for samples of the Totalp area (Fig. 4.11, 4.14).

Our biogeochemical analysis shows that the OM found in our samples is from reducing environment. Such environment could be aquatic sediments, subsurface waters and soils and hypolimnia of stratified lakes. A reducing environment is a place where oxygen is missing (free) and where iron cations could play as a reductant in the redox reactions.

The reducing environment is characteristic for the OM from the bulk rock. But is there a way to localize the OM in our samples? Is it the carbonate matrix that contain the OM or is the calcite veins that contain it, or serpentinite or is everywhere?

The majority of our samples from the carbonate staining and acetate peels method show a non-ferroan carbonate which could be interpreted as oxidising environment (Table 4.4).

Sample 19, a limestone from Totalp is a post-rift sediment and shows a ferroan carbonate matrix and first generation of veins, which means that these two carbonate textures are from reducing environment and most likely have similar age (Fig. 4.12). This is validated by previous research indicating that in Totalp unit post-rift sediments are poorly oxygenated (hemi)-pelagic (Weissert and Bernoulli 1985). The second generation of vein in this sample is non-ferroan from an oxidizing environment, probably occurring later (Fig. 4.12, Table 4.4).

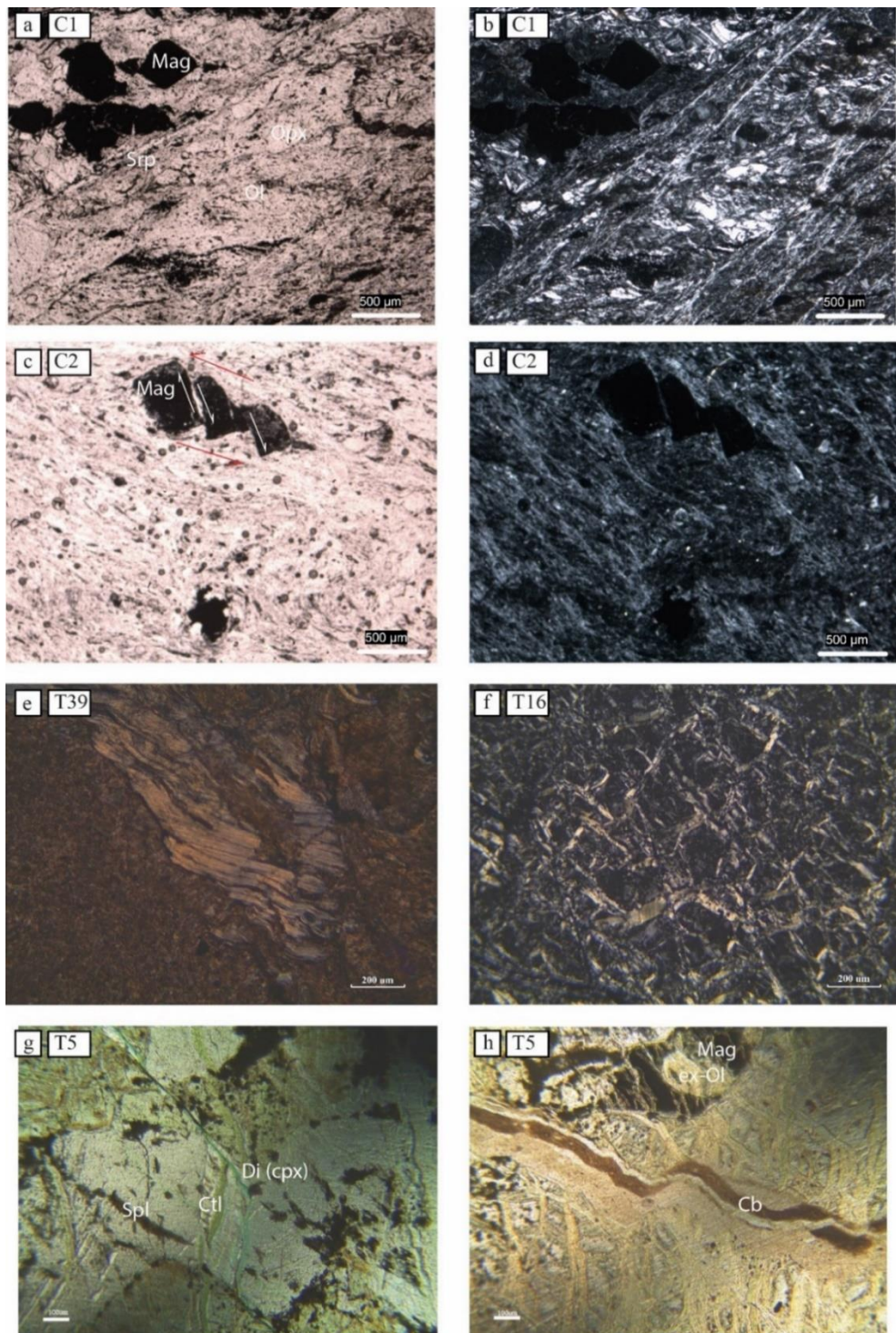
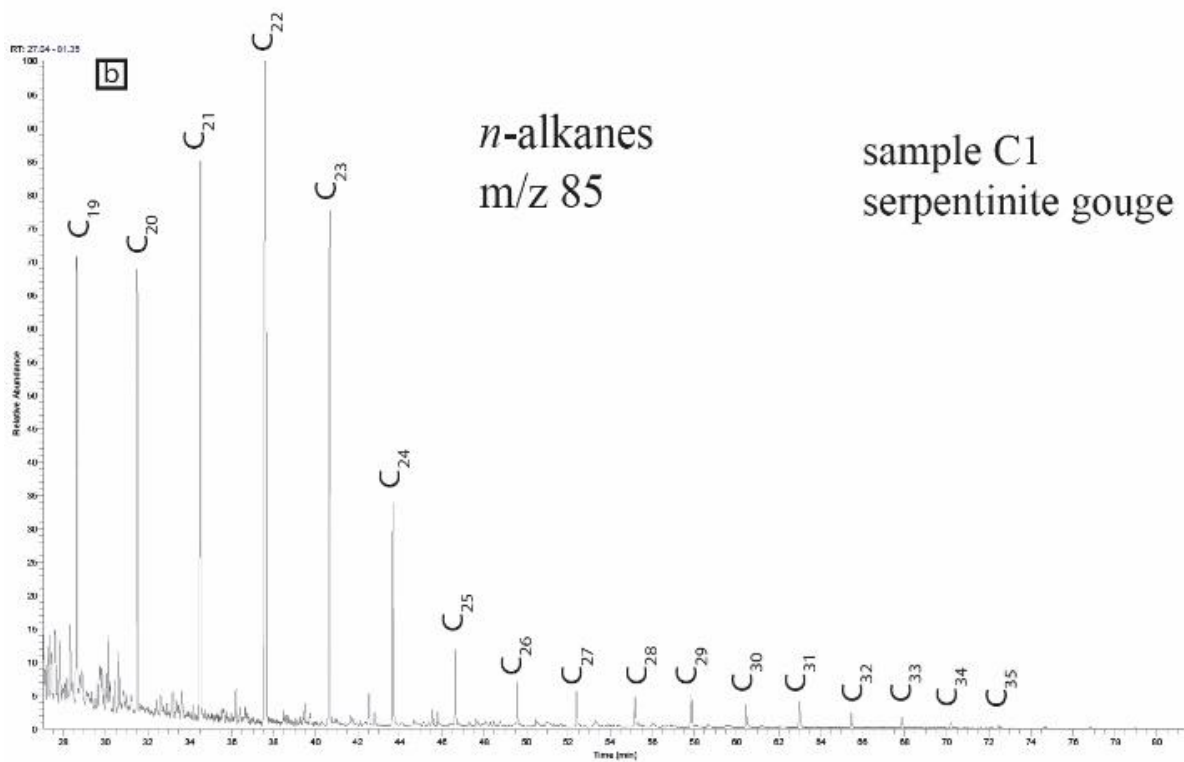
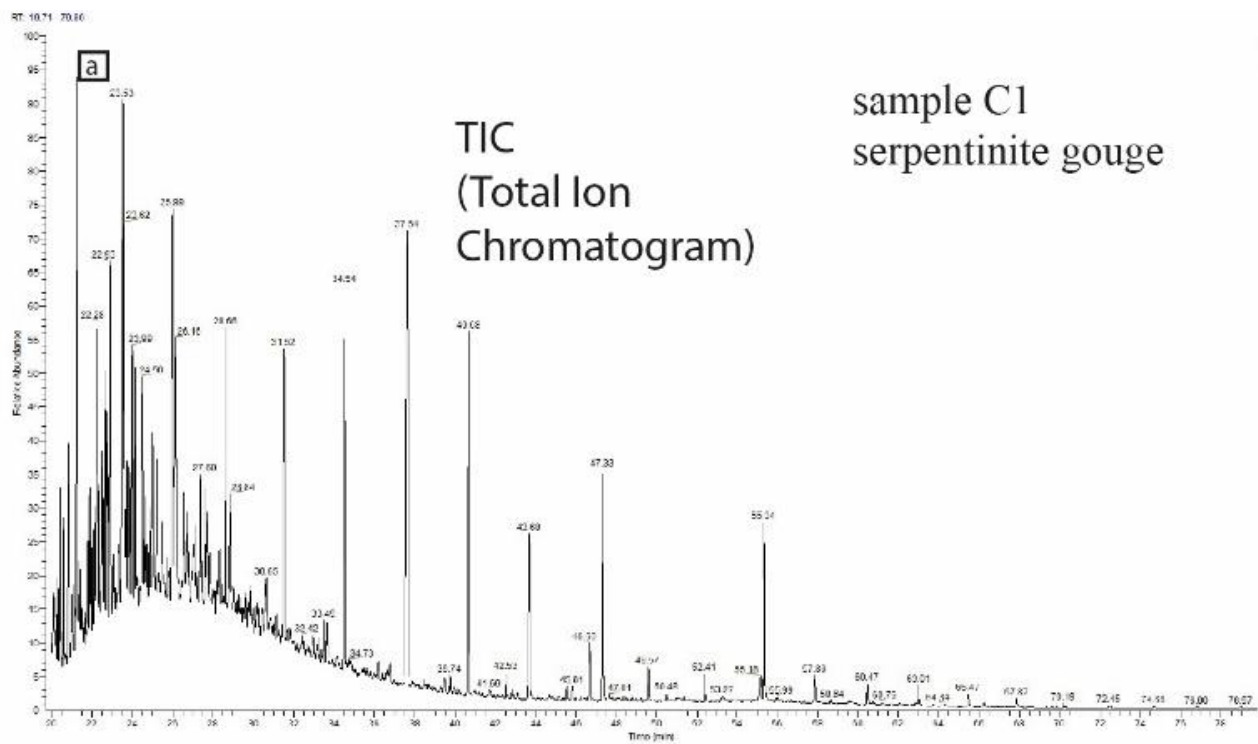


Figure 4.7. Thin sections from Chenaillet (a-d) and Totalp (e-h). a-d. serpentinite gouge and serpentinite cataclasite with foliated matrix and (table 1). e. opicalcite representing serpentinite clast in a carbonate matrix. f. mesh structure of serpentinite g-h. serpentinite mesh structure with olivine completely serpentinised, rest of clinopyroxene, later chrysotile veins cross-cutted by carbonate vein (see B.1).



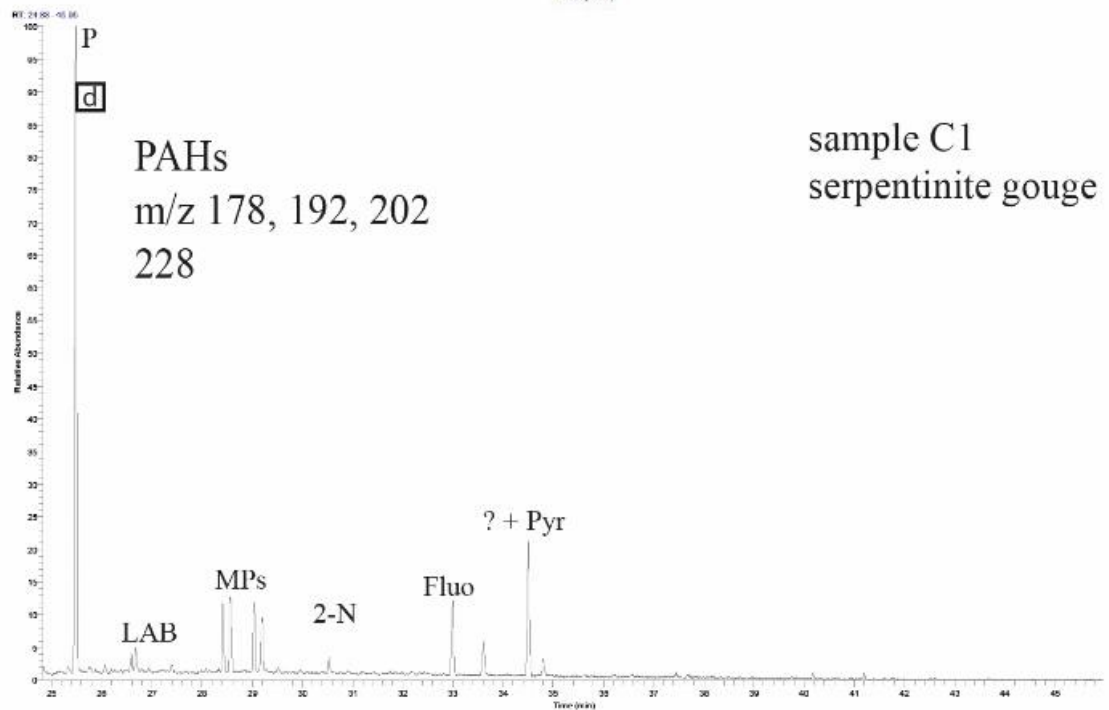
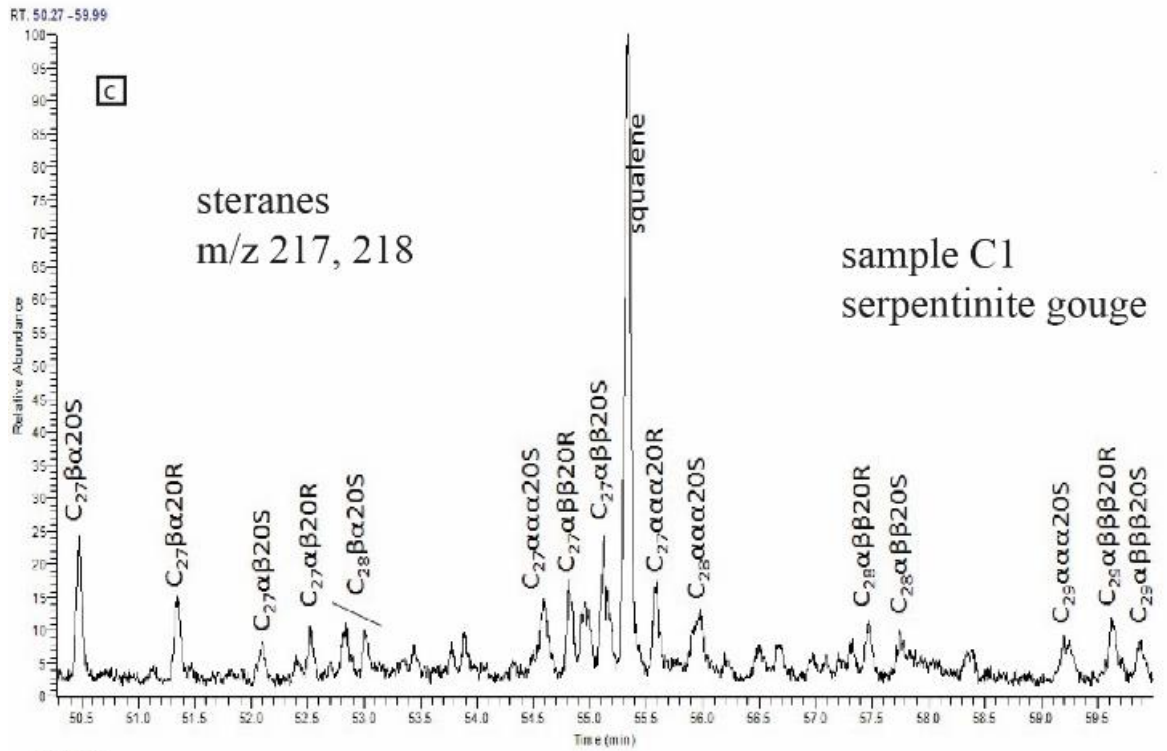
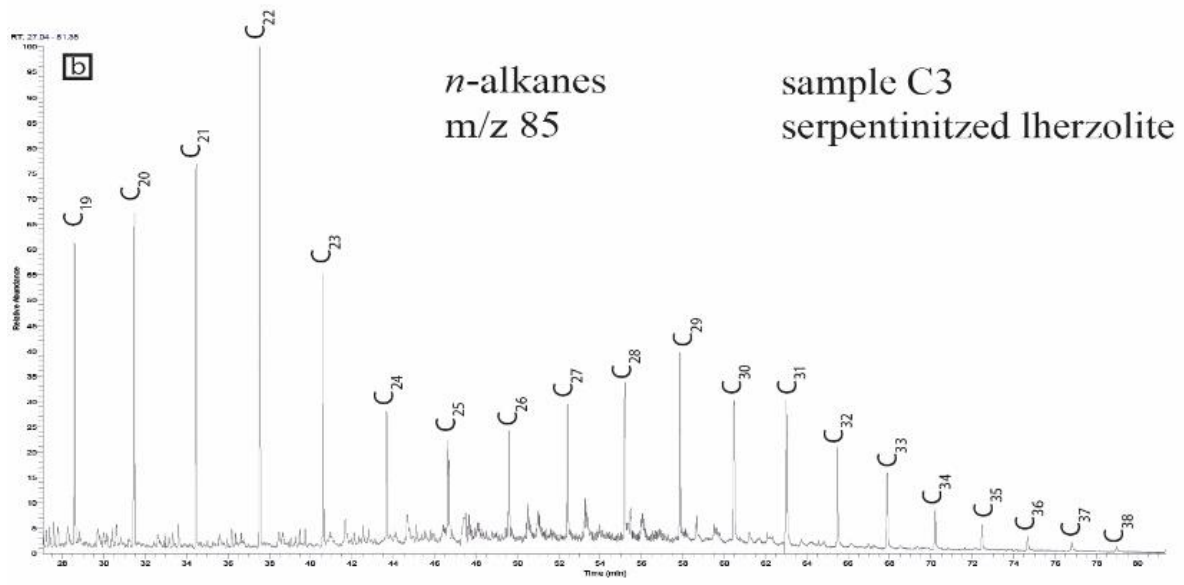
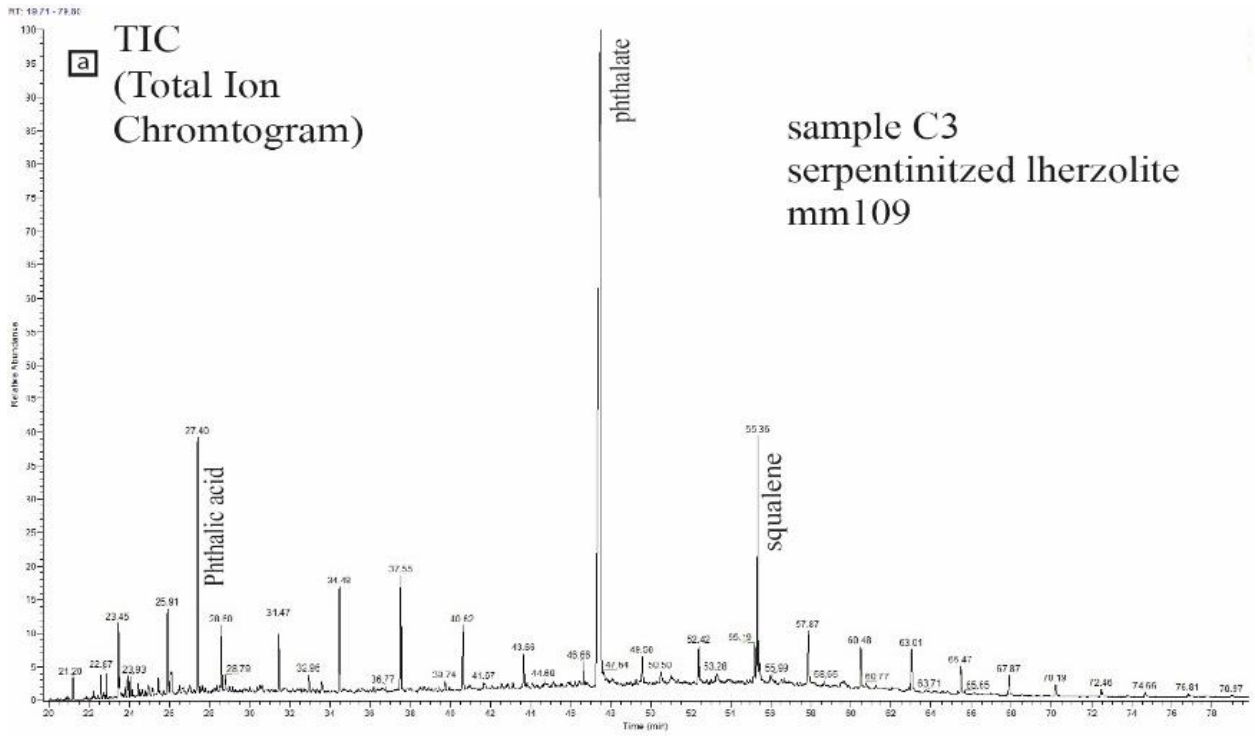
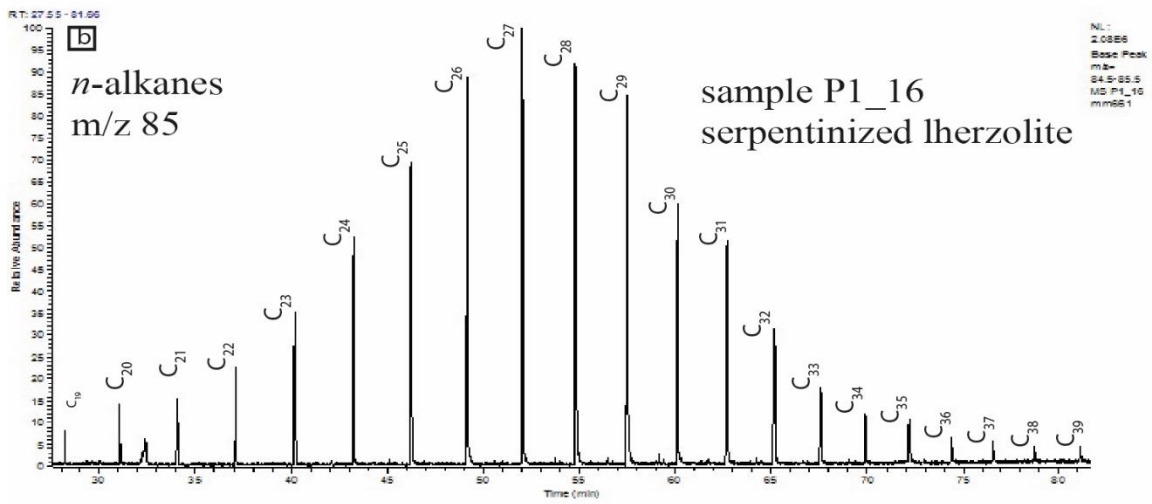
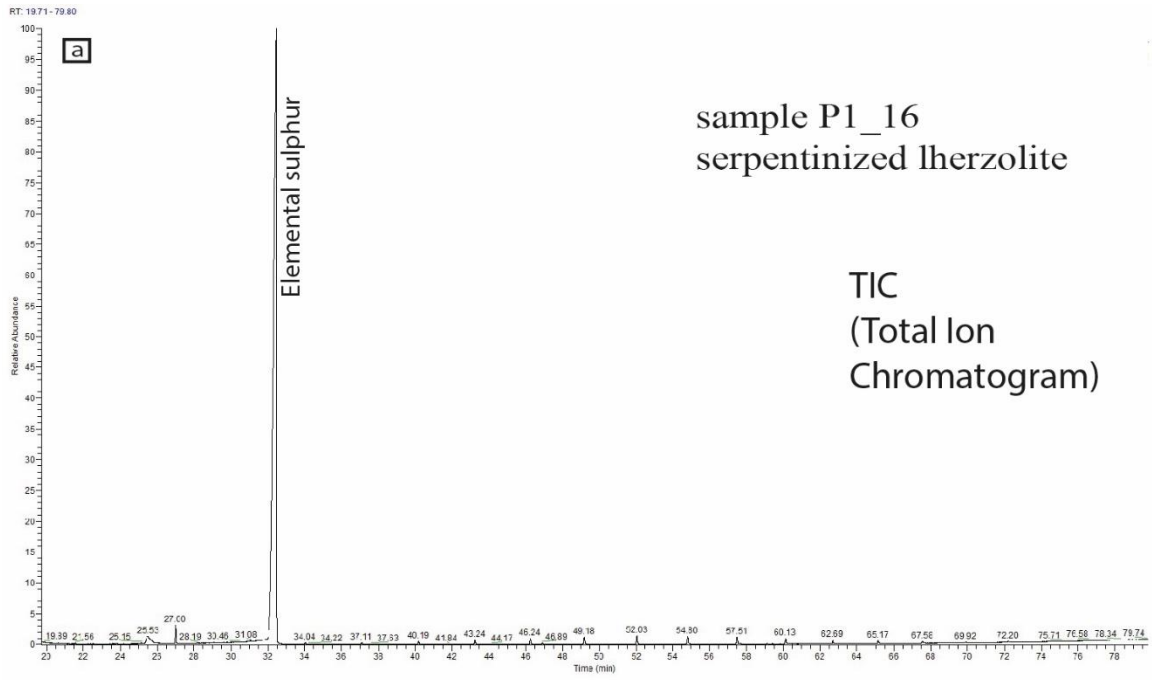


Figure 4.8. Representative mass chromatograms of the HCs of a serpentinite gouge C1 (Chenaillet). a) Total Ion Chromatogram b) *n*-alkanes distribution (m/z 85) c) sterane distribution (m/z 217, 218) d) PAH distribution (m/z 178, 192, 202, 228). For abbreviations see appendix.







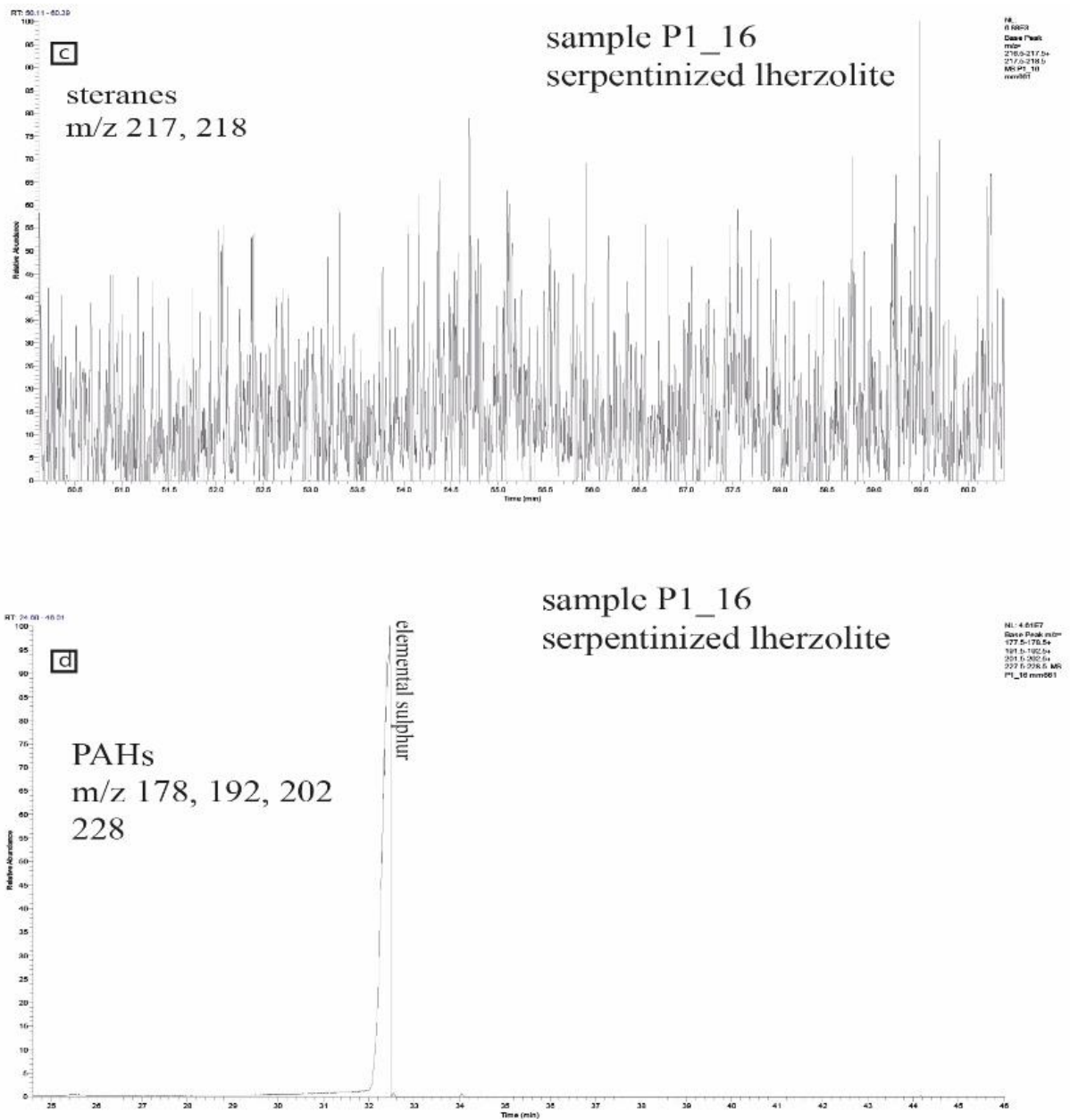


Figure 4.10. Representative mass chromatograms of the HCs of serpentinite sample P\_1\_16 from sulphide mine. a) Total Ion Chromatogram b) *n*-alkanes distribution (m/z 85) c) sterane distribution (m/z 217, 218) d) PAH distribution (m/z 178, 192, 202, 228). For abbreviations see appendix.

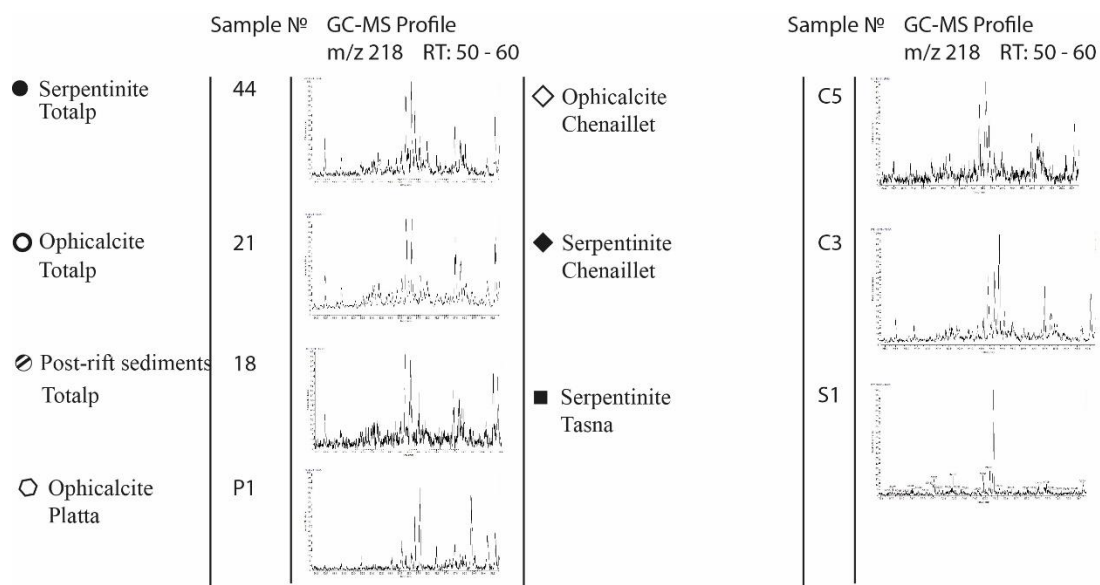
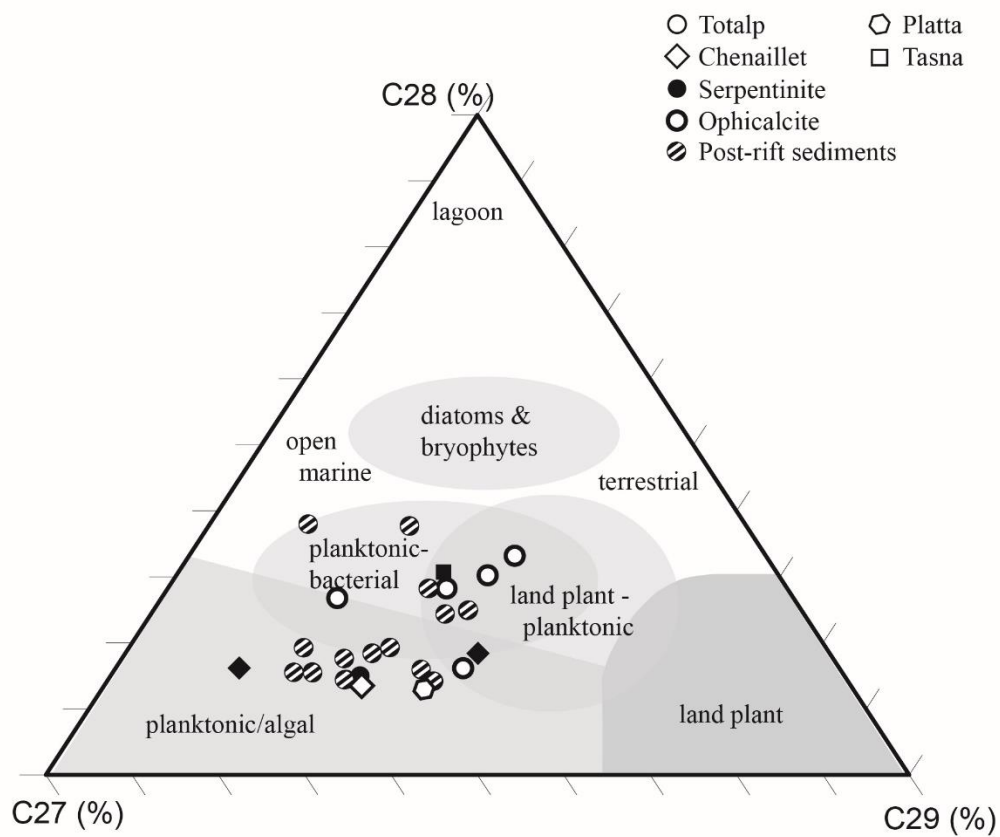


Figure 4.11. Sterane ternary distribution of the analysed samples for the studied areas for the  $\alpha\beta\beta$  and  $\alpha\alpha\alpha$  steranes, modified after Mateeva et al. 2017. The interpretation of depositional environment is from Patrycja Wójcik-Tabol & Ślącza (2015). A gas chromatogram from each group is presented with retention time 50 to 60.

Samples showing OM originating from reducing environment by isoprenoids/*n*-alkanes ratios – 24,25,29,33, 39 and 44, have non-ferroan veins and carbonate matrix. This could indicate that the OM is not related to the carbonate – veining or matrix but rather in the serpentinite.

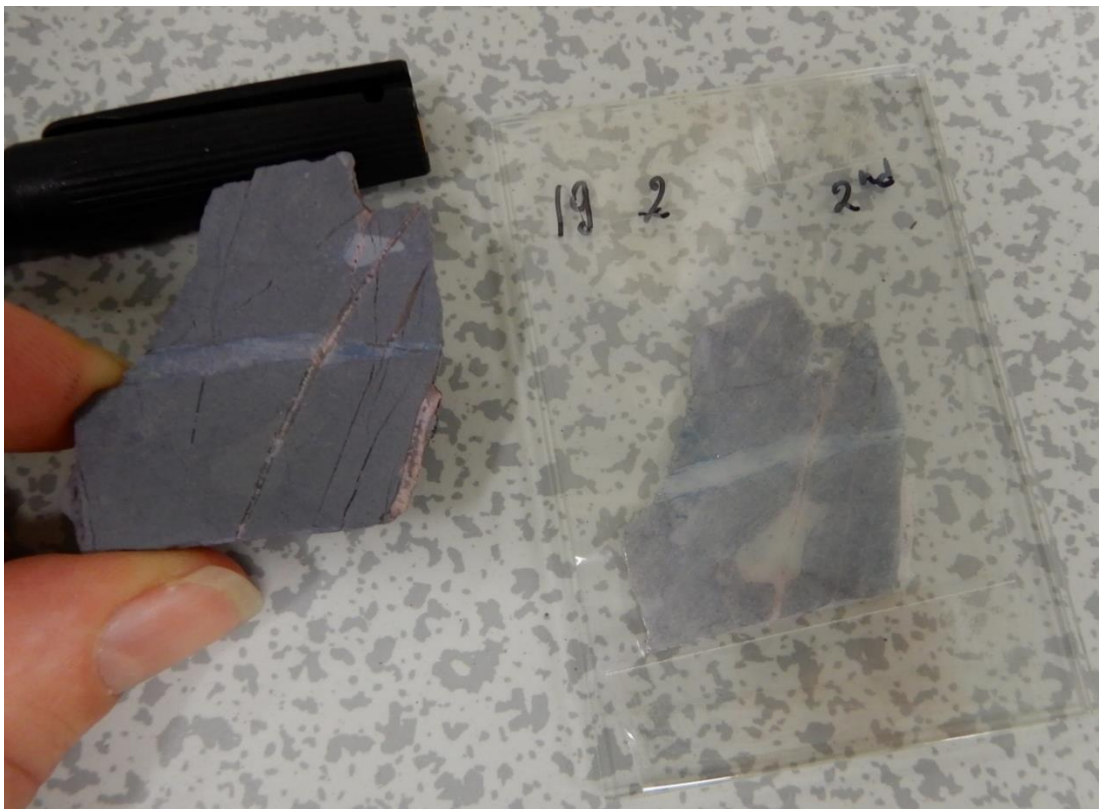


Figure 4.12 Carbonate staining of sample 19, a limestone from Totalp. It is clearly seen in blue the limestone matrix and horizontal bigger calcite veins and in pink several veins almost perpendicular to the blue one.

Table 4.4. Table showing the result from carbonate staining. Where the staining shows blue colour, it is interpreted as reducing environment, where the colour is pink is interpreted as oxidizing environment.

	Sample	Litho	Ferroan carbonate (reducing) or non-ferroan carbonate	
			Veins	Matrix
T o t a l P	16	serp. lherzolite	oxidizing	/
	19	limestone with 2 generations of veins	1st - reducing 2nd - oxidizing	reducing
	24	Serpentinite with numerous calcite veins	oxidizing	/
	25	tectono-sedimentary breccia (calcite and serpentine veins separating serpentine clasts; clasts supported)	oxidizing	/
	29	Tectono-sedimentary ophicalcite with carbonate matrix, sparic calcite veins and rare serpentine clasts	oxidizing	oxidizing
	33	serp. lherzolite with rest of cpx minerals, <0.5mm serpentine veins, <0.5mm rare calcite veins	oxidizing	/
	39b	serp. lherzolite with rest of cpx minerals, <0.5mm serpentine veins, <0.5mm rare calcite veins	oxidizing	/
	39	tectono-sedimentary ophicalcite (carbonate matrix with serpentine clasts and calcite veins)	oxidizing	oxidizing
	44	Serpentinite with numerous calcite veins	oxidizing	/
	63	3 sort of carbonate matrix and calcite veins	oxidizing	2 - oxidizing, 3th one before veining - reducing
	72	tectono-sedimentary breccia with serpentine clasts broken calcite veins	oxidizing	/
T a s s n a	S9	serp. lherzolite	oxidizing	/
	S10	type of carbonate veining (red-brown micrite surrounded by 2nd type)	oxidizing	1st - oxidizing 2nd - reducing
Platta	P1	serp. basalt with <1mm len	reducing	/

#### 4.5.2.1. Tasna

Hydrocarbons of Tasna only include steranes and hopanes ( $C_{29}\alpha\beta$  and  $C_{30}\alpha\beta$ ) in two samples (S1 serpentinite and S2 black shale) (Table 4.2) and their concentrations are low. Lab contamination of HCs of sample S8 occurred and data are not included in Table 4.2.

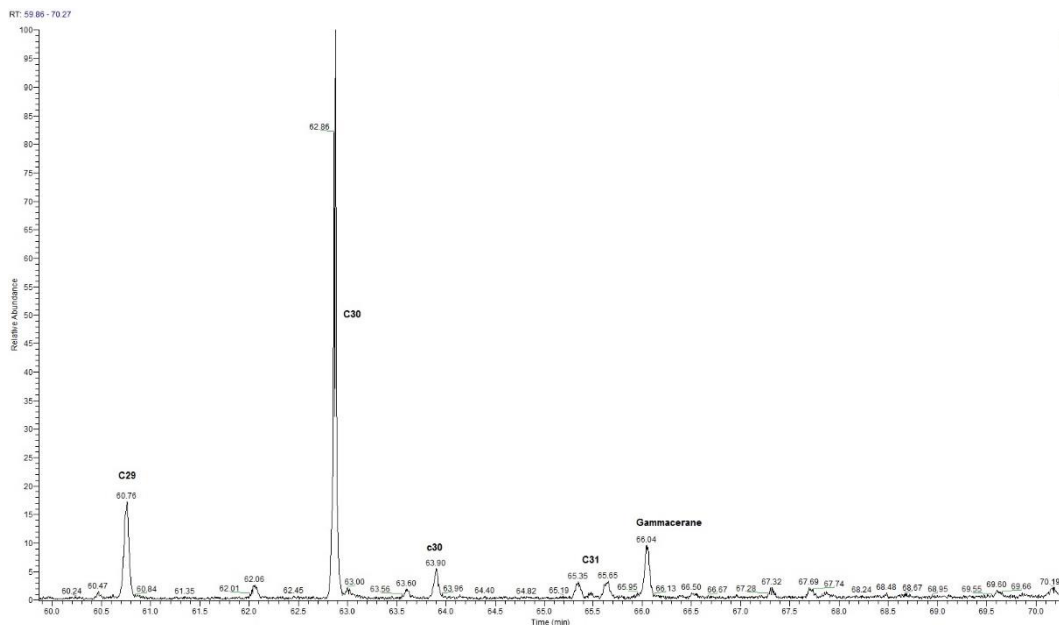


Figure 4.13. Mass chromatograms ( $m/z$  191) of sample P1 (serpentinised basalt) showing the distribution of hopanes (including gammacerane)

#### 4.5.2.2. Totalp

A detailed description of Totalp has been presented by Mateeva *et al.* (2017) and the findings are summarized here. HC (0.03ppb to 2500 ppb) in serpentinised lherzolite, ophicalcites and post-rift sediments were dominated by *n*-alkanes ( $C_{16}$ – $C_{40}$ ), PAHs, steranes and hopanes, with distribution consistent with those in the other three OCT areas described here. The inorganic carbon and organic carbon amounts are variable from 14 to 106000 and 19 to 647 ppm, respectively, and reflect the amount of carbonate and the lithological diversity at Totalp.

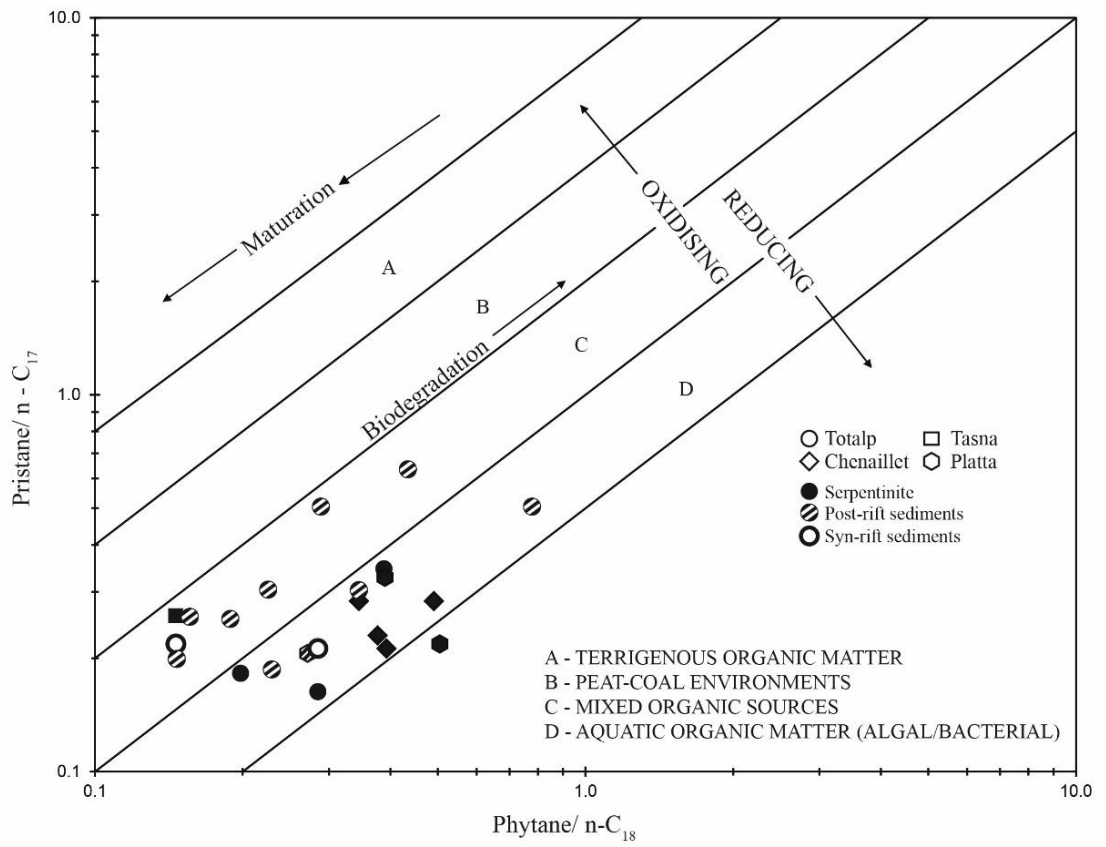
#### 4.5.2.3. Platta

The two serpentinite gouges (samples P3, P5) show dominance of  $C_{29}\alpha\beta > C_{30}\alpha\beta$  hopane while the ophicalcite sample P2 shows hopanes with different dominance  $C_{30}\alpha\beta > C_{29}\alpha\beta \gg C_{31}\alpha\beta$  S and R. A serpentinite basalt (sample P1) has the greatest range of hopanes  $C_{30}\alpha\beta > C_{29}\alpha\beta \gg$  Gammacerane  $> C_{30}\beta\alpha > C_{31}\alpha\beta$  S and R  $> C_{32}\alpha\beta$  S and R (Fig. 4.13). Gammacerane has been used with  $C_{30}$  hopane to calculate the gammacerane index (gammacerane/ $C_{30}$  hopane = 0.1) which serves to distinguish between oxic or anoxic environment (Kaiho et al. 2016).

Hydrocarbons isolated from the sulphide-copper mine samples did not include any steranes or hopanes and are not different in HC amount or distribution than other Platta samples (Table 4.2).

#### 4.5.2.4. Chenaillet

Samples from Chenaillet have the highest concentrations of HC from the three areas (Table 4.2). The samples contain hopanes ( $C_{29}\alpha\beta$ ,  $C_{29}Ts$ ,  $C_{30}\alpha\beta$ ,  $C_{31}\alpha\beta$  S and R,  $C_{30}\beta\beta$ ,  $C_{32}\alpha\beta$  S and R and  $C_{31}\beta\beta$ ) decreasing from  $C_{29}\alpha\beta$  to  $C_{32}\alpha\beta$  R. The serpentinised mantle in the Chenaillet contained the most PAH compounds (eg. P, MPs, Fluo) whereas the ophicalcite samples contain only Fluo (Table 4.3, Fig. 4.8, 4.9 d). The samples from Chenaillet did not have sufficient TOC to permit isotopic analysis on organic carbon (Table 4.2).



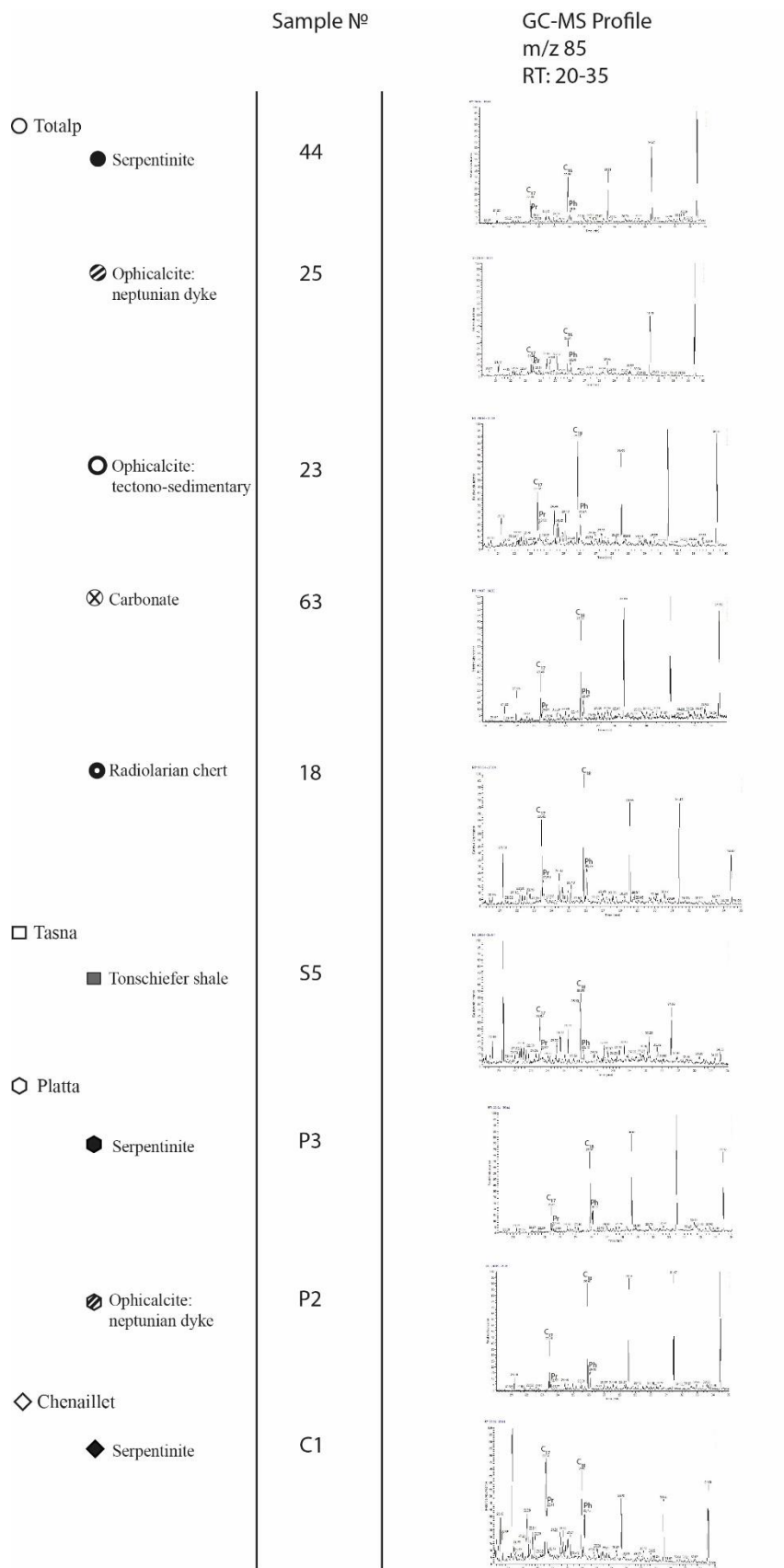


Figure 4.14. Plot of pristane/n-C17 vs phytane/n-C18 for Platta, Tasna, Chenaillet and Totalp samples used to identify depositional environment and OM type (Peters et al. 1999, Mateeva et al.2017). A gas chromatogram from each group is presented with retention time 20 to 35.

### 4.5.3. Carbon isotopes

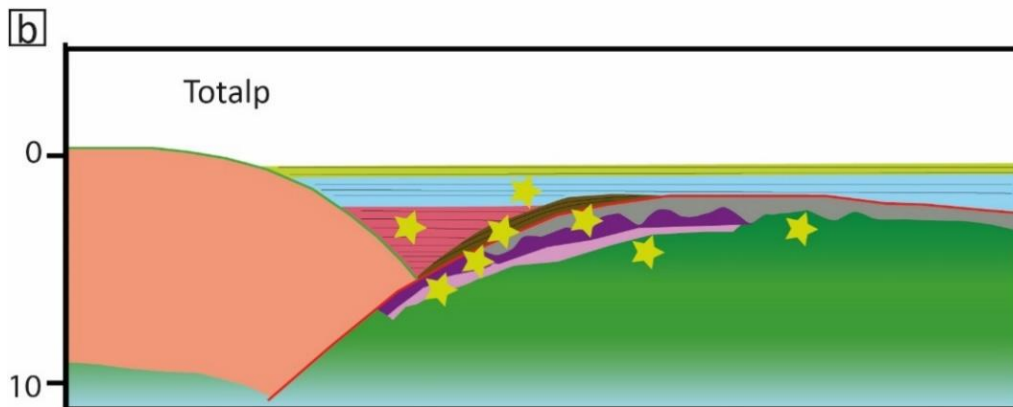
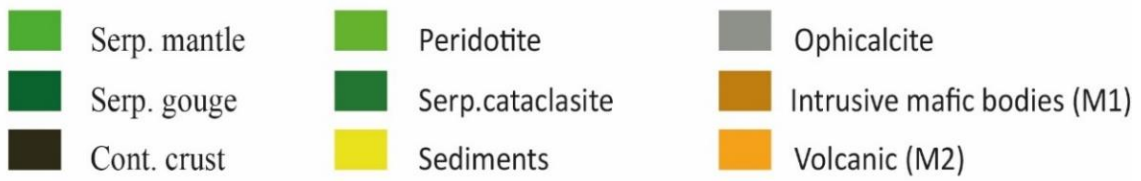
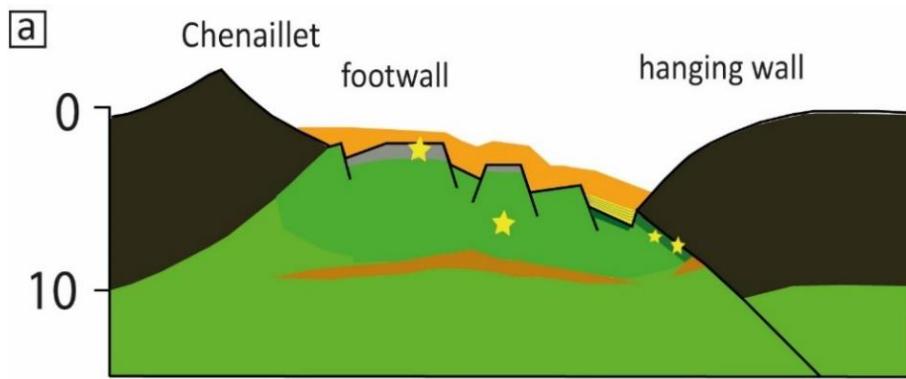
Only one sample, a post-rift sediment from Tasna (sample S5), had organic carbon contents high enough to allow isotopic analysis, with  $\delta^{13}\text{C}_{\text{org}} = -26.2\text{‰}$  VPDB. Of five samples from Totalp, the organic carbon isotopic composition range between  $\delta^{13}\text{C}_{\text{org}} = -26.02\text{‰}$  to  $-27.4\text{‰}$  VPDB (Mateeva et al. 2017).

$\delta^{18}\text{O}_{\text{SMOW}}$  of the calcite veins have values between 12.2 to 24.5‰ (12.2 to 16.4‰ for Platta; 16.7 to 19.2‰ for Tasna and 18.8 to 24.5‰ for Totalp) and the  $\delta^{13}\text{C}_{\text{VPDB}}$  are between -1.1 to 5.4‰ for Tasna; -0.78 to 1.9‰ for Totalp and 1.02 to 2‰ for Platta (Fig.B.5). These are similar to values previously reported for Alpine ophiolites (e.g. Davos-Parsenn, Arosa areas (Früh-Green et al. 1990; Engström et al. 2007)). The stable isotopic composition of a second generation of calcite veins in opicalcite (sample P2) is  $\delta^{13}\text{C}_{\text{VPDB}} = 1.02\text{‰}$  and  $\delta^{18}\text{O}_{\text{VPDB}} = -14.1\text{‰}$  (Table 4.5). The isotopic composition of a first generation calcite veins from a serpentinite basalt (sample P1) were  $\delta^{13}\text{C}_{\text{VPDB}} = 2.04\text{‰}$  and  $\delta^{18}\text{O}_{\text{VPDB}} = -18.12\text{‰}$  (Table 4.5).

Stable isotopic analyses of calcite veins from opicalcites from Tasna gave values from  $\delta^{13}\text{C}_{\text{VPDB}} = -1.1\text{‰}$  to 5.4‰ and  $\delta^{18}\text{O}_{\text{SMOW}} = 17.5\text{‰}$  to 19.2‰ (Table 4.5). For calcite veins from the serpentinite peridotite above the Moho limit, Tasna unit the isotopic composition was  $\delta^{13}\text{C}_{\text{VPDB}} = 0.21\text{‰}$  and  $\delta^{18}\text{O}_{\text{SMOW}} = 16.7\text{‰}$  (Table 4.5).

### 4.5.4. Fossil geological emplacement at the Tethys ocean

Conceptual sketch representing the geological emplacement and related lithology of the four studied areas (Tasna, Totalp, Chenaillet and Platta) on the seafloor (Fig. 4.15). These sketches serve to visualise the lithology and their place on the seafloor and with the serpentinised mantle to which our sampling strategy is based.



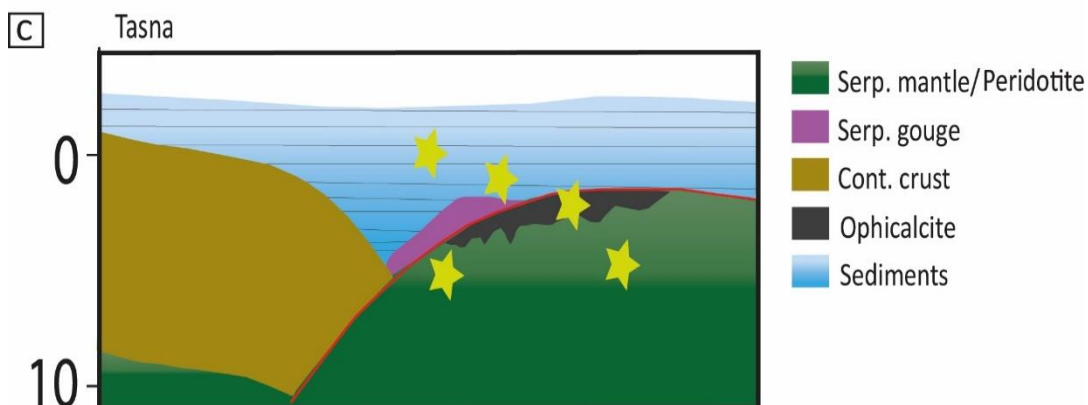


Figure 4.15 Conceptual sketch visualising different lithology on the seafloor. For these sketches software Stretch was used to draw the detachment normal faults.

Table 4.5 Table showing the carbon and oxygen isotopic results of the carbonate texture on samples from Tasna and Platta.

rock type	sample number	Carbonate texture	$\delta^{13}\text{C}_{\text{VPDB}}$ (‰) Ca veins	$\delta^{18}\text{O}_{\text{SMOW}}$ (‰) Ca veins
<b>Tasna</b>				
serp.lherzolite	S9	sparitic calcite in veins	-1.1	17.5
	S10	calcite veins surrounded by pink	0.21	19.2
Ophicalcite	S6	carbonate vein matrix	5.4	16..7
	P2		1.32	16.3
	P14	later generation sparitic calcite in veins	1.02	16.4
Serp. basalt	P1	thick ovals calcite cross cutted by small rare calcite veins, follow the direction of the basalt minerals	2.04	12.2

#### 4.5.5. Platta Sulphide mine

Fourteen samples from the sulphide deposit were analysed because of their presumed hydrothermal origin and therefore the possibility of the occurrence of methanotrophic biosystem (Fig. 4.5).

The sulphide deposit contains the sulphides -marcasite, chalcopyrite, pyrrhotite, and the oxydes, magnetite, ilvaite, as well as other minerals as chlorite, garnet and pyroxene (Table 4.6, 4.7). The host rock is lizardite of greenschist facies metamorphic grade.

Table 4.6. Table showing results from XRF for the samples from Platta sulphide mine

	10 <sup>4</sup> -10 <sup>5</sup> ppm	10 <sup>3</sup> -10 <sup>4</sup> ppm	10 <sup>2</sup> -10 <sup>3</sup> ppm	10-100 ppm	0-10 ppm
P_1_16	Fe, Al, Si, Mg	Ni, Mn, Cr, Ca, S	Zn, V, Ti, K, Ba, Cs, Te, P, Cl	/	Sr
P_2_16	Fe, Ca, Al, Si, Mg	Mn, Ti	Zr, Zn, Ni, Cr, V, Sc, K, S, Ba, Cs, Te, P, Cl	Sr, Cu, Sn	Nb
P_3_16	Fe, Al, Si, Mg	Ni, Mn, Cr, Ti, Ca	V, K, Ba, Cs, Te, P, Cl	Zn, Cu, Sn	Sr
P_8_16	Fe, Al, Si, Mg	Ni, Cr, S	Mn, Ti, Ca, K, Ba, Cs, Te, P, Cl	Zn, V	Sr, U
P_12_16	Fe, Ca, Al, Si, Mg	Mn, Ti	Zr, Ni, Cr, V, Sc, Ba, Cs, Te, Ag, P, Cl	Sr, Zn, Sb, Sn, Cd, Pd	/
P_14_16	Fe, Ca, Al, Si, Mg	Ni, Cr, S	Zn, Cu, Mn, V, Ti, Sc, K, Ba, Cs, Te, P, Cl	Sn	/
P_18_16	Fe, Ca, Al, S, Si, Mg	Cu, Mn, Cr	Zn, Ni, V, Ti, K, Ba, Cs, Te, P, Cl	As, Sn	Sr, Bi
P15	Fe, S, Si, Mg	Mn, Cr, Ca, K, Al	Zn, Cu, Ni, V, Ti, Ba, Cs, Te, P, Cl	Sn	/

Table 4.7. Table showing mineralogical composition of sulphide mine's samples from XRD analyses.

Samples	XRD
P_1_16	serpentinite T1, ilvaite(CaFeO(Si <sub>2</sub> O <sub>7</sub> )), chlorite ClO <sub>2</sub> , chalcopyrite
P_2_16	lizardite, chlorite, garnet and pyroxene
P_3_16	serpentinite T1, ilvaite(CaFeO(Si <sub>2</sub> O <sub>7</sub> )), chlorite ClO <sub>2</sub> , chalcopyrite
P_12_16	lizardite and ilvaite
P_14_16	
P_18_16	
P15	lizardite, marcassie, pyrrhotite, magnetite, chalcopyrite

Sulphide with their presence could relate to different deposit and source conditions. Sulphur is from the sulphate from seawater and oxidation of sulphide mineral due to the extensive circulation of seawater (Alt et al. 2013). Pyrrhotite, one of the sulphide

minerals found in these exposures is common in high temperature hydrothermal veins and in contact-metamorphic deposits, while marcasite is formed from elemental sulphur under acidic conditions and forms in metalliferous veins (Deer et al. 1992). Pyrite and chalcopyrite are also the major sulphide presented in the upper mantle (Vaughan and Corkhill 2017) and minerals as pyrite, pyrrhotite, and marcasite, are ubiquitous in hydrothermal ore deposits (Fontboté et al. 2017). Elemental sulphur ( $S_8$ ) which is abundant in these samples could be derived from weathering of sulphides such as pyrrhotite or from bacterial activity (Heymann et al. 2003). The sulphide are related from non-stoichiometric equilibration in phases in serpentinites (Burkhard 1989). These minerals are characteristic for a hydrothermal environment, but this criterion alone is not sufficient to identify a hydrothermal vent positively. The most occurrent mineral in these samples ilvaite usually occurs with magnetite, zinc and copper ores bodies. Ilvaite could also be the replacement mineral of olivine after FeO and MgO removal and CaO, H<sub>2</sub>O and O<sub>2</sub> addition under high fluid to rock ratio, low CO<sub>2</sub>, low O<sub>2</sub> and moderate temperature (Naslund et al. 1983).

#### **4.6. Interpretation and discussion**

Rocks from the Tasna, Platta and Chenaillet OCT areas have similar distributions of HCs to the Totalp area, previously described by Mateeva et al. 2017. The different distributions (e.g. C<sub>max</sub>) and amounts of HC within the same lithology could reflect the heterogeneity of the collected samples (e.g. clasts, veins) (Table 4.2).

The Tasna unit has the lowest concentrations of HCs, probably due to higher temperatures experienced during Alpine metamorphism (~<350 °C ) (Manatschal et al. 2006).

The TOC data are variable and depend on lithology and the percentage of carbonate in the samples. No positive correlation between concentrations of TOC and HCs is apparent.

#### 4.6.1. Source of OM

##### 4.6.1.1. Carbon isotopes

The isotopic values of carbon isotopes for the Tasna and Totalps samples  $\delta^{13}\text{C}_{\text{org}} = -26.02$  to  $-27.4\text{‰}$  VPDB are similar to preserved marine organic matter in rocks of ages between 170 to 120Ma ( $\delta^{13}\text{C}_{\text{org}}$  between  $-26$  and  $-29\text{‰}$  VPDB) (Schidlowski 1988; Hayes et al. 1999). During this period, the average isotopic fractionation ( $\epsilon_{\text{TOC}}$ ) was between 28 and 32‰, indicating maximal fractionation of carbon isotopes by phytoplanktonic producers (Hayes et al. 1999).

$$\epsilon_{\text{TOC}}f_o + \delta_i = \delta_a \quad (\text{Eq. 4.9})$$

(Hayes et al. 1999)

where  $\epsilon_{\text{TOC}}$  is the average isotopic fractionation between TOC ( $\delta_a$ ) and sedimentary carbonate ( $\delta_o$ ),  $\delta_i$  is the incoming carbon and  $f_o$  is the oxygen fugacity (Hayes et al. 1999). This is not altered by the serpentinisation process (Birner et al. 2016). The large fractionation implies that dissolved  $\text{CO}_2$  concentration were low in surface water during fixation of carbon by photosynthesis (Meyers and Shaw 1996).

The measured values are also similar to those found in different modern environments, hydrothermal system from the Galapagos ( $\delta^{13}\text{C}_{\text{org}} = -27.4\%$ ) and the Guaymas Basin ( $\delta^{13}\text{C}_{\text{org}} = -25$  to  $-21\%$ ) originating from chemoautolithotrophic bacteria (Orem et al. 1990), methanotrophic nutrition from MAR hydrothermal vent Menez Gwen ( $\delta^{13}\text{C}_{\text{org}} = -24.9$  to  $-34\%$ ) detected in mussel gills (Pond et al. 1998) or marine particulate organic carbon (POC) ( $\delta^{13}\text{C}_{\text{org}} = -20$  to  $-30\text{‰}$ ; (Des Marais 2001)). Assuming that methane assimilation leads to OM depleted in  $^{13}\text{C}$  by 15-50‰ relative to the methane source, our values would be from  $-10$  to  $+35\text{‰}$  and very different from the minimal values for anaerobic oxidatzing methane (AOM) of  $\delta^{13}\text{C}_{\text{org}} = -39.2$  to  $-41.8\text{‰}$  and therefore cannot be interpreted as derived from anaerobic methanotroph (ANME) (Barker and Fritz 1981; Elvert et al. 2000; Hinrichs and Boetius 2002). However, even in modern environments, where methanotroph biosystem exists as is the case in the active and extinct carbonate chimney of Lost City Hydrothermal Field (LCHF), the  $\delta^{13}\text{C}_{\text{org}}$  show a marine OM with  $\delta^{13}\text{C}_{\text{org}} = -21.5$  to  $-2.8\text{‰}$  VPDB. This demonstrates the predominance of the marine OM over

methanotrophic biosystem (Bradley et al. 2009). Therefore, the isotopic data are inconclusive with respect to the origin of the OM and the existence of a methanotrophic biosystem.

#### 4.6.1.2. Biomarkers

The biomarkers (steranes, isoprenoids, and hopanes) present are consistent with a marine-derived OM.

Gammacerane ( $m/z$  191) in serpentinised basalt near the Marmorera lake (sample P1) derives from organisms producing its molecular precursor in a reducing environment and could be related to hypersaline bottom-water anoxia and water column stratification (Fig.4.13) (Damsté et al. 1995; Takishita et al. 2012; Kaiho et al. 2016). This hypersaline environment could indicate generally low biological diversity and high production (Ten Haven et al. 1987). This type of environment could also be due to hydrothermal fluids generating water stratification. Based on the isoprenoid/ $n$ -alkanes ratios, the gammacerane index (gammacerane/ $C_{30}$   $\alpha\beta$  hopanes) = 0.11 and Pr/Phy < 1.3 indicate the depositional environment is a reducing (suboxic) environment with weak stratification (Fig. 4.14) (Brooks et al. 1969; Ten Haven et al. 1987; Kaiho et al. 2016).

The presence of hopanes indicates the presence of fossil bacterial and pristane and phytane could be derived from archaea, zooplankton or from photosynthetic algae (Brassell et al. 1981; De Rosa and Gambacorta 1988; Sachse et al. 2012; Rontani et al. 2013; Kaiho et al. 2016). The high  $C_{29}/C_{30}$  ratios (>1) indicate samples are sourced from rocks rich in carbonaceous organic matters (El Nady et al. 2014). The ternary sterane diagram indicate that the OM originates from a mixed marine source of planktonic algae/bacteria and the isoprenoid/ $n$ -alkane ratios indicate reducing environment with marine OM (Fig. 4.11, 4.14) (Mateeva et al. 2017).

The biomarkers together with the isotopic data are consistent with marine-derived OM rather than being specific to a methanotrophic biosystem. The OM is probably derived from the particulate and dissolved organic matter (POM, DOM) originating from phytoplankton, zooplankton remains and marine detritus. Our biomarkers are

also similar to hydrocarbons (*n*-alkanes up to C<sub>40</sub>, isoprenoids (pristane, phytane and squalane), hopanes and steranes) produced in the Lost City hydrothermal field (LCHF) by the incorporation of seawater dissolved organic carbon ( $\leq 0.45 \mu\text{m}$ ) and to organic compounds that are dominant also in a low-temperature metamorphism ( $<200 \text{ }^\circ\text{C}$ ) (Delacour et al. 2008b).

#### 4.6.2. Thermal history of OM

The PAHs are used to distinguish the thermal history of OM, for example a pyrogenic source ( $T = 350 \text{ }^\circ\text{C}$  to more than  $1200 \text{ }^\circ\text{C}$  (Abdel-Shafy and Mansour 2016)) would be characterized by ratios such as  $P/A < 5$  (Neff et al. 2005);  $\text{Fluo}/\text{Pyr} > 1$  (Neff et al. 2005; Motelay-Massei et al. 2007);  $\text{Benz}/\text{Benz}+\text{Chry} > 0.35$  (Yunker et al. 2002), while petrogenic sources ( $T=100\text{-}150 \text{ }^\circ\text{C}$ ) could last millions of years (Abdel-Shafy and Mansour 2016) characterized by  $P/A > 5$  (Neff et al. 2005);  $\text{Fluo}/\text{Pyr} < 1$  (Neff et al. 2005; Motelay-Massei et al. 2007);  $\text{Benz}/\text{Benz}+\text{Chry} < 0.2$  (Yunker et al. 2002) (Table 4.3).

Our PAHs ratios support the idea of a mixed temperature origin (petrogenic, pyrogenic) with  $\text{MP}/\text{P}$  values consistently between 0.5 and 1,  $\text{MPAHs}/\text{PAHs} < 0.8$ ,  $\text{BaA}/\text{BaA}+\text{Chry} > 0.3$ ,  $\text{Fluo}/\text{Pyr}$  mostly  $< 1$ , while abundance of low molecular weight species and dominance of P series over Chry series could suggest a petrogenic source (Table 4.3) (Garrigues et al. 1995; Yunker et al. 2002; Motelay-Massei et al. 2007; Saha et al. 2009; Saha et al. 2012). The PAHs in our samples could be interpreted as pyrolytic residues (Geissman et al. 1967) from OM alteration during hydrothermal activity  $T > 300 \text{ }^\circ\text{C}$  (Kawka and Simoneit 1990b) or low-grade metamorphism (Heymann et al. 2003). Unresolved peaks of PAHs are not included in the ratio calculations. However, our PAHs are different from modern antropogenic contamination (presence of HMW PAHs) including biomass combustion with  $(\text{IndPy}/(\text{IndPy}+\text{BghiP})) > 0.5$  (Yunker et al. 2002),  $\text{Fluo}/(\text{Fluo}+\text{Pyr}) > 0.5$  (De La Torre-Roche et al. 2009) and characterized by  $T$  of 300 to  $880 \text{ }^\circ\text{C}$  (McGrath et al. 2003), coal burning with  $\text{BaA}/(\text{BaA}+\text{Chry}) = 0.2$  to  $0.35$  (Akyüz and Çabuk 2010) or petroleum combustion with  $\text{IndPy}/(\text{IndPy}+\text{BghiP}) = 0.2$  to  $0.5$  (Yunker et al. 2002),

Fluo/(Fluo+Pyr)=0.4 to 0.5 (De La Torre-Roche et al. 2009) and also have a different distribution (Tobiszewski and Namieśnik 2012) (Table 4.3, see Glossary).

#### **4.6.3. Transport mechanism of OM**

In the four fossil Tethyan OCT areas that we have investigated, HCs were present in all lithologies in different amounts and their distributions are consistent with an origin from marine seawater (Mateeva et al. 2017). It is necessary to consider the transport mechanism of the OM into the basement rock.

We do not find evidence of upward transported methane-rich serpentinised fluid into the mantle rock or the overlying lithology. This does not support the existence of F-T reactions associated with serpentinisation being responsible for abiotic life. The OM is probably derived from POM and DOM from the overlying water column. Most of this organic matter will be incorporated into remineralized lithologies and some will be buried in sediments e.g. (Suess 1980; Meyers 1994). The infiltration of marine fluids through the sedimentary column into the basement rock may be caused by dynamic tectonic processes such as faulting, fracturing, or fluid pore circulation (Beard and Hopkinson 2000; Delacour et al. 2008c). Circulation of seawater via pore fluid transport of DOM in the upper meters of the basement rock and production of carbonate veins through supply of dissolved inorganic carbon (DIC) during the initial rock/water interaction at the seafloor is likely to have introduced OM into the rock (Früh-Green et al. 1990; Ménez et al. 2012; Mateeva et al. 2017). The OM may have migrated with seawater fluids from sediments into the serpentinised mantle through fractures caused by tectonic and crystallization stresses (Delacour et al. 2008c; Farough et al. 2016). This fracture permeability is not reliant on matrix permeability (Farough et al. 2016) and may be generated during mantle exhumation. The formation of pyrolytic PAHs likely occurred during the high temperature initial contact between the DOM containing fluid and the rock (Mateeva et al. 2017).

In summary, the OM found in the serpentinised mantle and overlying lithologies in the four Tethyan OCT areas was of marine origin and not methanotrophic (Mateeva et al. 2017).

#### 4.6.4. Origin of calcite veins

The isotopic signals can be related to each of the polyphaser geological history of the veins including three main geological settings related to fluids rock interactions from ocean floor of the passive margins to an obducted metamorphose outcrops (Fig.4.16 b ) (Früh-Green et al. 1990; Heydari 1997).

The carbon and oxygen isotopic results are compared to values and interpretation already done in the areas and to values related to the evolution of a passive margin environment (Heydari 1997).

At the initial stages of rifting of the oceanic crust (i.e. MOR) carbonate precipitation may involve mantle derived CO<sub>2</sub> ( $\delta^{18}\text{O}_{\text{SMOW mantle}} = 5.3 \pm 0.6\text{‰}$  (Carmody et al. 2013), mostly in MOR environment, Ca from DIC of dissolved limestone and marine water where the  $\delta^{18}\text{O}$  of the calcite vein would be more affected by the  $\delta^{18}\text{O}$  of the water being in bigger quantity.

A second generation of veins would occur with the hemi-pelagic to pelagic sediments in more reducing environment as shown by carbonate staining.

A later set of veins formed during burial and diagenesis (increase of  $\delta^{18}\text{O}_{\text{SMOW water}}$  with increasing temperature e.g.  $\delta^{18}\text{O}_{\text{SMOW water}} = 18\text{‰}$  for 6km depth (Heydari 1997)) and was related to the rock water ratio (i.e.  $\delta^{18}\text{O}_{\text{SMOW basalt}} = 5.5$  to  $7\text{‰}$  (Muehlenbachs 1986) vs  $\delta^{18}\text{O}_{\text{SMOW ocean}} = 0\text{‰}$ ).

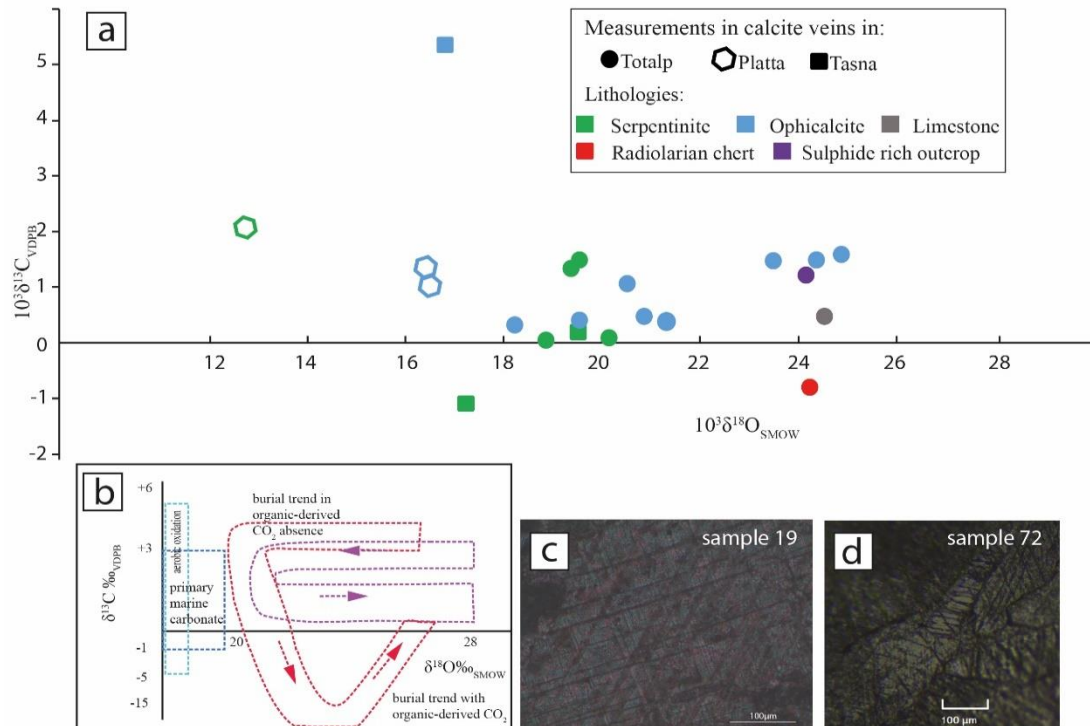


Figure 4.16. a) Carbon and oxygen isotopic composition of calcite veins in Tasna and Platta samples compared to Totalp samples and to in-situ sample from modern ocean seafloor (Mateeva et al. 2017). b) Summarized graph explaining the global range of carbon and oxygen isotopic composition in passive margin settings, modified after Kiriakoulakis (1997), Heydari (1997) c). calcite grain from one calcite veins sample 19 limestone, Totalp, showing twinning d) calcite grains from a calcite vein in sample 72 vein supported serpentinite breccia, Totalp unit.

A last generation of veins formed during obduction and was related to low grade metamorphism and lastly veins of post-accretionary Alpine tectonics with isotopic signature not modified by the metamorphism (Früh-Green et al. 1990).

Different generation of veins are distinguished by their textural features using cathodoluminescence technique rather than isotopic values. The sparitic calcite is extracted all from calcite veins with grains having a different history representing thin to thick patchy twinning representing low to large deformation from  $T < 200^\circ\text{C}$  to  $> 250^\circ\text{C}$  (Fig. 4.16 c, d) (Burkhard 1993). Thus our isotopic signal is an average of the three time stages described above and depend of factors such as composition of pre-metamorphic protolith, volatilization effects, fluid/rock ratios, and temperature of exchange (Valley 1986).

The  $\delta^{13}\text{C}_{\text{VPDB}}$  values are consistent with seawater-derived early diagenetic calcite (Fig. 4.16 b) (Hudson 1977; Coleman et al. 1993; Heydari 1997). The  $\delta^{18}\text{O}_{\text{SMOW}}$  values of

the calcite veins for the majority of samples vary between 12 to 25‰ and indicate calcite precipitation during shallow burial (<250 m), not influenced by organic carbon derived CO<sub>2</sub> but typical of Cretaceous calcite (Fig. 4.16 b) (Dix and Mullins 1992; Heydari 1997).

Our value of  $\delta^{13}\text{C}_{\text{VPDB}}$  do not seem to change by metamorphism from primary marine values, while the  $\delta^{18}\text{O}_{\text{SMOW}}$  change, by degree of metamorphism from the primary carbonate values  $\delta^{18}\text{O}_{\text{SMOW}} \approx 30\text{‰}$  (Sharp 2009). The temperature of Alpine metamorphism, from prehnite-pumpellyite to greenschist facies (Manatschal and Nievergelt 1997; Manatschal et al. 2006; Manatschal et al. 2011; Mateeva et al. 2017) is related with a decrease of oxygen isotope values (Sharp 2009).

Calcite precipitation temperatures, through even ambiguous, are calculated using the oxygen isotope data and the equations:

$$1000 \ln \alpha = 2.78(10^6 x T^{-2}) - 2.89 \quad (\text{Eq. 4.10})$$

(O'Neil et al. 1969)

$$\alpha_{A-B} = (1000 + \delta_A)/(1000 + \delta_B) \quad (\text{Eq. 4.11})$$

Where  $\delta_A$  is  $\delta^{18}\text{O}_{\text{mineral}}$  and  $\delta_B$  is  $\delta^{18}\text{O}_{\text{water}}$  in SMOW and T is the temperature in Kelvin.

A value of  $\delta^{18}\text{O}_{\text{SMOW}} = -1\text{‰}$  typical of seawater in the ice free world during the Jurassic is taken for these calculations (Sharp 2009; Schwarzenbach et al. 2013). For the  $\delta^{18}\text{O}_{\text{SMOW}} \text{ water} = 0\text{‰}$ , typical for modern ocean water the resulting temperature of calcite precipitation changes with a maximum of 7 °C. The temperature calculated for calcite precipitation in the Totalp area is between 39 and 74 °C, between 94 and 136 °C for Platta and between 71 and 91 °C for Tasna OCT. These values are similar to those previously found in the Ligurian ophiolite (49 – 151 °C) (Schwarzenbach et al. 2013) or modern hydrothermal systems (Atlantis massif (Früh-Green et al. 2003), MAR 15°20'N (Bach et al. 2011), MAR 23°N (Alt and Shanks 2003)) for calcite veins originating from seawater circulation (50 to 150 °C) (Alt et al. 2013). The calculated temperature for calcite precipitation with a  $\delta^{18}\text{O}_{\text{SMOW}} \text{ water} = -1$  to +1 in the Totalp

and Tasna areas, are not consistent with the hydrothermal fluid circulation associated with the opicalcite (100 – 150 °C) but with the wide range temperature (37 – 115 °C) of a fluid dominated open system during the early Alpine accretion and metamorphism (Weissert and Bernoulli 1985; Früh-Green et al. 1990).

#### **4.6.5. Platta Sulphide mine: Is the sulphide – serpentinite deposit a fossil hydrothermal vent?**

For the genesis of sulphide minerals, we may consider three possibilities, 1) a hydrothermal origin related to serpentinisation processes, 2) magmatic origin or, 3) biogenic formation from sulphate-reducing bacteria (Becking and Moore 1961; Burkhard 1989; Rickard et al. 2017).

1<sup>st</sup> type: Hydrothermal origin

A hydrothermal origin could relate to volcanogenic massive sulphide deposits – VMS or Ni-Cu deposits, a fossil deposit of seafloor massive sulphide deposits SMS associated with hydrothermal vents.

Hosted rock in VMS could be submarine mafic to ultramafic rocks and their brecciated equivalent and the sulphide presented here are encountered or characteristic of VMS (Taylor et al. 1995; Fallon et al. 2017). One of the main characteristic of VMS mineralization is upward and outward zonation from Cu to Zn-Pb, in our case a zonation is observed but no Pb is present and more samples are required to see this relationship (Table 4.6) (Rasmussen 2000). The VMS deposits are also characterized by Cu, Zn, Pb and Ba anomalies which is not our case (Table 4.6).

For this outcrop to be a fossil hydrothermal vents system it would have a different history. A hydrothermal vent system is characterized by fast pelagic sediment accumulation including ferrous oxides of hydrothermal origin which can be preserved (Haymon 1989; Montgomery and Kerr 2009). Haymon describes the evolution from a black smoker to an inactive white smoker back in 1983. First the temperature of the black smoker decreases, worm tubes start to appeared and the fluid composition

changes to amorphous silica, barite and pyrite (Haymon 1983). The individual white smoker created later, will be infilled with sulphide until it becomes inactive and dissolves to rubble form. Some of the minerals as anhydrite and caminite will be completely absent in the inactive vents while others will appeared from the oxidation of the sulphide minerals (oxyhydroxides, chlorides and hydrous sulphates) (Haymon 1983). Thus the hydrothermal vents on the surface will completely disappear after a few thousands of years (Haymon 1983). The black smokers lie directly on the magmatic basement (basalt) and have as deposits minerals sphalerite, wurtzite, iron-sulphides (pyrite, marcasite, melnikovite, rare pyrrhotite) and rare copper – sulphides (chalcopyrite, cubanite, covellite, digenite) (Haymon 1983), other minor minerals as amorphous silica, barite, talc, native sulphur, iron oxyhydroxides, jarosite, gypsum and caminite (Haymon 1983).

The hydrothermal vents are associated with low-diversity but highly productive biosystems originating on chemosynthetic biosystem and deposits of iron, copper, and zinc sulfides originated by the mixture of hydrothermal fluids ( $\leq 400$  °C) and seawater (Grassle 1987; Herzig and Hannington 1995; Van Dover 1995; Little et al. 1999). The high temperature on the hydrothermal vents could explain the lack of biomarkers other than *n*-alkanes and the post-depositional PAHs in the Marmorera sulphide deposit. For a hydrothermal sulphide to be added during serpentinisation the temperature must be between 350- 400° C (Alt et al. 2013).

This massive hydrothermal sulphide deposit with its emplacement and its lithology might indicate a hydrothermal sulphide system hosted by serpentinite, however further mineralogical and textural data is needed, the criteria used are not sufficient to identify this environment with certainty.

2<sup>nd</sup> type : Sulphide deposits could be of a magmatic origin due to their mineralogical associations, texture and ore chemistry, which is the case of CO-Ni-As deposit in Oberengadin region and Val Malenco, Alps (Burkhard 1989; Barnes et al. 2017). The magmatic sulphide ore deposits are sulphide liquid enriched in chalcophile elements (Ni and Cu) zoned and originate from silicate magma (Barnes et al. 2017). These

natural smelters are dominated by Ni and Cu or platinum group elements and Au which is not the case in our outcrop (Table 4.6) (Barnes et al. 2017).

3<sup>rd</sup> type: The biogenic formation of sulphide relate to sulphate reducing microorganisms (SRM) and their characteristic to utilize sulphate ( $\text{SO}_4^{2-}$ ) in anaerobic environment to produce hydrogen sulphide ( $\text{H}_2\text{S}$ ) that lead to production of pyrite, iron sulphides (mackinawite and greigite) (Vaughan and Corkhill 2017). As it was pointed earlier (chapter 2) these SRM (SRM = SRB + sulphate reducing archaea SRA) are the most likely to be related to methanotroph in anaerobic environments. For this bacterial sulphate reduction to happen and later to create these minerals, OM, sulphate ( $\text{SO}_4^{2-}$ ), anaerobic environment and iron-bearing minerals to provide the iron ( $\text{Fe}^{2+}$ ) are needed (Vaughan and Corkhill 2017). Modern marine anoxic sediments are the dominant place for this iron sulphide minerals' origin, but it is not believed that this origin could explain the large sulphide outcrop in Platta.

4<sup>th</sup> type: Hydrothermal mineralisation is said to occur along fault zones due to seismically made fluid pulse as transport mechanism (Sibson et al. 1975). This mechanism move substantial amount of mineralising fluid ( $10^{10}$  litres) from one crustal environment to another (Sibson et al. 1975). This hydrothermal transport would probably suggest that the host rock, e.g. serpentinite would probably be low in elements that are in high proportions in the hydrothermal deposit. However, these hydrothermal deposits are vein deposits with episodic mineralisation, which is not the Platta sulphide mine case. The analyses of hydrocarbons in this area suggest a marine environment and not a migration from the host rock, as it would be the case if there were seismic pumping transport in a tectonically active area.

Hydrothermal fluids related to the origin of sulphide could be differentiate to magmatic, seawater or even metamorphic fluids distinguished by their isotopes  $\delta^{34}\text{S}$  (Alt and Shanks 2006).

This massive hydrothermal sulphide deposit with its emplacement and its lithology might indicate a hydrothermal sulphide system hosted by serpentinite related also to

some extend to biological origin of sulphide. Based on literature and this restrain findings, the arguments are not sufficient to identify this environment.

#### **4.7. Summary**

The results from the Tasna, Platta and Chenaillet areas are very similar to those previously described for the Totalp area except for their lower quantity and variety of HC. The OM found in the Alpine OCT samples is from a marine OM derived from sediments which was then transported into serpentinitised mantle where it was thermally altered. No organic biomarkers related to a methanotrophic biosystem were found in the sampled lithology. Are our results indication that methanotrophic biosystem is non-existent in these environments or that the marine OM is dominant and conceal the methanotroph signal?

Important remaining open questions are whether OM was mostly associated with the carbonate precipitation in the basement unit. Or whether the OM could reach and be preserved as deep as the fluids leading to serpentinitisation taking into account the depth where the maximum habitable temperature of every living organism (120 °C) is reached.

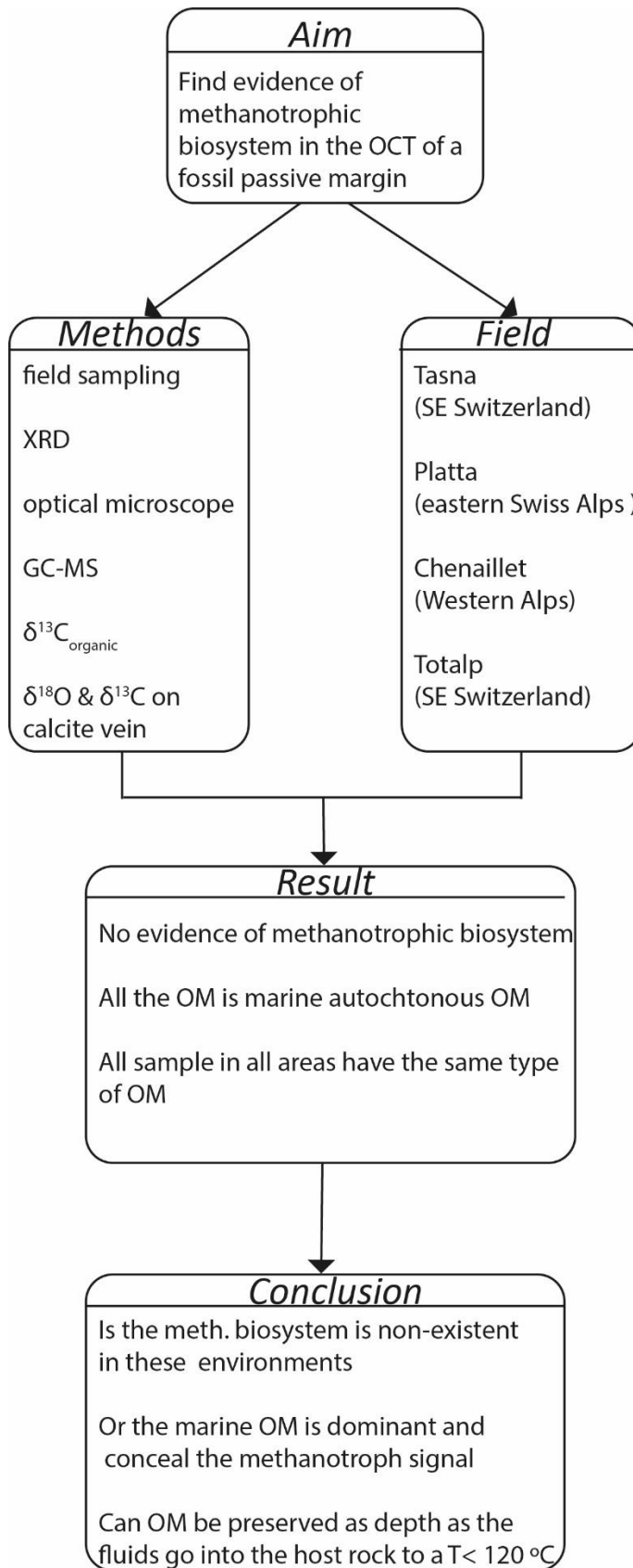


Figure 4.17. Summary flow charts of chapter 4



## Chapter 5

# **5. Organic matter in Ocean Continent Transitions of present- day magma-poor rifted margin: the examples of Iberia and Newfoundland**



## 5.1. Abstract

Serpentinisation and concomitant reduction of CO<sub>2</sub> to methane at modern hydrothermal vents has been observed to support methanotrophic biosystems at mid-ocean ridges. Exhumation of mantle within ocean regions and its subsequent serpentinisation is a common occurrence. It is possible that methanotrophy is not restricted to hydrothermal vents systems alone and could be pervasive within serpentinised exhumed oceanic mantle.

The ocean-continent transition (OCT) of magma-poor rifted continental margins provides an opportunity to investigate this. Serpentine, intrusive magmatic rocks and the overlying sediments (mainly breccia and one clayey limestone) collected as part of the Ocean Drilling Program (ODP) from the Iberian and Newfoundland margin, were analysed to find evidence of methanotrophic bacteria related to the serpentinisation process.

Samples from the OCT of Newfoundland (ODP Leg 210) contain *n*-alkanes, PAHs and isoprenoids (pristane, phytane) while those from the OCT of Iberian (ODP Legs 149 and 173) also contained detectable steranes and hopanes. However, the distribution and composition of hydrocarbons suggest that the OM may not be indigenous to the rocks.

The only clear evidence of Archaean bacteria was provided from GDGTs (0 – 3), crenarchaeol and isomers from the clayey limestone (149/897C/1A/63R1) at the Iberian Margin and these were likely derived from overlying oceanic waters. There were no detectable GDGTs in any of the igneous and metamorphic rocks. Hydrocarbon fingerprinting using polar plots suggests that any organic compounds in these samples were probably introduced from the drilling mud.

Our analysis has not found evidence of methanotrophy within the IODP samples examined and does not support the existence of a pervasive or significant

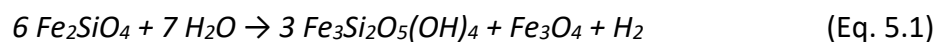
methanotrophic biosystem within the serpentinised exhumed mantle of the Newfoundland or Iberian OCTs.

## 5.2. Introduction

Since their discovery in 1977, more than 400 hydrothermal vents have been visually identified, providing unique biosystems using chemosynthetic energy produced by water-rock interactions ([vents-data.interridge.org](http://vents-data.interridge.org)) (Kelley and Shank 2010).

Some hydrothermal vents (e.g. Lost city, Mount Saldanha 36°34'N, Nibelungen 8°18'S, Rainbow 36°14'N on mid-Atlantic ridge MAR) are partially supported by energy derived from serpentinisation and host methanotrophic biosystems among other bio-communities e.g. (Bischoff et al. 2006; Konn et al. 2009). This type of hydrothermal vent is found only at slow spreading (SSR) ocean ridges (e.g. mid-Atlantic ridge MAR), being driven by the heat derived from mantle serpentinisation and magmatic sources (Bach and Früh-Green 2010). However, serpentinisation is not confined to hydrothermal vents alone. Serpentinised exhumed mantle may account for ~25% of the ocean floor formed at SSRs and is often associated with high concentrations of organic matter (OM) (MAR; 4-6°N) (Ménez et al. 2012; Alt et al. 2013). This raises the question of whether bio-systems could be associated with serpentinisation that occurs away from the hydrothermal vents.

Serpentinisation provides a sustainable source of metabolic energy in the form of electrons that are necessary for the micro-organisms to biosynthesize organic molecules *via* the hydration of peridotite minerals as shown for olivine in Eq.5.1 (e.g. (Russell et al. 2010).



The  $\text{H}_2$  produced by the reaction could react with  $\text{CO}_2$  at high pressure and temperature *via* Fisher-Tropsh type reactions, which are anaerobic and abiotic (Eq.5.2):



Methanotrophic bacteria in consort with sulphate-reducing bacteria can use the CH<sub>4</sub> produced as their source of carbon and electrons, transforming the reactants to hydrogen sulphide and hydrogen carbonate (Eq.5.3).



Anaerobic methanotrophic microorganisms remove almost 90% of all the CH<sub>4</sub> produced in marine anoxic sedimentary environments, and only 2% is lost to the atmosphere; hence, they have a significant role in regulating this greenhouse gas (Reeburgh et al. 1996; Hinrichs et al. 2000).

Methanotrophic biosystems are recognised by an unusually depleted δ<sup>13</sup>C isotopic composition and biomarkers such as crocetane (Thiel et al. 1999; Bian et al. 2001), sn-2-hydroxyarchaeol (Hinrichs et al. 1999), archaeol (Hinrichs et al. 1999), biphytanic diacids (Birgel et al. 2008), glycerol ethers (Hinrichs et al. 1999), and C<sub>20</sub>, C<sub>25</sub> sn-2 hydroxy isoprenoid glycerol diethers for anaerobic methanotrophic archaea type 2 ANME-2 (Stadnitskaia et al. 2008) (Fig. 5.1).

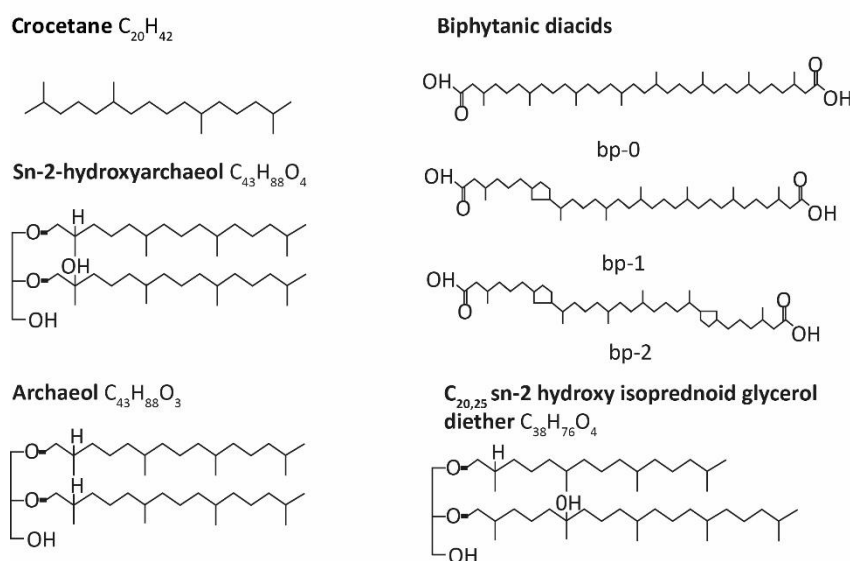


Figure 5.1. Chemical structures of the hydrocarbon biomarkers for anaerobic methanotrophs.

In this Chapter, samples of serpentinite and the overlying lithologies collected from Ocean Drilling Program (ODP) cores from the Iberian and Newfoundland margins are investigated to test for the presence of methanotrophs. Understanding the relationship between serpentinitisation and the methanotrophic bacteria away from

prolific hydrothermal vents is important in the understanding of the role of SSRs in the global carbon cycle on a geological timescale and the connection, if any, between serpentinisation and organic matter production.

### **5.3. Iberia and Newfoundland continental margins, examples of a magma-poor rifted margins with serpentinised exhumed mantle**

The Iberia-Newfoundland conjugate rifted margins (Péron-Pinvidic and Manatschal 2008) are currently the best studied hyper-extended, magma-poor rift system in the world through deep-sea drilling (ODP Legs 103, 149, 173, 210) and supporting geophysical studies (Sawyer et al. 1994; Whitmarsh et al. 1998b; Beard et al. 2002; Manatschal et al. 2009). The Iberia-Newfoundland conjugate rifted margin result from the opening of the North Atlantic and the separation of the North American and Iberian plates during continental rifting in the early Cretaceous (e.g.(Sawyer et al. 1994; Whitmarsh and Wallace 2001)).

The structure of a magma-poor margins has been described elsewhere (Unternehr et al. 2010; Sutra et al. 2013; Masini et al. 2014). Samples selected for analysis from Iberian margin IODP drilling are from the exhumed mantle domain which separates oceanic crust from hyper-extended (and hyper-thinned) continental crust. Our selected IODP samples on the Newfoundland margin contain serpentinised mantle, however their tectonic context is uncertain.

#### **5.3.1. Iberia-Newfoundland margins and serpentinisation**

During the ODP Leg 103 expedition (Boillot et al. 1980; Boillot 1986), serpentinised mantle rocks were discovered between continental and oceanic crust at the OCT of the Galicia Bank segment of the Iberian margin (Boillot et al. 1980; Whitmarsh et al. 2001a; Manatschal et al. 2006). Later ODP drilling expeditions (Legs 149, 173 and 210) combined with seismic reflection and refraction data showed that exhumation extends over tens to hundreds of kilometres on both the Iberian and the conjugate Newfoundland margins. Within regions of exhumed mantle, the distribution of

serpentinisation with depth is uncertain, however some evidence suggests that it occurs within the footwall of large extensional faults (Alt and Shanks 1998; Whitmarsh et al. 2001a; Manatschal et al. 2006; Andreani et al. 2007; Reston and McDermott 2011; Bayrakci et al. 2016) and is intense within the upper 2 km or so, rapidly decreasing with depth to less than 5% at 5 km depth (Skelton 2005).

The mantle rocks are usually highly serpentinised with calcite veins cross-cutting in places (e.g. NW Iberia) (Boillot et al. 1989). The depth of serpentinisation at the OCT on the west Galician margin was estimated to be from 2.5 to 6 km, depending on the sediment cover (Boillot et al. 1989). Serpentinisation at the cooling Iberian margin occurred at temperatures of 150 °C and below, and carbonate precipitation (calcite veins in serpentinite, ophicalcite) occurred over a temperature range 13 °C – 44 °C (Agrinier and Cannat 1997; Schwarzenbach et al. 2013). In previous studies of the cores from the Iberian margin, lizardite and chrysotile were identified, but not antigorite and they were also characterized by brittle deformation and calcite veins (Sawyer et al. 1994).

Serpentinised mantle peridotites were exhumed along the Iberian and Newfoundland margins during Valanginian to Aptian times (Müntener and Manatschal 2006). The serpentinised peridotites from the Newfoundland margin are interpreted to be depleted spinel harzburgites, resulting from a high degree of melting by exhumation of a former subarc mantle (Müntener and Manatschal 2006). Those at the Iberian margin are less depleted spinel harzburgites than those of the Newfoundland margin, and show a wide-ranging degree of partial melting and re-fertilization of an earlier depleted arc related peridotite (Müntener and Manatschal 2006). The Newfoundland margins mantle samples have clinopyroxene which contain lower  $\text{Al}_2\text{O}_3$  (<4 wt.%),  $\text{Na}_2\text{O}$  (<0.6 wt.%) and  $\text{TiO}_2$  (<0.15 wt.%) and higher Cr (>0.154 wt.%) than the Iberian clinopyroxenes indicating a residual composition probably arc related (Müntener and Manatschal 2006).

Evidence from ODP Sites on the Iberia- Newfoundland margin (e.g. Sites 897, 1068, 1070, 1277) indicates that the serpentinised mantle in the OCT is locally intruded by

diachronous intrusions (Beard et al. 2002; Manatschal et al. 2009). These occurred during continental breakup and are also visible on seismic sections consistent with observed high seismic velocities e.g. (Péron-Pinvidic et al. 2007; Manatschal et al. 2009).

### 5.3.2. Chosen ODP Sites for Analysis

We present the results of analysis of serpentinites from ODP Sites 897C, 1068A, 1070A and 1277A. These sites were chosen because they are situated in the OCT zones of the Iberia-Newfoundland margins on basement highs and where drilling penetrated the serpentinitised mantle. Descriptions of locations and rocks recovered from drilling can be found in the relevant Initial Reports of the ODP Legs (Sawyer et al. 1994; Whitmarsh et al. 1998c; Tucholke and Sibuet 2007b) (Fig. 5.2, Table 5.1).

Site 897C (40°50.328'N, 12°28.440'W) is situated in the Iberian Abyssal plain over the north-south basement ridge in a water depth of 5315 m and penetrated 744.9m into the sea-bed where it encountered serpentinitised peridotite (Sawyer et al. 1994).

Site 1070 (40°47.778'N, 12°43.430'W) is also situated on the Iberian Abyssal Plain, 20 km west of the peridotite ridge over an elongated basement ridge in a water depth of 5321 m and close to magnetic anomaly M1 (Fig. 5.2, Table 5.1) (Whitmarsh et al. 1998d). Drilling at Site 1070 reached serpentinitised peridotite at a penetration of 680 mbsf (Whitmarsh et al. 1998d).

Site 1068 (40°40.955'N, 11°36.720'W) is also from Leg 173 and is situated in the southern edge of the Iberian margin in a water depth of 5044 m (Fig. 5.2, Table 5.1) (Whitmarsh et al. 1998c). Led by reflection seismicity, Site 1068 encountered serpentinitised mantle at a penetration of 893 mbsf (Fig. 5.2) (Whitmarsh et al. 1998c; Manatschal et al. 2009).

Site 1277 (45°11.800'N, 44°22.600'W) at the Newfoundland margin is drilled on a basement ridge at a water depth of 4628 m and encountered serpentinitised mantle at 142 mbsf penetration. This well was located a few kilometres from magnetic

anomaly M1 (Tucholke and Sibuet 2007a) where the mantle was exhumed at ~127 Ma (Fig. 5.2, Table 5.1).

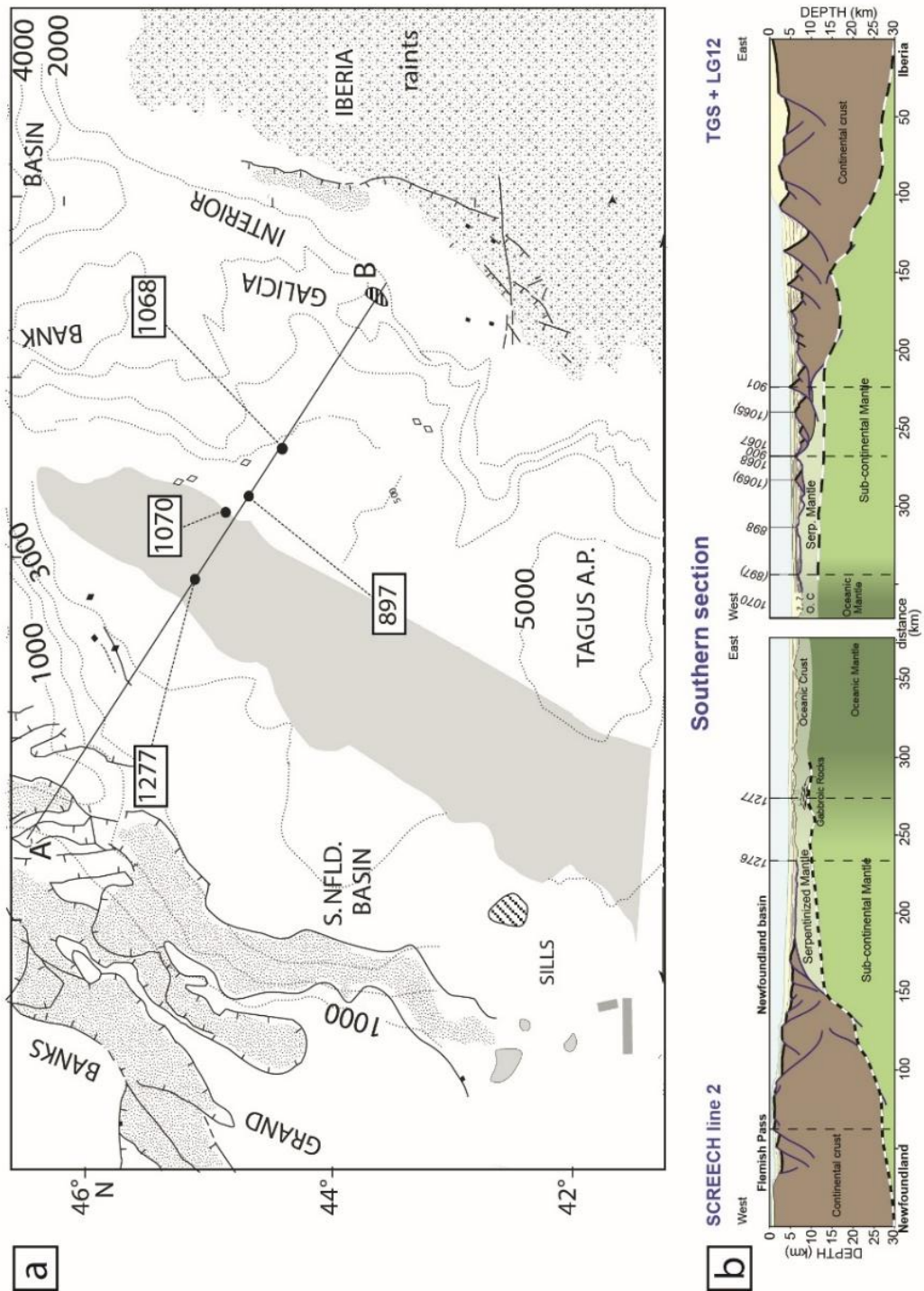


Figure 5.2. Maps and figure showing the locality of the chosen ODP sites on the Iberian and Newfoundland margins. A- Simplified map showing the position of the four sites modified from Jagoutz et al. 2007. B – Figure showing the position and main lithology of the sites (Sutra et al. 2013).

#### 5.3.2.1. Sites 897C

Site 897C consists of different kinds of sediments (claystone, dolomite, sandstone, pelagic/hemipelagic facies, calcareous turbidite) representing mass flow deposits (syn- and post-tectonic sediments) and serpentinised mantle at the base (Sawyer et al. 1994). The sediments of this unit are dated from early Pleistocene to Hauterivian. Sample (149/897C/1A/63R1 91-95.5) investigated in this study belongs to the sub-unit IV (648.7-677.5 mbsf), including sediments of early Aptian to early-late Hauterivian (~125 Ma), dated using fossil stratigraphy (Sawyer et al. 1994). This sample (149/897C/1A/63R1 91-95.5) is a clayey limestone, without any serpentinite clasts (Fig. 5.3, Table 5.1). The sedimentation rate at ODP Site 897 was high for the turbidites and low for the carbonates and other sediments (Sawyer et al. 1994).

The mass flow deposits, of Early Cretaceous age, contain clasts of serpentinised mantle and are therefore post-serpentinisation and exhumation (Sawyer et al. 1994).

Calcite filling of fractures within serpentinised mantle are observed in the shallower penetration but are absent beneath 677 mbsf penetration (Sawyer et al. 1994; Whitmarsh et al. 1998a). No ophicalcites were found.

The peridotites are spinel- and plagioclase-bearing harzburgites and lherzolites with minor pyroxenites and dunites (Whitmarsh & Wallace, 2001) and are replaced by a serpentinite mesh texture composed of serpentine ± magnetite + bastite, with only relics of olivine and pyroxene (Alt and Shanks 1998; Schwarzenbach et al. 2012). The main serpentine is lizardite without the presence of talc or antigorite (Agrinier et al., 1996). Sample (149/897C/63R2 92-97.5) is a clayey limestone deposited by mass flow (Table 5.1).

Methane concentrations measured in the Pliocene-Pleistocene turbidite from Site 897 suggest methanogenic bacterial activity, but the  $\delta^{13}\text{C}_{\text{Org}}$  is typical of marine algae (Meyers and Shaw 1996). For Site 897C (cores 63R- 1 and 63R- 2), the measured organic carbon was low (0.42 to 0.75%) with a high C/N ratio (17.7 & 37) suggesting land plant inputs (Sawyer et al. 1994). The C/N ratios of sediments from shallower

cores (59R to 61R) from the same site had low TOC (<0.1%) and low organic C/N ratios (<5), which was explained by the low amounts of carbon and high absorption of ammonium ions by clay minerals during the diagenesis of OM (Müller 1977; Sawyer et al. 1994). OM is primarily marine from algal production and land plant detritus preserved by rapid transport and burial (Sawyer et al. 1994). Headspace methane measured during the drilling has values in the range of 104 to 105 ppm from 50 to 100 mbsf where the C1/C2 ratios indicated an in-situ biogenic origin (Sawyer et al. 1994).

#### 5.3.2.2. Site 1068A

The core from Site 1068A contains sediments (claystone, silt and sandstone from core 1 to 15), breccia (from core 15 to 20), serpentinite breccia (part of core 20 and 21) and serpentinitised peridotites (from core 21 to 29). The serpentinitised peridotites are lizardite and chrysotile in a mesh texture (Whitmarsh et al. 1998c; Beard and Hopkinson 2000), tectonically exhumed during nonvolcanic rifting (Beard and Hopkinson 2000). The breccias overlying the mantle exhibit hydrothermal alteration from the upward serpentinitised fluids due to rodingitization of amphibolite, presence of hydrogarnet, zeolite, chlorite and high concentration of methane (Beard and Hopkinson 2000).

Gabbroic magmatism occurred at 247 Ma as determined by U-Pb dating of zircons in the amphibolites at Site 1068 (Gardien and Paquette 2004). Later intrusions are dated at 167-132 Ma by  $^{39}\text{Ar}$ - $^{40}\text{Ar}$  ages of hornblende and 142-133 Ma by  $^{39}\text{Ar}$ - $^{40}\text{Ar}$  ages of plagioclases (Jagoutz et al. 2007).

Sample (173/1068A/20R7/18-21) is a breccia with angular to sub-angular clasts of metagabbro in a matrix of calcite and chlorite. Sample (173/1068A/20R7/82-87) is a serpentinite breccia with clasts of dunite in a matrix of serpentine, chlorite and calcite (Fig. 5.3, Table 5.1) (Whitmarsh et al. 1998b).

#### 5.3.2.3. Site 1070A

Core material recovered from Hole 1070A includes, from top to bottom, post-rift sediments (early Oligocene and late Aptian), tectono-sedimentary breccias overprinted by tectonics hydrothermal events, pegmatite gabbros and gabbroic intrusions in a serpentinised highly altered peridotite (~ 10m) and finally massive serpentinised basement (> 70-95%) (Whitmarsh et al. 1998b). Serpentinite breccias, gouges and cataclasites from this site have been previously compared with the Totalp unit of the eastern Swiss Alps (Chapter 3), in terms of deformation and carbonate texture (Masini et al. 2013). The gabbroic pegmatites are intrusive within the serpentinised mantle (173/1070A/9R2 64-69), have a source from enriched mid-ocean ridge basalts (E-MORB) and are dated at  $127 \pm 4$  Ma by U-Pb on zircons from altered albitite (Beard et al. 2002). The crustal accretion at this Site is dated at 127 Ma and the mantle exhumation is dated at late Aptian time (112-119 Ma) (Table 5.1) (Whitmarsh and Wallace 2001; Jagoutz et al. 2007). Three samples from this site representing serpentinite breccia, gabbro and serpentinised peridotite were analysed (fig. 5.3, Table 5.1).

Depth (mdsf)	Name/Litho	TIC profile	TC (%) +/- 0.07%	TOC (ppm) +/- 0.6%	HC (ppb) +/- 15ppb
133.42	210/1277A/5R1 82-87 basalt		0.2	302	2500
135.68	210/1277A/5R3 15-22 pegmatite gabbro		0.1	302	2500
142.91	210/1277A/6R1 81-86 serpentinized peridotite		0.2	302	2500

Newfoundland margin



Depth (mdsf)	Name/Litho	TIC profile	TC (%) +/- 0.07%	TOC (ppm) +/- 0.6%	HC (ppb) +/- 15ppb
650.64	149/897C/1A/63R1 91-95.5 clayey limestone				
672.53	149/897C/63R2 92-97.5 serpentinized peridotite				
	173/1070A/8R5 48.5-55 serpentinite breccia				



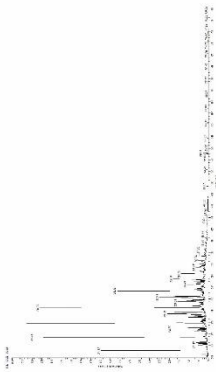
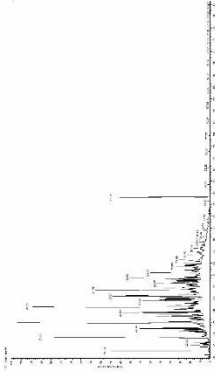
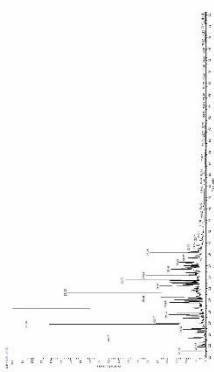
Depth (mssf)	Iberia margin	Name/Litho	TIC profile	TC (%) +/- 0.07%	TOC (ppm) +/- 0.6%	HC (ppb) +/- 15ppb
678.32		173/1070A/9R2 64-69 coarse-grained (pegmatite) gabbro				
686.32		173/1070A/10R1 42.5-47 serpentinite peridotite				
892.26		173/1068A/20R7 18-21 breccia 173/1068A/20R7 82-87				

Figure 5.3. Images of the taken samples with their depth (mbsf – meters below se floor), ODP number and lithology, TC, TOC and HC values with their analytical uncertainty (see Table 2). There is no apparent correlation between measured data and depth for the small number of sample.

#### 5.3.2.4. Site 1277A

The rocks drilled at ODP Site 1277A contain, from top to bottom, 60cm of sediments (sandstone, ferruginous sediments and hyaloclastite breccia), three types of basalt flows, debris flows and sandstones with clasts of gabbro and serpentinite. These all overlay the serpentinitised mantle basement (a strongly altered serpentinitised harzburgite) that is intruded by two minor gabbroic dykes (Tucholke et al. 2004). No sediments were recovered in the core. ODP Site 1277 is similar to ODP Site 1070 in term of its magmatic evolution (Jagoutz et al. 2007). The age of the alkaline and MOR-basaltic (MORB) magmatism are determined by  $^{39}\text{Ar}$ - $^{40}\text{Ar}$  ages age ( $128\pm 3\text{Ma}$  and  $<91.6\pm 0.3\text{Ma}$ ) and show that MORB magmatism occurs after mantle exhumation and serpentinitisation (Jagoutz et al. 2007). The 210/1277A/5R1 82-87 samples chosen for analysis were basalts that are interbedded with debris flow containing serpentinite and gabbro clasts (Fig. 5.3, Table 5.1). Sample 210/1277A/5R3 15-22 from a gabbroic intrusion and sample 210/1277A/6R1 81-86 from a serpentinitised peridotite were also chosen for analyses (fig. 5.3, Table 5.1).

#### 5.3.3. IODP cores and contamination

It is important to prevent samples becoming contaminated when analysing trace amounts of organic matter (OM); this starts with the collection of the samples. In 1995, the ODP drilling controlled contamination by using different types of drill fluid. For ODP Legs 173 (1997) and 210 (2003) the fluid used was a high- viscosity mud sweep called sepiolite, while for ODP Leg 149 (1994) the drilling mud was bentonite (Andrews et al. 2016).

Table 5.1. Results by samples IODP sites including mineralogy and texture observed in hand specimens and the texture on the calcites used for the isotopic analyses ( $\delta^{13}\text{CVPDB}$  and  $\delta^{18}\text{OVPDB}$ ).

No Sample	Lithology	depth (mbsf)	coordinates (UTM) Latitude Longitude	geological situation OCT and	drilling fluid (seawater + )	age	macroscopic description	texture	carbonate texture	$\delta^{13}\text{C}_{\text{vms}}$ (%)	$\delta^{18}\text{O}_{\text{vms}}$ (%)
<b>Iberian Abyssal Plain</b>											
149/897C/63R2 92-97.5 Return to Iberia	clayey limestone	649.61	40°50.33'N 12°28.44'W	IAP (Iberian Abyssal Plain)	bentonite	Aptian-Albian	mass flow deposit, non-tilted fine sediment	very fine grained			
149/897C/63R2 92-97.5 Return to Iberia	serp.peridotite	650.64	40°50.33'N 12°28.44'W		bentonite	Aptian-Albian	light green srp with oliv+px+spinel showing brittle deformation	mesh serpentinite	spartic calcite in veins	-0.71	0.05
173/1068A/20R7 18-21	breccia	892.26	40°40.955'N 11°36.720'W		sepiolite	Barremian	fine green-grayish matrix (calc+chl) and sub-rounded mm to cm clasts of metagabbro	matrix supported breccia			
173/1068A/20R7 82-87	breccia serp	892.9	40°40.955'N 11°36.720'W	IAP hyper-extended continental crust	sepiolite	Barremian	fine gray matrix (srp+chl+cal) and angular to sub-rounded millimetric clasts of dunite	matrix supported breccia			
173/1070A/8R5 48.5-55	serp.breccia	672.535	40°47.779'N 12°43.430'W		sepiolite		Greenish matrix from granular calcite with angular to rounded 0.1mm to 0.5mm clasts of serp. peridotite gabbro composed of large plg and px with interstitial amp and oxides. Alteration & veins minis: prehnite, zeolite, vesuvianite and chl	matrix supported breccia			
173/1070A/9R2 64-69	coarse-grained gb	678.32	40°47.779'N 12°43.430'W	IAP, close to magnetic anomaly M1 and 30km west of J anomaly	sepiolite			coarse hypidiomorphic igneous			
173/1070A/10R1 42.5-47 Newfoundland margin	serp.peridotite	686.325	40°47.779'N 12°43.430'W		sepiolite		lz+chl+sub-angular to angular 0.2 to 0.6mm bastite+ minor spl+chl from lherzolite; small calcite veins	pseudomorphitic			
<b>Newfoundland margin</b>											
210/1277A/5R1 82-87	basalt flow	133.42	45°11.8002'N 44°22.5999'E	on basement ridge km of magnetic anomaly M1	sepiolite	Barremian	yellowish brown colour plg, px, plw with fine calcite vein	aphyritic to fine grained (<0.1-0.5mm)	spartic calcite in veins	2.55	-0.09
210/1277A/5R3 15-22	gabbro	135.68	45°11.8002'N 44°22.5999'E		sepiolite	Barremian	phenocryst of oxidised px, plg, px and oliv serpentized foliated peridotite with strong cataclaste overprint, oxidised, calcite veins and <2mm px	pegmatitic	spartic calcite in veins		
210/1277A/6R1 81-86	serp.peridotite	142.91	45°11.8002'N 44°22.5999'E		sepiolite	Barremian		pseudomorphitic foliated	spartic calcite in veins	2.16	-0.12

Bentonite is a clay composed of smectite, quartz, feldspars and small amounts of mica and/or illite (Gieskes et al. 1986). Sepiolite is a clay mineral ( $\text{Mg}_4\text{Si}_6\text{O}_{15}(\text{OH})_2 \cdot 6\text{H}_2\text{O}$ ) that occurs as a secondary mineral associated with serpentine (Anthony et al. 2000). The cores collected on some ODP Legs (129, 185, 201 801, 1149) were examined for microbial contamination (prokaryotic cells) potentially introduced during drilling, by using chemical and particulate tracers (perfluorocarbon and fluorescent microspheres) and were then compared to surface seawater (Smith et al. 2000b; House et al. 2003). A cautious estimate of the amount of contamination from the drilling fluid in the core was of the order of 1-10 bacteria  $\text{g}^{-1}$  of core material (Smith et al. 2000a). Seawater is the biggest source of contamination of drill fluids with OM (Smith et al. 2000a).

Even the use of a portable coring tool could introduce microorganisms, as indicated by a bromide tracer (Haldeman et al. 1995). The RV Joides Resolution (IODP program, expedition 301) uses only surface seawater with drilling fluid and any contamination is monitored using perfluorocarbon tracers (PFTs) (Lever et al. 2006). Contamination is not dependent on depth of drilling, but decreases towards the centre of the core and is greater in sediments than in basalt, while contamination in clay is greater than in fine sand (Lever et al. 2006). The drilling fluids can also be detected by X-ray diffraction (XRD) since the fluid is injected during coring (France-Lanord et al. 2016). On expeditions with specific microbiological objectives (expedition 337), the drilling fluid employed was ASTEX-S SAS, with a known GC-MS profile (Inagaki et al. 2013). However, tests for contamination only deal with microbial contamination, and do not usually determine the organic composition of drilling muds and core materials.

#### **5.4. Methods**

To search for OM content and evidence of methanotrophs, samples were chosen not only from serpentinised mantle but also from overlying sediment and magmatic intrusive rocks (Fig. 5.3). ODP core samples for analyses were also selected for their consolidation and integrity. Sediment samples were chosen for their proximity to serpentinised mantle. Basalt and gabbro samples in close contact with serpentinite

were also chosen as this type of lithology is also known to support hydrogen-based biosystems (Anderson et al. 1998).

IODP drilling core samples are restricted in terms of their amount available for analysis compared to Alpine outcrops samples, where the amount is unlimited. The samples were taken from the IODP Bremen core repository and had not been specially stored for organic geochemistry analysis (<https://www.marum.de/en/Research/IODP-Bremen-Core-Repository.html>).

#### **5.4.1. Sample preparation**

The samples were cut with water as a lubricant, as required, at the Marum centre (Bremen, Germany) and wrapped in pre-combusted foil (400 °C) to limit contamination. Upon return to the laboratory the samples were cleaned with de-ionised water (18 MΩ cm<sup>-1</sup> resistivity; Milli-Q) and rinsed with re-distilled dichloromethane (DCM) before and after cutting into small pieces (<2cm), sonicated with de-ionised water (10 min; Milli-Q) before transfer to the Tema mill. The weight of the samples varied from 40 to 90 g and due to the small amounts, no outer edges were removed. In order to assess lab contamination, blanks composed of DCM:methanol (9:1) solution were subjected to the same procedures as the samples. The size of the sample did not permit thin sections and for this reason previous literature is used, especially the proceedings of the International Ocean Drilling Program IODP (Sawyer et al. 1994; Whitmarsh et al. 1998c; Whitmarsh et al. 1998d; Tucholke et al. 2004).

#### **5.4.2. Geochemical analyses**

Total organic carbon (TOC) values were obtained from 1 to 5 mg of bulk sample powder, decarbonated through addition of 10% HCL at 25 °C. Analyses of total carbon (TC) and TOC were carried out in a Carlo Erba Instrument NC2500 elemental analyser. The TC results are reported as a wt % while the TOC values are reported as ppm due to their low levels. The analytical uncertainty for this method is 0.012% and the variability of our analysed samples is 0.6% for organic carbon and 0.06% for inorganic carbon.

Stable isotopic analyses of organic carbon were not performed due to insufficient TOC. Carbon and oxygen isotope measurements were performed on calcite extracted manually from calcite veins from three samples containing visible veins. Carbon and oxygen isotope values were normalized to IAEA-CH7 calibration material and reported using the standard  $\delta$ -notation with Vienna-Pee Dee Belemnite (VPDB) reference material. A VG SIRA 10MS Isocarb (common acid bath) was used to calculate the CO<sub>2</sub> conversation from the calcite (McCrea 1950; Craig 1957; Friedman and O'Neil 1977; Swart et al. 1991).

Calcite precipitation temperatures can be calculated using the oxygen isotope data and O'Neil (1969) equations (Eq.5. 4, 5.5):

$$1000\ln\alpha = 2.78(10^6x T^{-2}) - 3.39 \quad (\text{Eq. 5.4})$$

$$\alpha_{A-B} = (1000 + \delta_A)/(1000 + \delta_B) \quad (\text{Eq. 5.5})$$

where the isotope values are calculated in SMOW for A - mineral and B - seawater and the temperature (T) in Kelvin. Based on previous calculations the oxygen isotopic composition of modern seawater is assumed to be  $\delta^{18}\text{O}_{\text{seawater(SMOW)}} = 0\text{‰}$  (Agrinier and Cannat 1997; Schwarzenbach et al. 2013). This values changes to  $\delta^{18}\text{O}_{\text{seawater(SMOW)}} = -1\text{‰}$  in an ice free world e.g. Late Cretaceous), which is insignificant of terms of result given in a range (Schwarzenbach et al. 2013).

Soxhlet extraction was used to extract bitumen from powdered bulk rock with a DCM:methanol (9:1) solution for 24 hours (method modified from (Wolff et al. 1995)). The eluent from an alumina column (alumina, sodium sulphate using heptane as solvent) was diluted in hexane (200  $\mu\text{L}$ ) and analysed by gas chromatography (GC) and GC-mass spectrometry (GC-MS). A GC Trace 1300 fitted with a split-splitless injector, GC column (DB-5MS non-polar 5% phenyl and 95% methyl silicone stationary phase, 60 m 0.25 mm i.d., film thickness 0.1  $\mu\text{m}$ ) using helium as a carrier gas (2 mL  $\text{min}^{-1}$ ) was coupled with a Thermoquest ISQMS single quadrupole mass spectrometer. The GC oven temperature was programmed from 60 to 170  $^{\circ}\text{C}$  after 1 minutes at 6  $^{\circ}\text{C min}^{-1}$ , then from 170 to 315  $^{\circ}\text{C}$  at 2.5  $^{\circ}\text{C min}^{-1}$  and finally held at 315

°C for 15 minutes. GC–MS was carried out in full data acquisition mode, providing mass spectra of compounds eluting from 20 to 90 minutes; these were identified by comparison with the literature and with authentic reference materials where available (e.g. PAHs-polynuclear aromatic hydrocarbons). 5 $\alpha$ (H)-Cholestane was used as an external reference material for quantification; response factors were assumed to be 1, hence data are semi-quantitative. Data were processed using XCalibur 1.2 software (ThermoScientific).

The mean carbon number, MC# (Peltzer and Gagosian 1989) of *n*-alkanes was calculated over the carbon number range C<sub>16</sub>-C<sub>32</sub> (Eq.5.6). Carbon preference indices (CPI) of *n*-alkanes (Peters et al. 2005a) were calculated over the carbon number range C<sub>16</sub>-C<sub>21</sub> because the HMW *n*-alkanes are present only in trace amounts (Eq.5.7; Table 2).

$$MC\# = \frac{\sum([C_i] \times C_i)}{\sum [C_i]} \quad (\text{Eq. 5.6})$$

where [C<sub>i</sub>] = concentration of the *n*-alkane with C<sub>i</sub> carbon number

$$CPI = \frac{\sum(\text{odd } C_{17} - C_{21})}{\sum(\text{even } C_{16} - C_{20})} \quad (\text{Eq. 5.7})$$

Kovats indices were calculated for unknown compounds using the formula (Eq.5.8):

$$KI = 100 \times \frac{n + RT_{\text{unknown}} - RT_n}{RT_N - RT_n} \quad (\text{Eq. 5.8})$$

where RT is the retention time and n and N are the carbon numbers of the *n*-alkanes with lower and higher carbon number eluting prior to and after the unknown, respectively.

The bitumen extract of one sediment sample (149/897C/1A/63R1), characterised by relatively high amounts of HCs, was sent to the University of Bristol to isolate and identify specific biomarkers (i.e. GDGTs- glycerol dibiphytanyl glycerol tetraethers), using a method based on high-performance liquid chromatography with atmospheric pressure chemical ionisation–mass spectrometry (HPLC/APCI-MS, ThermoFisher Scientific TSQ Quantum Access with a ThermoFisher Scientific Accela PDA Detector). HPLC was carried out using two Waters Acquity UPLC BEH Hilic columns (2.1 mm x

150 mm x 1.7 µm) with isocratic flow rate of 0.2 mL/min to attain normal phase separation. The targeted biomarkers were eluted for 25 minutes with 82% hexane and 18% n-hexane/iPA 9:1, then the gradient of the n-hexane/iPA 9:1 was changed linearly from 35% over 25 minutes, to 100% over 30 minutes. The acquisition was carried out using selective ion monitoring mode (SIM) to increase the sensitivity and the data were analysed from the [M+H]<sup>+</sup> peaks using Xcalibur software.

For the GDGTs, several indices are calculated to indicate their origin, water temperature and history (Eq.5.9 – 5.12). They are resistant to oxidation and geological degradation (Zhang et al. 2011). The Branched Isoprenoid Tetraether (BIT) indicates the input of terrestrial OM (Eq.5.9) (Hopmans et al. 2000):

$$BIT = \frac{(GDGT - 1) + (GDGT - 2) + (GDGT - 3)}{(GDGT - 1) + (GDGT - 2) + (GDGT - 3) + (Cren)} \quad (\text{Eq. 5.9})$$

The methane index (MI) is used to determine methane-rich environments and therefore potentially the presence of a methanotrophic community (Eq.5.10) (Zhang et al. 2011):

$$MI = \frac{(GDGT - 1) + (GDGT - 2) + (GDGT - 3)}{(GDGT - 1) + (GDGT - 2) + (GDGT - 3) + (Cren) + (Cren.isomer)} \quad (\text{Eq. 5.10})$$

The tetraether index TEX<sub>86</sub> correlates with annual mean sea surface temperature and gives a temperature proxy applied to sediments old as 140My (Eq.5. 11) (Schouten et al. 2002):

$$TEX_{86} = \frac{(GDGT - 2) + (GDGT - 3) + (Cren.isomer)}{(GDGT - 1) + (GDGT - 2) + (GDGT - 3) + (Cren.isomer)} \quad (\text{Eq. 5.11})$$

Finally the ring index (RI) describes the average number of rings which differs between marine samples (1.4 to 3.3) and high surface water temperature (Eq.5.12) (Pearson et al. 2004):

$$RI = \frac{1 \times (GDGT - 1) + 2 \times (GDGT - 2) + 3 \times (GDGT - 3) + 4 \times (GDGT - 4)}{(GDGT - 1) + (GDGT - 2) + (GDGT - 3) + (GDGT - 4)} \quad (\text{Eq. 5.12})$$

## 5.5. Results: carbon and hydrocarbon distributions

Table 5.2 Results by IODP sites including TC (%), TOC (ppm) and total HC concentration ppb. For the *n*-alkanes: the carbon number range (*n*-alkanes range), the maximum carbon number (C<sub>max</sub>), carbon preference index (CPI values) and mean carbon number (MC#) are shown.

rock type	sample number	Total Carbon (%)	Total C <sub>organic</sub> ppm	Hydrocarbons (HC) ppb	<i>n</i> -alkanes				Hopanes	PAHs
					Range	C <sub>max</sub>	CPI	Mean C#		
Iberia margin										
clayey limestone	149/897C/1A/63R1 91-95.5	4.33	302	2470	16-35, tr 36-39	23	1.20	23	***	***
serp.peridotite	149/897C/63R2 92-97.5	3.20	120	2.5	16-32	19	0.53	19	BDL	*
Newfoundland margin										
breccia	173/1068A/20R7 18-21	0.12	8	163	trace 16-21, 25	24	0.75	24	BDL	BDL
breccia serp	173/1068A/20R7 82-87	0.07	91	700	16-21, tr 22-29	23	1.02	23	*	BDL
serp.breccia	173/1070A/8R5 48.5-55	3.51	68	1580	16-22, tr 23-32	18	0.93	18	BDL	*
coarse-grained gb	173/1070A/9R2 64-69	0.03	191	1806	16-21, tr 22-34	18	0.94	18	BDL	*
serp.peridotite	173/1070A/10R1 42.5- 47	1.44	80	219	16-22, tr 23-33	19	0.90	19	BDL	*
Newfoundland margin										
basalt flow	210/1277A/5R1 82-87	1.37	200	105	16-25, tr 26-32	19	1.06	19	BDL	*
gabbro	210/1277A/5R3 15-22	0.12	86	235	16-21, tr 22-32	19	0.99	19	BDL	*
serp.peridotite	210/1277A/6R1 81-86	2.98	15	32	16-20, tr 21-32	18	0.94	18	BDL	BDL

1.1.1 Hydrocarbon distribution in the sediment sample (149/897C/1A/63R1 91-95.5)

Sample number	Lithology	steranes	hopanes	PAHs
<b>Iberian Abyssal Plain</b>				
149/897C/1A/63R1 91-95.5	clayey limestone	C29 $\alpha\alpha$ and $\alpha\beta$ S, R > dia C29 > C27 R > C28 $\alpha\beta$ 20S	C29 $\alpha\beta$ , C30 $\alpha\beta$ , C31 $\alpha\beta$ S, R; C30 $\beta\beta$ ; C31 $\beta\beta$ , C32 $\alpha\beta$ S, R, C34 $\alpha\beta$ S, R	P, Fluo, Chry, BaA, BbF, BF, Benz, DBT, MDBT, 2MDBT, MPs
149/897C/63R2 92-97.5	serp.peridotite	BDL	BDL	P, Fluo
<b>Return to Iberia</b>				
173/1068A/20R7 18-21	breccia	BDL	BDL	BDL
173/1068A/20R7 82-87	breccia serp	C27 20R, S > dia C27 20R, S > C28 $\alpha\beta\beta$ S, R > C29 20R, S	C29 $\alpha\beta$ , C30 $\alpha\beta$	BDL
173/1070A/8R5 48.5-55	serp.breccia	BDL	C29 $\alpha\beta$ , C30 $\alpha\beta$	BDL
173/1070A/9R2 64-69	coarse-grained gb	BDL	C29 $\alpha\beta$ , C30 $\alpha\beta$	BDL
173/1070A/10R1 42.5-47	serp.peridotite	BDL	BDL	P, MPs
<b>Newfoundland margin</b>				
210/1277A/5R1 82-87	basalt flow	BDL	BDL	P, Fluo, MPs
210/1277A/5R3 15-22	gabbro	BDL	BDL	P, Fluo
210/1277A/6R1 81-86	serp.peridotite	BDL	BDL	BDL

Table 5.3 Table showing the identified *n*-alkanes, PAHs, steranes and hopanes in the samples. For the abbreviations of the names see glossary. Where Phenanthrene, P; Fluoranthene, Fluo; Chrysene, Chry; Benzo(a)anthracene, BaA; Benzo(b)fluoranthene, BbF; Benzo (k) fluoranthene BF; Benzo(a)pyrene, Benz; Dibenzothiophene (DBT), methyl DBT (MDBT) and methylP (3,2,1 and 9 MPs).

The sediment sample (897/63R1), from almost 650 m below the seafloor and 28m above the serpentinised mantle, has the highest TC, TOC and HCs values, 4.33%, 302 ppm and 2470 ppb, respectively (Table 5.2). This sediment sample is the richest of our batch in terms of HCs.

It contains *n*-alkanes from C<sub>16</sub> to C<sub>35</sub> with traces of C<sub>36</sub> to C<sub>39</sub>, steranes, hopanes, PAHs, isoprenoids (pristane and phytane), LMW alkanes and branched alkanes (Fig. 5.4, Table 5.2, 5.3). The distribution of hopanes included C<sub>29</sub> to C<sub>30</sub> αβ; C<sub>31</sub>, C<sub>32</sub> and C<sub>34</sub> αβ 22S and 22R and C<sub>30</sub> and C<sub>31</sub> ββ compounds (Table 5.3). The PAHs include only LMW ≤ 252 (Fig. 5.4, Table 5.3). The CPI is 1.20 showing slight odd over even predominance (Table 5.2). Pristane is more abundant than phytane.

GDGTs were present in 897/63R1 and include the isoprenoidal GDGTs with 0 to 3 rings, crenarchaeol and its regioisomer, as well as minor components identified as branched GDGTs (GDGT Ia-c, GDGTIIa-b, GDGT IIIa) (Fig. 5.6). The indices (BIT, MI, TEX<sub>86</sub> and RI) calculated from the data using equations 8 to 11 are shown in Figure 5.6.

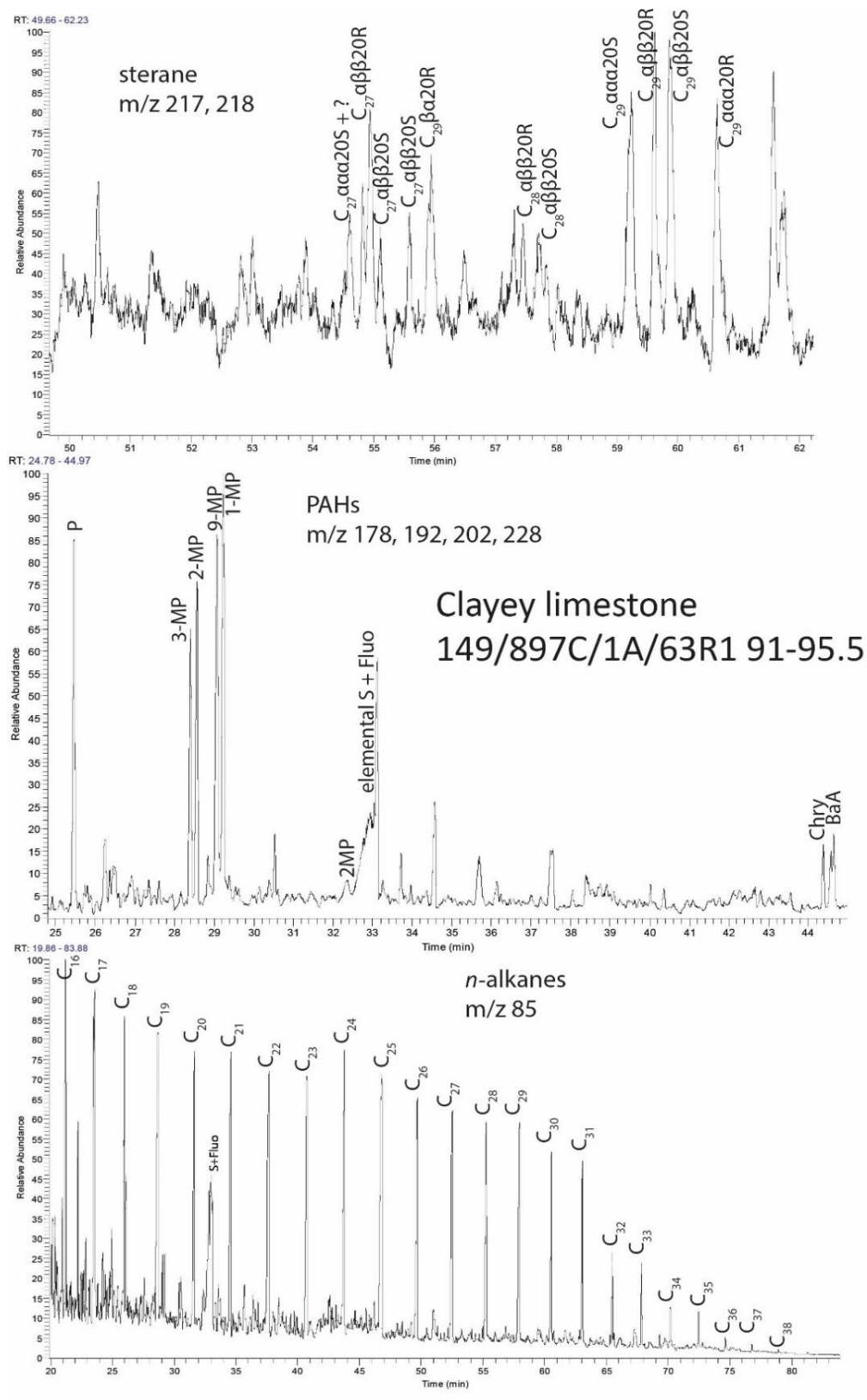


Figure 5.4. Ion chromatogram profile of the clayey limestone sample for *n*-alkanes (m/z 85), PAHs and steranes (m/z 217, 218).

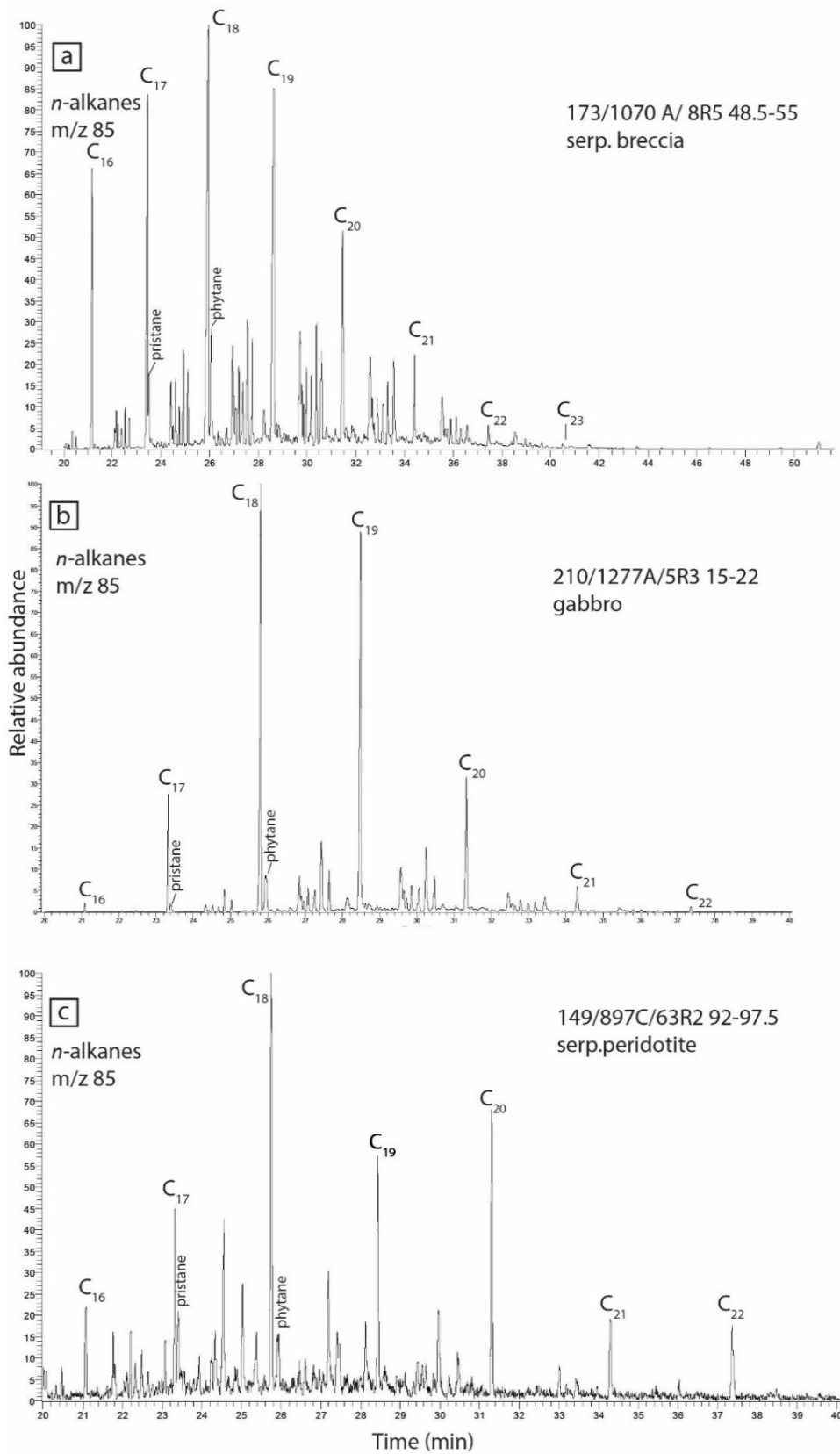
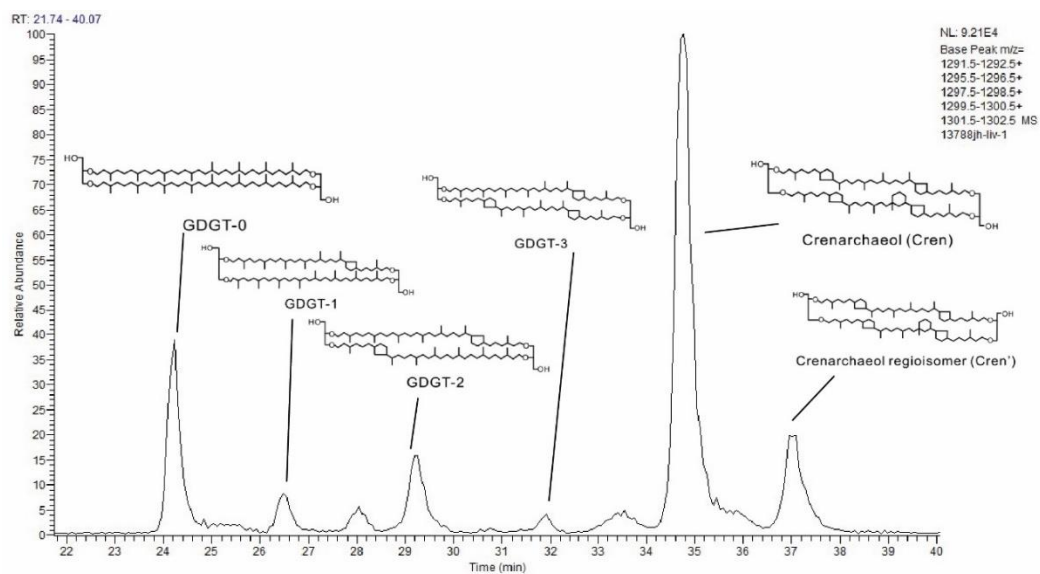


Figure 5.5. Ion chromatogram (m/z 85) of the *n*-alkanes of three samples. a. and b. serp. breccia from leg 173 Iberian margin b. gabbro from leg 210 Newfoundland showing similar distribution c. serpentinised peridotite from leg 149 Iberian margin.



Sample Name	lithology	<i>i</i> GDGTs (%)	<i>br</i> GDGTs (%)	BIT	GDGT-0/Crenarchaeol	RI	TEX <sub>86</sub>	MI
149/897C/1A/63R1 91-95.5	clayey limestone	81	19	0.2	0.29	1.9	0.89	0.18

Figure 5.6. GDGTs results for sedimentary sample 897/63R1. Different ratios result from the GDGTs are given using formulas described in methodology section.

### 5.5.1. Hydrocarbons in other lithologies

TC and TOC values varied from 0.07 to 3.51% and 8 to 200 ppm respectively, reflecting the heterogeneity of different lithologies (Table 5.2). There is no clear relationship between TC, TOC and HC amounts, although the number of samples taken was too small to test statistical significance (Fig. 5.3, Table 5.2). The Iberian and Newfoundland margins had a relatively low sedimentation rate and the missing sedimentary core could indicate that the TOC was reworked. This could explain the low amount of TOC found in the Iberian and Newfoundland margin.

*n*-alkanes are the dominant compounds in the total ion chromatogram (TIC) with short-chain compounds from C<sub>16</sub> to C<sub>21</sub> being most abundant and with traces from C<sub>22</sub> to C<sub>32</sub>; the majority of samples from Legs 173 and 210 having a C<sub>max</sub> = 18 and 19 (Table 5.2). The *n*-alkanes from ODP Leg 149 at the Iberian margin are more abundant and range from C<sub>16</sub> to C<sub>32</sub> (Table 5.2). Steranes were present only in the serpentinite breccia 1068A/20R7 82-87 (Table 5.2, 5.3). The hopanes  $\alpha\beta$  hopanes, mainly C<sub>29</sub> and C<sub>30</sub> were present in breccia and gabbros from ODP Leg 173 (Table 5.2) (Mackenzie et al. 1980). Steranes and hopanes in the Newfoundland margin samples were below

detection limits (Table 5.2, 5.3). Low molecular PAHs (P, MP, Flu) were the only PAHs present in the samples (Table 5.2). The samples from ODP Legs 173 and 210, at the Iberian and Newfoundland margins, respectively contained very similar alkanes profiles ( $m/z$  85) (Fig. 5.5). When isoprenoids were present, pristane was always more abundant than phytane.

### 5.5.2. Carbonate isotopes

The isotopic composition of the carbonate from the calcite veins were  $\delta^{13}C_{VPDB} = -0.71\text{‰}$  and  $\delta^{18}O_{VPDB} = 0.05\text{‰}$  for one sample 897C/63R2 at the Iberian margin with a relatively small range  $\delta^{13}C_{VPDB} = 2.16\text{‰}; 2.55\text{‰}$  and  $\delta^{18}O_{VPDB} = -0.12\text{‰}; -0.09\text{‰}$  for two samples 12771/5R1 and 1277A/6R1 from the Newfoundland margin (Table 5.1).

## 5.6. Discussion

### 5.6.1. Origin of organic matter from biomarkers of sediment samples (149/897C/1A/63R1 91-95.5)

#### 5.6.1.1. Biomarkers

The dominance of pristane over phytane ( $Pr/Ph = 2.86$ ) suggests an oxic environment of deposition for the sediment (Table 5.4) (Peters and Moldowan 1993). Together with the pristane/ $n$ - $C_{17}$  and phytane/ $n$ - $C_{18}$  (4.06 and 2.33, respectively) this suggests a mixed open marine source for the OM, mainly bacterial, deposited under dysoxic condition with low maturation level (Table 5.4) (Peters and Moldowan 1993; Peters et al. 2005b; Vu et al. 2009). The low maturation level indicated by the isoprenoids/ $n$ -alkanes ratios is also confirmed by the steranes thermal maturity ratios ( $\alpha\alpha\alpha 20S/\alpha\alpha\alpha 20S + \alpha\alpha\alpha 20R$   $C_{27} = 0.76$ ,  $\alpha\beta\beta/\alpha\alpha\alpha + \alpha\beta\beta$   $C_{27} = 0.71$ ,  $\alpha\beta\beta/\alpha\alpha\alpha + \alpha\beta\beta$   $C_{29} = 0.52$  and  $\alpha\alpha\alpha 20S/\alpha\alpha\alpha 20S + \alpha\alpha\alpha 20R$   $C_{29} = 0.49$ ) (Table 5.4).

Hopane/sterane ratios are used to indicate the inputs of eukaryotes (algae, higher plants) and prokaryotes (bacteria) input in the source rock (Peters et al. 2005a; El Diasty et al. 2016) (Table 5.4). The high value (4.8) in this sediment sample suggests terrigenous or microbial reworked OM inputs (Table 5.4) (Peters et al. 2005a). The  $C_{30}$  hopane is dominant over  $C_{29}$  compound, with ratio = 0.6 typical for the clayey

limestone lithology (Table 5.4) (Gurgey 1999). Steranes are dominated by C<sub>29</sub> compounds (73.6%; cf. C<sub>27</sub> - 19.5%) and C<sub>28</sub> - 6.9%) which could derive either from terrigenous or marine OM (Volkman 1988; Nichols et al. 1990; Peters and Moldowan 1993; Wójcik-Tabol and Ślącza 2015). These results are comparable with results found from the science party of ODP Site 897 indicating that the source of OM in the sediments in these legs are from marine algal production and land plant detritus composed of less-reactive materials (Sawyer et al. 1994).

PAHs are related to high temperature environments under three headings: i) pyrogenic involving incomplete combustion and pyrolysis of OM, ii) petrogenic by slow maturation of OM during burial, or iii) a diagenetic origin by alteration of biogenic compounds in sediments (Baumard et al. 1998; Magi et al. 2002). With respect to our geological environment, the PAHs could reflect OM alteration during hydrothermal activity  $T > 300$  °C (Kawka and Simoneit 1990b) or derive from pyrolytic residues (Geissman et al. 1967) related to the anoxic thermochemical decomposition of the OM within a contact zone of intrusive magma. The distribution of LMW PAHs (MW <252) with two and three rings could be explained by their higher solubility in water, which made them more easily transferable into the sediments (Table 5.2) (Baumard et al. 1998; Mackay and Callcott 1998; Johnsen et al. 2005). PAH ratios can differentiate between the three type of origin ratio as  $MP/P < 2$  with 0.85 and  $BaA/BaA+Chry=0.5$  thus indicating a pyrogenic source (Colombo et al. 1989; Garrigues et al. 1995; Yunker et al. 2002). From Fluo and Pyrene, both PAHs associated with LT combustion only Fluo is present, which could show higher amounts of oxidized organic matter related to its hydrogen index values, which we do not have (Inagaki et al. 2013).

Table 5.4. Biomarkers ratios used to indicate the source input and thermal maturity.

	Ratios	149/897C/1A/ 63R1 91-95.5	149/897C / 63R2 92-97.5	173/1068A / 20R7 18- 21	173/1068A/ 20R7 82-87	173/1070A/ 8R5 48.5- 55	173/1070A/ 9R2 64-69	173/1070A/ 10R1 42.5- 47	210/1277A / 5R1 82-87	210/1277A / 5R3 15- 22	210/1277A / 6R1 81-86
Source input and paleodepositional environment	Pr/n -C <sub>17</sub>	4.06	0.63	X	0.02	0.11	0.01	0.11	0.10	0.07	0.09
	Ph/n -C <sub>18</sub>	2.33	0.01	X	0.28	0.17	0.01	0.14	0.13	0.16	0.11
	Pr/Ph	2.86	2.06	X	0.29	0.39	X	0.31	0.15	0.08	0.22
	hop/ster	4.80	X	X	0.16	X	X	X	X	X	X
	C <sub>29</sub> /C <sub>30</sub> hopane	0.60	X	X	0.81	1.85	1.71	X	X	X	X
Thermal maturity	αα20S/αα20S+αα20R C <sub>27</sub>	0.76	X	X	0.50	X	X	X	X	X	X
	αββ/ααα+αββ C <sub>27</sub>	0.71	X	X	0.41	X	X	X	X	X	X
	αββ/ααα+αββ C <sub>29</sub>	0.52	X	X	0.71	X	X	X	X	X	X
	ααα20S/ααα20S+ααα20R C <sub>29</sub>	0.49	X	X	X	X	X	X	X	X	X

### 5.6.2. GDGTs (Glycerol dibiphytanyl glycerol tetraethers)

GDGTs were identified in the sediment sample (897C/1A/63R1) from the Iberian margin. They are the main membrane constituents of cultured thermophilic archaea (Schouten et al. 2000; Kuypers et al. 2001). The overall distribution of *i*GDGTs with a dominance of crenarchaeol, followed by its isomer and GDGT-0 is typical of Thaumarchaeota (Damsté et al. 2002; Schouten et al. 2002) that are chemolithoautotrophic ammonium-oxidizers, non-thermophilic and non-methanotrophic Archaea, typical of marine surficial sediments and the most likely source of crenarchaeol (Damsté et al. 2002; Schouten et al. 2002; Zhang et al. 2011; Schouten et al. 2013; Pan et al. 2016).

Several indices calculated from GDGTs give additional information and confirm the presence of non-methanotrophic archaea. The BIT index (0.2) indicates a clear predominance of marine OM, because of the absence of br-GDGTs, which are characteristic of soil bacteria (Fig. 5.6) (Damsté et al. 2002; Hopmans et al. 2004). The MI index defines the contribution of methanotrophic Euryarchaeota in methane flux and AOM (Zhang et al. 2011). The range of MI values is always between 0 and 1 with AOM distribution at MI > 0.5 being indicative of methanotrophy (Zhang et al. 2011). The MI index of 0.18 in the sediment sample indicates a likely absence of AOM consortia and dominance of non-methanotrophic marine microbial input, probably Thaumarchaeota (Fig. 5.6) (Zhang et al. 2011; Pan et al. 2016). This is confirmed by the dominance of crenarchaeol over GDGT 1-4 that are typical for methanotrophs (ANME-1) (Schouten et al. 2013).

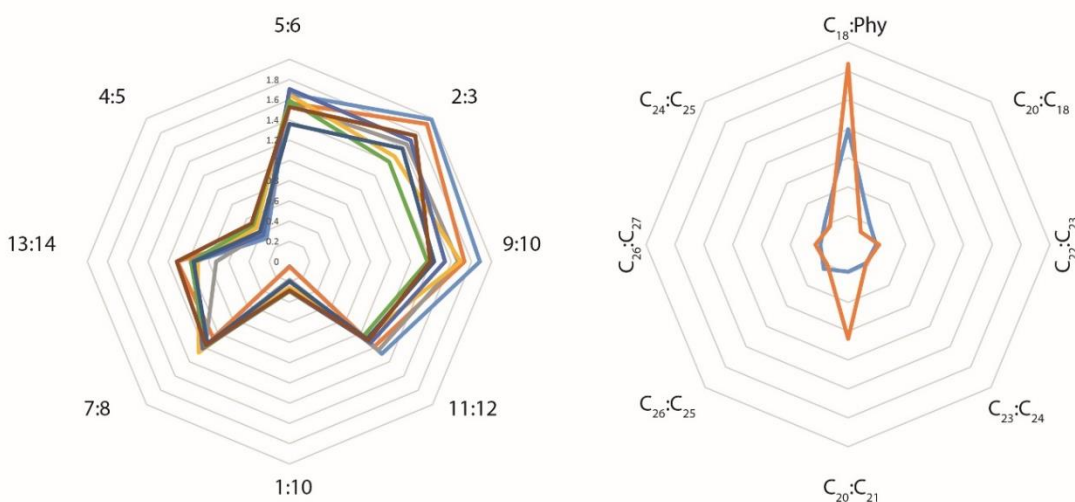
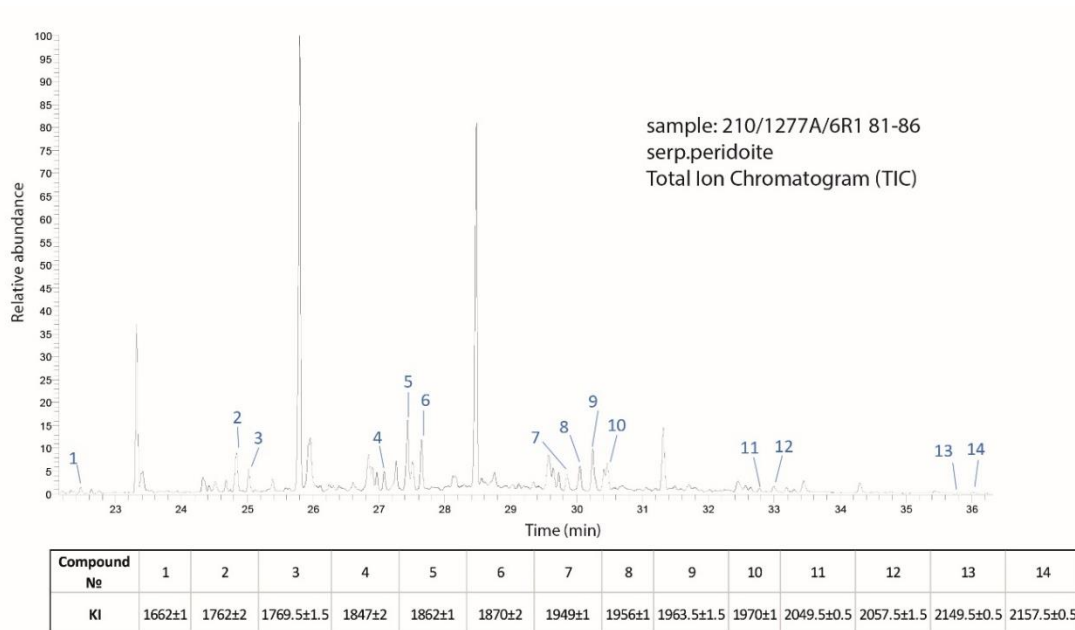
The TEX<sub>86</sub> index equates to a sea surface temperature of 32 °C. This index was linearly correlated with the temperature of ocean surface water during Cretaceous (SST > 28 °C and from 30 to 40 °C in mid-Cretaceous tropical ocean) (Fig. 5.6) (Schouten et al. 2000; Schouten et al. 2013). The number of cyclopentane rings of the iso-GDGTs in Archaea depends on environmental factor such as pH and temperature with the numbers of rings increasing with temperature (Gabriel and Chong 2000; Schouten et al. 2013). This temperature index is not biased by high AOM, and is supported by

values of  $MI \leq 0.3$  and  $BIT < 0.4$  and is typical for the early Cretaceous period (Fig. 5.6) (Prah and Wakeham 1987; Müller et al. 1998).

### 5.6.3. HCs in other lithologies

The absence of steranes and hopanes and the presence of PAHs in the magmatic samples of the Newfoundland margin could be attributed to the margin greater thermal gradient probably attributed to additional post-rift magmatic intrusions compared to the Iberian margin or its pre-rift subduction history (Müntener and Manatschal 2006; Peron-Pinvidic et al. 2010). However more samples from both margins would be necessary to confirm this. The sterane distribution of the serpentinite breccia (1068A/20R7/82-87) is dominated by  $C_{27}$  and  $C_{28}$ , indicating a depositional environment of marine organic matter by planktonic -bacteria (Peters et al. 2005a; Volkman 2005; Wójcik-Tabol and Ślącza 2015). This reducing (anoxic/suboxic) marine depositional environment is also confirmed by the isoprenoids (pristane, phytane)/ $n$ -alkanes ratios (Table 5.4) (1070A/8R5: 0.11, 0.17; 1070A/10R1: 0.11, 0.14). PAH ratios can differentiate between the three type of origin ratio as  $MP/P < 2$  with 0.85 for 897C/1A/63R1, 0.85 for 1277A/5R1 and 1.09 for 1070A/10R1 and  $BaA/BaA+Chry=0.5$  thus indicating a pyrogenic source (Table 5.4) (Colombo et al. 1989; Garrigues et al. 1995; Yunker et al. 2002).

The similarity in the GC-MS chromatograms of the distribution of alkanes ( $m/z$  85) between many samples from different lithologies in ODP Legs 173 and 210 is striking (Fig. 5.5). This is clearly shown by a star-diagram comparing various alkane ratios (Fig. 5.7). This type of diagram is used for fingerprinting oil origin in reservoir evaluation (Sofer 1984). Comparison of the ratios of eight pairs of peaks in the samples having identical Kovat's indices (KI) in a star-plot diagram shows a similar distribution that is likely to be generated from a single source (Fig. 5.7) (Kamali et al. 2013). Given the similarity of distribution ratios in many different samples (Fig. 5.5, 5.7), this raises the possibility of contamination by drilling mud since blanks allowed us to exclude a contamination from the laboratory (Fig. 5.4, 5.5). Two samples from ODP Leg 149



Leg 173 Iberian margin (Site 1068A, 1070A)  
and Leg 210 Newfoundland margin (Site 1277A):

- 1277A/5R1 82-87
- 1277A/5R3 15-22
- 1277A/6R1 81-86
- 1068A/20R7 18-21
- 1070A/8R5 48.5-55
- 1070A/9R2 64-69
- 1070A/10R1 42.5-47
- 1068A/20R7 82-87

Leg 149 Iberian margin -Site 897C

- 897C/1A/63R1 91-95.5 clayey limestone
- 897C/63R2 92-97.5 serp. peridotite

Figure 5.7. A star-plot diagram of alkane ratios from eight igneous and metamorphic samples from ODP Legs 173 and 210 from Iberian and Newfoundland margin showing similar distribution pattern. The peaks are shown in the GC-MS profile with their approximated RT and KI is shown in the table. We could propose that a contamination is realistically conceivable. The second star-plot diagram shows the distribution pattern of *n*-alkanes and isoprenoids for the two samples from ODP Leg 149 Site 897C (1A/63R1/91-95.5 clayey limestone and 63R2/92-97.5 serp. peridotite) using a different kind of drilling mud (bentonite) and showing different path from the samples from ODP Legs 173 and 210 and from each other.

were drilled using a different fluid and have different HC distributions (Fig. 5.5 c, Fig. 5.7).

Contamination from the drilling fluid is also possible in the sediment sample, however due to its higher organic matter concentration, as the total bacterial populations is usually measured to be greatest near the sediment surface ( $2.50 \times 10^9$  cells mL<sup>-1</sup>) with general decreasing with depth throughout the core (Wellsbury et al. 2000), it does not have the same consequence (Fig. 5.4).

#### **5.6.4. Carbonate isotopes - source temperature**

The carbon isotopes in the calcite veins of the Iberia Newfoundland margins have typical oceanic inorganic carbon signatures  $\delta^{13}\text{C}_{\text{PDB}} \approx 0\text{‰}$  e.g. (Sharp 2017). Our  $\delta^{13}\text{C}_{\text{PDB}}$  and  $\delta^{18}\text{O}_{\text{PDB}}$  results are in the same range for the Iberian Margin as those in other studies with an average value of  $0 \pm 2\text{‰}$  and  $0 \pm 3\text{‰}$  (Meyers and Shaw 1996; Schwarzenbach et al. 2013) (Table 5.1). The oxygen isotope of inorganic carbon is around 0‰ with  $\delta^{18}\text{O}_{\text{PDB}} = -0.12$  to  $0.05\text{‰}$  due to a long water-rock interaction associated with decreasing water-rock ratio through time (Bowers and Taylor 1985; Shanks 2001) (Table 5.1). The  $\delta^{13}\text{C}_{\text{VPDB}}$  values are consistent with aerobic oxidation and are similar to primary marine carbonate (Table 5.1).

The temperature of carbonate precipitation calculated for the Iberia margin is 17.2 °C for serpentinite sample 897C/63-2 and 17.9 °C to 18 °C for Site 1277A (1277A/5R1 basalt flows and 1277A/6R1 serpentinites) at the Newfoundland margin. These temperatures conform to the ones typical of the carbonation on Iberia passive margin (13 °C to 44 °C) (Agrinier and Cannat 1997; Schwarzenbach et al. 2013). Furthermore, they reflect the absence of volcanism or earlier basement cooling during the final stages of the continental rifting (Sawyer et al. 1994; Whitmarsh and Wallace 2001; Schwarzenbach et al. 2013).

## 5.7. Conclusion

*“Strict proof plays no part in human life outside mathematics. ...  
Rational demonstration is powerless in the face of some of the most  
elementary realities”*

*David Hume, 1711- 1776*

The sediment sample (149/897C/1A/63R1) from the Iberian Margin contains the most OM derived from a marine OM source including Thaumarchaeota, other bacteria and terrigenous detritus and reached a low maturation under dysoxic depositional environment.

Alkane distributions in metamorphic and magmatic samples from the Iberian and Newfoundland margins (ODP Legs 173 and 210) indicate that there is possibility of contamination of hard rock samples by comparing their HC ratios. Other HCs have different distributions and ratios in the samples and could be indigenous to the rocks. If so, the OM derives from a mixed source dominantly algal/bacterial deposited in reducing environment.

The microbial community originates from the open ocean, thus the OM would have been deposited on the seafloor and its presence in the different lithology would be influenced by the distance from the seafloor and the lithology, especially a sedimentary one (e.g. clay minerals) and not related to serpentinisation of mantle and methanotrophic biosystems (Labonté et al. 2017).

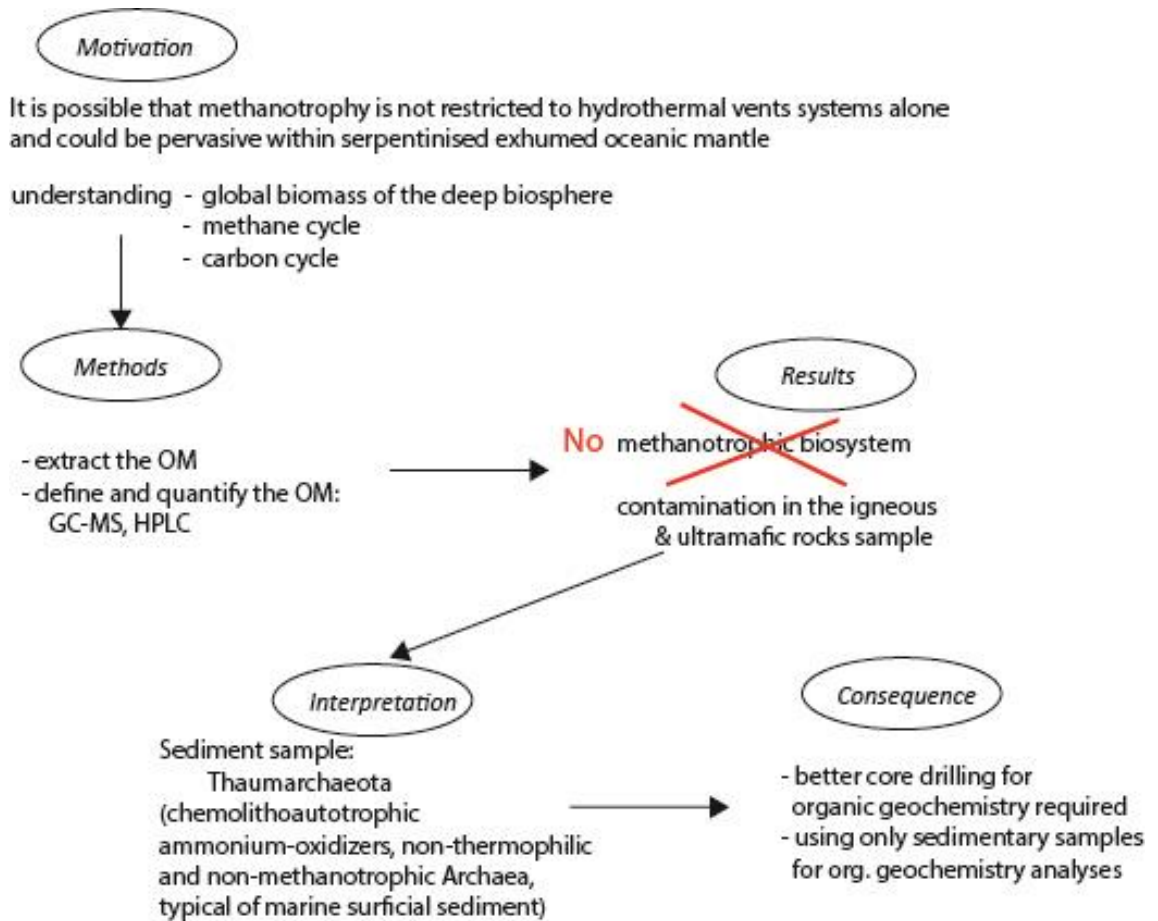


Figure 5.8. Summary flow charts of chapter 5



## Chapter 6

# 6. Discussion and Summary

*“I have steadily endeavoured to keep my mind free so as to give up any hypothesis, however much beloved (and I cannot resist forming one on every subject), as soon as facts are shown to be opposed to it.”*

*Charles Darwin (1809 – 1882)*



## **A.1. Abstract**

Serpentinisation is considered to have been involved in the origin of early life and chemosynthetic bio-systems. Serpentinisation and concomitant reduction of CO<sub>2</sub> to methane at modern hydrothermal vents could support hydrogen-driven microbial environments including methanotrophic biosystems. It is important for the understanding of the sub-surface and the fate of methane to determine if methanotrophic biosystems are locally restricted to hydrothermal vents or if they are more pervasive, being linked with the exhumation of serpentinised mantle at the seafloor. Fossil and *in-situ* samples from ocean-continent transitions (OCTs), were investigated for biomarker evidence of abiotic methane oxidation (i.e. markers for methanotrophs).

All of the analysed samples contain OM of marine origin. The paleo-depositional conditions, and thermal maturity of the OM were also assessed.

There was no evidence of methanotrophic biosystems or any kind of biosystem related to the serpentinite. There could be several reasons for this, from their absence to the limitations of the analytical methods. It is likely that methanotrophic biosystems is therefore related to serpentinisation can only flourish under optimal conditions (*e.g.* at hydrothermal vents).

Nevertheless, based on the analytical detection limits for organic biomarkers and using a thought experiment, I place an upper bound on the biomass of methanotrophs that could be supported by serpentinisation.

## **6.1. OM in the target samples**

Organic matter (OM) was present in all samples from the four fossils Alpine OCT areas (Totalp, Platta, Tasna and Chenaillet) and from *in-situ* samples from the OCT areas of Iberian and Newfoundland conjugated margins.

Hydrocarbons identified in the fossil Tethys Alpine OCT include *n*-alkanes, isoprenoids (pristane and phytane), steranes, hopanes and PAHs, while those in the modern

settings also contain branched and cyclic alkanes. Similar distributions of biomarkers in Totalp, Platta, Chenaillet and Tasna indicate similar environments, despite different metamorphic histories (e.g. Fig. 6.1). In the case of the sedimentary sample from the Iberian margin (149/897C/63R1) the OM plots away from the Alpine cluster (e.g. Fig. 6.1). Due to suspected contamination of the other ODP cores samples those data are not presented (see Chapter 5).

Most OM was deposited in a reducing environment, except for the sedimentary sample from Iberian margin (Figs. 6.1 to 6.3). This conclusion is supported by isoprenoids/*n*-alkanes ratio, pristane/phytane vs. CPI and the plots of  $C_{27}/(C_{27}+C_{29})$  regular steranes against pristane/phytane ratios indicating the depositional environment as pelagic anoxic in most cases (Figs. 6.1 to 6.3) (Powell and McKirdy 1973; Hossain et al. 2009; Adegoke et al. 2015). The OM is from a mixed marine of planktonic-algae or bacteria origin with a planktonic-algae dominance (Figs. 6.1,6.4).

A *n*-alkanes tend to increase in relative abundance with thermal maturation, while those of hopanes and isoprenoids are inversely correlated with the temperature history (Mißbach et al. 2016). Considering that the Alpine metamorphism was in the range of prehnite-pumpellyite to greenschist facies, the different maturation behaviour of the biogenic organic compounds could explain why the *n*-alkanes dominate. The variable amounts of HCs within the same lithology could reflect the heterogeneity of the collected samples (e.g. clasts, veins). The highest concentrations of HCs in the Alpine samples, all lithologies considered, were at Chenaillet, followed by Totalp, Platta and then Tasna (Fig. 6.6). This could be explained by the temperature history with metamorphism being highest at Tasna and lower at Chenaillet and Totalp. Steranes, hopanes and isoprenoids distributions are consistent with a marine source. The PAHs and *n*-alkanes are more common HCs, but their distributions are not consistent with contamination. Furthermore, carbon isotopic composition of OM is again consistent with a marine origin.

In addition, compounds detected in our samples, that are known to be lab handling contaminants (e.g. *phthalate*), are shown in appendix A and are not considered

further.

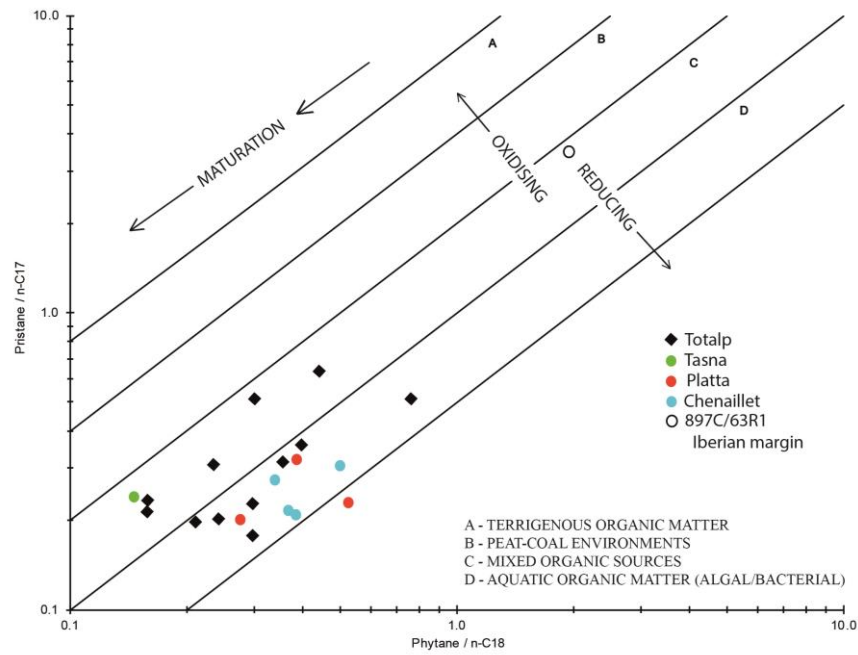


Figure 6.1 Plot of pristane/*n*-C17 vs phytane/*n*-C18 shows the depositional environment. Isoprenoids/*n*-alkanes ratio (pristane/phytane) show consistency in the results with rather reducing environment. Only one sample, the clayey limestone from site 897C, Iberian margin shows very low maturation compare to the other samples. Modified after Mateeva et al. 2017.

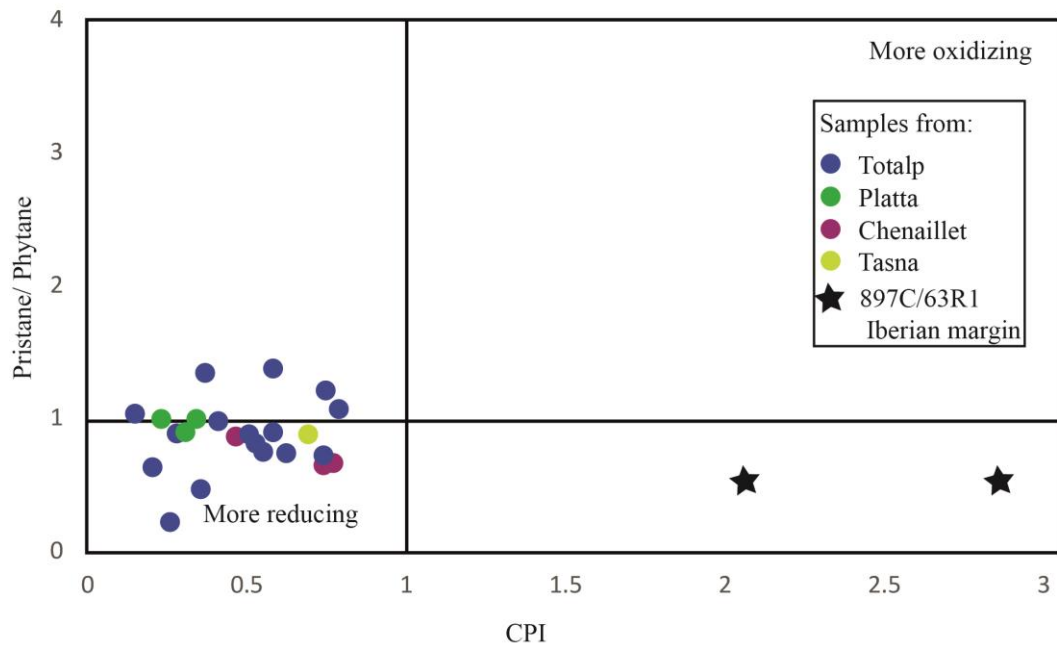


Figure 6.2 Pristane/phytane ratios versus CPI (*n*-alkanes) confirms the depositional environment conditions (Meyers and Snowdon 1993).

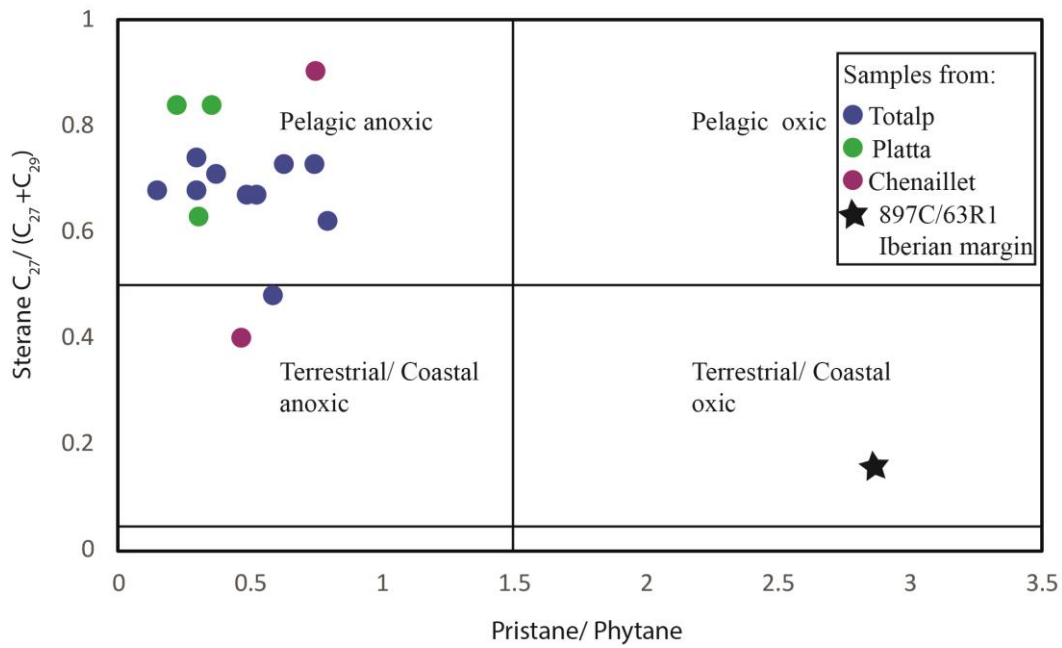


Figure 6.3 Sterane C<sub>27</sub>/(C<sub>27</sub>+C<sub>29</sub>) vs Pristane/phytane ratios showing depositional environment conditions and source input. Here, it indicates mostly a pelagic anoxic environment (Powell 1988).

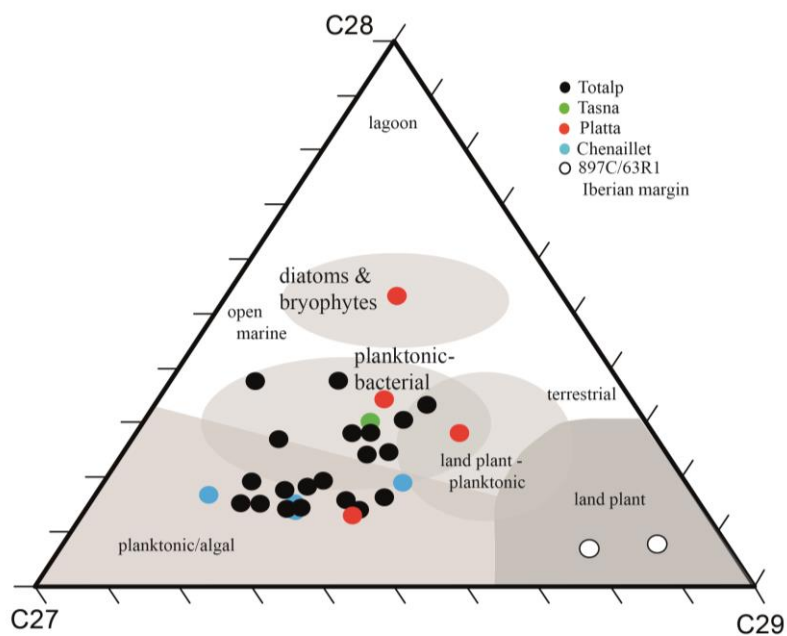


Figure 6.4 Sterane ternary distribution ( $\alpha\beta$  steranes). Classification is after Patrycja Wójcik-Tabol & Ślaczka (2015). For the sediment sample from the Iberian margin (149/897C/63R1) both  $\alpha\beta$  (left side) and  $\alpha\alpha$  (right side) type steranes are shown both displaying the input of terrestrial OM. Modified after Mateeva et al. 2017.

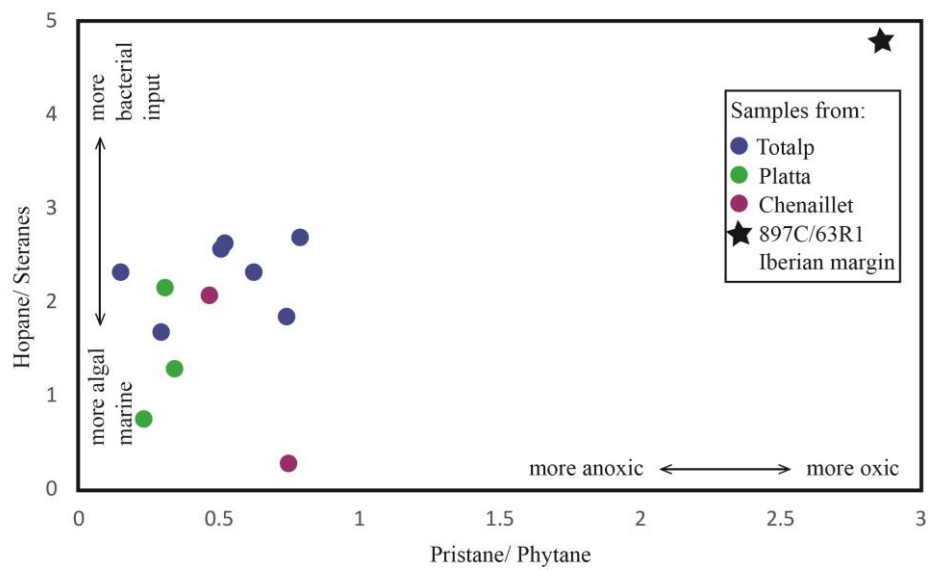


Figure 6.5 Hopane/steranes versus pristane/phytane ratios differentiates between algal and bacterial source input, as well as depositional environment conditions anoxic or oxic (El Diasty and Moldowan 2012).

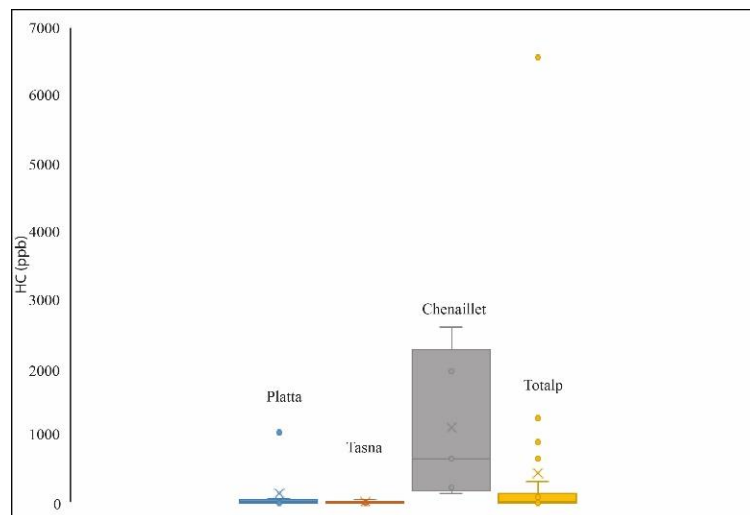


Figure 6.6 Mean, median and standard deviations of HC concentrations in the four studied Alpine areas.

## 6.2. Evidence of methanotrophic biosystem

*“No amount of factual knowledge can guarantee the truth of a scientific law:  
the laws simply do not follow deductively from factual observations”*

*Arthur Schopenhauer, 1788-1860*

The biomarkers, their distributions and the carbon isotopic data for OM, indicate an open marine source with no evidence of *in-situ* production of OM in sub-surface.

In addition, no specific biomarkers (e.g. crocetane) consistent with methane oxidation were found in our fossil or *in-situ* samples (Chapter 2.4.2).

Similar distributions of biomarkers, with the exception of squalane (irregular acyclic isoprenoid), were found at the active hydrothermal vents at Lost City (n-alkanes < C<sub>40</sub>, pristane, phytane, hopanes and steranes) where marine OM dominates (Delacour et al. 2008c). The difficulty in finding methanotrophic biomarkers, is because they are swamped by marine OM. For example, the isotopic composition ( $\delta^{13}\text{C}_{\text{org}}$ ) of OM at Lost City is -28.9‰ to -21.5‰ i.e. typically marine, yet anaerobic methanotroph of type ANME-1 is detected by biomarker such as squalane and analyses of 16S rRNA gene (Brazelton et al. 2006; Delacour et al. 2008b). The stable isotope ratio measurements in this hydrothermal vent are supposed to be difficult to interpret because of the limited DIC and the multiple possible sources of CH<sub>4</sub> (methanogens, serpentinization-associated reactions and anaerobic and aerobic methanotrophy) (Brazelton et al. 2006).

Mixing of microbial with non-microbial (thermogenic or abiotic) methane could occur also with a minimal variation along the carbon isotopic signal of methane  $\delta^{13}\text{C}_{\text{CH}_4}$  (Etiope and Sherwood Lollar 2013). Nevertheless using  $\delta^{13}\text{C}_{\text{CH}_4}$  with carbon isotopic signal of ethane  $\delta^{13}\text{C}_{\text{C}_2\text{H}_6}$  could be used to detect this mixture even if the fraction of biotic gas is less than 10% (Etiope and Sherwood Lollar 2013).

Table 6.1. Table showing the organic carbon data for 6 analysed samples from the Alpine Tethys OCT.

Area	Sample	$10^3 \delta^{13}C_{VPDB}$
Totalp	T1 sedim. ophicalcite	-27.4
	T19 limestone	-26.9
	T64 carbonate	-26.3
	T39 tec-sed. ophicalcite	-27.7
	T9 rew. Tec-sed. Breccia	-26.5
Tasna	S5 Tonschiefer shale	-26.2

The organic carbon isotopic signal of six Alpine samples was  $\delta^{13}C_{org} = -26.8 \pm 0.6\%$  VPDB in the range of OM at Lost City, where there is evidence for methanotrophy (Delacour et al. 2008b). Nevertheless, taken together with the biomarker data, I conclude that the OM in the Alpine samples is overwhelmingly marine (Table 6.1).

### 6.3. An upper bound on methanotrophic biomass associated with serpentinised mantle?

In this section, the organic geochemistry results are examined further to explore the total methanotrophic biosystem that may be hosted by the serpentinisation process. Methanotrophs consume more than 90% of the  $CH_4$  produced in the ocean, making them important for the global carbon cycle and climate change (Reeburgh 2007). Thus, it is important to quantify the methanotrophic biomass and its contribution to the oxidation of methane.

Results from organic geochemical analyses do not show the presence of any specific methanotrophic biomarkers, so it is assumed that these biomarkers are below the analytical detection limit and the latter represents an upper bound of what might exist in nature. We make the assumption that this upper bound of methanotrophic biomass based on field sample analysis is linked to the total methanotrophic biosystem hosted by the serpentinisation process. In the following analysis we also assume that our estimates of the biomass specifically apply to the Alpine Tethys OCT geographic region and a specific geological time corresponding to the time of mantle exhumation in the Jurassic around 160 Ma.

I will detail the quantitative calculation used to estimate the upper bound of methanotrophic biomass and compare these estimates with biomass in the serpentinised host rock and methanotrophic biomass globally.

*The laboratory detection limit of crocetane and the upper bound of methanotroph cells per unit mass of serpentinised mantle rock sample.*

The detection limits of an individual biomarker using the described analytical method is estimated to be  $\kappa = 53$  pg (Fig. 6.7). This is the absolute analytical detection limit and is independent of the sample and standard concentration. It is received by the GC-MS method for estimation of detection limit using external standard and the spectrum of the smallest compound (Fig. 6.7) (Nakashima and Hayashi 2016).

Next, I consider the number of microbial cells required to allow a detectable signal of crocetane. The following calculations are clarification to those presented in the schema in figure 6.7.

Let us assume that the mass of a microbial cell is  $\lambda$ , note that ANME-1, -2 and -3 have not been cultured to date, so data are not currently available (Girguis et al. 2005), and the concentration of crocetane in a dry cell of ANME-1 is  $\beta$  (Eq. 6.1, Fig. 6.7).

The average mass of crocetane per microbial cell  $\chi$  is therefore:

$$\chi = \lambda \cdot \beta \quad (\text{Eq. 6.1})$$

Assuming  $\lambda = 6.25 \times 10^{-10}$  g and  $\beta = 4.5 \mu\text{g}\cdot\text{g}^{-1}$  (Tanner 1948; Blumenberg et al. 2004), the average mass of crocetane per microbial cell would be:

$$\chi = 2.8 \times 10^{-16} \text{ g}$$

The number of cells,  $\sigma$ , required to detect crocetane is therefore:

$$\sigma = \kappa / \chi \quad (\text{Eq. 6.2})$$

Using  $\kappa = 53$  pg and  $\chi = 2.8 \times 10^{-16}$  g this gives the number of required cells for crocetane detection (Fig. 6.7):

$$\sigma = 1.9 \times 10^4 \text{ cells}$$

For the geochemical laboratory analysis, a sample of 100 g of dry rock was taken and used to produce 50  $\mu\text{L}$  of extract dissolved in DCM for analysis. Of this 50  $\mu\text{L}$ , only 1  $\mu\text{L}$  was injected into the GCMS. As a consequence, the detection limit of the sampling and analysis method used relates to 2 g of rock sample. The detection limit of  $1.9 \times 10^4$  cells derived above therefore is for 2 g of rock sample (Fig. 6.7).

Hence the detection limit,  $\mu$ , of the number of methanotroph cells/kg of dry rock sample =  $0.95 \times 10^6$  cells/kg

This is the maximum amount of methanotroph biomass per unit rock sample derived from the detection limit. This result is derived for our fossil Alpine samples and is based on two major assumptions. Firstly, regarding the dry mass of an AOM cell, this is not known due to the difficulty of growing in pure culture e.g. (Girguis et al. 2005). Secondly, the OM and biomarkers are assumed to be 100% preserved which is never the case due to bio- and thermal- degradation.

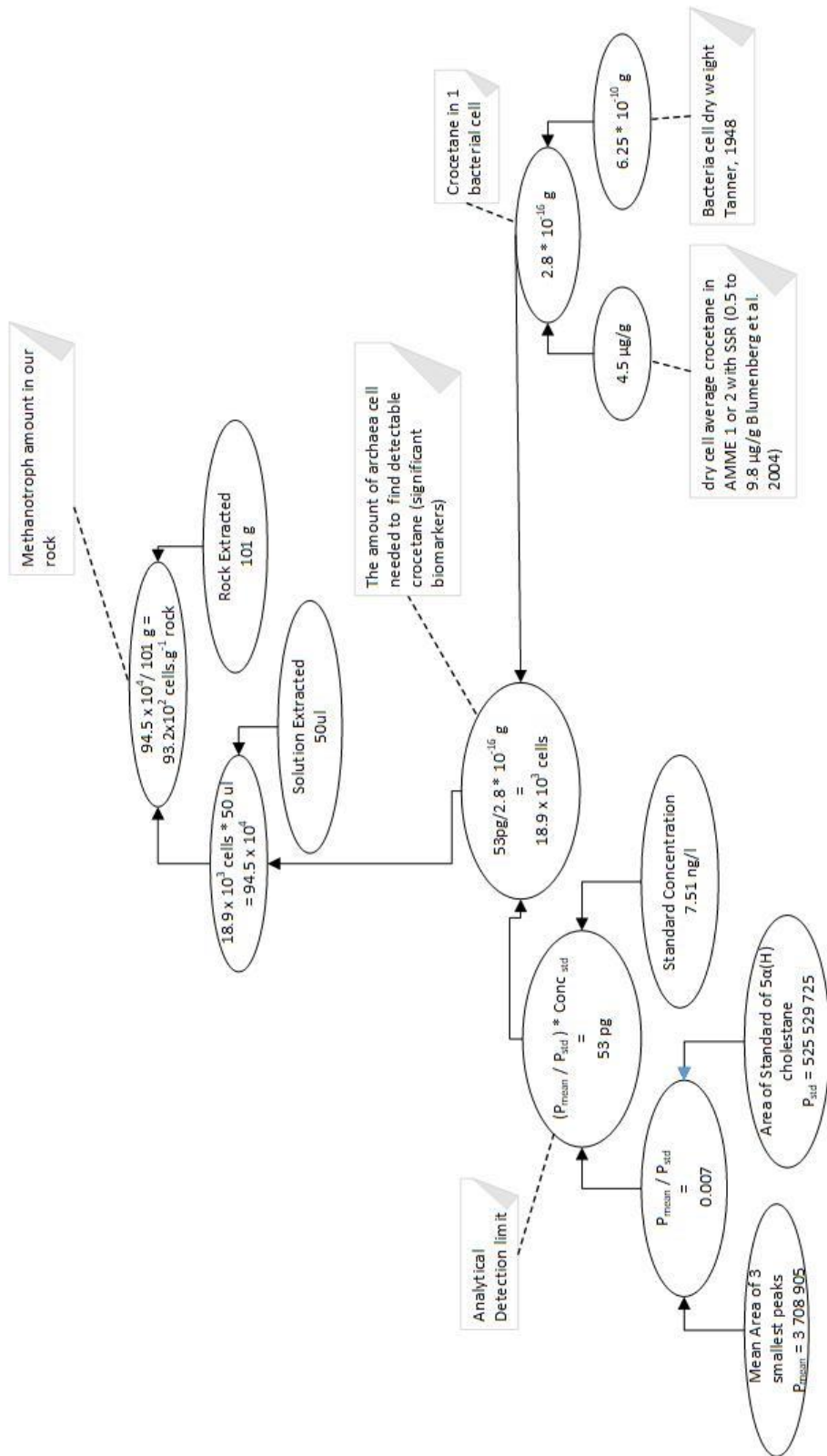


Figure 6.7 Scheme showing the calculation of maximum amount of methanotrophic biomass per unit rock sample.

*The calculation of global quantity of serpentinized mantle host material for methanotrophs*

The host material for anaerobic methanotrophs is assumed to be serpentinised mantle and its overlying sediments where methanotrophs have been found (Reeburgh 2007). For this study, the volume and mass of serpentinised mantle host material under the seafloor is of particular interest. This serpentinised mantle is formed by the exhumation of oceanic mantle which occurs at slow-spreading ocean ridges and magma poor rifted margins. The global fraction of the oceanic domain which consists of exhumed mantle,  $F_{\text{exm}}$ , is not precisely known but is likely to be within the limits of 0.05 and 0.15 (Alt et al. 2013). The global fraction of the Earth's surface,  $O_{\text{earth}}$ , which is oceanic is approximately 0.65.

The surface area,  $A_{\text{em}}$ , of the Earth which consists of exhumed mantle surface is:

$$A_{\text{exm}} = A_{\text{earth}} \times O_{\text{earth}} \times F_{\text{exm}} \quad (\text{Eq. 6.3})$$

Where  $A_{\text{earth}}$  is the total Earth surface area which is  $5.1 \times 10^{14} \text{ m}^2$ .

The volume of serpentinised mantle can be calculated from  $A_{\text{exm}}$  and the distribution of serpentinised mantle with depth. This distribution of serpentinised mantle with depth is complex (Skelton et al. 2005; Cooper 2010), consisting of a high fraction (approximately 100%) down to depths of 1500 to 2000 m beneath the sea-floor then decaying exponentially with depth (with approximately 5% at 5000 m depth beneath the sea-floor). Integration of this serpentinisation distribution with depth gives an equivalent thickness of serpentinised mantle of approximately 3000 m.

The global volume of serpentinised mantle  $V_{\text{sp}}$  may be calculated from:

$$V_{\text{sp}} = A_{\text{exm}} \cdot t_{\text{sp}} \quad (\text{Eq. 6.4})$$

where  $t_{\text{sp}}$  is the equivalent thickness of serpentinised mantle.

The thickness of serpentinised mantle which may contain metamorphic biosystems has been calculated to have lower and upper bounds of 1 and 1000 m (ANME at 1443 mbs in sediments at site 1276 Roussel et al. 2008; bacteria at 750 mbsf in sediments

Wellsbury et al. 2000). This thickness (1 to 1000 m) is much less than the integrated thickness of serpentinised mantle (3000 m).

The mass of serpentinised mantle,  $M_{sp}$ , can be determined assuming its density,  $\rho_{sp}$ . I consider the density of serpentinised mantle to be  $2600 \text{ kg.m}^{-3}$  corresponding to serpentinised mantle with 10% magnetite content (Skelton et al. 2005; Cooper 2010).

$$M_{sp} = V_{sp} \cdot \rho_{sp} \quad (\text{Eq. 6.5})$$

Assuming  $F_{exm} = 0.1$  for the oceanic fraction of exhumed mantle oceanic Earth and  $t_{sp} = 100 \text{ m}$  for the thickness of serpentinised mantle that may be methanotrophic, the mass of serpentinised mantle is calculated to be  $8.6 \times 10^{18} \text{ kg}$ .

#### *Calculation of the global methanotrophic biomass*

Considering the global mass of serpentinised mantle and the estimated maximum mass of methanotrophs per kg of serpentinised mantle,  $\mu$ , based on the laboratory detection limit of crocetane, a global mass of methanotrophs,  $M_{gmt}$ , can be calculated (Eq.6.6).

$$M_{gmt} = (M_{sp} \cdot \mu) \quad (\text{Eq. 6.6})$$

The global mass of methanotrophs,  $M_{gmt}$ , is shown in figure 6.8 as a function of the serpentinised mantle oceanic fraction,  $F_{exm}$ , and the thickness of serpentinised mantle supporting methanotrophs,  $t_{sp}$ . This global mass of methanotrophs assumes that all methanotrophs within the Earth's present oceanic domains has been preserved. In addition, the total mass is highly dependent on the thickness of the layer of serpentinised mantle capable of supporting methanotrophs.

The predicted global mass of methanotrophs, shown in figure 6.8, may be compared with the present day global total bio-mass of  $1.56 \times 10^{15} \text{ kg}$  of C ( $0.56 \times 10^{15} \text{ kg}$  C without bacteria, increasing to  $1 \times 10^{15} \text{ kg}$  C for prokaryotes (bacteria + archaea)) (Whitman et al. 1998; Groombridge and Jenkins 2000). It is important to note that while the total global biomass represents bio-mass alive today, the estimate of the

predicted global mass of methanotrophs represent that created within the present global ocean domain over the last 160 Ma.

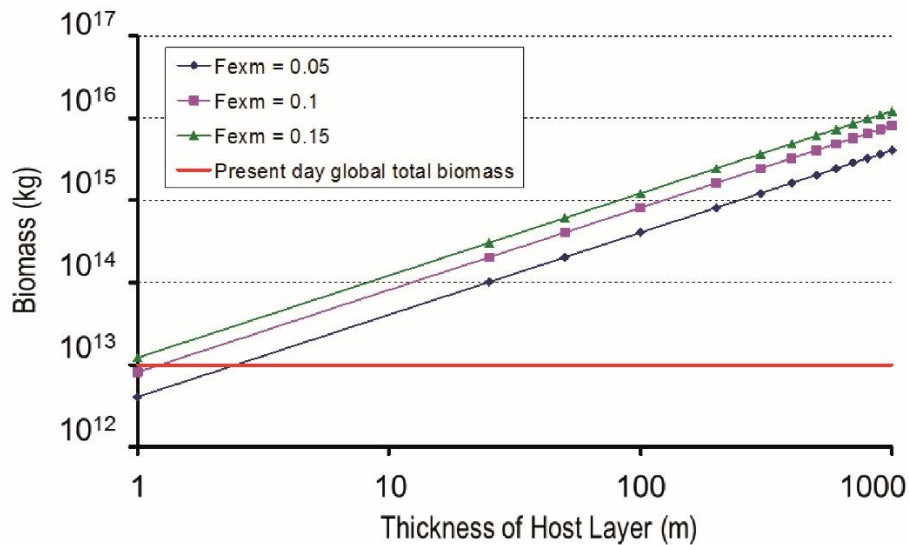


Figure 6.8 Logarithmic plot showing the global mass of methanotrophs (in y) as a function of the thickness of serpentinised mantle that may host methanotrophs (in x). Here taken between 1 and 1000 m. The percentage of exhumed mantle on the ocean floor,  $f$ , is shown for three values 0.05, 0.1 and 0.15%. It is compared with the present day global total bio-mass.

*Comparison of productions rates of estimated upper bound of oceanic global methanotrophic biomass with that of present day oceanic global biomass.*

The upper bound of global methanotrophic biomass calculated from the detection limit of crocetane is for all serpentinised exhumed mantle created between the present day and the age of the oldest existing oceanic crust which is approximately 180 Ma (Müller et al. 1997). In contrast the present-day oceanic biomass is estimated to have a life span of 10 years. This period is the maximum life span of the Antarctic krill, a species with the largest oceanic biomass (Eq.6.8) (Nicol and Endo 1997). It is better to compare biomass production rates than to compare the biomass of our estimated oceanic methanotrophic biomass, over 160 Ma with the present-day oceanic bio mass.

Our estimate of methanotrophic biomass production,  $R_{gmt}$ , is therefore:

$$R_{gmt} = M_{gmt} / 180 \text{ Myr} \quad (\text{Eq. 6.7})$$

The best available estimate of present day oceanic biomass is  $5-10 \times 10^{12}$  kg (Groombridge and Jenkins 2000) .

Assuming 10 years for the oceanic biomass life span gives a present-day oceanic biomass production rate,  $R_{ocbm}$ , (Eq.6.8):

$$R_{ocbm} = 10 \times 10^{12} / 10 \text{ kg/yr} \quad (\text{Eq. 6.8})$$

or

$$R_{ocbm} = 10^{12} \text{ kg/yr}$$

In figure 6.9 the present-day oceanic biomass production rates are compared with our estimate of average production rates for oceanic methanotrophs over the last 180 Myr which depend on the thickness of the serpentinised mantle layer that could support methanotrophs, and the fraction of oceanic crust that is exhumed serpentinised mantle.

While figure 6.8 shows that the methanotrophic may dominate the oceanic biomass though the deep biosphere biomass, their productions rates are orders of magnitude less than that of the present-day oceanic biomass. Our estimates of the oceanic methanotrophic biomass are an upper bound based on the detection limit of crocetane. It is still challenging to estimate the biomass of methanotrophs and whether they should be included in this total oceanic biomass estimation (Jørgensen 2012).

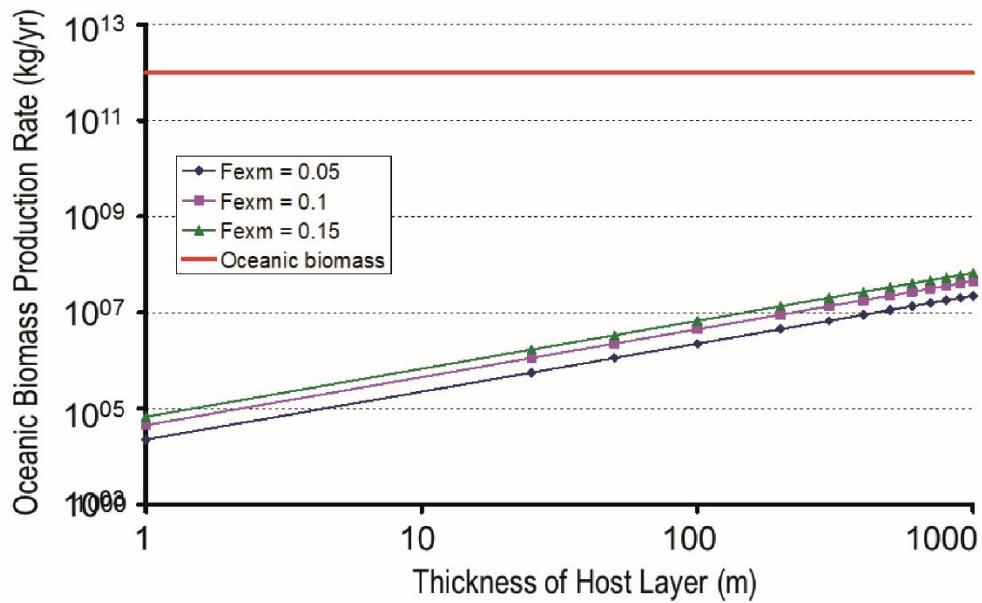


Figure 6.9 Logarithmic plot comparing the annual rate of mass per year of the calculated methanotrophs with the oceanic biomass.

*Second thought experiment to estimate the CH<sub>4</sub> production rates from the serpentinisation process*

Present day production of dissolved H<sub>2</sub> has been observed during the early stages of serpentinisation at depths shallower than 2 km in the MARK area (Kane Fracture Zone, Mid Atlantic Ridge) (Andreani et al. 2013). H<sub>2</sub> production depends on Fe(III) availability, which depends on the degree of serpentinisation. Experiments show that most H<sub>2</sub> is produced between 250-450 °C, or from 10-70% serpentinisation and that the Fe(III) is mostly in serpentinite (Marcaillou 2012; Andreani et al. 2013). For example, the dissolved H<sub>2</sub> released during serpentinisation at the MARK maximises at around 140 mM at a degree of serpentinisation of 10-18% and decreases to <10mM when this is >60% (Andreani et al. 2013). Where the degree of serpentinisation is > 80%, as well as low temperature (50-150 °C), Fe(III) is dominantly in magnetite (Marcaillou 2012; Andreani et al. 2013). Even if the degree of serpentinisation could be mathematically related to the amount of dissolved H<sub>2</sub>, there is a lack of observations of H<sub>2</sub> release away from hydrothermal vents.

Next, I will assume that only serpentinisation is producing dissolved H<sub>2</sub>. Depending on the inclusion of the Fe (III) in the Fe-minerals, different amounts of H<sub>2</sub> would be produced. Analytical methods consisting of  $\mu$ -Xanes analyses and measured on two different length-scales on serpentine minerals from ODP Leg 153, MARK, MAR show that for the formation of 1kg of serpentine 0.26 mol of H<sub>2</sub> is produced for total Fe(III) in magnetite and 0.325-0.335 mol of H<sub>2</sub> for 15-27% Fe(III) incorporation in serpentine, (Andreani et al. 2013). The latest incorporation of Fe(III) is observed under natural condition during early stage of serpentinization from 2 to 4 km in the MARK area (Andreani et al. 2013). Serpentinisation experiments in pure water at T = 300 °C and P = 300 Bar over 70 days using non-altered spinel-lherzolite and measured with X-ray Absorption Near Edge Structure spectroscopy shows an average rate of production of H<sub>2</sub> of 1.464 mol kg<sup>-1</sup> y<sup>-1</sup>, where the theoretical average rate H<sub>2</sub> is calculated to be 1.917 mol kg<sup>-1</sup> y<sup>-1</sup> (Marcaillou et al. 2011). If all the H<sub>2</sub> reacts with CO to form methane (FTT reaction) or with CO<sub>2</sub> (Sabatier reaction) there would be a ratio of 3:1 or 4:1 of H<sub>2</sub> to CH<sub>4</sub>. Hence, the amount of H<sub>2</sub> measured by Marcaillou et al. (2011), divided by an average of 3.5 will give 0.42 mol CH<sub>4</sub> kg rock<sup>-1</sup>y<sup>-1</sup>. The lack of better understanding of the CO availability and the boundary of CO<sub>2</sub> methanation in different geological oceanic settings make this an upper bound of abiotic methane generation. FTT or Sabatier reaction show condition above 200 °C and P>1 atm (McCollom and Seewald 2013; Etiope and Ionescu 2014). Considering the previous calculation of the total mass of serpentinite and a thickness of 2 km, a total mass of serpentinite of 1.89 x 10<sup>20</sup> kg was calculated (Eq. 6.2, 6.3). Taking in account that the oldest oceanic crust is 180 Ma, the serpentinisation rate per year, S<sub>rate</sub> can be calculated to 1.05 x 10<sup>12</sup> kg y<sup>-1</sup> (Müller et al. 1997).

$$M_{sp} / 180 \text{ Ma} = S_{rate} \quad (\text{Eq. 6.9})$$

Using the value for methane production of 0.42 mol CH<sub>4</sub> kg rock<sup>-1</sup>y<sup>-1</sup> gives a total of 4.41 x10<sup>11</sup> mol y<sup>-1</sup> of CH<sub>4</sub> for the total hosted serpentinised peridotite, S<sub>CH4</sub>.

$$S_{CH4} = CH_4 \text{ rate} \cdot S_{rate} \quad (\text{Eq. 6.10})$$

This result compares to the present day natural sources of CH<sub>4</sub> (wetlands, termites and ocean) of 9.97 x10<sup>12</sup> mol y<sup>-1</sup> (160 Mt CH<sub>4</sub> y<sup>-1</sup>) (Etiope and Klusman 2002), or the

present annual rate of CH<sub>4</sub> production by methanogens 18.7 x10<sup>14</sup> mol CH<sub>4</sub> y<sup>-1</sup> (300 Tg CH<sub>4</sub> y<sup>-1</sup>) (Reeburgh 2007). Another comparison could be done with a CH<sub>4</sub> flux 5 x 10<sup>9</sup> mol y<sup>-1</sup> estimated for the Mid-Atlantic ridge, which originates from the Mid-Ocean ridges and serpentinisation (Reeburgh 2007). These comparisons could show the great efficacy of the methanotrophs but more likely that the experimental estimation of CH<sub>4</sub> produced by serpentinisation is unrealistic.

### *Problems*

The annual production of abiotic CH<sub>4</sub> based on an average serpentinisation rate is clearly high. Going further with our assumptions methanotrophs amount could be found based on its efficacy. This upper limit of abiotic produced methane by serpentinisation could be consumed by the methanotrophs with the same efficiency as any other source of methane (e.g. methanogens), estimated to be around 90% (Reeburgh 2007).

The AOM consortia ANME and SRB coexist in the sulphate-methane transition zone (SMTZ) above the methanogenic zone, from the sediment surface to around 40 cm depth, and are absent between 2 and 4 km depth in metamorphic rocks (Reeburgh 2007). Even the distance between the zone producing abiotic CH<sub>4</sub> and SMTZ is problematic.

In addition, despite observations of serpentinisation fuelling methanotrophic bio-systems at hydrothermal vents, these systems are difficult to detect even in active hydrothermal vents.

Serpentinisation is a known process that produces dissolved H<sub>2</sub> and CH<sub>4</sub> (via FTT) in ultramafic-hosted hydrothermal systems however, only in the Lost city and Logatchev 2 hydrothermal vents is there a possible link between this process, FTT and methanotrophic biosystem. Rainbow is an ultramafic and serpentinisation-derived vent that contains organic compounds (CH<sub>4</sub> and others) from a mixed origin including FTT, but does not contain any ANMEs. The von Damm Vent Field contains ANMEs but the CH<sub>4</sub> is delivered from hydrothermal CH<sub>4</sub>-rich fluid formed by the plutonic rock's

magmatic volatile fluid over millions of years (McDermott et al. 2015). In Loki's Castle black smoker, the ANMEs utilise CH<sub>4</sub> of thermogenic composition (Baumberger et al. 2016). Other hydrothermal vents where exothermic serpentinisation reactions do not play any role still contain ANME such as Guyamas Basin, Shrimp Hole, Piccard (Reveillaud et al. 2016). Thus, it would be difficult to estimate the ANMEs quantifying only the serpentinite Earth's mass.

An estimation of the upper bound on methanotrophs for fossil Alpine systems was found, however these estimates need to be viewed critically given the assumptions of the calculations and the lack of actual evidence. Even if ANMEs play a significant role in the global carbon cycle and climate change, their consumption of CH<sub>4</sub> is not well quantified and factors controlling them are still unknown even with time, CH<sub>4</sub> and interspecies interaction (SRB). There is still more to be understood about serpentinisation its extent, how far off-axis the process is active and its relationship with bio-systems in different environments.

#### **6.4. Recommendation**

*"Harry, there is never a perfect answer in this messy, emotional world.*

*Perfection is beyond the reach of humankind,*

*beyond the reach of magic." Dumbledore, J.K. Rowling*

Although no evidence for a methanotrophic bio-system was found in the Alpine Tethys OCT samples of exhumed serpentinised mantle and overlying lithologies, the identifiable biomarkers and isotopic data are consistent with a marine origin for OM which persisted 160 My after their formation at a rifted margin, despite having experienced Alpine obduction. The OM in all sampled lithologies including the exhumed mantle rocks is consistent with marine origin from planktonic algae and bacteria deposited in a reducing environment, with the OM migrating into the serpentinite most likely from the overlying seawater or sediment cover. I do not believe that drilling to recover samples deeper than the ones from the surface

outcrops would provide evidence of methanotrophs because of issues of contamination and detection limits (see Chapter 5).

For samples from ODP cores, two possible suggestions could be made. The only sediment sample taken from the IODP Bremen repository showed a marine OM source including Thaumarchaeota, bacteria and terrigenous detritus which reached a low maturation under dysoxic depositional conditions. The HCs from the in-situ samples from the Iberian and Newfoundland margins were consistent with probable contamination from core drilling. This issue could be resolved by using core material specifically collected for microbiology or by analysing the specific drilling mud used for the core drilling and extract its OM signature from the samples. In the first case, the IODP Bremen Core repository propose a deep-frozen (-80 °C) subseafloor core store for geomicrobiological analysis. The proportion of microbiological sample material available compared to the deep-sea floor is negligible. Less than 50 samples by expedition (to date expeditions 307, 336 and 357) have related to a main aim of microbiology. These samples could possibly provide evidence of methanotrophy and could give stronger biomarker signatures at concentrations required for analysing the carbon isotopic signatures of the different compounds. The OM signature being derived from an open marine microbial community could be influenced by the distance from the sea floor and sediment type (i.e. lithology), which could lead to the understanding that we are capable to date to analyse well the OM in core drilled sediments due to its higher content.

Lipid analyses do not allow the description of the entire microbial diversity, however due to the amount and variety of biomarkers in the studied lipids analyses might provide the best way forward for this type of research (Rossel et al. 2008).

## **6.5. Remaining questions**

*"Towards the door we never opened" T.S.Eliot, Four Quartets*

*"Science may set limits to knowledge, but should not set limits to imagination."*

*Bertrand Russel, 1872-1970.*

The primary aim of this research was to establish whether methanotrophic biosystems are localised and only flourish in the conditions generated by hydrothermal vents or are pervasive with the region of serpentinisation on the seafloor. While methanotrophy in hydrothermal vents have been investigated previously, research had not been carried out in the OCT areas of magma poor margins. The most efficient way to do that would be to collect samples from a modern hydrothermal vent and samples from equal distance by moving away from the vents. This will provide a profile containing different lithology including serpentinised mantle and could determine if the organic matter is localised on the hydrothermal system or pervasive within the serpentinite basement.

IODP expedition 357 was developed at the end of 2015 and had a primary goal to study the relationship between serpentinisation and microbial activity (Früh-Green et al. 2016). One of the goals was to observe if the serpentinisation process supported microbial activity only in hydrothermal vents by drilling in the Atlantis massif (i.e. Lost city) and in a transect across the southern wall of the massif. To date, there are no publications supporting a closed link between serpentinisation and microbial activity including methanotrophic bio-systems.

Methanotrophy could be related to serpentinisation only under specific conditions, for example in hydrothermal vents. Perhaps these results are not very optimistic in regard to the serpentinisation and methane production on other planets. Study about the abiotic methane origin on Mars shows that other reactions rather than the serpentinisation process are a more probable cause consistent with the episodically produced methane (Webster et al. 2015). Such reactions are driven by ultraviolet (UV) light striking carbon-containing meteoroids and cosmic dust (Webster et al. 2015).

This research raises more questions than its primary aim:

Why do we see the same OM in the fossil samples from the Alpine Tethys OCT and in-situ samples from the Iberian and Newfoundland margin?

Is the OM homogenously distributed throughout the sample – e.g. breccia OM more in the carbonate matrix, carbonate veins or clasts?

If marine OM prevails on the seafloor surface, is it possible to find a better biological signal of a methanotroph biosystem deeper in the mantle (e.g. serpentinised mantle not in contact with overlying lithology and at a greater distance and up to a depth of 7 km)?

Could biomarkers be used more successfully in a fossil environment characterised by little or inexistent metamorphism to narrow temperature history and depositional environment?

Provided the quantity of sample needed for analyses, even bigger samples would be needed to separate different parts (e.g. clasts, veins). Carbonate staining and acetate peel method constraint this answer for the carbonate (appendix B).

During this project it became apparent that no biomarker or lipid open library exists as it does for fatty acids. Furthermore, such a library does not exist for the variety of contaminants that exist in laboratory environment or elsewhere. Therefore, I recommend that an open library for biomarkers, lipids and contaminants be compiled in a similar manner as that in place for fatty acids.

## **6.6. Contribution**

*“It's been a long road  
Gettin' from there to here  
It's been a long time  
But my time is finally here”*

*Diane Warren, 1998 Faith of the heart*

This project was undertaken to establish whether methanotrophic biosystems are localised and only flourish in the conditions generated by hydrothermal vents or are pervasive within the region of exhumed mantle and active serpentinisation.

This work establishes that there is OM in fossil serpentinised mantle and overlying lithologies of the Alpine Tethys which is not due to the serpentinisation process. Indeed, the OM found in both fossil and in-situ samples of serpentinised mantle show marine OM from algae and bacteria rather than a methanotrophic biosystem. The same type of OM is found in the overlying lithology supporting again the fact that this OM did not originate from the serpentinisation process. Along with several reasons why evidence of a methanotrophic biosystem was not found, the most obvious reason would be that the serpentinisation process is simply not enough to produce and support this kind of system away from hydrothermal vents.

Even if serpentinisation was central to prove the emergence of life from abiotic processes, the only conclusive evidence is found in alkaline hydrothermal vents (Russell et al. 1989; Shock 1992; Kelley et al. 2001; Holm et al. 2006; Proskurowski et al. 2006). The serpentinisation leading to FTT, is a mechanism that reduces CO<sub>2</sub> by producing H<sub>2</sub>. However, H<sub>2</sub> could also be produced by magma diageneses and from friction with other rocks. Furthermore, FTT compete with the biotic mechanisms of anaerobic methanogen to produce methane. With this in mind, we cannot assume that serpentinisation is the only process that could produce life regardless of the surrounding environmental conditions.

This is the first time that organic geochemistry methods have been used to identify biological biosystems in the fossil Tethys ocean. The findings of this investigation were similar to those of earlier geological studies.

The methane produced (CH<sub>4</sub>) from the serpentinisation process is expected to represent an important carbon source. However, the large amount of dissolved organic carbon observed appeared to be the major pool of carbon in the studied fossil Tethyan environment.

My results indicate that anaerobic methanotrophs are constrained within the hydrothermal environment. Their contribution in the shallow fossil subsurface would be negligible if existent and the OM would be dominant by DOC and/or biodegradation. Their presence in deep biosphere sediments and magmatic or

metamorphic rock in passive margin could not be confirmed due to drilling fluid contamination. In conclusion the methanotrophic contribution to energy flow and carbon assimilation remains very limited.

On a geological point of view this research was pioneering in explaining the geological history of an exhumed then obducted fossil seafloor using biomarkers.



# A. Appendix A Organic geochemistry

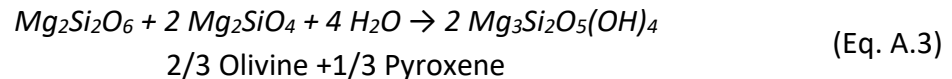
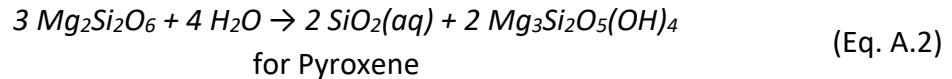
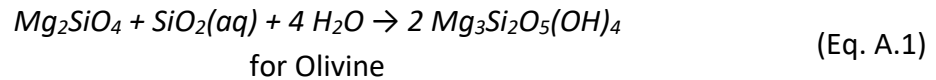
Appendix A relates to organic geochemistry and contains: explanation of what organic compound is, a table with the molecular ions used for the GC-MS, 2D structure presentation of the biomarkers, GC-MS profiles and a list of contaminants found in our samples; serpentinisation formulae, methods path and drilling mud analysis. The 2d structure molecular presentation is taken from the Open Chemistry database of the National Center for Biotechnology Information, software Thermo XCalibur 3.1. library and the Biomarker guide (Peters et al. 2005b; Kim et al. 2015)s



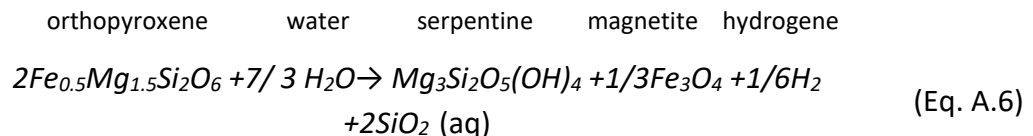
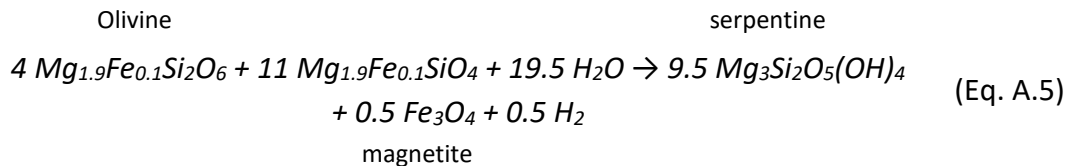
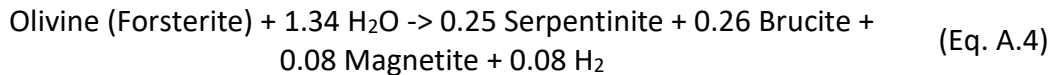
## A.1. Serpentinisation chemistry

In this section I will present several formulae describing different paths of the mineralogical and chemical alteration during serpentinisation. Some of this path are observed only in laboratory experiments.

For the magnesium-rich Olivine (Forsterite) and Pyroxene:

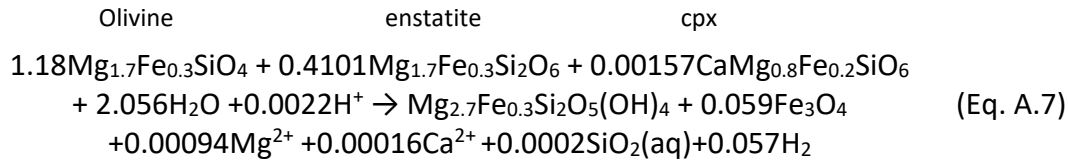


No H<sub>2</sub> production during these processes due to no oxidation of iron. When the ultramafic minerals olivine and pyroxene contain iron Fe, a hydrogen H<sub>2</sub> creation is possible:

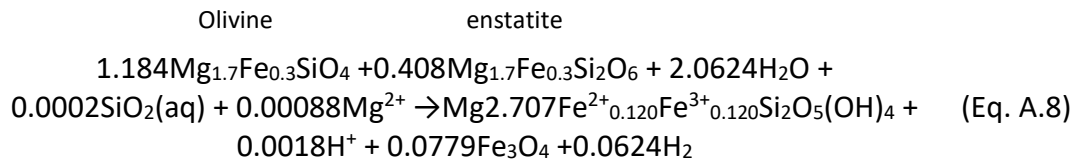


During experimentation, the chemistry in the reaction could be followed for each step of the serpentinisation (Marcaillou et al. 2011):

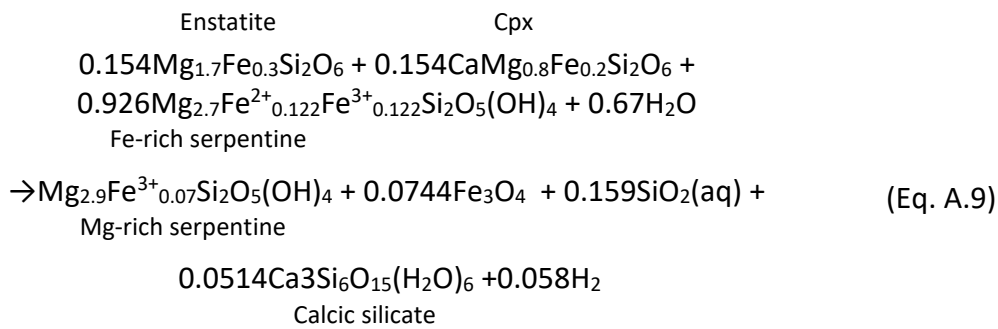
Early serpentinisation stage:



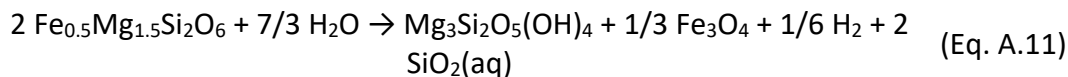
Intermediate serpentinisation stage:



Final serpentinisation stage:



Generalised formula for olivine and orthopyroxene assumed for the H<sub>2</sub> production:

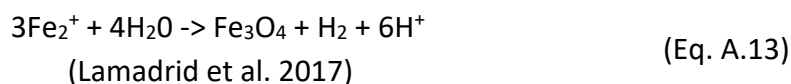


(Marcaillou et al. 2011)

Two-stage serpentinisation are observable from Mg-rich olivine to serpentinite and Fe-brucite (Bach et al. 2006; McCollom and Bach 2009):

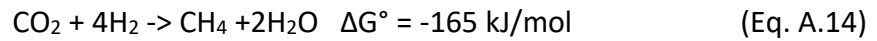


The oxidation of iron during serpentinisation also produced magnetite:

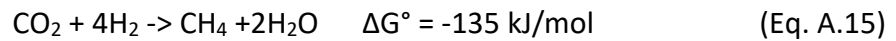


The formulae below show that there is no unique path for methane at the seafloor (table 2.3).

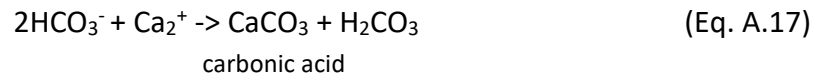
The inorganic anaerobic Fisher-Tropsch (FT) – Sebatier type reaction:



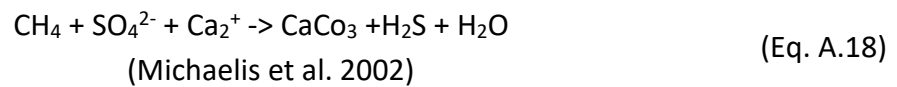
Same as the hydrogenotrophic methanogenesis reaction:



CO<sub>2</sub> could also react with water:



AOM – SRB consortia that produce methane derived bicarbonate:



## A.2. Ions used for single ion monitoring SIM in GC-MS analyses

Table 6.2 Table showing the ions used for single ion monitoring (SIM) during GC-MS analyses.

m/z (molecular ion)	Compound name
57	<i>n</i> -alkane/isoprenoids
85	<i>n</i> -alkane/isoprenoids
123	Secohopanes/sesquiterpanes
127	<i>n</i> -alkane/isoprenoids
177	norhopanes/1 methyl hopane
183	isoprenoids
191	hopanes/terpanes/tricyclics
205	methylhopanes
217	steranes/diasteranes
218	$\alpha\beta\beta$ steranes
231	methyl steranes
370	C27 hopane
372	colostane = C27 steranes and diasteranes
386	C28
398	C29 hopanes
400	C29 steranes and diasteranes
412	C30 pentacyclics
414	C30 steranes and diasteranes
426	C31 hopanes
440	C33 hopanes

### A.3. Hydrocarbons found in our samples

Hydrocarbons found in the samples consist of *n*-alkanes, PAHs, steranes, hopanes and the isoprenoids pristane and phytane.

For each compound the molecular and skeletal formula (chemical structure) is given using as reference the Open chemistry database of (<https://pubchem.ncbi.nlm.nih.gov/>) and the Biomarker guide (Peters and Moldowan 1993)

#### *n*-alkanes

The *n*-Alkanes are very common hydrocarbons and have a linear single arrangement of the carbon atoms. They are linear chain hydrocarbon and have general chemical formula  $C_nH_{2n+2}$ .

pentadecane  $C_{15}H_{32}$



Hexadecane  $C_{16}H_{34}$



By adding one carbon atom one line is add to the linair straight-chain and the name are as follow:

$C_1$  Hen-

$C_4$  Te-

$C_7$  Hepta-

C<sub>2</sub> Do-

C<sub>5</sub> Pen-

C<sub>8</sub> Octa-

C<sub>3</sub> tri-

C<sub>6</sub> Hexa-

C<sub>9</sub> Nona-

H<sub>10-19</sub> -decane

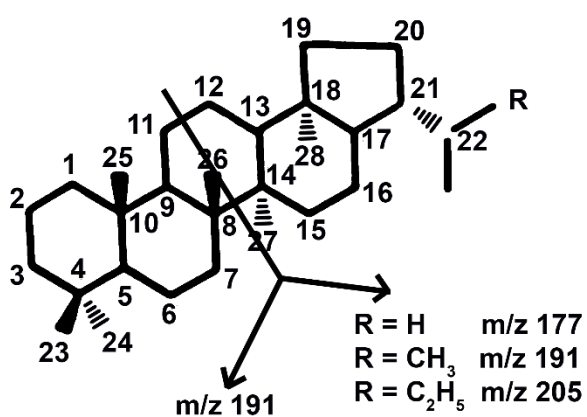
H<sub>20-29</sub> -cosane

H<sub>30-39</sub> -triacontane

H<sub>40-49</sub> -tetracontane

## Hopane

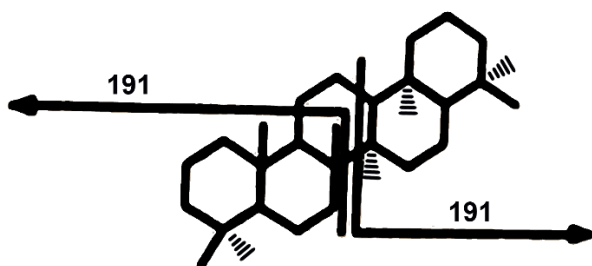
Hopanes contain four cyclohexane rings and one cyclopentane ring. They have stereochemistry around C-17 and C-22 of  $\alpha$  or  $\beta$  and around C-22 of R or S (22S or 22R homolog) (Peters and Moldowan 1993). Hopanes of  $\beta\alpha$  series are known as moretanes and with more than  $>C_{30}$  are called homohopanes (homo- methylene group in addition) (Peters and Moldowan 1993).



C<sub>30</sub>-17 $\alpha$ , 21 $\beta$ (H)-Hopane

29 $\alpha\beta$  17 $\alpha$ (H), 21 $\beta$ (H)-Norhopane

30 $\alpha\beta$  17 $\alpha$ (H), 21 $\beta$ (H)-Hopane



Gammacerane C<sub>30</sub>H<sub>52</sub>

31 $\alpha$  $\beta$  S 17 $\alpha$ (H), 21 $\beta$ (H)-22S-Homohopane

31 $\alpha$  $\beta$  R 17 $\alpha$ (H), 21 $\beta$ (H)-22R-Homohopane

30 $\beta\beta$  17  $\beta$ (H), 21 $\beta$ (H)-hopane

32 $\alpha\beta$  S 17 $\alpha$ (H), 21 $\beta$ (H)- 22S- Homohopane

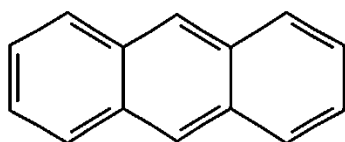
32 $\alpha\beta$  R 17 $\alpha$ (H), 21 $\beta$ (H)- 22R- Homohopane

34 $\alpha\beta$  R 17 $\alpha$ (H), 21 $\beta$ (H)-22R- Homohopane

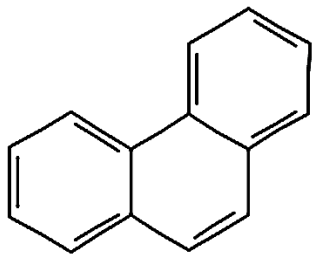
34 $\alpha\beta$  S 17 $\alpha$ (H), 21 $\beta$ (H)-22R- Homohopane

### PAH Polynuclear Aromatic Hydrocarbons

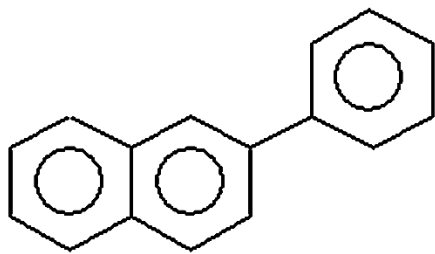
The PAHs are composed of one or more aromatic rings.



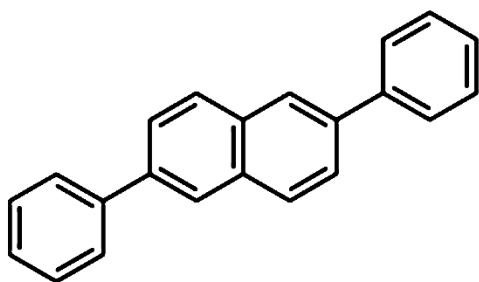
A Anthracene  $C_{14}H_{10}$



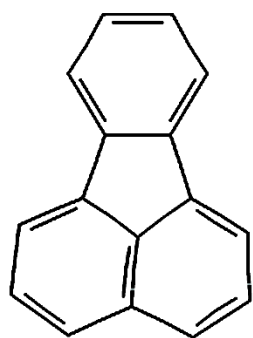
P Phenanthrene  $C_{14}H_{10}$



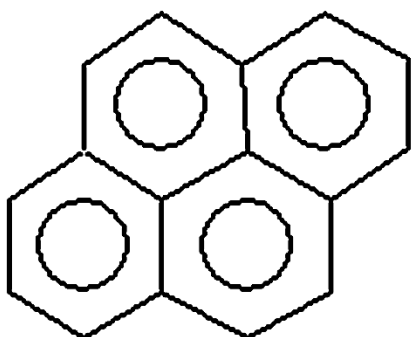
2N 2-phenyl Naphthalene



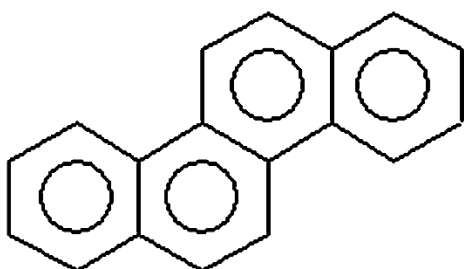
2,6- diphenylnaphthalene  $C_{22}H_{16}$



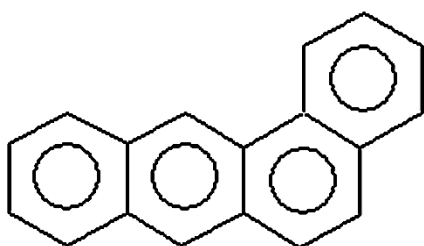
Fluo Fluoranthene  $C_{16}H_{10}$



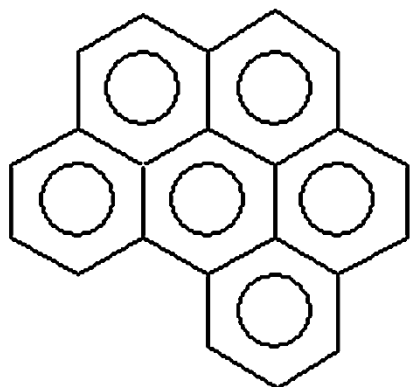
Pyr Pyrene  $C_{16}H_{10}$



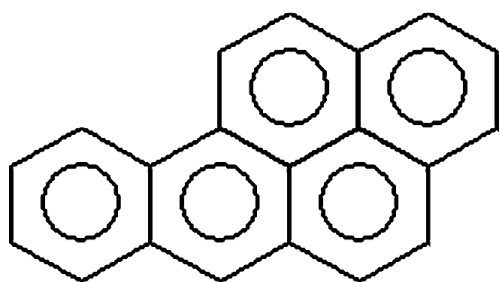
Chry Chrysene  $C_{18}H_{12}$



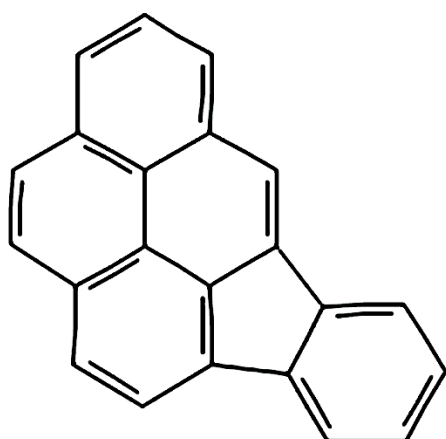
BaA Benzo(a)anthracene  $C_{18}H_{12}$



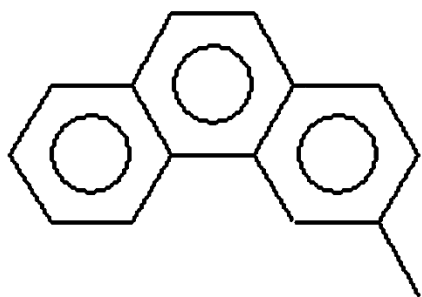
BghiP Benzo (ghi) perylene  $C_{22}H_{12}$



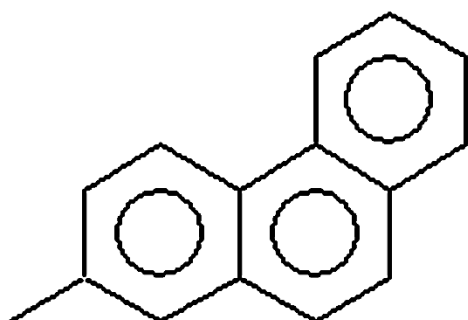
Benz Benzo(a)pyrene  $C_{20}H_{12}$



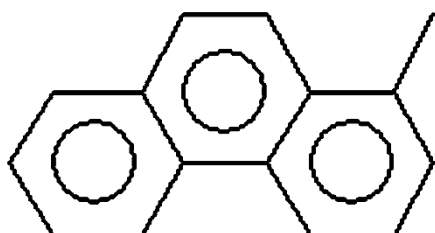
IndPy Indeno(1,2,3-cd)pyrene  $C_{22}H_{12}$



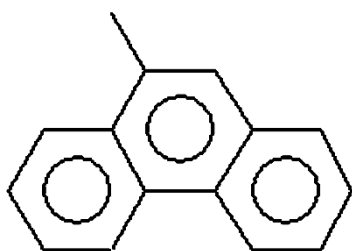
3 MPs 3-methylphenanthrene  $C_{15}H_{12}$



2 MPs 2-methylphenanthrene  $C_{15}H_{12}$



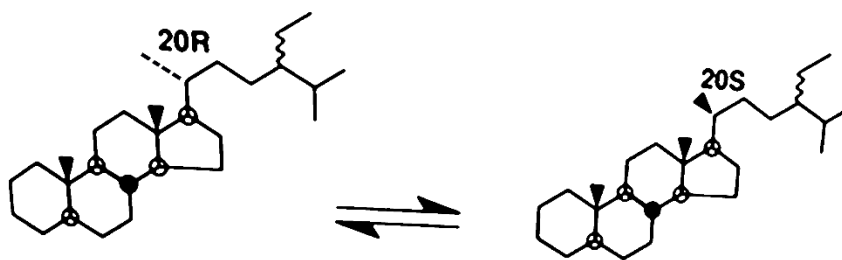
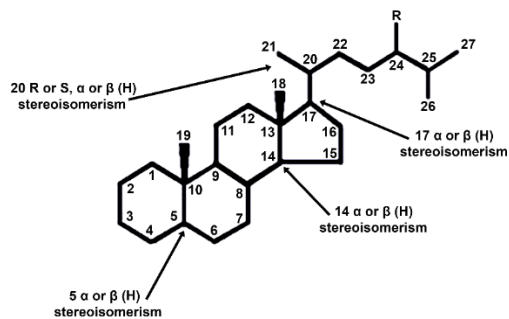
1 MPs 1-methylphenanthrene  $C_{15}H_{12}$

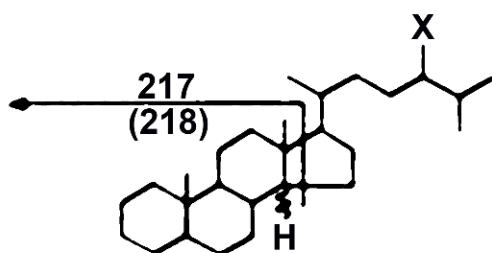


9 MPs 9-methylphenanthrene  $C_{15}H_{12}$

## Steranes

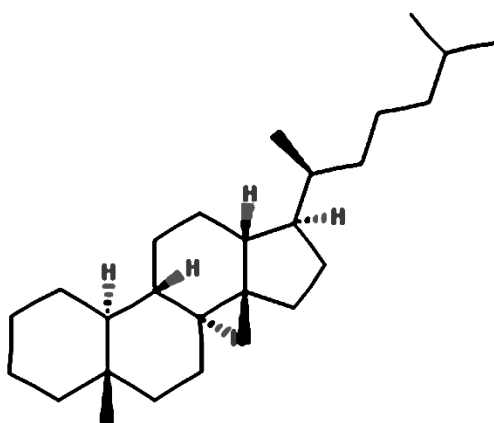
Steranes derive from sterols found in eukaryotic organisms (Peters and Moldowan 1993). The sterol precursor contains a hydroxyl group ( $\text{HO}^-$ ) which is not present in the steranes. The molecular structures of steranes are complex as they have different stable stereoisomers, but not all stereoisomers are found in living organisms (Peters and Moldowan 1993). The configuration  $20R \alpha\alpha$  from sterols will evolve, as stereoisomers  $\alpha\alpha R$ ,  $\alpha\alpha S$ ,  $\alpha\beta R$  and  $\alpha\beta S$  in ratio 1:1:1:3 (Peters and Moldowan 1993). All sterols in living organism are in the  $20R$  configuration and in the sediments and petroleum are of mixture of  $24R$  and  $24S$  ( $\text{C}_{28}$ ) (Peters and Moldowan 1993).





**m/z 217 14 $\alpha$ (H) – Steranes**

**m/z 218 14 $\beta$ (H) – Steranes**



13 $\beta$  (H),17 $\alpha$  (H), 20S-diacholestane

C27 $\beta\alpha$ 20S 20S 13 $\beta$  (H),17 $\alpha$  (H)-diacholestane

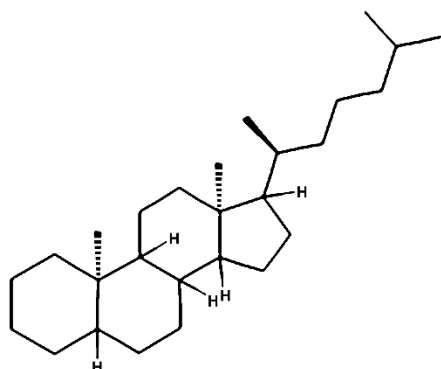
C27 $\beta\alpha$ 20R 20R 13 $\beta$  (H),17 $\alpha$  (H)-diacholestane

C27 $\alpha\beta$ 20S 20S 13 $\beta$ (H),17 $\alpha$  (H)-diacholestane

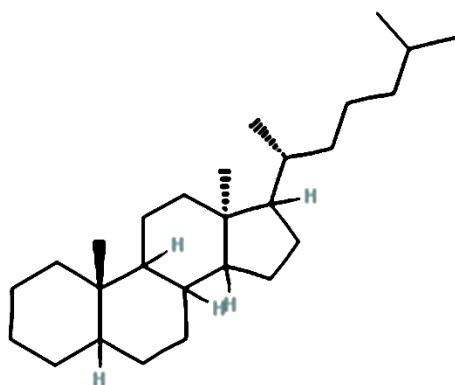
C27 $\alpha\beta$ 20R 20S 13 $\beta$ (H),17 $\alpha$  (H)-diacholestane

C28 $\beta\alpha$ 20S 20S 24-methyl-13 $\beta$ (H),17 $\alpha$ (H)- diacholestane

C<sub>28</sub>β<sub>α</sub>20R 20R 24-methyl-13β(H),17α(H)- diacholestane

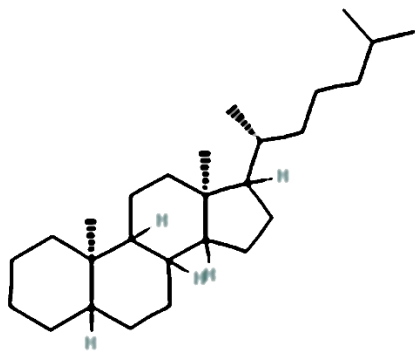


C<sub>27</sub>αα<sub>α</sub>20S 20S 5α(H), 14α(H), 17α(H)-cholestane (C<sub>27</sub>H<sub>48</sub>)

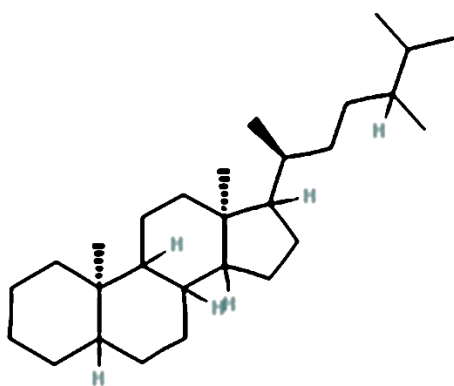


C<sub>27</sub> αββ20R 20R 5α (H), 14α (H), 17α (H)-cholestane

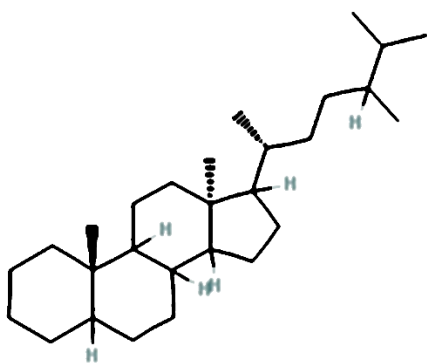
C<sub>27</sub> αββ20S 20S 5α (H), 14α(H), 17α (H)-cholestane



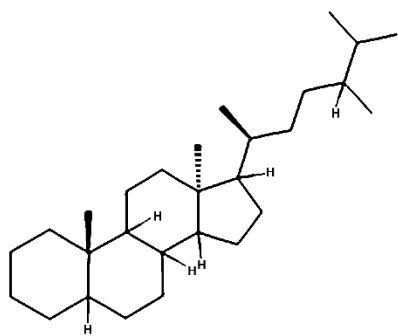
C27 $\alpha\alpha\alpha$ 20R 20R 5 $\alpha$ (H), 14 $\alpha$ (H), 17 $\alpha$ (H)-cholestane



C28 $\alpha\alpha\alpha$ 20S 20S 24-methyl-5 $\alpha$ (H), 14 $\alpha$ (H), 17 $\alpha$ (H)-cholestane (C<sub>28</sub>H<sub>50</sub>)

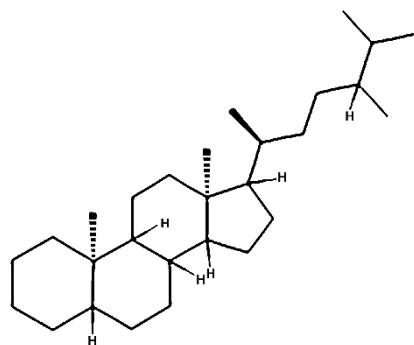


C28 $\alpha\beta\beta$ 20R 20R 24-methyl-5 $\alpha$ (H), 14 $\alpha$ (H), 17 $\alpha$ (H)-cholestane

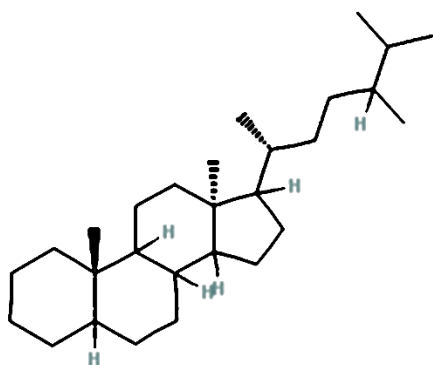


C28 $\alpha\beta\beta$ 20S 20S 24-methyl-5 $\alpha$ (H), 14 $\alpha$ (H), 17 $\alpha$ (H)- cholestane

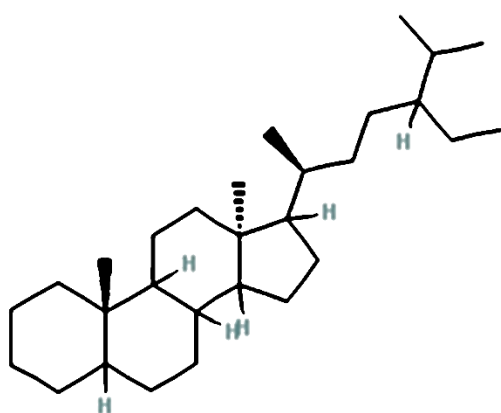
C28 $\alpha\alpha\alpha$ 20R 20R 24-methyl-5 $\alpha$ (H), 14 $\alpha$ (H), 17 $\alpha$ (H)- cholestane



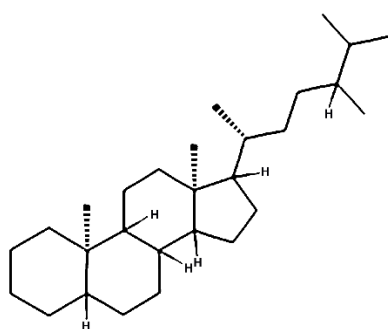
C29 $\alpha\alpha\alpha$ 20S 20S 24-ethyl-5 $\alpha$ (H), 14 $\alpha$ (H), 17 $\alpha$ (H)- cholestane



C29 $\alpha\beta\beta$ 20R 20R 24-ethyl-5 $\alpha$ (H), 14 $\alpha$ (H), 17 $\alpha$ (H)- cholestane



C29 $\alpha\beta\beta$ 20S 20S 24-ethyl-5 $\alpha$ (H), 14 $\alpha$ (H), 17 $\alpha$ (H)- cholestane

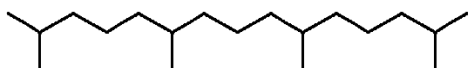


C29 $\alpha\alpha\alpha$ 20R 20R 24-ethyl-5 $\alpha$ (H), 14 $\alpha$ (H), 17 $\alpha$ (H)- cholestane

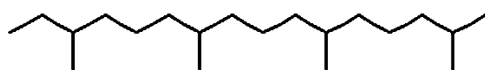
## Isoprenoids

Isoprenoids are also hydrocarbons and very important biomarkers. They consist of five carbon atoms each of them connected with 2 bonds to the previous carbon atom and with a single bond to the others two. In our sample the isoprenoids are pristane  $C_{19}H_{40}$  and phytane  $C_{20}H_{42}$  and the biomarker for methanotrophic is crocetane  $C_{20}H_{42}$ .

Pristane  $C_{19}H_{40}$  linear isoprenoid



Phytane  $C_{20}H_{42}$  linear isoprenoid contain one methylene group ( $-CH_2$ ) more than pristane

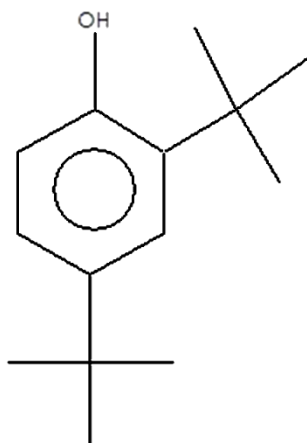


### A.4. Other contaminants

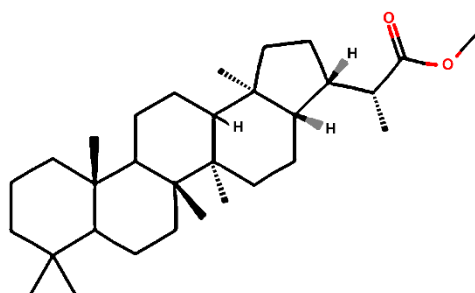
#### A.4.1. 2,4-Di-tert-butylphenol

$RT \approx 19$

2,4-Di-tert-butylphenol  
Formula C<sub>14</sub>H<sub>22</sub>O, MW 206, CAS# 96-76-4, Entry# 177130  
Phenol, 2,4-bis(1,1-dimethylethyl)-



At the beginning of this study the blank used for the samples from the Alps was a pure quartz powder (grains between nm) heated at 200 °C. During the study this blank show content of *n*-alkanes and a big amount of sulphur when grounded. Later several tested involving silica gel (BDH Laboratory, precipitated acid washed) heated in different temperature (200, 400 and 600 °C) were tested for organic matter. In each temperature they show organic matter in the form of *n*-alkanes. The silica was shown to be ineffective blank. For this reason the blank used later was only the solution used for the extraction (DCM:MeOH 9:1).



### A.4.2. Hopanoic acid

RT  $\approx$  70

$C_{31}H_{52}O_2$

Molecular weight = 456

Peaks = 191, 410

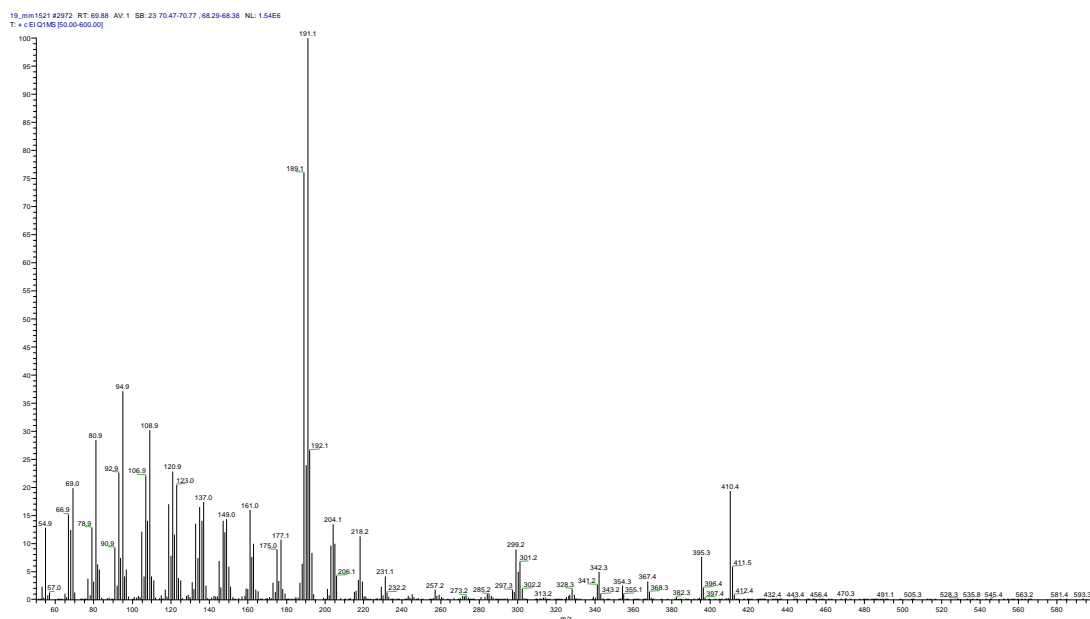


Figure 6.10. Mass spectrum of hopanoic acid.

### A.4.3. Dimethylpolysiloxane

RT= 71

Ions (m/z) = 207

Source: Septum bleed or methyl silicone column bleed

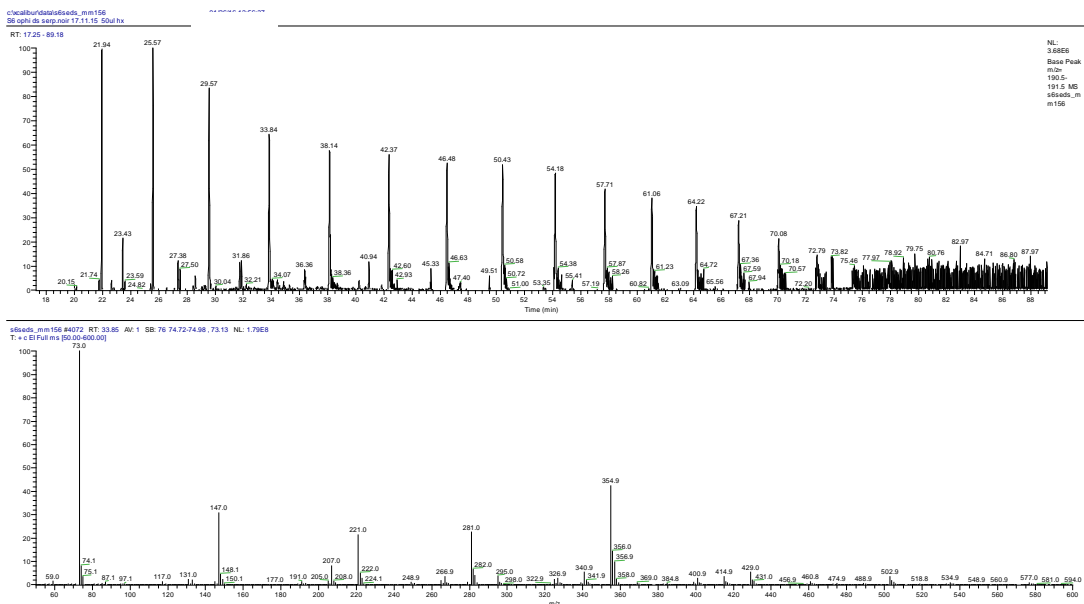
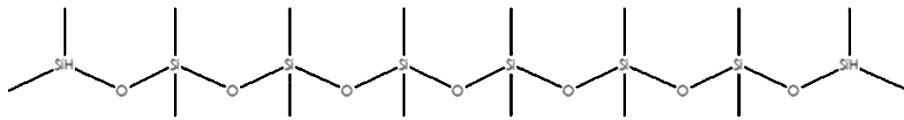
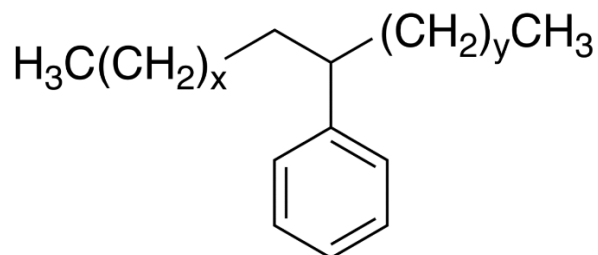


Figure 6.11. A chromatogram showing a column bleeding and the mass spectrum of Dimethylpolysiloxane.

#### A.4.4. Linear alkylbenzene (LAB) $C_6H_5C_nH_{2n+1}$



Source: dishwashing liquid using to clean the Tema Mill before the hot tap water rinsing and the cleaning with methanol.

## Ions (m/z): 91, 92

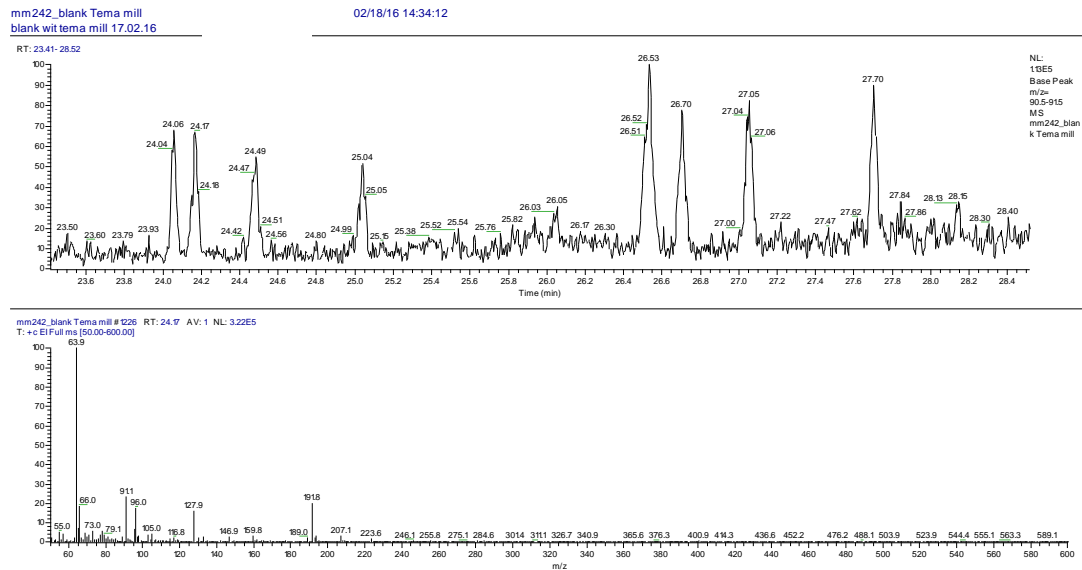


Figure 6.12 Gas chromatogram showing different LABs and the mass spectrum of a chosen molecule in RT =24.17

### A.5. Hydrocarbons biomarkers for anaerobic methanotrophs

#### Hydrocarbons:

crocetane (2,6,11,15-tetramethyl- hexadecane);

unsaturated crocetanes with up to two double bonds;

PMI (2,6,10,15,19-pentamethylcosane);

unsaturated PMIs with up to five double bonds;

#### Glycerol Diethers:

archaeol (2,3-di-O-phytanyl-sn-glycerol);

sn-2-hydrox-yarchaeol (2-O-3-hydroxyphytanyl-3-O-phytanyl-sn-glycerol)

#### Ether-bond cleaved lipids:

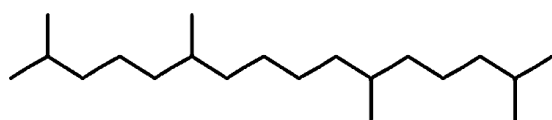
phytane (3,7,11,15-tetramethylhexadecane);

hydroxyphytane (3-hydroxy-3,7,11,15-tetramethylhexadecane);

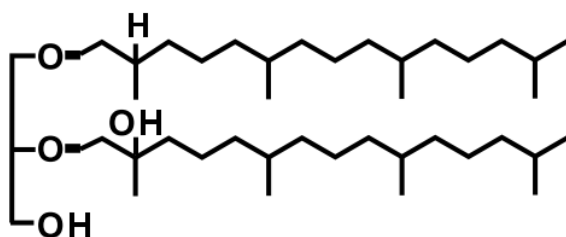
C40:0 (3,7,11,15,18,22,26,30-octamethyldotriacontane);

C40:1 [1-(1,5,8,12,16,20-hexamethyldocosyl)-3-(4-methylhexyl)-cyclopentane];

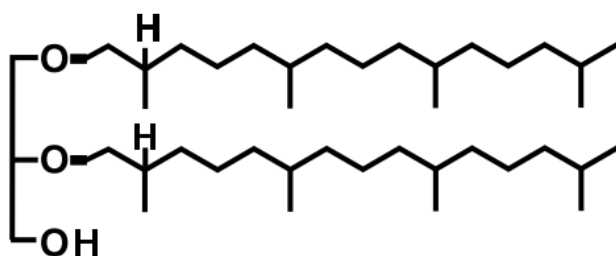
C40:2 (1,1'-(1,5,8,12-tetramethyl-1,12-dodecandiyl)-bis[3-(4-methylhexyl)-cyclopentane]).



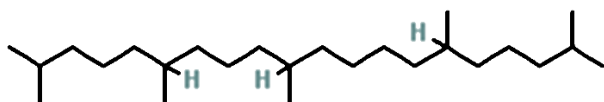
**Crocetane** C<sub>20</sub>H<sub>42</sub> (m/z 300,150)



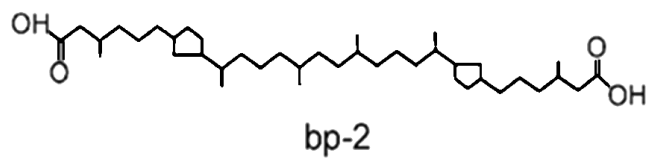
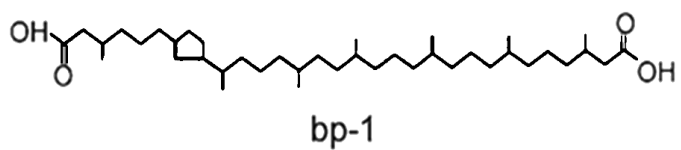
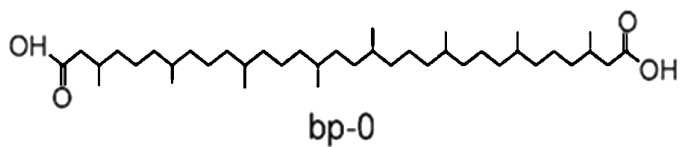
**Sn-2-hydroxyarchaeol** C<sub>43</sub>H<sub>88</sub>O<sub>4</sub>



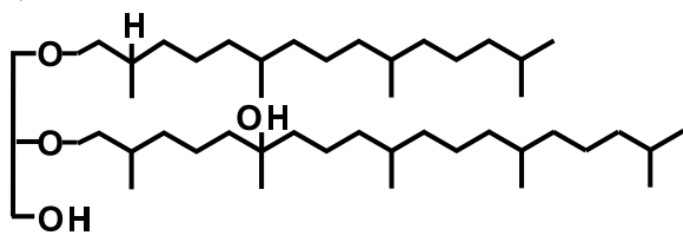
**Archaeol** C<sub>43</sub>H<sub>88</sub>O<sub>3</sub>



PMI (2,6,10,15,19-pentamethylicosane)



### Biphytanic diacids



### Glycerolethers

$C_{20}$ ,  $C_{25}$  sn-2 hydroxy isoprenoid glycerol diether  $C_{38}H_{76}O_4$

## B. Appendix B: Methods



**B.1. Thin sections images**

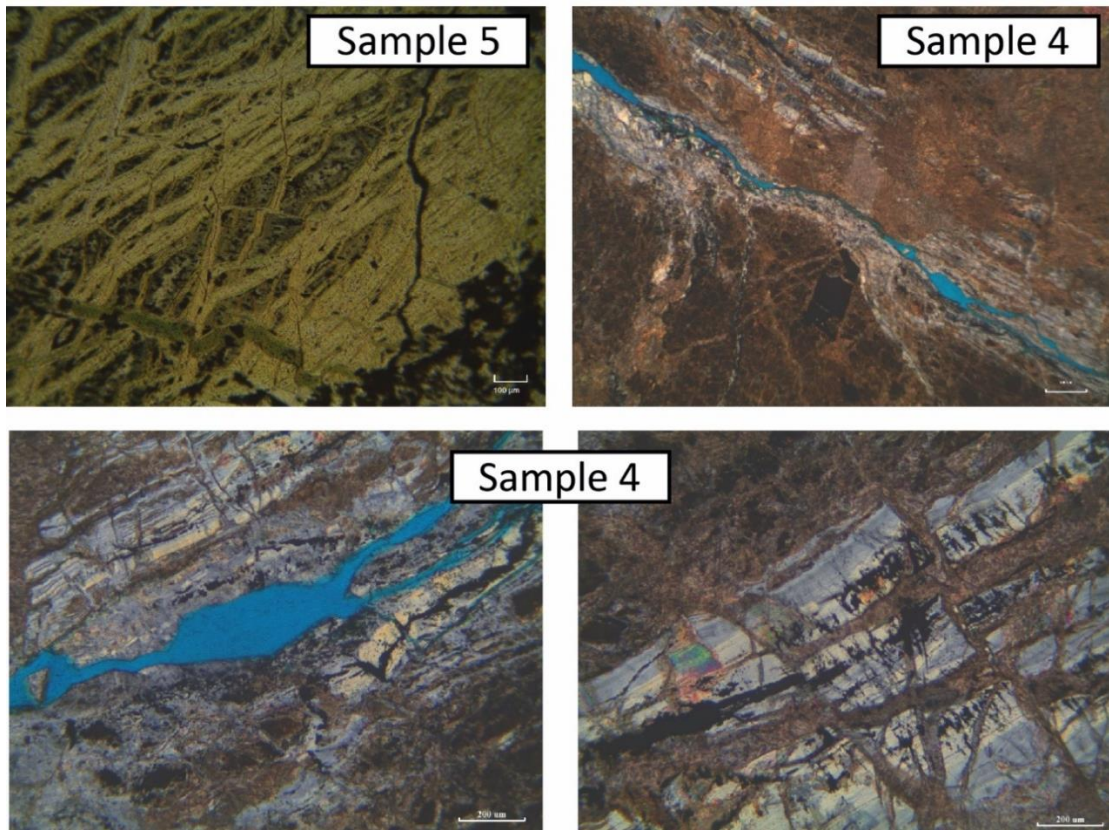


Figure 6.13 An additional panel with thin section images from Totalp. Sample 5 is serpentinised Iherzolite and sample 4 is ophicalcite.

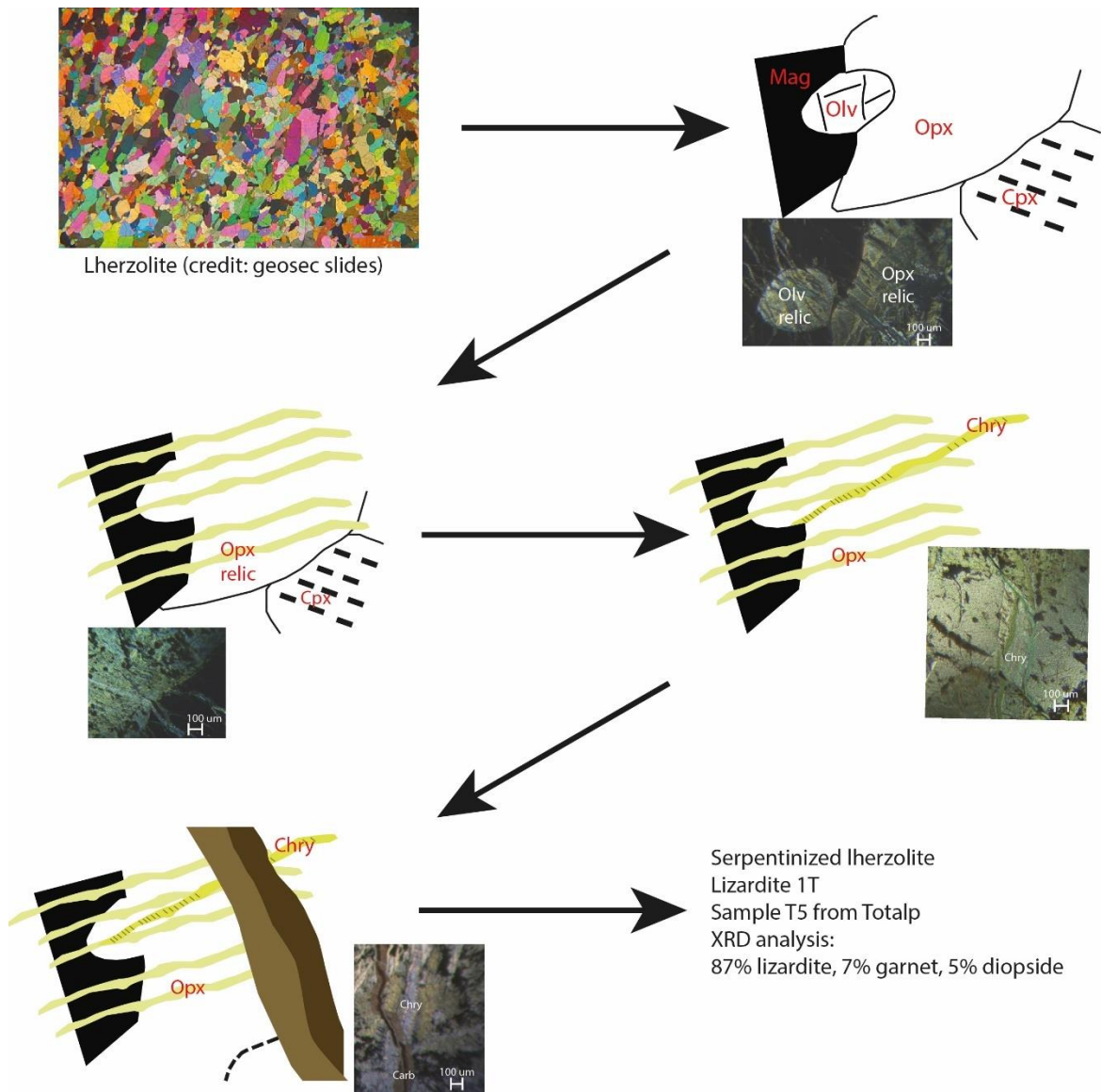
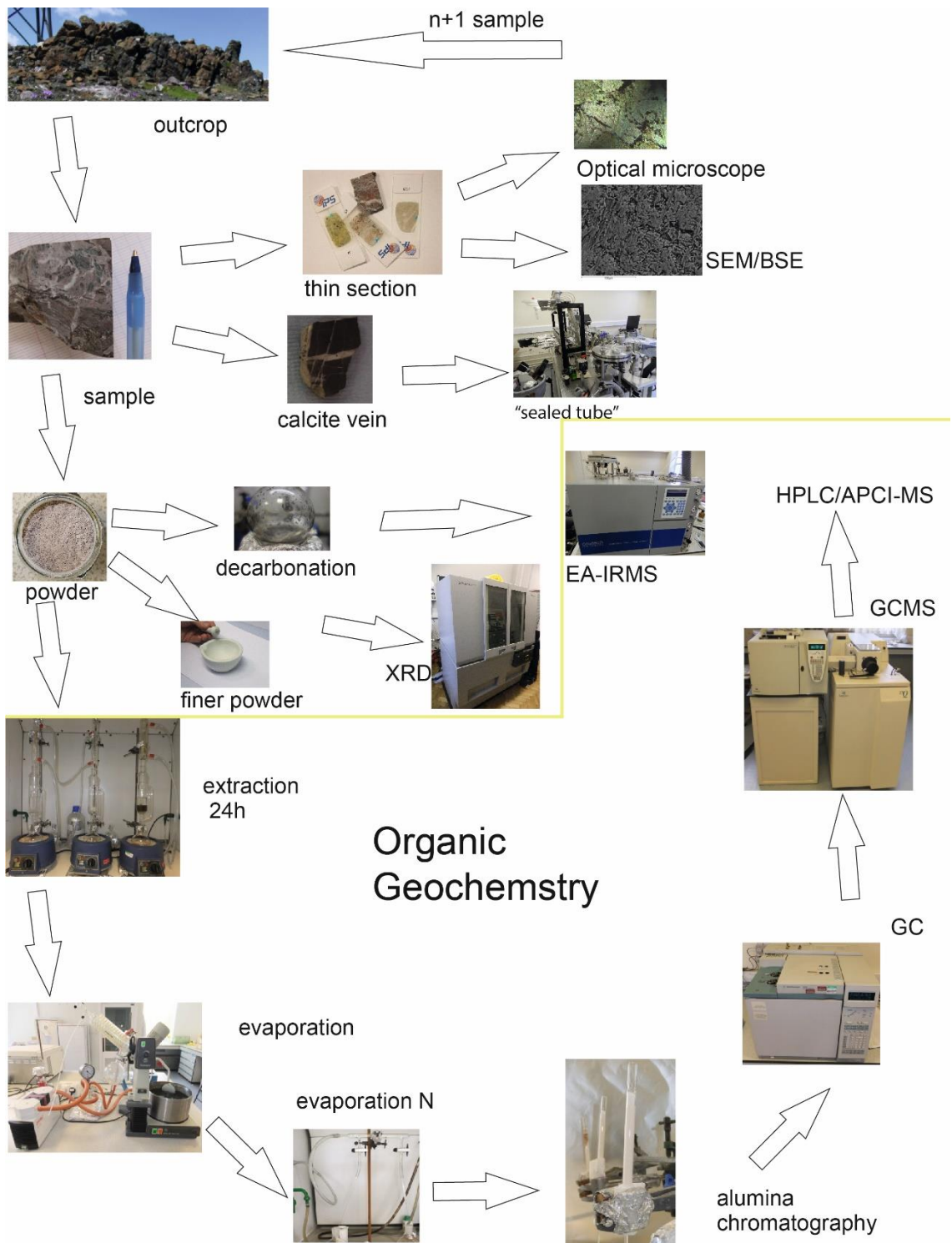


Figure 6.14. Sketch summarising the serpentinisation based on sample 5 from Totalp. Pyroxene is still present in the serpentinite but not olivine. This could be due to the fact that in low fluid flux serpentinisation start with olivine and in later stage in more open fluid condition magnetite appeared (Bach et al. 2006). The oxydes are magnetite and spinel. Chrysotile and carbonate veins are observed in thin section but invisible to the naked eye. The samples represent also later fluid veins and fractures (coloured in baby blue).

## B.2. Methods





IODP Bremen Core Repository



sample



calcite manual extraction from vein



"sealed tube" method



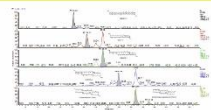
powder



decarbonation HCl



EA-IRMS



HPLC/APCI-MS

GCMS



GC



alumina chromatography



extraction 24h

+ blank same procedures (DCM:MeOH 9:1)

# Organic Geochemistry



evaporation

evaporation N



## C. Appendix C : Mass spectrum and Gas chromatogram

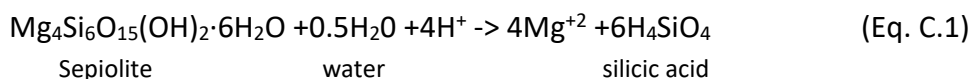


## C.1. Sepiolite drilling mud

Dry powder samples of sepiolite before being mixed with seawater or used as a drilling mud, were received from the IODP 367 cruise.

If the objective of the IODP expedition is not related to microbial life or hydrocarbon, the organic geochemistry done on the cruises is limited to carbonate and elemental analyses techniques.

During drilling, the mud sweeps, sepiolite, is mixed with seawater and is used to sweep the excess solids from the holes (Escutia et al. 2010):



The samples all had very similar GC-MS profiles raising the question of possible contamination comparison with the blanks allowed us to exclude a contamination from the laboratory analyses (Fig.C.2).

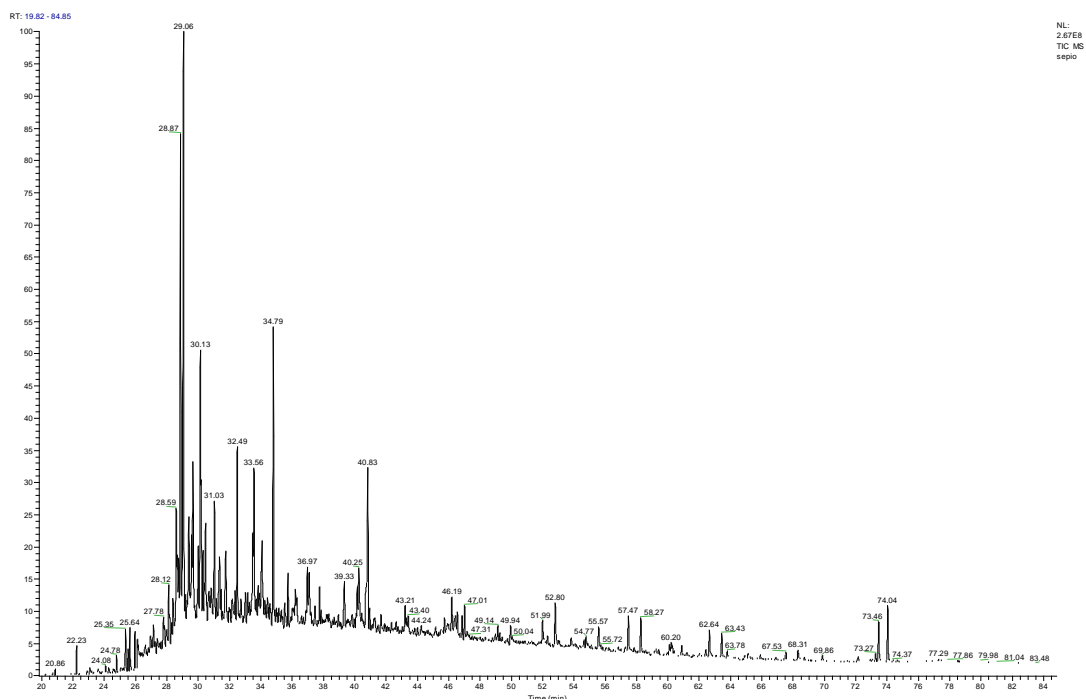


Figure 6.15 Gas chromatogram profiles of a drilling mud (sepiolite).

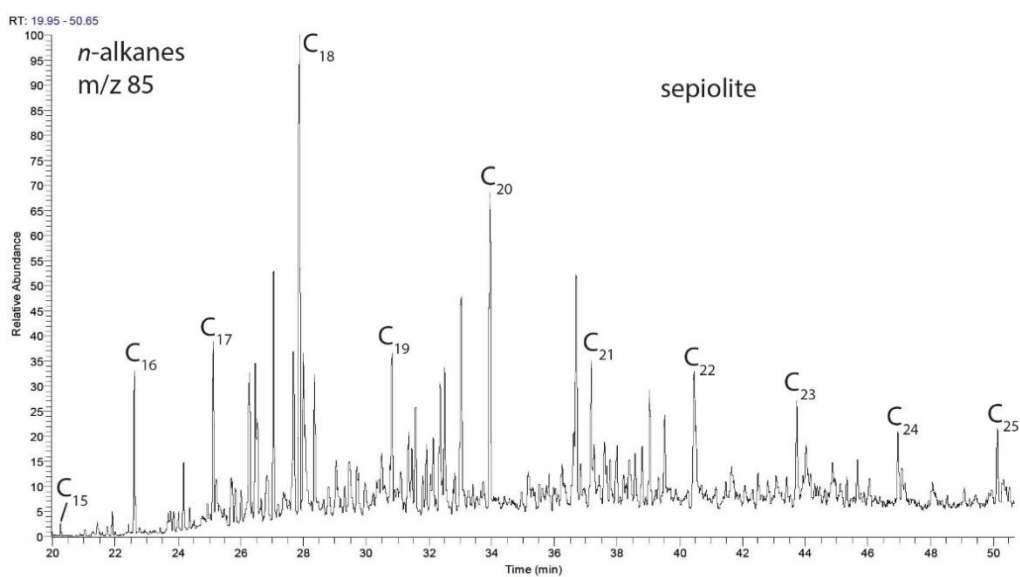
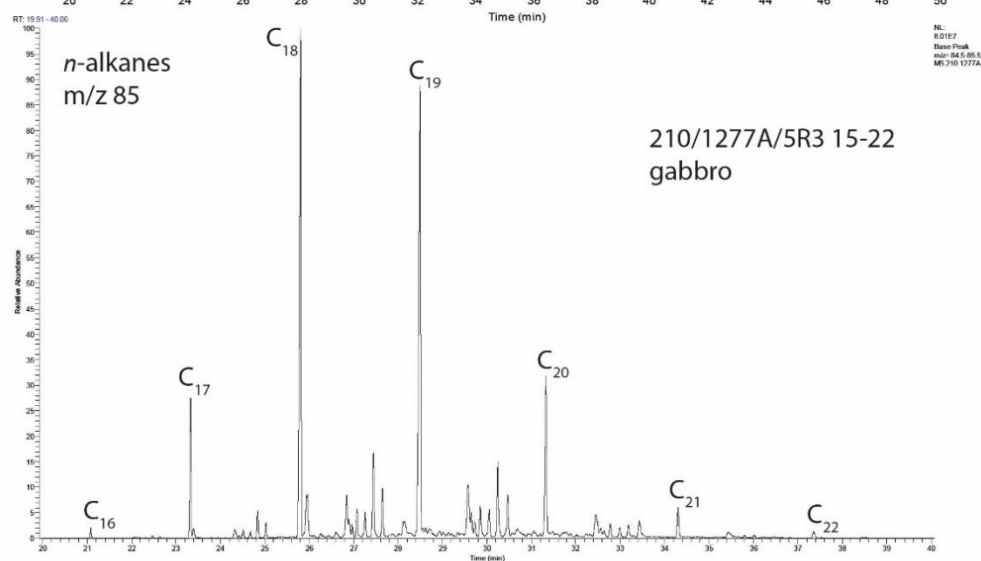
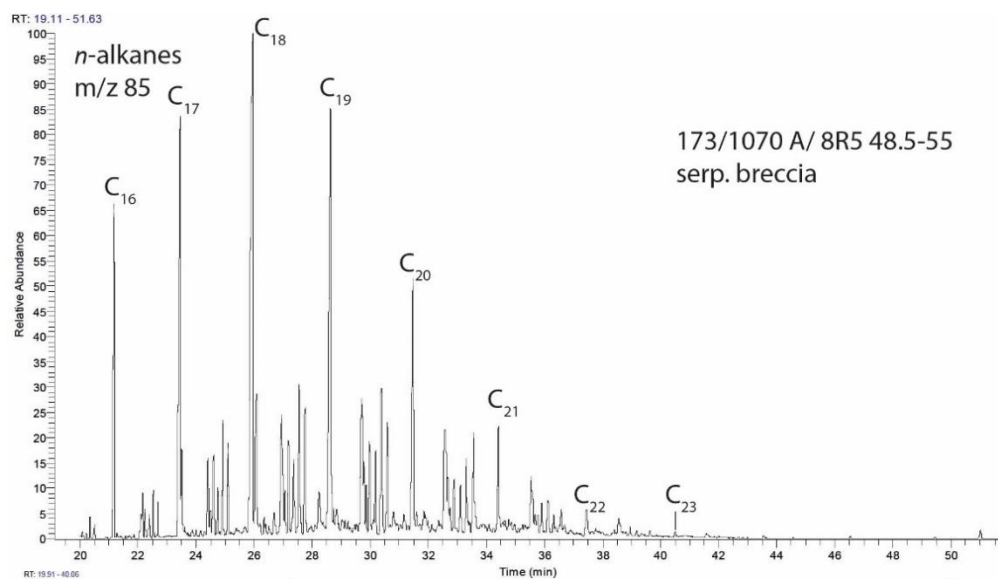


Figure 6.16 Ion chromatogram (m/z 85) from two samples and sepiolite. The three ion chromatograms show a dominance of C18 *n*-alkane.

The chromatography showed a distribution in which C<sub>18</sub> is the dominant alkane, which is the same as the profile of a sample of drilling fluid (Fig.C.1). Thus, we tested for possible contamination from the drilling fluid (sepiolite) by comparing the ratios of eight pairs of peaks in the samples having similar RT and the same KI in a star-plot diagram (Fig.C.3). The two samples from Leg 149 do not feature in the calculation as they were drilled with a different fluid and the sediment sample presents a different chromatogram profile (Fig. 5.7). The ratios of these eight paired peaks samples were almost identical but differed from the sepiolite (Fig.C.3).

Thus, we tested for possible contamination from the drilling fluid (sepiolite) by comparing the ratios of eight pairs of peaks in the samples having similar RT and the same KI in a star-plot diagram (Fig.C.3). The ratios of these eight paired peaks samples were almost identical, but differed from the sepiolite (Fig.C.3).

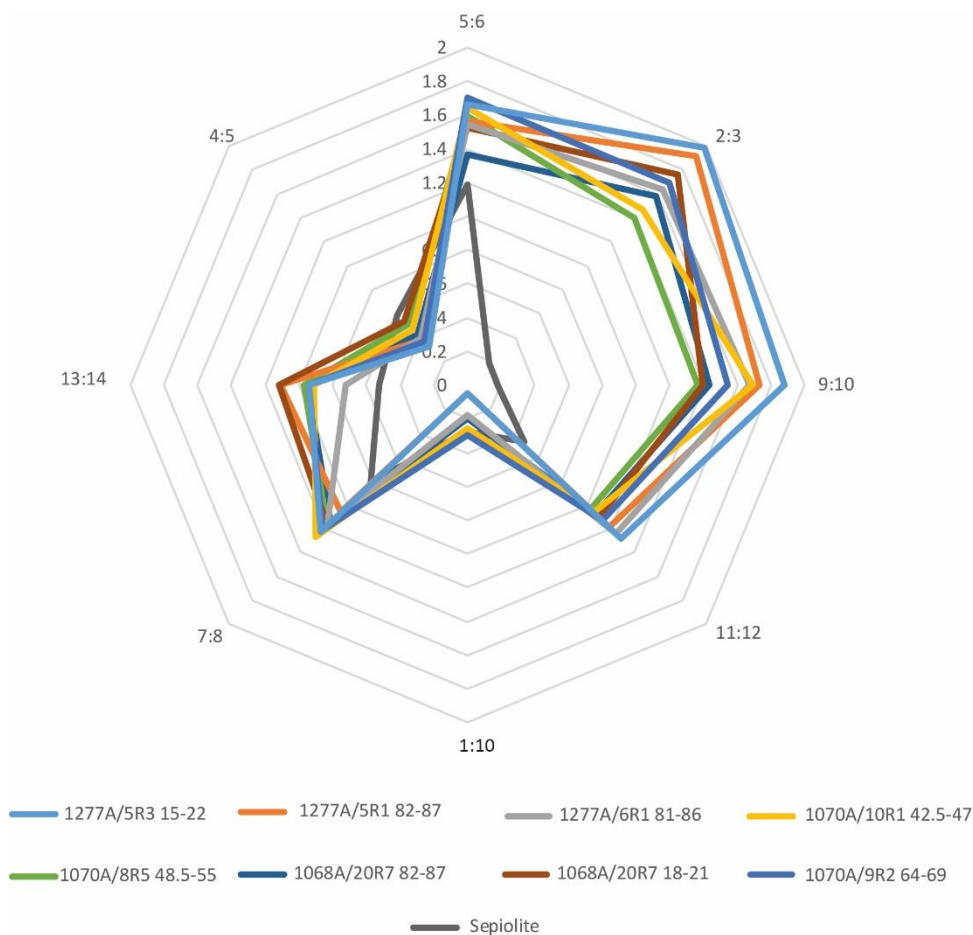
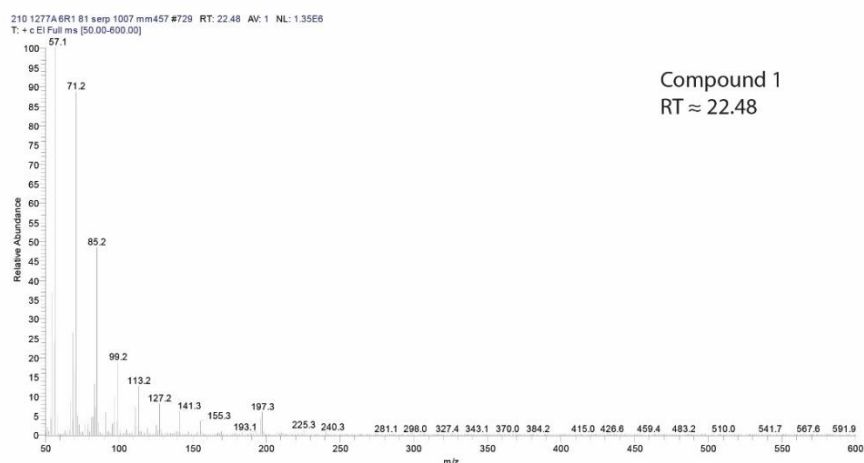
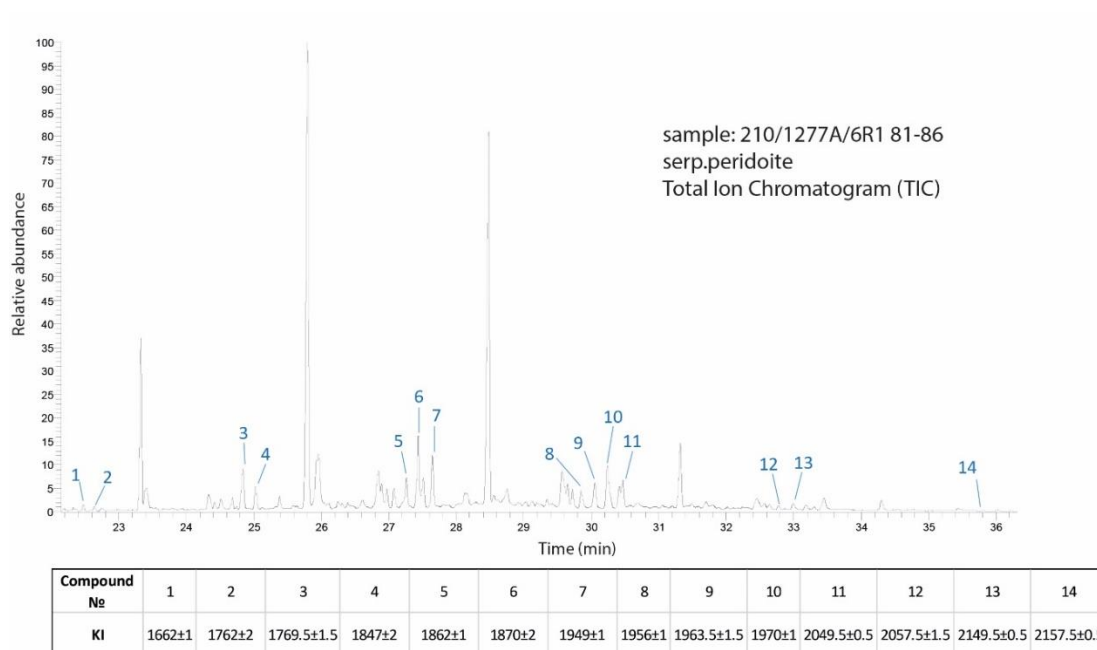


Figure 6.17 A star-plot diagram of alkane ratios from eight igneous and metamorphic samples from Legs 173 and 210 from Iberian and Newfoundland margin from figure 5.7 compared to sepiolite.

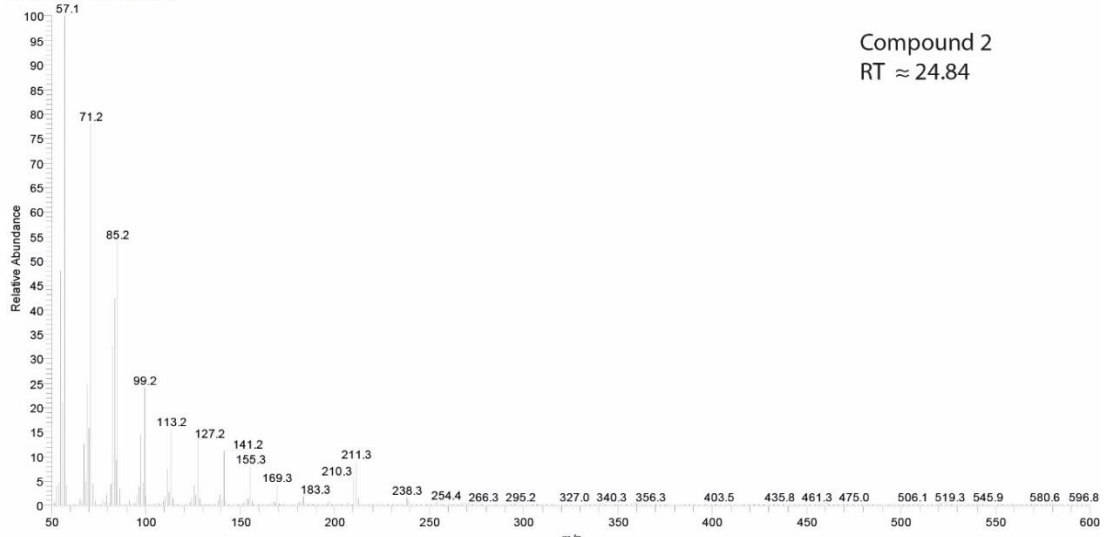
I would like to thank Michael Nirrengarten for sending me a sepiolite powder sample from the IODP cruise 367.

## C.2. Mass spectrum profiles

Ion chromatogram profiles (GC-MS) and mass spectrum profiles of the cyclic and branches alkanes of our samples presented in figure 5.7 chapter 5.

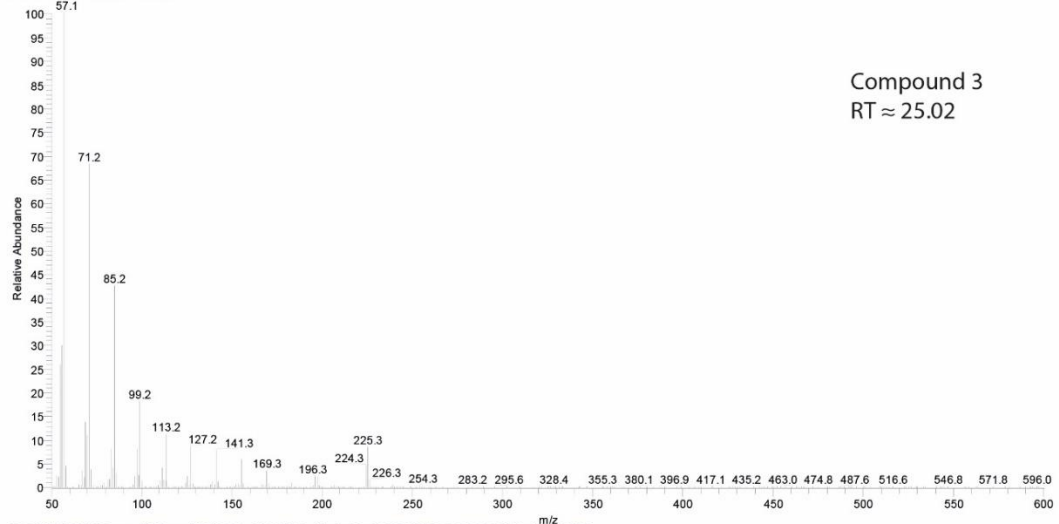


210 1277A6R1 81 serp 1007 mm457 #1423 RT: 24.84 AV: 1 NL: 7.03E6  
T: + c EI Full ms [50.00-600.00]



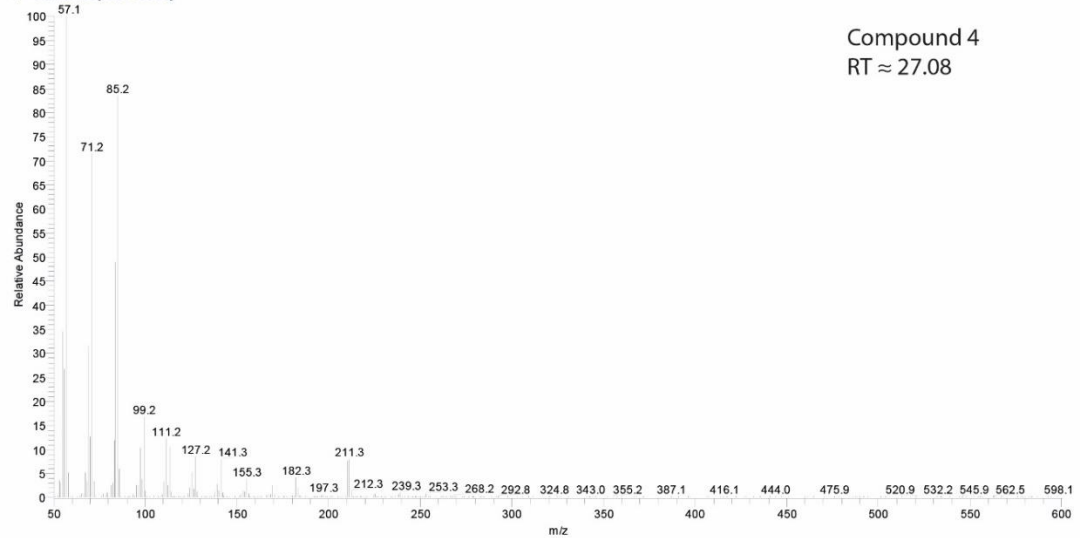
Compound 2  
RT ≈ 24.84

210 1277A6R1 81 serp 1007 mm457 #1478 RT: 25.02 AV: 1 SB: 20 27.94-27.98 , 26.68-26.70 NL: 4.87E6  
T: + c EI Full ms [50.00-600.00]



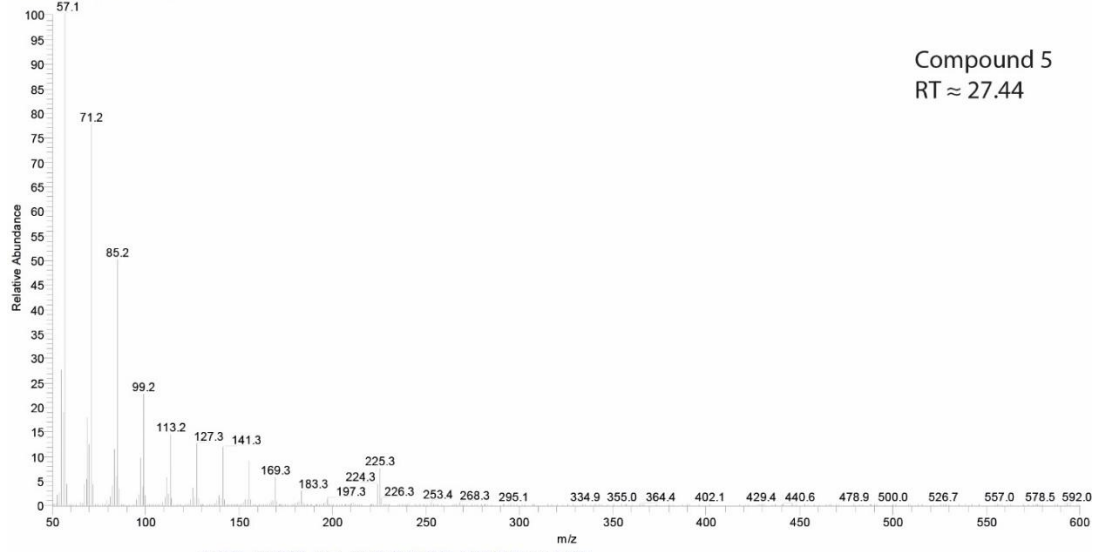
Compound 3  
RT ≈ 25.02

210 1277A6R1 81 serp 1007 mm457 #2083 RT: 27.08 AV: 1 SB: 20 27.94-27.98 , 26.68-26.70 NL: 3.37E6  
T: + c EI Full ms [50.00-600.00]

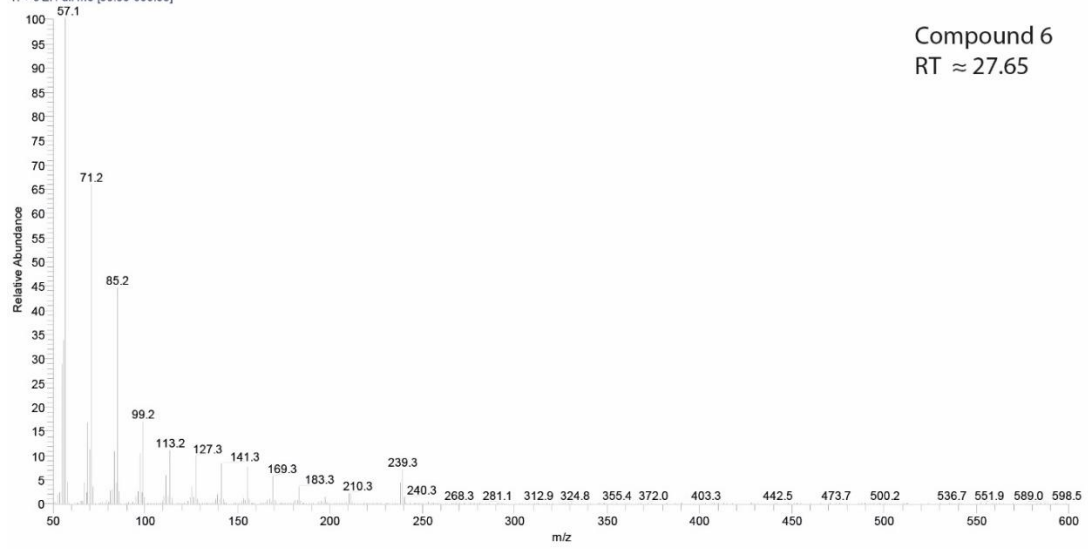


Compound 4  
RT ≈ 27.08

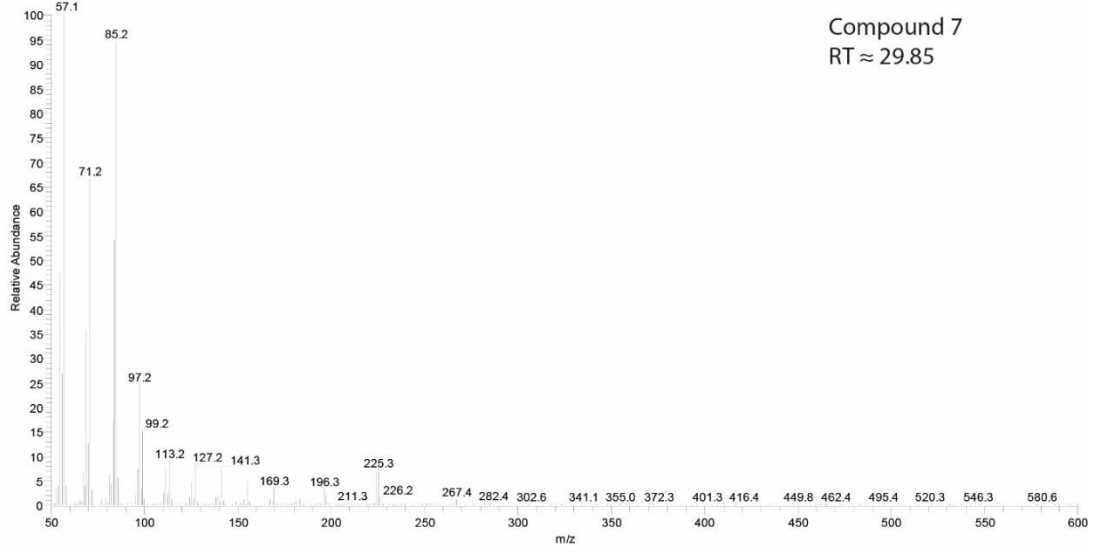
210 1277A6R1 81 serp 1007 mm457 #2188 RT: 27.44 AV: 1 SB: 20 27.94-27.98, 26.68-26.70 NL: 1.48E7  
T: + c EI Full ms [50.00-600.00]



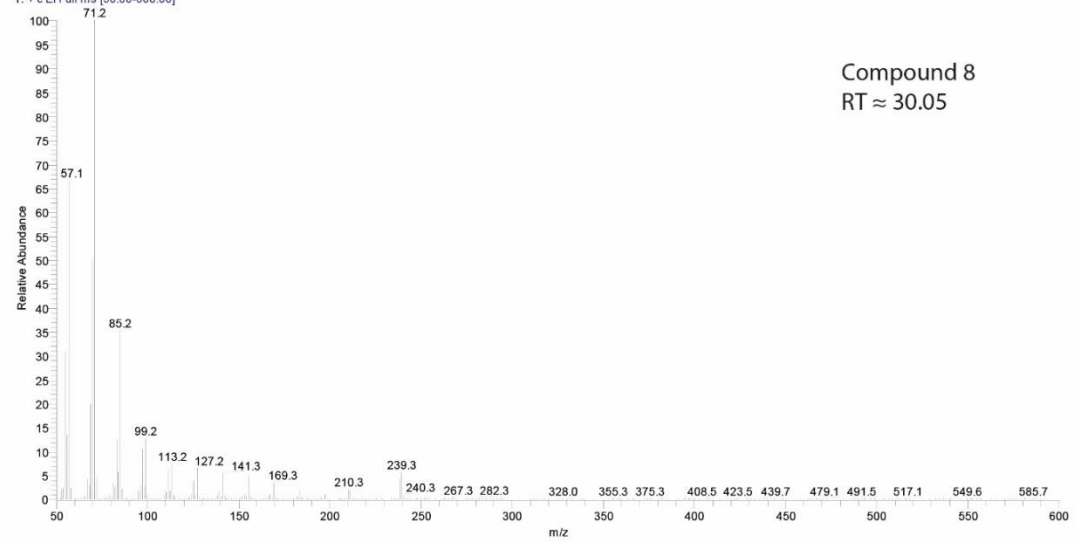
7 #2250 RT: 27.65 AV: 1 SB: 20 27.94-27.98, 26.68-26.70 NL: 1.13E7  
T: + c EI Full ms [50.00-600.00]



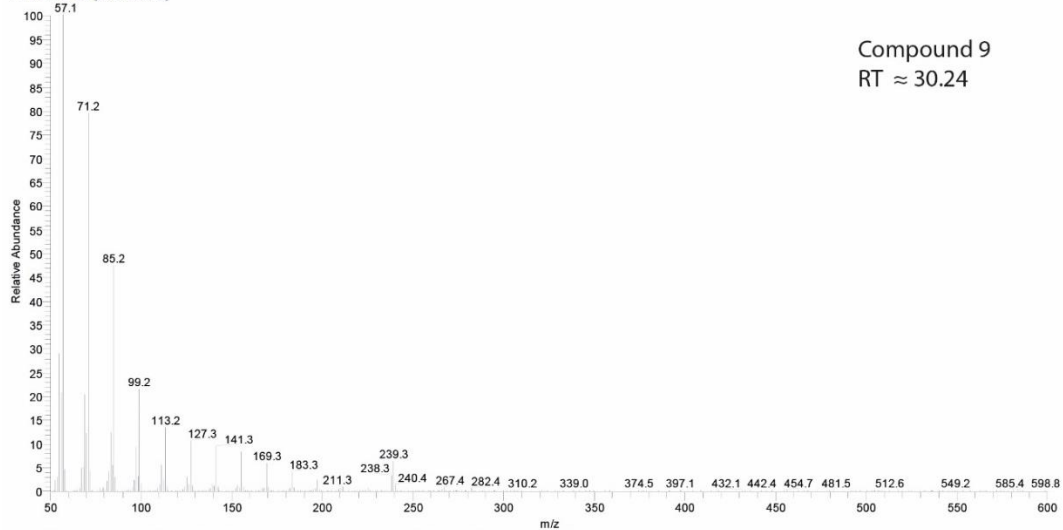
210 1277A6R1 81 serp 1007 mm457 #2898 RT: 29.85 AV: 1 SB: 33 30.85-30.91 , 28.90-28.95 NL: 2.44E6  
T: + c EI Full ms [50.00-600.00]



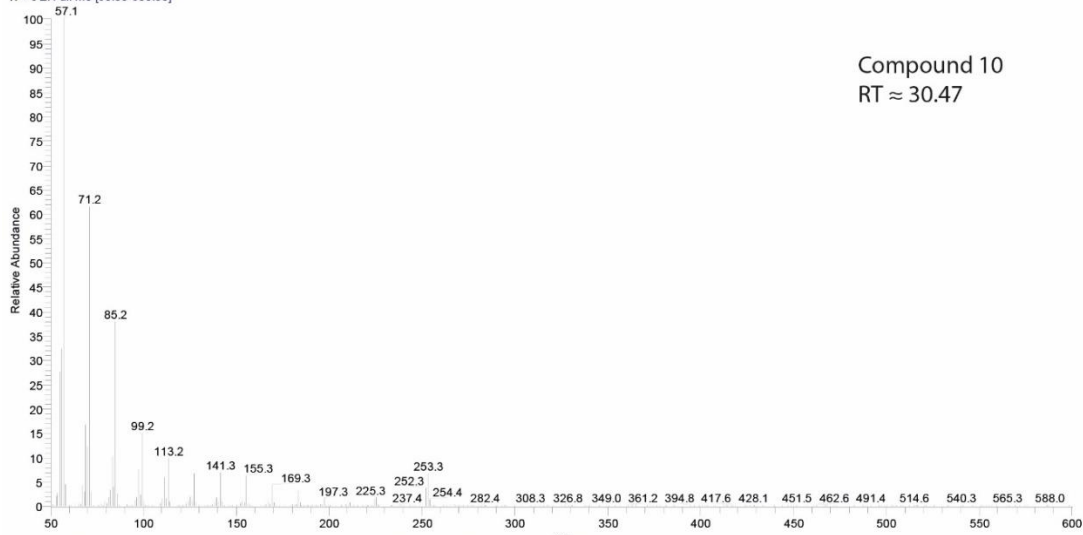
210 1277A6R1 81 serp 1007 mm457 #2958 RT: 30.06 AV: 1 SB: 21 30.79-30.84 , 29.23-29.24 NL: 5.13E6  
T: + c EI Full ms [50.00-600.00]



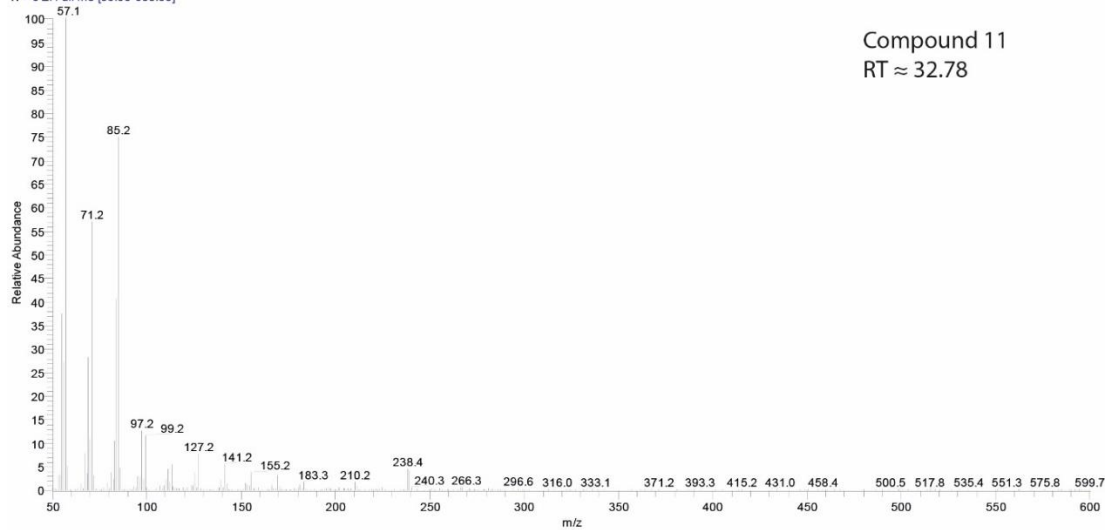
210 1277A6R1 81 serp 1007 mm457 #3012 RT: 30.24 AV: 1 SB: 21 30.79-30.84, 29.23-29.24 NL: 8.51E6  
T: + c EI Full ms [50.00-600.00]



210 1277A6R1 81 serp 1007 mm457 #3079 RT: 30.47 AV: 1 SB: 21 30.79-30.84, 29.23-29.24 NL: 6.20E6  
T: + c EI Full ms [50.00-600.00]



210 1277A6R1 81 serp 1007 mm457 #3757 RT: 32.78 AV: 1 SB: 52 33.90-34.05, 32.26-32.29 NL: 8.24E5  
T: + c EI Full ms [50.00-600.00]



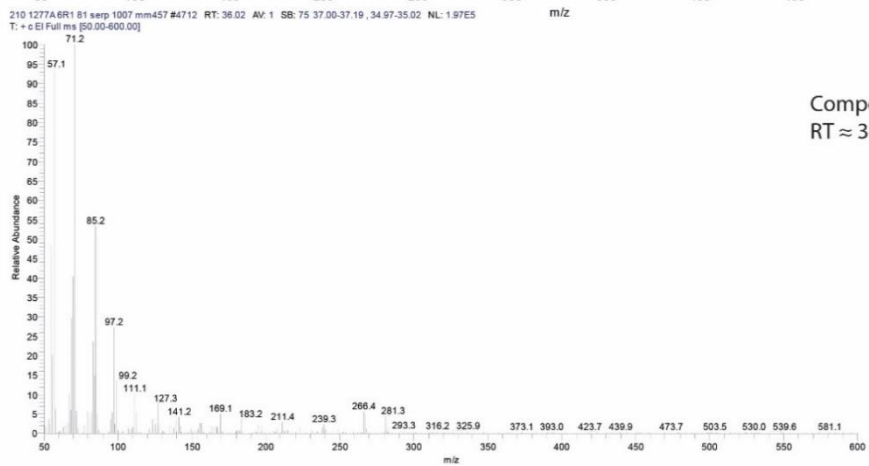
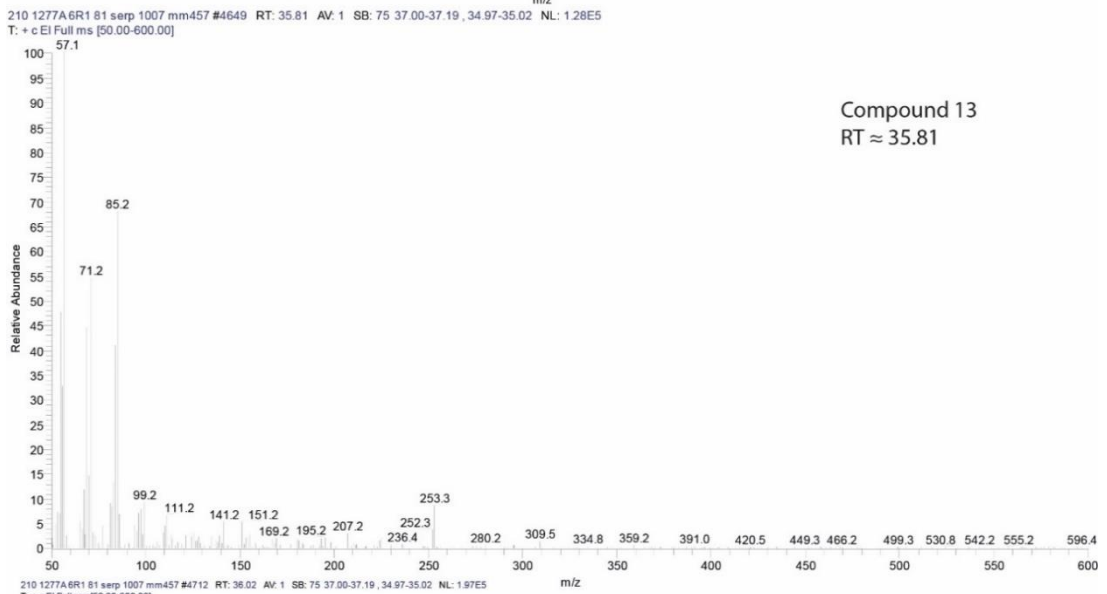
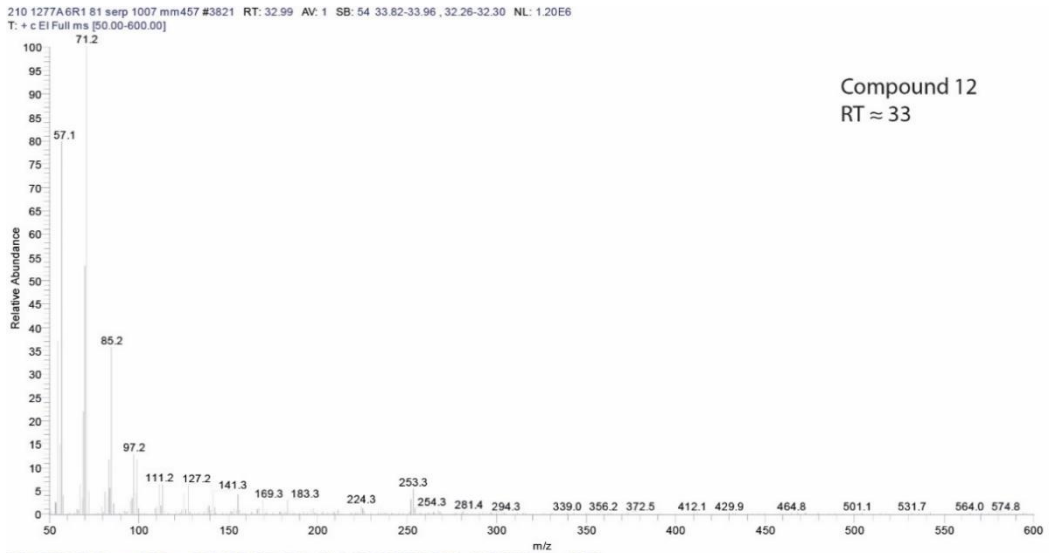


Figure 6.18 Mas spectrum of the cyclic and branches alkanes used in figure 5.7.



## 7. Bibliography

- Abdel-Shafy, H. I., & Mansour, M. S. M. (2016). A review on polycyclic aromatic hydrocarbons: Source, environmental impact, effect on human health and remediation. *Egyptian Journal of Petroleum*, 25, 107-123.
- Adegoke, A. K., Yandoka, B. M. S., Abdullah, W. H., Akaegbobi, I. M. (2015). Molecular geochemical evaluation of Late Cretaceous sediments from Chad (Bornu) Basin, NE Nigeria: implications for paleodepositional conditions, source input and thermal maturation. *Arabian Journal of Geosciences*, 8, 1591-1609.
- Agrinier, P., & Cannat, M. (1997). Oxygen isotopic constraints on serpentinization processes in ultramafic rocks from the Mid-Atlantic Ridge (23°N). *Proceedings of the Ocean Drilling Program, Scientific Results*, 153.
- Akyüz, M., & Çabuk, H. (2010). Gas–particle partitioning and seasonal variation of polycyclic aromatic hydrocarbons in the atmosphere of Zonguldak, Turkey. *Science of the total environment*, 408, 5550-5558.
- Allen, D. E., & Seyfried Jr, W. E. (2003). Compositional controls on vent fluids from ultramafic-hosted hydrothermal systems at mid-ocean ridges: An experimental study at 400°C, 500 bars. *Geochimica et Cosmochimica Acta*, 67, 1531-1542.
- Allen, D. E., & Seyfried Jr, W. (2004). Serpentinization and heat generation: constraints from Lost City and Rainbow hydrothermal systems. *Geochimica et Cosmochimica Acta*, 68, 1347-1354.
- Alt, J. C., & Shanks, W. C. (1998). Sulfur in serpentinized oceanic peridotites: Serpentinization processes and microbial sulfate reduction. *Journal of Geophysical Research*, 103, 9917.
- Alt, J. C., & Shanks, W. (2003). Serpentinization of abyssal peridotites from the MARK area, Mid-Atlantic Ridge: Sulfur geochemistry and reaction modeling. *Geochimica et Cosmochimica Acta*, 67, 641–653.
- Alt, J. C., & Shanks, W. C. (2006). Stable isotope compositions of serpentinite seamounts in the Mariana forearc: Serpentinization processes, fluid sources and sulfur metasomatism. *Earth and Planetary Science Letters*, 242, 272-285.
- Alt, J. C., Shanks, W. C., Bach, W., Paulick, H., Garrido, C. J., Beaudoin, G. (2007). Hydrothermal alteration and microbial sulfate reduction in peridotite and gabbro exposed by detachment faulting at the Mid-Atlantic Ridge, 15° 20' N (ODP Leg 209): A sulfur and oxygen isotope study. *Geochemistry, Geophysics, Geosystems*, 8.
- Alt, J. C., Shanks, W. C., Crispini, L., Gaggero, L., Schwarzenbach, E. M., Früh-Green, G. L., Bernasconi, S. M. (2012). Uptake of carbon and sulfur during seafloor

- serpentinization and the effects of subduction metamorphism in Ligurian peridotites. *Chemical Geology*, 322-323, 268-277.
- Alt, J. C., Schwarzenbach, E. M., Früh-Green, G. L., Shanks, W. C., Bernasconi, S. M., Garrido, C. J., Crispini, L., Gaggero, L., Padrón-Navarta, J. A., Marchesi, C. (2013). The role of serpentinites in cycling of carbon and sulfur: Seafloor serpentinization and subduction metamorphism. *Lithos*, 178, 40-54.
- Amend, J. P., & McCollom, T. M. (2009). Energetics of biomolecule synthesis on early Earth. *Chemical evolution II: from the origins of life to modern society*, 1025, 63-94.
- Anderson, R. T., Chapelle, F. H., Lovley, D. R. (1998). Evidence against hydrogen-based microbial ecosystems in basalt aquifers. *Science*, 281, 976-977.
- Andreani, M., Mével, C., Boullier, A. M., Escartin, J. (2007). Dynamic control on serpentine crystallization in veins: constraints on hydration processes in oceanic peridotites. *Geochemistry, Geophysics, Geosystems*, 8.
- Andreani, M., Muñoz, M., Marcaillou, C., Delacour, A. (2013).  $\mu$ XANES study of iron redox state in serpentine during oceanic serpentinization. *Lithos*, 178, 70-83.
- Andrews, G. D., Schmitt, A. K., Busby, C. J., Brown, S. R., Blum, P., Harvey, J. (2016). Age and compositional data of zircon from sepiolite drilling mud to identify contamination of ocean drilling samples. *Geochemistry, Geophysics, Geosystems*, 17, 3512-3526.
- Anthony, J., Bideaux, R., Bladh, K., Nichols, M. (2000). Handbook of Mineralogy–Vol. IV (Arsenates, Phosphates, Vanadates).– Mineral Data Publishing. Tucson, Arizona.
- Arshad, A., Speth, D. R., de Graaf, R. M., den Camp, H. J. O., Jetten, M. S., Welte, C. U. (2015). A metagenomics-based metabolic model of nitrate-dependent anaerobic oxidation of methane by Methanoperedens-like archaea. *Frontiers in microbiology*, 6.
- Baaske, P., Weinert, F. M., Duhr, S., Lemke, K. H., Russell, M. J., Braun, D. (2007). Extreme accumulation of nucleotides in simulated hydrothermal pore systems. *Proceedings of the National Academy of Sciences*, 104, 9346-9351.
- Bach, W., Garrido, C. J., Paulick, H., Harvey, J., Rosner, M. (2004). Seawater-peridotite interactions: First insights from ODP Leg 209, MAR 15 N. *Geochemistry, Geophysics, Geosystems*, 5.
- Bach, W., Paulick, H., Garrido, C. J., Ildefonse, B., Meurer, W. P., Humphris, S. E. (2006). Unraveling the sequence of serpentinization reactions: petrography, mineral chemistry, and petrophysics of serpentinites from MAR 15°N (ODP Leg 209, Site 1274). *Geophysical Research Letters*, 33, L13306.
- Bach, W., & Früh-Green, G. L. (2010). Alteration of the oceanic lithosphere and implications for seafloor processes. *Elements*, 6, 173-178.
- Bach, W., Rosner, M., Jöns, N., Rausch, S., Robinson, L. F., Paulick, H., Erzinger, J. (2011). Carbonate veins trace seawater circulation during exhumation and uplift of mantle rock: results from ODP Leg 209. *Earth and Planetary Science Letters*, 311, 242-252.

- Bailey, S. W. (1969). Polytypism of trioctahedral 1: 1 layer silicates. *Clays and Clay Minerals*, 17, 355-371.
- Barker, J. F., & Fritz, P. (1981). Carbon isotope fractionation during microbial methane oxidation. *Nature*, 293, 289-291.
- Barnes, J., & Sharp, Z. (2006). Achlorine isotope study of DSDP/ODP serpentinized ultramafic rocks: Insights into the serpentinization process. *Chemical Geology*, 228, 246-265.
- Barnes, S. J., Holwell, D. A., Le Vaillant, M. (2017). Magmatic sulfide ore deposits. *Elements*, 13, 89-95.
- Baross, J., & Hoffman, S. (1985). Submarine hydrothermal vents and associated gradient environments as sites for the origin and evolution of life. *Origins of life and evolution of the biosphere*, 15, 327-345.
- Barriga, F., Fouquet, Y., Almeida, A., Biscoito, M., Charlou, J., Costa, R., Dias, A., Marques, A., Miranda, J., Olu, K. (1998). Discovery of the Saldanha hydrothermal field on the FAMOUS segment of the MAR (36°30' N). *Eos Trans. AGU*, 79.
- Batuyev, B. N., Krotov, A. G., Markov, V. F., Cherkashev, G. A., Krasnov, S. G., Lisitsyn, Y. D. (1994). Massive sulfide deposits discovered and sampled at 14°45'N, Mid-Atlantic Ridge. *BRIDGE Newsletter*, 6, 6-10.
- Baumard, P., Budzinski, H., Michon, Q., Garrigues, P., Burgeot, T., Bellocq, J. (1998). Origin and bioavailability of PAHs in the Mediterranean Sea from mussel and sediment records. *Estuarine, Coastal and Shelf Science*, 47, 77-90.
- Baumberger, T., Früh-Green, G. L., Thorseth, I. H., Lilley, M. D., Hamelin, C., Bernasconi, S. M., Okland, I. E., Pedersen, R. B. (2016). Fluid composition of the sediment-influenced Loki's castle vent field at the ultra-slow spreading Arctic Mid-Ocean ridge. *Geochimica et Cosmochimica Acta*, 187, 156-178.
- Bayrakci, G., Minshull, T., Sawyer, D., Reston, T. J., Klaeschen, D., Papenberg, C., Ranero, C., Bull, J., Davy, R., Shillington, D. (2016). Fault-controlled hydration of the upper mantle during continental rifting. *Nature Geoscience*, 9, 384-388.
- Beal, E. J., House, C. H., Orphan, V. J. (2009). Manganese- and iron-dependent marine methane oxidation. *Science*, 325, 184-187.
- Beard, J. S., & Hopkinson, L. (2000). A fossil, serpentinization-related hydrothermal vent, Ocean Drilling Program Leg 173, Site 1068 (Iberia Abyssal Plain): Some aspects of mineral and fluid chemistry. *Journal of Geophysical Research: Solid Earth (1978–2012)*, 105, 16527-16539.
- Beard, J. S., Fullagar, P. D., Sinha, A. K. (2002). Gabbroic pegmatite intrusions, Iberia Abyssal Plain, ODP Leg 173, Site 1070: Magmatism during a transition from non-volcanic rifting to sea-floor spreading. *Journal of Petrology*, 43, 885-905.
- Becking, L. B., & Moore, D. (1961). Biogenic sulfides. *economic geology*, 56, 259-272.

- Beltenev, V., Ivanov, V., Shagin, A., Sergeyev, M., Rozhdestvenskaya, I., Shilov, V., Debretzova, I., Cherkashev, G., Samovarov, M., Poroshina, I. (2005). New hydrothermal sites at 13 N, Mid-Atlantic Ridge. *InterRidge News*, 14, 14-16.
- Berner, R. A. (1984). Sedimentary pyrite formation: An update. *Geochimica et Cosmochimica Acta*, 48, 605-615.
- Bernoulli, D., & Weissert, H. (1985). Sedimentary fabrics in Alpine ophiolites, south Pennine Arosa zone, Switzerland. *Geology*, 13, 755-758.
- Bernoulli, D. 2001. "Where did Gustav Steinmann see the trinity." Geological Society of America Abstracts with Programs.
- Bernoulli, D., Manatschal, G., Desmurs, L., Muntener, O. (2003). Where did Gustav Steinmann see the trinity? Back to the roots of an Alpine ophiolite concept. *Special papers - geological society of America*, 373, 93-110.
- Bernoulli, D., & Jenkyns, H. C. (2009). Ophiolites in ocean–continent transitions: from the Steinmann Trinity to sea-floor spreading. *Comptes Rendus Geoscience*, 341, 363-381.
- Beslier, M.-O., Girardeau, J., Boillot, G. (1990). Kinematics of peridotite emplacement during North Atlantic continental rifting, Galicia, northwestern Spain. *Tectonophysics*, 184, 321-343.
- Bian, L., Hinrichs, K. U., Xie, T., Brassell, S. C., Iversen, N., Fossing, H., Jørgensen, B. B., Hayes, J. M. (2001). Algal and archaeal polyisoprenoids in a recent marine sediment: molecular isotopic evidence for anaerobic oxidation of methane. *Geochemistry, Geophysics, Geosystems*, 2.
- Birgel, D., Thiel, V., Hinrichs, K.-U., Elvert, M., Campbell, K. A., Reitner, J., Farmer, J. D., Peckmann, J. (2006). Lipid biomarker patterns of methane-seep microbialites from the Mesozoic convergent margin of California. *Organic geochemistry*, 37, 1289-1302.
- Birgel, D., Elvert, M., Han, X., Peckmann, J. (2008). 13 C-depleted biphytanic diacids as tracers of past anaerobic oxidation of methane. *Organic geochemistry*, 39, 152-156.
- Birner, S. K., Warren, J. M., Cottrell, E., Davis, F. A. (2016). Hydrothermal alteration of seafloor peridotites does not influence oxygen fugacity recorded by spinel oxybarometry. *Geology*, 44, 535-538.
- Biscoito, M., Almeida, A., Segonzac, M. (2006). Preliminary biological characterization of the Saldanha hydrothermal field at the Mid-Atlantic Ridge (36 degrees 34'N, 32 degrees 26'W, 2200 m). *Cahiers de biologie marine*, 47, 421-427.
- Blumenberg, M., Seifert, R., Reitner, J., Pape, T., Michaelis, W. (2004). Membrane lipid patterns typify distinct anaerobic methanotrophic consortia. *Proceedings of the National Academy of Sciences of the United States of America*, 101, 11111-11116.
- Blumer, M. (1957). Removal of elemental sulfur from hydrocarbon fractions. *Analytical chemistry*, 29, 1039-1041.

- Boetius, A., Ravenschlag, K., Schubert, C. J., Rickert, D., Widdel, F., Gieseke, A., Amann, R., Jorgensen, B. B., Witte, U., Pfannkuche, O. (2000). A marine microbial consortium apparently mediating anaerobic oxidation of methane. *Nature*, 407, 623-626.
- Boetius, A. (2005). Lost city life. *Science*, 307, 1420-1422.
- Bogolepov, V. (1970). Problem of serpentinization of ultrabasic rocks. *International Geology Review*, 12, 421-432.
- Boillot. (1986). Tectonic denudation of the upper mantle along passive margins: a model based on drilling results (ODP leg 103, western Galicia margin, Spain). *Tectonophysics*, 132, 335-342.
- Boillot, G., Grimaud, S., Mauffret, A., Mougnot, D., Kornprobst, J., Mergoïl-Daniel, J., Torrent, G. (1980). Ocean-continent boundary off the Iberian margin: a serpentinite diapir west of the Galicia Bank. *Earth and Planetary Science Letters*, 48, 23-34.
- Boillot, G., Feraud, G., Recq, M., Girardeau, J. (1989). Undercrusting by serpentinite beneath rifted margins. *Nature*, 341, 523-525.
- Bonatti, E., Lawrence, J. R., Morandi, N. (1984). Serpentinization of oceanic peridotites: temperature dependence of mineralogy and boron content. *Earth and Planetary Science Letters*, 70, 88-94.
- Boone, D. R., Johnson, R. L., Liu, Y. (1989). Diffusion of the interspecies electron carriers H<sub>2</sub> and formate in methanogenic ecosystems and its implications in the measurement of K<sub>m</sub> for H<sub>2</sub> or formate uptake. *Applied and environmental microbiology*, 55, 1735-1741.
- Boschi, C., Früh-Green, G. L., Delacour, A., Karson, J. A., Kelley, D. S. (2006). Mass transfer and fluid flow during detachment faulting and development of an oceanic core complex, Atlantis Massif (MAR 30 N). *Geochemistry, Geophysics, Geosystems*, 7.
- Boschi, C., Dini, A., Früh-Green, G. L., Kelley, D. S. (2008). Isotopic and element exchange during serpentinization and metasomatism at the Atlantis Massif (MAR 30 N): insights from B and Sr isotope data. *Geochimica et Cosmochimica Acta*, 72, 1801-1823.
- Bougault, H., Charlou, J. L., Fouquet, Y., Needham, H. D., Vaslet, N., Appriou, P., Baptiste, P. J., Rona, P. A., Dmitriev, L., Silantiev, S. (1993). Fast and slow spreading ridges: structure and hydrothermal activity, ultramafic topographic highs, and CH<sub>4</sub> output. *Journal of Geophysical Research: Solid Earth*, 98, 9643-9651.
- Bowers, T. S., & Taylor, H. P. (1985). An integrated chemical and stable-isotope model of the origin of Mid-ocean Ridge Hot Spring Systems. *Journal of Geophysical Research: Solid Earth*, 90, 12583-12606.
- Boyet, M., Blichert-Toft, J., Rosing, M., Storey, M., Télouk, P., Albarède, F. (2003). <sup>142</sup>Nd evidence for early Earth differentiation. *Earth and Planetary Science Letters*, 214, 427-442.

- Bradley, A. S., Hayes, J. M., Summons, R. E. (2009). Extraordinary  $^{13}\text{C}$  enrichment of diether lipids at the Lost City Hydrothermal Field indicates a carbon-limited ecosystem. *Geochimica et Cosmochimica Acta*, 73, 102-118.
- Bradley, A. S., & Summons, R. E. (2010). Multiple origins of methane at the Lost City Hydrothermal Field. *Earth and Planetary Science Letters*, 297, 34-41.
- Brassell, S. C., Wardroper, A. M. K., Thomson, I. D., Maxwell, J. R., Eglinton, G. (1981). Specific acyclic isoprenoids as biological markers of methanogenic bacteria in marine sediments. *Nature*, 290, 693-696.
- Brazelton, W. J., Schrenk, M. O., Kelley, D. S., Baross, J. A. (2006). Methane- and sulfur-metabolizing microbial communities dominate the Lost City hydrothermal field ecosystem. *Applied and Environmental Microbiology*, 72, 6257-6270.
- Bristow, T. F., & Grotzinger, J. P. (2013). Sulfate availability and the geological record of cold-seep deposits. *Geology*, 41, 811-814.
- Brock, T., & Madigan, M., 1991. *Biology of microorganisms*. 6th. NJ, Englewood Cliffs: Prentice-Hall. Ed.
- Brocks, J. J., Logan, G. A., Buick, R., Summons, R. E. (1999). Archean molecular fossils and the early rise of eukaryotes. *Science*, 285, 1033-1036.
- Brooks, J., Gould, K., Smith, J. (1969). Isoprenoid hydrocarbons in coal and petroleum. *Nature*, 222, 257-259.
- Budin, I., Bruckner, R. J., Szostak, J. W. (2009). Formation of protocell-like vesicles in a thermal diffusion column. *Journal of the American Chemical Society*, 131, 9628-9629.
- Burkhard, D. J., & O'Neil, J. R. (1988). Contrasting serpentinization processes in the eastern Central Alps. *Contributions to Mineralogy and Petrology*, 99, 498-506.
- Burkhard, D. J. (1989). Co-Ni-As sulphides in serpentinites of different metamorphic grade in the eastern Central Alps (Switzerland and Italy). *Mineralogy and Petrology*, 41, 65-71.
- Burkhard, M. (1993). Calcite twins, their geometry, appearance and significance as stress-strain markers and indicators of tectonic regime: a review. *Journal of Structural Geology*, 15, 351-368.
- Canfield, D. E., Jørgensen, B. B., Fossing, H., Glud, R., Gundersen, J., Ramsing, N. B., Thamdrup, B., Hansen, J. W., Nielsen, L. P., Hall, P. O. (1993). Pathways of organic carbon oxidation in three continental margin sediments. *Marine geology*, 113, 27-40.
- Cannat, M., Manatschal, G., Sauter, D., Péron-Pinvidic, G. (2009). Assessing the conditions of continental breakup at magma-poor rifted margins: What can we learn from slow spreading mid-ocean ridges? *Comptes Rendus Geoscience*, 341, 406-427.
- Cannat, M., Fontaine, F., Escartín, J. (2010). Serpentinization and associated hydrogen and methane fluxes at slow spreading ridges. 188, 241-264.

- Cardace, D., Hoehler, T., McCollom, T., Schrenk, M., Carnevale, D., Kubo, M., Twing, K. (2013). Establishment of the Coast Range ophiolite microbial observatory (CROMO): drilling objectives and preliminary outcomes. *Scientific Drilling*, 16, 45-55.
- Carmody, L., Barry, P. H., Shervais, J. W., Kluesner, J. W., Taylor, L. A. (2013). Oxygen isotopes in subducted oceanic crust: A new perspective from Siberian diamondiferous eclogites. *Geochemistry, Geophysics, Geosystems*, 14, 3479-3493.
- Caruso, L. J., & Chernosky, J. (1979). The stability of lizardite. *The Canadian Mineralogist*, 17, 757-769.
- Cassani, F., Gallango, O., Talukdar, S., Vallejos, C., Ehrmann, U. (1988). Methylphenanthrene maturity index of marine source rock extracts and crude oils from the Maracaibo Basin. *Organic geochemistry*, 13, 73-80.
- Cavanaugh, C. M., Levering, P. R., Maki, J. S., Mitchell, R., Lidstrom, M. E. (1987). Symbiosis of methylotrophic bacteria and deep-sea mussels. *Nature*, 325, 346-348.
- Charlou, J. L., Dmitriev, L., Bougault, H., Needham, H. D. (1988). Hydrothermal CH<sub>4</sub> between 12°N and 15°N over the Mid-Atlantic Ridge. *Deep Sea Research Part A. Oceanographic Research Papers*, 35, 121-131.
- Charlou, J. L., & Donval, J. P. (1993). Hydrothermal methane venting between 12°N and 26°N along the Mid-Atlantic Ridge. *Journal of Geophysical Research*, 98, 9625-9642.
- Charlou, J. L., Fouquet, Y., Bougault, H., Donval, J. P., Etoubleau, J., Jean-Baptiste, P., Dapigny, A., Appriou, P., Rona, P. A. (1998). Intense CH<sub>4</sub> plumes generated by serpentinization of ultramafic rocks at the intersection of the 15°20'N fracture zone and the Mid-Atlantic Ridge. *Geochimica et Cosmochimica Acta*, 62, 2323-2333.
- Charlou, J. L., Donval, J. P., Fouquet, Y., Jean-Baptiste, P., Holm, N. (2002). Geochemistry of high H<sub>2</sub> and CH<sub>4</sub> vent fluids issuing from ultramafic rocks at the Rainbow hydrothermal field (36°14'N, MAR). *Chemical Geology*, 191, 345-359.
- Charlou, J. L., Donval, J. P., Konn, C., Ondréas, H., Fouquet, Y., Jean-Baptiste, P., Fourré, E. (2010). High production and fluxes of H<sub>2</sub> and CH<sub>4</sub> and evidence of abiotic hydrocarbon synthesis by serpentinization in ultramafic-hosted hydrothermal systems on the Mid-Atlantic Ridge. *Diversity of Hydrothermal Systems on Slow Spreading Ocean Ridges*, 265-296.
- Cherkashov, G., Poroshina, I., Stepanova, T., Ivanov, V., Bel'Tenev, V., Lazareva, L., Rozhdestvenskaya, I., Samovarov, M., Shilov, V., Glasby, G. (2010). Seafloor massive sulfides from the northern equatorial Mid-Atlantic Ridge: New discoveries and perspectives. *Marine Georesources and Geotechnology*, 28, 222-239.
- Childress, J. J., Fisher, C., Brooks, J., Kennicutt, M., Bidigare, R., Anderson, A. (1986). A methanotrophic marine molluscan (*Bivalvia*, *Mytilidae*) symbiosis: Mussels fueled by gas. *Science (Washington)*, 233, 1306-1308.
- Christensen, N. I. (1972). The abundance of serpentinites in the oceanic crust. *The Journal of Geology*, 709-719.

- Coleman, M., Raiswell, R., Brown, A., Curtis, C., Aplin, A., Ortoleva, P., Gruszczynski, M., Lyons, T., Lovley, D., Eglinton, G. (1993). Microbial mineralization of organic matter: mechanisms of self-organization and inferred rates of precipitation of diagenetic minerals [and Discussion]. *Philosophical Transactions of the Royal Society of London A: Mathematical, Physical and Engineering Sciences*, 344, 69-87.
- Coleman, R. (1971). Plate tectonic emplacement of upper mantle peridotites along continental edges. *Journal of Geophysical Research*, 76, 1212-1222.
- Coleman, R., & Keith, T. (1971). A chemical study of serpentinization—Burro Mountain, California. *Journal of Petrology*, 12, 311-328.
- Colombo, J. C., Pelletier, E., Brochu, C., Khalil, M., Catoggio, J. A. (1989). Determination of hydrocarbon sources using n-alkane and polyaromatic hydrocarbon distribution indexes. Case study: Rio de la Plata estuary, Argentina. *Environmental Science & Technology*, 23, 888-894.
- Connelly, D. P., Copley, J. T., Murton, B. J., Stansfield, K., Tyler, P. A., German, C. R., Van Dover, C. L., Amon, D., Furlong, M., Grindlay, N. (2012). Hydrothermal vent fields and chemosynthetic biota on the world's deepest seafloor spreading centre. *Nature communications*, 3, 620.
- Cooper, C. J. 2010. "Anomalous bathymetry and mass heterogeneity at the conjugate Iberia and Newfoundland rifted margins." University of Liverpool.
- Craig, H. (1957). Isotopic standards for carbon and oxygen and correction factors for mass-spectrometric analysis of carbon dioxide. *Geochimica et Cosmochimica Acta*, 12, 133-149.
- Crespo-Medina, M., Meile, C., Hunter, K., Diercks, A., Asper, V., Orphan, V., Tavormina, P., Nigro, L., Battles, J., Chanton, J. (2014). The rise and fall of methanotrophy following a deepwater oil-well blowout. *Nature Geoscience*, 7, 423-427.
- Damsté, J. S. S., Kenig, F., Koopmans, M. P., Köster, J., Schouten, S., Hayes, J., de Leeuw, J. W. (1995). Evidence for gammacerane as an indicator of water column stratification. *Geochimica et Cosmochimica Acta*, 59, 1895-1900.
- Damsté, J. S. S., Schouten, S., Hopmans, E. C., van Duin, A. C., Geenevasen, J. A. (2002). Crenarchaeol the characteristic core glycerol dibiphytanyl glycerol tetraether membrane lipid of cosmopolitan pelagic crenarchaeota. *Journal of Lipid Research*, 43, 1641-1651.
- De La Torre-Roche, R. J., Lee, W.-Y., Campos-Díaz, S. I. (2009). Soil-borne polycyclic aromatic hydrocarbons in El Paso, Texas: Analysis of a potential problem in the United States/Mexico border region. *Journal of Hazardous Materials*, 163, 946-958.
- de Ronde, C. E., Baker, E. T., Massoth, G. J., Lupton, J. E., Wright, I. C., Feely, R. A., Greene, R. R. (2001). Intra-oceanic subduction-related hydrothermal venting, Kermadec volcanic arc, New Zealand. *Earth and Planetary Science Letters*, 193, 359-369.
- De Rosa, M., & Gambacorta, A. (1988). The lipids of archaebacteria. *Progress in lipid research*, 27, 153-175.

- Deer, W. A., Howie, R. A., Zussman, J., (1992), An introduction to the rock-forming minerals pp.). Longman London.
- Deguchi, S., & Tsujii, K. (2007). Supercritical water: a fascinating medium for soft matter. *Soft Matter*, 3, 797-803.
- Delacour, A., Früh-Green, G. L., Bernasconi, S. M., Kelley, D. S. (2008a). Sulfur in peridotites and gabbros at Lost City (30 N, MAR): Implications for hydrothermal alteration and microbial activity during serpentinization. *Geochimica et Cosmochimica Acta*, 72, 5090-5110.
- Delacour, A., Früh-Green, G. L., Bernasconi, S. M., Schaeffer, P., Kelley, D. S. (2008b). Carbon geochemistry of serpentinites in the Lost City Hydrothermal System (30 N, MAR). *Geochimica et Cosmochimica Acta*, 72, 3681-3702.
- Delacour, A., Früh-Green, G. L., Bernasconi, S. M., Schaeffer, P., Kelley, D. S. (2008c). Carbon geochemistry of serpentinites in the Lost City Hydrothermal System (30°N, MAR). *Geochimica et Cosmochimica Acta*, 72, 3681-3702.
- Delacour, A., Früh-Green, G. L., Frank, M., Gutjahr, M., Kelley, D. S. (2008d). Sr-and Nd-isotope geochemistry of the Atlantis Massif (30 N, MAR): implications for fluid fluxes and lithospheric heterogeneity. *Chemical Geology*, 254, 19-35.
- Des Marais, D. J. (2001). Isotopic evolution of the biogeochemical carbon cycle during the Precambrian. *Reviews in mineralogy and geochemistry*, 43, 555-578.
- Desbruyères, D., Biscoito, M., Caprais, J. C., Colaço, A., Comtet, T., Crassous, P., Fouquet, Y., Khripounoff, A., Le Bris, N., Olu, K., Riso, R., Sarradin, P. M., Segonzac, M., Vangriesheim, A. (2001). Variations in deep-sea hydrothermal vent communities on the Mid-Atlantic Ridge near the Azores plateau. *Deep Sea Research Part I: Oceanographic Research Papers*, 48, 1325-1346.
- Deschamps, F., Guillot, S., Godard, M., Chauvel, C., Andreani, M., Hattori, K. (2010). In situ characterization of serpentinites from forearc mantle wedges: timing of serpentinization and behavior of fluid-mobile elements in subduction zones. *Chemical Geology*, 269, 262-277.
- Deschamps, F., Godard, M., Guillot, S., Chauvel, C., Andreani, M., Hattori, K., Wunder, B., France, L. (2012). Behavior of fluid-mobile elements in serpentines from abyssal to subduction environments: examples from Cuba and Dominican Republic. *Chemical Geology*, 312, 93-117.
- Deschamps, F., Godard, M., Guillot, S., Hattori, K. (2013). Geochemistry of subduction zone serpentinites: A review. *Lithos*, 178, 96-127.
- Desmurs, L., Manatschal, G., Bernoulli, D. (2001). The Steinmann trinity revisited: mantle exhumation and magmatism along an ocean- continent transition: the Platta nappe, eastern Switzerland. *the geological society of london*, 235-266.
- Desmurs, L., Müntener, O., Manatschal, G. (2002). Onset of magmatic accretion within a magma-poor rifted margin: a case study from the Platta ocean-continent transition, eastern Switzerland. *Contributions to Mineralogy and Petrology*, 144, 365-382.

- Devey, C., Lackschewitz, K., Baker, E. (2005). Hydrothermal and volcanic activity found on the southern Mid-Atlantic Ridge. *Eos*, 86, 209.
- Dewey, J. F., & Bird, J. M. (1970). Mountain belts and the new global tectonics. *Journal of Geophysical Research*, 75, 2625-2647.
- Dias, A., Mills, R., Da Costa, I. R., Costa, R., Taylor, R., Cooper, M., Barriga, F. (2010). Tracing fluid–rock reaction and hydrothermal circulation at the Saldanha hydrothermal field. *Chemical Geology*, 273, 168-179.
- Dias, A., Früh-Green, G., Bernasconi, S., Barriga, F. (2011). Geochemistry and stable isotope constraints on high-temperature activity from sediment cores of the Saldanha hydrothermal field. *Marine geology*, 279, 128-140.
- Dias, Á. S., & Barriga, F. J. (2006). Mineralogy and geochemistry of hydrothermal sediments from the serpentinite-hosted Saldanha hydrothermal field (36° 34' N; 33° 26' W) at MAR. *Marine geology*, 225, 157-175.
- Dick, H. J., Lin, J., Schouten, H. (2003). An ultraslow-spreading class of ocean ridge. *Nature*, 426, 405-12.
- Dickson, J. (1965). A modified staining technique for carbonates in thin section. *Nature*, 205, 587-587.
- Dietrich, V., (1970), Die Stratigraphie der Platta-Decke: Fazielle Zusammenhänge zwischen Oberpenninikum und Unterostalpin pp.). Geologisches Institut der Eidg. Technischen Hochschule und der Universität Zürich.
- Dietrich, V., (1972), Die sulfidischen Vererzungen in den Oberhalbsteiner Serpentinitten: ein Beitrag zur Kenntnis der alpinen Metamorphosen und des Gebirgsbaues im südlichen Graubünden (128 pp.). Schweiz: Kümmerly & Frey.
- Diment, W. H. (1964). Thermal conductivity of serpentinite from Mayaguez, Puerto Rico, and other localities. *National Academy of Sciences, National Research Council Publication*, 1188, 92-106.
- Dix, G. R., & Mullins, H. T. (1992). Shallow-burial diagenesis of deep-water carbonates, northern Bahamas: Results from deep-ocean drilling transects. *Geological Society of America Bulletin*, 104, 303-315.
- Douville, E., Charlou, J., Oelkers, E., Bienvu, P., Colon, C. J., Donval, J., Fouquet, Y., Prieur, D., Appriou, P. (2002). The rainbow vent fluids (36° 14' N, MAR): the influence of ultramafic rocks and phase separation on trace metal content in Mid-Atlantic Ridge hydrothermal fluids. *Chemical Geology*, 184, 37-48.
- Dunlop, D. J., & Prévot, M. (1982). Magnetic properties and opaque mineralogy of drilled submarine intrusive rocks. *Geophysical Journal International*, 69, 763-802.
- Dyment, J., & Arkani-Hamed, J. (1995). Spreading-rate-dependent magnetization of the oceanic lithosphere inferred from the anomalous skewness of marine magnetic anomalies. *Geophysical Journal International*, 121, 789-804.

- Dyment, J., Arkani-Hamed, J., Ghods, A. (1997). Contribution of serpentized ultramafics to marine magnetic anomalies at slow and intermediate spreading centres: insights from the shape of the anomalies. *Geophysical Journal International*, 129, 691-701.
- Ehlmann, B., Mustard, J., Murchie, S. (2010). Geologic setting of serpentine deposits on Mars. *Geophysical Research Letters*, 37.
- El Diasty, W. S., & Moldowan, J. (2012). Application of biological markers in the recognition of the geochemical characteristics of some crude oils from Abu Gharadig Basin, north Western Desert–Egypt. *Marine and Petroleum Geology*, 35, 28-40.
- El Diasty, W. S., Ghonaim, A. A., Mostafa, A., El Beialy, S., Edwards, K. (2016). Biomarker characteristics of the Turonian–Eocene succession, Belayim oilfields, central Gulf of Suez, Egypt. *Journal of the Association of Arab Universities for Basic and Applied Sciences*, 19, 91-100.
- El Nady, M. M., Harb, F. M., Mohamed, N. S. (2014). Biomarker characteristics of crude oils from Ashrafi and GH oilfields in the Gulf of Suez, Egypt: An implication to source input and paleoenvironmental assessments. *Egyptian Journal of Petroleum*, 23, 455-459.
- Elvert, M., Suess, E., Greinert, J., Whiticar, M. J. (2000). Archaea mediating anaerobic methane oxidation in deep-sea sediments at cold seeps of the eastern Aleutian subduction zone. *Organic geochemistry*, 31, 1175-1187.
- Engström, A., Skelton, A., Grassineau, N. (2007). Isotopic and petrological evidence of fluid–rock interaction at a Tethyan ocean–continent transition in the Alps: implications for tectonic processes and carbon transfer during early ocean formation. *Geofluids*, 7, 401-414.
- Epin, M.-E., Manatschal, G., Amann, M. (2017). Defining diagnostic criteria to describe the role of rift inheritance in collisional orogens: the case of the Err-Platta nappes (Switzerland). *SJG*.
- Escartin, J., Hirth, G., Evans, B. (1997a). Nondilatant brittle deformation of serpentinites: Implications for Mohr-Coulomb theory and the strength of faults. *Journal of Geophysical Research: Solid Earth*, 102, 2897-2913.
- Escartin, J., Hirth, G., Evans, B. (1997b). Effects of serpentization on the lithospheric strength and the style of normal faulting at slow-spreading ridges. *Earth and Planetary Science Letters*, 151, 181-189.
- Escartin, J., Hirth, G., Evans, B. (2001). Strength of slightly serpentized peridotites: Implications for the tectonics of oceanic lithosphere. *Geology*, 29, 1023-1026.
- Escutia, C., Brinkhuis, H., Klaus, A., Scientists, E. (2010). Wilkes Land Glacial History: Cenozoic East Antarctic Ice Sheet evolution from Wilkes Land margin sediments. In (ed.), *Proceedings of the Integrated Ocean Drilling Program, Preliminary Reports*.
- Etioppe, G., & Klusman, R. W. (2002). Geologic emissions of methane to the atmosphere. *Chemosphere*, 49, 777-789.

- Etioppe, G., & Sherwood Lollar, B. (2013). Abiotic methane on Earth. *Reviews of Geophysics*, 51, 276-299.
- Etioppe, G., & Ionescu, A. (2014). Low-temperature catalytic CO<sub>2</sub> hydrogenation with geological quantities of ruthenium: a possible abiotic CH<sub>4</sub> source in chromitite-rich serpentinized rocks. *Geofluids*, 5, 438-452.
- Etioppe, G. (2015). Seepage in Serpentinised Peridotites and on Mars. In (ed.), *Natural Gas Seepage*, (pp.141-163): Springer.
- Evamy, B. (1969). The precipitational environment and correlation of some calcite cements deduced from artificial staining. *Journal of Sedimentary Research*, 39.
- Evans, B. W. (2004). The serpentinite multisystem revisited: chrysotile is metastable. *International Geology Review*, 46, 479-506.
- Evans, B. W., Hattori, K., Baronnet, A. (2013). Serpentinite: what, why, where? *Elements*, 9, 99-106.
- Fabiańska, M., Kozielska, B., Bielaczyc, P., Woodburn, J., Koniecznyński, J. (2016). Geochemical markers and polycyclic aromatic hydrocarbons in solvent extracts from diesel engine particulate matter. *Environmental Science and Pollution Research*, 23, 6999-7011.
- Fallon, E. K., Petersen, S., Brooker, R. A., Scott, T. B. (2017). Oxidative dissolution of hydrothermal mixed-sulphide ore: An assessment of current knowledge in relation to seafloor massive sulphide mining. *Ore Geology Reviews*.
- Farough, A., Moore, D., Lockner, D., Lowell, R. (2016). Evolution of fracture permeability of ultramafic rocks undergoing serpentinization at hydrothermal conditions: An experimental study. *Geochemistry, Geophysics, Geosystems*, 17, 44-55.
- Florineth, D., & Froitzheim, N. (1994). Transition from continental to oceanic basement in the Tasna Nappe (Engadine Window, Graubunden, Switzerland)-evidence for Early Cretaceous Opening of the Valais ocean. *Schweizerische Mineralogische und Petrographische Mitteilungen*, 74, 437-448.
- Flügel, E., (2013), *Microfacies of carbonate rocks: analysis, interpretation and application* (pp.). Springer Science & Business Media.
- Fontboté, L., Kouzmanov, K., Chiaradia, M., Pokrovski, G. S. (2017). Sulfide minerals in hydrothermal deposits. *Elements*, 13, 97-103.
- Fouquet, Y., Cherkashov, G., Charlou, J., Ondréas, H., Birot, D., Cannat, M., Bortnikov, N., Silantyev, S., Sudarikov, S., Cambon-Bonavita, M. (2008). Serpentine cruise-ultramafic hosted hydrothermal deposits on the Mid-Atlantic Ridge: First submersible studies on Ashadze 1 and 2, Logatchev 2 and Krasnov vent fields. *InterRidge News*, 17, 15-19.
- Fouquet, Y., Cambon, P., Etoubleau, J., Charlou, J. L., Ondréas, H., Barriga, F. J., Cherkashov, G., Semkova, T., Poroshina, I., Bohn, M. (2010). Geodiversity of Hydrothermal Processes Along the Mid-Atlantic Ridge and Ultramafic-Hosted Mineralization: a New

Type Of Oceanic Cu-Zn-Co-Au Volcanogenic Massive Sulfide Deposit. *Diversity of Hydrothermal Systems on Slow Spreading Ocean Ridges*, 321-367.

- France-Lanord, C., Spiess, V., Klaus, A., Adhikari, R., Adhikari, S., Bahk, J., Baxter, A., Cruz, J., Das, S., Dekens, P. (2016). International Ocean Discovery Program. *Proceedings of the International Ocean Discovery Program Volume 354*.
- Frazer, J. W., & Crawford, R. (1963). Modifications in the simultaneous determination of carbon, hydrogen, and nitrogen. *Microchimica Acta*, 51, 561-566.
- Friedman, I., & O'Neil, J. R., (1977), Data of geochemistry: Compilation of stable isotope fractionation factors of geochemical interest pp.). US Government Printing Office.
- Froitzheim, N., & Manatschal, G. (1996). Kinematics of Jurassic rifting, mantle exhumation, and passive-margin formation in the Austroalpine and Penninic nappes (eastern Switzerland). *Geological Society of America Bulletin*, 108, 1120-1133.
- Froitzheim, N., & Rubatto, D. (1998). Continental breakup by detachment faulting: field evidence and geochronological constraints (Tasna nappe, Switzerland). *terra nova*, 10, 171-176.
- Fruh-Green, G. L., Connolly, J. A. D., Plas, A., S.Kelley, D., Grobety, B. (2004). Serpentinization of Oceanic Peridotites: Implications for Geochemical Cycles and Biological Activity. *The Subseafloor Biosphere at Mid-Ocean Ridges Geophysical Monograph Series*, 144.
- Früh-Green, G. L., Weissert, H., Bernoulli, D. (1990). A multiple fluid history recorded in Alpine ophiolites. *Journal of the Geological Society*, 147, 959-970.
- Früh-Green, G. L., Kelley, D. S., Bernasconi, S. M., Karson, J. A., Ludwig, K. A., Butterfield, D. A., Boschi, C., Proskurowski, G. (2003). 30,000 years of hydrothermal activity at the Lost City vent field. *Science*, 301, 495-498.
- Früh-Green, G. L., Orcutt, B. N., Green, S., Cotterill, C., McCaig, A. (2016). Expedition 357 preliminary report: Atlantis Massif serpentinization and life. *International Ocean Discovery Program Preliminary reports*.
- Gabriel, J. L., & Chong, P. L. G. (2000). Molecular modeling of archaeobacterial bipolar tetraether lipid membranes. *Chemistry and Physics of Lipids*, 105, 193-200.
- Gagliano, A. L., D'Alessandro, W., Tagliavia, M., Parello, F., Quatrini, P. (2014). Methanotrophic activity and diversity of methanotrophs in volcanic geothermal soils at Pantelleria (Italy). *Biogeosciences*, 11, 5865-5875.
- Gardien, V., & Paquette, J. (2004). Ion microprobe and ID-TIMS U–Pb dating on zircon grains from leg 173 amphibolites: evidence for Permian magmatism on the West Iberian margin. *terra nova*, 16, 226-231.
- Garrigues, P., Budzinski, H., Manitz, M., Wise, S. (1995). Pyrolytic and petrogenic inputs in recent sediments: a definitive signature through phenanthrene and chrysene compound distribution. *Polycyclic Aromatic Compounds*, 7, 275-284.

- Gebruk, A. V., Galkin, S., Vereshchaka, A., Moskalev, L., Southward, A. (1997). Ecology and biogeography of the hydrothermal vent fauna of the Mid-Atlantic Ridge. In (ed.), *Advances in Marine Biology*, (pp.93-144): Elsevier.
- Geissman, T., Sim, K., Murdoch, J. (1967). Organic minerals. Picene and chrysene as constituents of the mineral curtisite (idrialite). *Cellular and Molecular Life Sciences*, 23, 793-794.
- German, C., Baker, E., Mevel, C., Tamaki, K. (1998). Hydrothermal activity along the southwest Indian ridge. *Nature*, 395, 490-493.
- German, C., Colley, S., Palmer, M., Khripounoff, A., Klinkhammer, G. (2002). Hydrothermal plume-particle fluxes at 13 N on the East Pacific Rise. *Deep Sea Research Part I: Oceanographic Research Papers*, 49, 1921-1940.
- Giardini, A., Subbarayudu, G. V., Melton, C. E. (1976). The emission of occluded gas from rocks as a function of stress: Its possible use as a tool for predicting earthquakes. *Geophysical Research Letters*, 3, 355-358.
- Gieskes, J. M., Kastner, M., Erzinger, J., Boulègue, J., Hart, S. R., 1986. Geochemistry, minerals, color, rare earth elements and d18O at DSDP Hole 92-504B. In *Supplement to: Gieskes, JM et al. (1986): Geochemical studies in Hole 504B, Leg 92. In: Leinen, M; Rea DK; et al. (eds.), Initial Reports of the Deep Sea Drilling Project, Washington (U.S. Govt. Printing Office), 92, 547-562, doi:10.2973/dsdp.proc.92.136.1986: PANGAEA.*
- Girguis, P. R., Cozen, A. E., DeLong, E. F. (2005). Growth and population dynamics of anaerobic methane-oxidizing archaea and sulfate-reducing bacteria in a continuous-flow bioreactor. *Applied and environmental microbiology*, 71, 3725-3733.
- Glein, C. R., Baross, J. A., Waite, J. H. (2015). The pH of Enceladus' ocean. *Geochimica et Cosmochimica Acta*, 162, 202-219.
- Glombitza, C., Adhikari, R. R., Riedinger, N., Gilhooly III, W. P., Hinrichs, K.-U., Inagaki, F. (2016). Microbial sulfate reduction potential in coal-bearing sediments down to ~ 2.5 km below the seafloor off Shimokita Peninsula, Japan. *Frontiers in microbiology*, 7.
- Gonçalves, P. A., Mendonça Filho, J. G., Mendonça, J. O., da Silva, T. F., Flores, D. (2013). Paleoenvironmental characterization of a Jurassic sequence on the Bombarral sub-basin (Lusitanian basin, Portugal): insights from palynofacies and organic geochemistry. *International Journal of Coal Geology*, 113, 27-40.
- Gràcia, E., Charlou, J. L., Radford-Knoery, J., Parson, L. M. (2000). Non-transform offsets along the Mid-Atlantic Ridge south of the Azores (38 N–34 N): ultramafic exposures and hosting of hydrothermal vents. *Earth and Planetary Science Letters*, 177, 89-103.
- Grantham, P. J., & Wakefield, L. L. (1988). Variations in the sterane carbon number distributions of marine source rock derived crude oils through geological time. *Organic geochemistry*, 12, 61-73.
- Grassle, J. F. (1987). The ecology of deep-sea hydrothermal vent communities. *Advances in Marine Biology*, 23, 301-362.

- Greenberger, R. N., Mustard, J. F., Cloutis, E. A., Pratt, L. M., Sauer, P. E., Mann, P., Turner, K., Dyar, M. D., Bish, D. L. (2015). Serpentinization, iron oxidation, and aqueous conditions in an ophiolite: Implications for hydrogen production and habitability on Mars. *Earth and Planetary Science Letters*, 416, 21-34.
- Groombridge, B., & Jenkins, M. D., (2000), Global biodiversity: Earth's living resources in the 21st century pp.). World Conservation Press.
- Grotzinger, J. P., & Kasting, J. F. (1993). New constraints on Precambrian ocean composition. *The Journal of Geology*, 101, 235-243.
- Grotzinger, J. P., & Knoll, A. H. (1999). Stromatolites in Precambrian carbonates: evolutionary mileposts or environmental dipsticks? *Annual Review of Earth and Planetary Sciences*, 27, 313-358.
- Guillot, S., & Hattori, K. (2013). Serpentinites: essential roles in geodynamics, arc volcanism, sustainable development, and the origin of life. *Elements*, 9, 95-98.
- Gurgey, K. (1999). Geochemical characteristics and thermal maturity of oils from the Thrace Basin (western Turkey) and western Turkmenistan. *Journal of Petroleum Geology*, 22, 167-189.
- Halama, R., Bebout, G. E., John, T., Scambelluri, M. (2014). Nitrogen recycling in subducted mantle rocks and implications for the global nitrogen cycle. *International Journal of Earth Sciences*, 103, 2081-2099.
- Haldeman, D., Amy, P., Russell, C., Jacobson, R. (1995). Comparison of drilling and mining as methods for obtaining microbiological samples from the deep subsurface. *Journal of microbiological methods*, 21, 305-316.
- Halevy, I., Johnston, D. T., Schrag, D. P. (2010). Explaining the structure of the Archean mass-independent sulfur isotope record. *Science*, 329, 204-207.
- Harder, J. (1997). Anaerobic methane oxidation by bacteria employing <sup>14</sup>C-methane uncontaminated with <sup>14</sup>C-carbon monoxide. *Marine geology*, 137, 13-23.
- Haroon, M. F., Hu, S., Shi, Y., Imelfort, M., Keller, J., Hugenholtz, P., Yuan, Z., Tyson, G. W. (2013). Anaerobic oxidation of methane coupled to nitrate reduction in a novel archaeal lineage. *Nature*, 500, 567-570.
- Harrison, S., & Rajakaruna, N., (2011), Serpentine: the evolution and ecology of a model system pp.). Univ of California Press.
- Hartnett, H. E., Keil, R. G., Hedges, J. I., Devol, A. H. (1998). Influence of oxygen exposure time on organic carbon preservation in continental margin sediments. *Nature*, 391, 572-575.
- Hattori, K. H., & Guillot, S. (2007). Geochemical character of serpentinites associated with high-to ultrahigh-pressure metamorphic rocks in the Alps, Cuba, and the Himalayas: Recycling of elements in subduction zones. *Geochemistry, Geophysics, Geosystems*, 8.

- Hayes, J. M., Freeman, K. H., Popp, B. N., Hoham, C. H. (1990). Compound-specific isotopic analyses: A novel tool for reconstruction of ancient biogeochemical processes. *Organic geochemistry*, 16, 1115-1128.
- Hayes, J. M., Strauss, H., Kaufman, A. J. (1999). The abundance of  $^{13}\text{C}$  in marine organic matter and isotopic fractionation in the global biogeochemical cycle of carbon during the past 800 Ma. *Chemical Geology*, 161, 103-125.
- Haymon, R. M. (1983). Hydrothermal deposition on the East Pacific Rise at 21 N. *Journal of Geochemical Exploration*, 19, 493-495.
- Haymon, R. M. (1989). Hydrothermal processes and products on the Galapagos Rift and East Pacific Rise. In D.M. Hussong E.L. Winterer, & R.W. Decker (ed.), *The Eastern Pacific Ocean and Hawaii*, (pp.125-144): Geological Society of America.
- Herzig, P. M., & Hannington, M. D. (1995). Polymetallic massive sulfides at the modern seafloor a review. *Ore Geology Reviews*, 10, 95-115.
- Heydari, E. (1997). Hydrotectonic models of burial diagenesis in platform carbonates based on formation water geochemistry in North American sedimentary basins. In I.P. Montanez, J.M. Gregg&K.L.Shelton (ed.), *Basin-wide diagenetic patterns: Integrated petrologic, geochemical and hydrologic considerations*, (pp.53-79): Society of Economic Paleontologists and Mineralogists, Special Publication
- Heymann, D., Jenneskens, L. W., Jehlicka, J., Koper, C., Vlietstra, E. J. (2003). Biogenic fullerenes? *International Journal of Astrobiology*, 2, 179-183.
- Hilaret, N., & Reynard, B. (2009). Stability and dynamics of serpentinite layer in subduction zone. *Tectonophysics*, 465, 24-29.
- Hinrichs, K.-U., Hayes, J. M., Sylva, S. P., Brewer, P. G., DeLong, E. F. (1999). Methane-consuming archaeobacteria in marine sediments. *Nature*, 398, 802-805.
- Hinrichs, K.-U., Summons, R. E., Orphan, V., Sylva, S. P., Hayes, J. M. (2000). Molecular and isotopic analysis of anaerobic methane-oxidizing communities in marine sediments. *Organic geochemistry*, 31, 1685-1701.
- Hinrichs, K.-U., & Boetius, A. (2002). The anaerobic oxidation of methane: new insights in microbial ecology and biogeochemistry. In (ed.), *Ocean margin systems*, (pp.457-477): Springer.
- Hinrichs, K. U. (2002). Microbial fixation of methane carbon at 2.7 Ga: Was an anaerobic mechanism possible? *Geochemistry, Geophysics, Geosystems*, 3, 1-10.
- Hirth, G., & Guillot, S. (2013). Rheology and tectonic significance of serpentinite. *Elements*, 9, 107-113.
- Hodgkinson, M. R., Webber, A. P., Roberts, S., Mills, R. A., Connelly, D. P., Murton, B. J. (2015). Talc-dominated seafloor deposits reveal a new class of hydrothermal system. *Nature communications*, 6.

- Hoehler, T. M., Alperin, M. J., Albert, D. B., Martens, C. S. (1994). Field and laboratory studies of methane oxidation in an anoxic marine sediment: Evidence for a methanogen-sulfate reducer consortium. *Global Biogeochemical Cycles*, 8, 451-463.
- Holm, N. G., & Andersson, E. M. (1998). Hydrothermal systems. *The molecular origins of life*, 86-99.
- Holm, N. G., & Charlou, J. L. (2001). Initial indications of abiotic formation of hydrocarbons in the Rainbow ultramafic hydrothermal system, Mid-Atlantic Ridge. *Earth and Planetary Science Letters*, 191, 1-8.
- Holm, N. G., Dumont, M., Ivarsson, M., Konn, C. (2006). Alkaline fluid circulation in ultramafic rocks and formation of nucleotide constituents: a hypothesis. *Geochemical Transactions*, 7, 1-13.
- Holm, N. G., Oze, C., Mousis, O., Waite, J., Guilbert-Lepoutre, A. (2015). Serpentinization and the formation of H<sub>2</sub> and CH<sub>4</sub> on celestial bodies (planets, moons, comets). *Astrobiology*, 15, 587-600.
- Hopmans, E. C., Schouten, S., Pancost, R. D., van der Meer, M. T., Sinninghe Damsté, J. S. (2000). Analysis of intact tetraether lipids in archaeal cell material and sediments by high performance liquid chromatography/atmospheric pressure chemical ionization mass spectrometry. *Rapid Communications in Mass Spectrometry*, 14, 585-589.
- Hopmans, E. C., Weijers, J. W., Schefuß, E., Herfort, L., Damsté, J. S. S., Schouten, S. (2004). A novel proxy for terrestrial organic matter in sediments based on branched and isoprenoid tetraether lipids. *Earth and Planetary Science Letters*, 224, 107-116.
- Horita, J. (1999). Abiogenic Methane Formation and Isotopic Fractionation Under Hydrothermal Conditions. *Science*, 285, 1055-1057.
- Hossain, H. Z., Sampei, Y., Roser, B. P. (2009). Characterization of organic matter and depositional environment of Tertiary mudstones from the Sylhet Basin, Bangladesh. *Organic geochemistry*, 40, 743-754.
- House, C. H., Cragg, B. A., Teske, A., Party, S. 2003. "Drilling contamination tests during ODP Leg 201 using chemical and particulate tracers." Proceedings of the Ocean Drilling Program, Initial reports.
- Huang, W.-Y., & Meinschein, W. (1979). Sterols as ecological indicators. *Geochimica et Cosmochimica Acta*, 43, 739-745.
- Hudson, J. (1977). Stable isotopes and limestone lithification. *Journal of the Geological Society*, 133, 637-660.
- Inagaki, F., Hinrichs, K., Kubo, Y. 2013. "the Expedition 337 Scientists." Proceedings of the Integrated Ocean Drilling Program.
- Jagoutz, O., Müntener, O., Manatschal, G., Rubatto, D., Péron-Pinvidic, G., Turrin, B. D., Villa, I. M. (2007). The rift-to-drift transition in the North Atlantic: A stuttering start of the MORB machine? *Geology*, 35, 1087-1090.

- Jamtveit, B., & Hammer, Ø. (2012a). Sculpting of rocks by reactive fluids. *Geochemical Perspectives*, 1, 341-342.
- Jamtveit, B., & Hammer, Ø., (2012b), Sculpting of rocks by reactive fluids (140 pp.). *Geochemical Perspectives*, v. 3.
- Johnsen, A. R., Wick, L. Y., Harms, H. (2005). Principles of microbial PAH-degradation in soil. *Environmental Pollution*, 133, 71-84.
- Jørgensen, B. B. (1982). Mineralization of organic matter in the sea bed—the role of sulphate reduction.
- Jørgensen, B. B. (2012). Shrinking majority of the deep biosphere. *Proceedings of the National Academy of Sciences*, 109, 15976-15977.
- Juniper, S. 2004. "Impact of the development of seafloor massive sulphides on the vent ecosystem." *Proceedings, International Seabed Authority Workshop, Jamaica, Minerals other than polymetallic nodules of the International Seabed Area.*
- Kahl, W.-A., Jöns, N., Bach, W., Klein, F., Alt, J. C. (2015). Ultramafic clasts from the South Chamorro serpentine mud volcano reveal a polyphase serpentinization history of the Mariana forearc mantle. *Lithos*, 227, 1-20.
- Kaiho, K., Saito, R., Ito, K., Miyaji, T., Biswas, R., Tian, L., Sano, H., Shi, Z., Takahashi, S., Tong, J. (2016). Effects of soil erosion and anoxic–euxinic ocean in the Permian–Triassic marine crisis. *Heliyon*, 2, e00137.
- Kalyuzhnaya, M. G., Puri, A. W., Lidstrom, M. E. (2015). Metabolic engineering in methanotrophic bacteria. *Metabolic engineering*, 29, 142-152.
- Kamali, M. R., Abolghasemi, A., Bagheri, R., Kadkhodayi, A. (2013). Petroleum geochemistry and oil–oil correlation of the Fahliyan and Surmeh reservoirs in the Garangan and Chilingar oilfields, the Dezful embayment (Sw Iran). *Journal of Petroleum Exploration and Production Technology*, 3, 85-92.
- Kawka, O. E., & Simoneit, B. R. (1990a). Polycyclic aromatic hydrocarbons in hydrothermal petroleum from the Guaymas Basin spreading center. *Applied Geochemistry*, 5, 17-27.
- Kawka, O. E., & Simoneit, B. R. T. 1990b. "Polycyclic aromatic hydrocarbons in hydrothermal petroleum from the Guaymas Basin spreading center." *Applied Geochemistry*.
- Kelemen, P. B., & Hirth, G. (2012). Reaction-driven cracking during retrograde metamorphism: Olivine hydration and carbonation. *Earth and Planetary Science Letters*, 345, 81-89.
- Kelley, D. S., & Delaney, J. R. (1987). Two-phase separation and fracturing in mid-ocean ridge gabbros at temperatures greater than 700 C. *Earth and Planetary Science Letters*, 83, 53-66.
- Kelley, D. S. (2001). Black smokers: incubators on the seafloor. *Earth: Inside and Out*, 183-189.

- Kelley, D. S., Karson, J. A., Blackman, D. K., Fruh-Green, G. L., Butterfield, D. A., Lilley, M. D., Olson, E. J., Schrenk, M. O., Roe, K. K., Lebon, G. T., Rivizzigno, P., the, A. T. S. P. (2001). An off-axis hydrothermal vent field near the Mid-Atlantic Ridge at 30[deg] N. *Nature*, 412, 145-149.
- Kelley, D. S., Karson, J. A., Früh-Green, G. L., Yoerger, D. R., Shank, T. M., Butterfield, D. A., Hayes, J. M., Schrenk, M. O., Olson, E. J., Proskurowski, G. (2005). A serpentinite-hosted ecosystem: the Lost City hydrothermal field. *Science*, 307, 1428-1434.
- Kelley, D. S., & Shank, T. M. (2010). Hydrothermal systems: A decade of discovery in slow spreading environments. In C. W. Devey P. A. Rona, J. Dymont and B. J. Murton (ed.), *Diversity of Hydrothermal Systems on Slow Spreading Ocean Ridges*, (pp.369-407) Washington: American Geophysical Union.
- Kendrick, M. A., Scambelluri, M., Honda, M., Phillips, D. (2011). High abundances of noble gas and chlorine delivered to the mantle by serpentinite subduction. *Nature Geoscience*, 4, 807-812.
- Kennedy, M. J., Pevear, D. R., Hill, R. J. (2002). Mineral surface control of organic carbon in black shale. *Science*, 295, 657-660.
- Kessler, J. D., Valentine, D. L., Redmond, M. C., Du, M., Chan, E. W., Mendes, S. D., Quiroz, E. W., Villanueva, C. J., Shusta, S. S., Werra, L. M. (2011). A persistent oxygen anomaly reveals the fate of spilled methane in the deep Gulf of Mexico. *Science*, 331, 312-315.
- Killops, S., & Massoud, M. (1992). Polycyclic aromatic hydrocarbons of pyrolytic origin in ancient sediments: evidence for Jurassic vegetation fires. *Organic geochemistry*, 18, 1-7.
- Kim, S., Thiessen, P. A., Bolton, E. E., Chen, J., Fu, G., Gindulyte, A., Han, L., He, J., He, S., Shoemaker, B. A. (2015). PubChem substance and compound databases. *Nucleic acids research*, 44, D1202-D1213.
- Kiriakoulakis, K. 1997. "Organic geochemistry of early diagenetic concretions." EOES, PhD (350).
- Knittel, K., & Boetius, A. (2009). Anaerobic oxidation of methane: progress with an unknown process. *Annual review of microbiology*, 63, 311-334.
- Konn, C., Charlou, J.-L., Donval, J.-P., Holm, N., Dehairs, F., Bouillon, S. (2009). Hydrocarbons and oxidized organic compounds in hydrothermal fluids from Rainbow and Lost City ultramafic-hosted vents. *Chemical Geology*, 258, 299-314.
- Koschinsky, A. (2006). Discovery of new hydrothermal vents on the southern Mid-Atlantic Ridge (4° S-10° S) during cruise M 68/1. *InterRidge News*, 15, 9-15.
- Koschinsky, A., Garbe-Schönberg, D., Sander, S., Schmidt, K., Gennerich, H.-H., Strauss, H. (2008). Hydrothermal venting at pressure-temperature conditions above the critical point of seawater, 5 S on the Mid-Atlantic Ridge. *Geology*, 36, 615-618.

- Kuypers, M. M., Blokker, P., Erbacher, J., Kinkel, H., Pancost, R. D., Schouten, S., Damsté, J. S. S. (2001). Massive expansion of marine archaea during a mid-Cretaceous oceanic anoxic event. *Science*, 293, 92-95.
- Labonté, J. M., Lever, M. A., Edwards, K. J., Orcutt, B. N. (2017). Influence of Igneous Basement on Deep Sediment Microbial Diversity on the Eastern Juan de Fuca Ridge Flank. *Frontiers in microbiology*, 8.
- Lamadrid, H., Rimstidt, J. D., Schwarzenbach, E. M., Klein, F., Ulrich, S., Dolocan, A., Bodnar, R. J. (2017). Effect of water activity on rates of serpentinization of olivine.
- Lang, S. Q., Butterfield, D. A., Schulte, M., Kelley, D. S., Lilley, M. D. (2010). Elevated concentrations of formate, acetate and dissolved organic carbon found at the Lost City hydrothermal field. *Geochimica et Cosmochimica Acta*, 74, 941-952.
- Larson, B. I., Houghton, J. L., Lowell, R. P., Farough, A., Meile, C. D. (2015). Subsurface conditions in hydrothermal vents inferred from diffuse flow composition, and models of reaction and transport. *Earth and Planetary Science Letters*, 424, 245-255.
- Lavier, L. L., Roger Buck, W., Poliakov, A. N. (1999). Self-consistent rolling-hinge model for the evolution of large-offset low-angle normal faults. *Geology*, 27, 1127-1130.
- Lemoine, M., Tricart, P., Boillot, G. (1987). Ultramafic and gabbroic ocean floor of the Ligurian Tethys (Alps, Corsica, Apennines): In search of a genetic model. *Geology*, 15, 622-625.
- Lever, M. A., Alperin, M., Engelen, B., Inagaki, F., Nakagawa, S., Steinsbu, B. r. O., Teske, A., Scientists, I. E. (2006). Trends in basalt and sediment core contamination during IODP Expedition 301. *Geomicrobiology Journal*, 23, 517-530.
- Lewis, A. D., & Smewing, J. D. (1980). The Montgenevre ophiolite (Hautes Alpes, France): Meta—morphism and trace-element geochemistry of the volcanic sequence. *Chemical Geology*, 28, 291-306.
- Li, X.-H., Faure, M., Lin, W., Manatschal, G. (2013). New isotopic constraints on age and magma genesis of an embryonic oceanic crust: The Chenaillet Ophiolite in the Western Alps. *Lithos*, 160-161, 283-291.
- Little, C. T., Cann, J. R., Herrington, R. J., Morisseau, M. (1999). Late Cretaceous hydrothermal vent communities from the Troodos ophiolite, Cyprus. *Geology*, 27, 1027-1030.
- Ludwig, K. A., Kelley, D. S., Butterfield, D. A., Nelson, B. K., Früh-Green, G. (2006). Formation and evolution of carbonate chimneys at the Lost City Hydrothermal Field. *Geochimica et Cosmochimica Acta*, 70, 3625-3645.
- Macdonald, K. C., Becker, K., Spiess, F. N., Ballard, R. D. (1980). Hydrothermal heat flux of the “black smoker” vents on the East Pacific Rise. *Earth and Planetary Science Letters*, 48, 1-7.
- Mackay, D., & Callcott, D. (1998). Partitioning and physical chemical properties of PAHs. In (ed.), *PAHs and Related Compounds*, (pp.325-345): Springer.

- Mackenzie, A., Patience, R., Maxwell, J., Vandenbroucke, M., Durand, B. (1980). Molecular parameters of maturation in the Toarcian shales, Paris Basin, France—I. Changes in the configurations of acyclic isoprenoid alkanes, steranes and triterpanes. *Geochimica et Cosmochimica Acta*, 44, 1709-1721.
- Magi, E., Bianco, R., Ianni, C., Di Carro, M. (2002). Distribution of polycyclic aromatic hydrocarbons in the sediments of the Adriatic Sea. *Environmental Pollution*, 119, 91-98.
- Manatschal, G., & Nievergelt, P. (1997). A continent-ocean transition recorded in the Err and Platta nappes (Eastern Switzerland). *Eclogae Geologicae Helvetiae*, 90, 3-28.
- Manatschal, G., & Bernoulli, D. (1999). Architecture and tectonic evolution of nonvolcanic margins: Present-day Galicia and ancient Adria. *Tectonics*, 18, 1099-1119.
- Manatschal, G., Froitzheim, N., Rubenach, M., Turrin, B. D. (2001). The role of detachment faulting in the formation of an ocean-continent transition: insights from the Iberia Abyssal Plain. *Geological Society, London, Special Publications*, 187, 405-428.
- Manatschal, G., Muntener, O., Desmurs, L., Bernoulli, D. (2003). An ancient ocean-continent transition in the Alps: the Totalp, Err-Platta, and Malenco units in the eastern Central Alps (Graubünden and northern Italy). *Eclogae Geologicae Helvetiae*, 96, 131-146.
- Manatschal, G., Engström, A., Desmurs, L., Schaltegger, U., Cosca, M., Muntener, O., Bernoulli, D. (2006). What is the tectono-metamorphic evolution of continental break-up: The example of the Tasna Ocean–Continent Transition. *Journal of Structural Geology*, 28, 1849-1869.
- Manatschal, G., Muntener, O., Lavier, L. L., Minshall, T. A., Peron-Pinvidic, G. (2007). Observations from the Alpine Tethys and Iberia Newfoundland margins pertinent to the interpretation of continental breakup. *Geological Society, London, Special Publications*, 282, 291-324.
- Manatschal, G., E.Sutra, G.Peron-Pinvidic. (2009). The lesson from the Iberia-Newfoundland rifted margins: how applicable is it to other rifted margins? , 2, 27-37.
- Manatschal, G., & Muntener, O. (2009). A type sequence across an ancient magma-poor ocean–continent transition: the example of the western Alpine Tethys ophiolites. *Tectonophysics*, 473, 4-19.
- Manatschal, G., Sauter, D., Karpoff, A. M., Masini, E., Mohn, G., Lagabrielle, Y. (2011). The Chenaillet Ophiolite in the French/Italian Alps: An ancient analogue for an Oceanic Core Complex? *Lithos*, 124, 169-184.
- Marcaillou, C., Muñoz, M., Vidal, O., Parra, T., Harfouche, M. (2011). Mineralogical evidence for H<sub>2</sub> degassing during serpentinization at 300°C/300bar. *Earth and Planetary Science Letters*, 303, 281-290.
- Marcaillou, C. 2012. "Serpentinisation et production d'hydrogène en contexte de dorsale lente : approche expérimentale et numérique." Docteur, Institut des sciences de la Terre (ISTerre, Grenoble).

- Martin, W., Baross, J., Kelley, D., Russell, M. J. (2008). Hydrothermal vents and the origin of life. *Nature Reviews Microbiology*, 6, 805-814.
- Masini, E., Manatschal, G., Mohn, G., Weissert, H. (2013). The Alpine Tethys rifted margins: Reconciling old and new ideas to understand the stratigraphic architecture of magma-poor rifted margins. *Sedimentology*, 60, 174-196.
- Masini, E., Manatschal, G., Tugend, J., Mohn, G., Flament, J.-M. (2014). The tectono-sedimentary evolution of a hyper-extended rift basin: the example of the Arzacq–Mauléon rift system (Western Pyrenees, SW France). *International Journal of Earth Sciences*, 103, 1569-1596.
- Mateeva, T., Wolff, G. A., Manatschal, G., Picazo, S., Kuszniir, N. J., Wheeler, J. (2017). Preserved organic matter in a fossil Ocean Continent Transition in the Alps: the example of Totalp, SE Switzerland. *Swiss Journal of Geosciences*, 1-22.
- Mauffret, A., & Montadert, L. 1988. "Seismic stratigraphy off Galicia." Proc. Ocean Drill. Program Sci. Results.
- McCollom, T. M., & Shock, E. L. (1997). Geochemical constraints on chemolithoautotrophic metabolism by microorganisms in seafloor hydrothermal systems. *Geochimica et Cosmochimica Acta*, 61, 4375-4391.
- McCollom, T. M., & Seewald, J. S. (2006). Carbon isotope composition of organic compounds produced by abiotic synthesis under hydrothermal conditions. *Earth and Planetary Science Letters*, 243, 74-84.
- McCollom, T. M., & Bach, W. (2009). Thermodynamic constraints on hydrogen generation during serpentinization of ultramafic rocks. *Geochimica et Cosmochimica Acta*, 73, 856-875.
- McCollom, T. M. (2013). Laboratory simulations of abiotic hydrocarbon formation in Earth's deep subsurface. *Reviews in Mineralogy & Geochemistry*, 75, 467-494.
- McCollom, T. M., & Seewald, J. S. (2013). Serpentinites, Hydrogen, and Life. *Elements*, 9, 129-134.
- McCollom, T. M., & Donaldson, C. (2016). Generation of Hydrogen and Methane during Experimental Low-Temperature Reaction of Ultramafic Rocks with Water. *Astrobiology*, 16, 389-406.
- McCrea, J. M. (1950). On the isotopic chemistry of carbonates and a paleotemperature scale. *The Journal of Chemical Physics*, 18, 849-857.
- McDermott, J. M., Seewald, J. S., German, C. R., Sylva, S. P. (2015). Pathways for abiotic organic synthesis at submarine hydrothermal fields. *Proceedings of the National Academy of Sciences*, 112, 7668-7672.
- McGrath, T. E., Chan, W. G., Hajaligol, M. R. (2003). Low temperature mechanism for the formation of polycyclic aromatic hydrocarbons from the pyrolysis of cellulose. *Journal of Analytical and Applied Pyrolysis*, 66, 51-70.

- Melchert, B., Devey, C. W., German, C., Lackschewitz, K., Seifert, R., Walter, M., Mertens, C., Yoerger, D., Baker, E., Paulick, H. (2008). First evidence for high-temperature off-axis venting of deep crustal/mantle heat: The Nibelungen hydrothermal field, southern Mid-Atlantic Ridge. *Earth and Planetary Science Letters*, 275, 61-69.
- Ménez, B., Pasini, V., Brunelli, D. (2012). Life in the hydrated suboceanic mantle. *Nature Geoscience*, 5, 133-137.
- Mevel, C., Caby, R., Kienast, J.-R. (1978). Amphibolite facies conditions in the oceanic crust: Example of amphibolitized flaser-gabbro and amphibolites from the Chenaillet ophiolite massif (Hautes Alpes, France). *Earth and Planetary Science Letters*, 39, 98-108.
- Mével, C. (2003). Serpentinization of abyssal peridotites at mid-ocean ridges. *Comptes Rendus Geoscience*, 335, 825-852.
- Meyers, P. A., & Snowdon, L. R. (1993). Types and Thermal Maturity of Organic Matter Accumulated During Early Cretaceous Subsidence of the Exmouth Plateau, Northwest Australian Margin: Chapter 8.
- Meyers, P. A. (1994). Preservation of elemental and isotopic source identification of sedimentary organic matter. *Chemical Geology*, 114, 289-302.
- Meyers, P. A., & Shaw, T. J. 1996. "Organic Matter Accumulation, Sulfate Reduction, and Methanogenesis in Pliocene–Pleistocene Turbidites on the Iberia Abyssal Plain." Proceedings of the Ocean Drilling Program, Scientific Results.
- Michaelis, W., Seifert, R., Nauhaus, K., Treude, T., Thiel, V., Blumenberg, M., Knittel, K., Gieseke, A., Peterknecht, K., Pape, T., Boetius, A., Amann, R., Jørgensen, B. B., Widdel, F., Peckmann, J., Pimenov, N. V., Gulin, M. B. (2002). Microbial Reefs in the Black Sea Fueled by Anaerobic Oxidation of Methane. *Science*, 297, 1013-1015.
- Miller, D. J., & Christensen, N. I. 1997. "Seismic velocities of lower crustal and upper mantle rocks from the slow-spreading Mid-Atlantic Ridge, south of the Kane Transform Zone (MARK)." Proceedings of the Ocean Drilling Program. Scientific results.
- Mißbach, H., Duda, J.-P., Lünsdorf, N., Schmidt, B., Thiel, V. (2016). Testing the preservation of biomarkers during experimental maturation of an immature kerogen. *International Journal of Astrobiology*, 15, 165-175.
- Mohn, G., Manatschal, G., Müntener, O., Beltrando, M., Masini, E. (2010). Unravelling the interaction between tectonic and sedimentary processes during lithospheric thinning in the Alpine Tethys margins. *International Journal of Earth Sciences*, 99, 75-101.
- Mohn, G., Manatschal, G., Beltrando, M., Masini, E., Kuszniir, N. (2012). Necking of continental crust in magma-poor rifted margins: Evidence from the fossil Alpine Tethys margins. *Tectonics*, 31.
- Montgomery, H., & Kerr, A. C. (2009). Rethinking the origins of the red chert at La Désirade, French West Indies. *Geological Society, London, Special Publications*, 328, 457-467.

- Moore, D. E., Lockner, D., Summers, R., Shengli, M., Byerlee, J. (1996). Strength of chrysotile-serpentine gouge under hydrothermal conditions: Can it explain a weak San Andreas fault? *Geology*, 24, 1041-1044.
- Morita, R. (1999). Is H<sub>2</sub> the universal energy source for long-term survival? *Microbial ecology*, 38, 307-320.
- Motelay-Massei, A., Ollivon, D., Garban, B., Tiphagne-Larcher, K., Zimmerlin, I., Chevreuril, M. (2007). PAHs in the bulk atmospheric deposition of the Seine river basin: source identification and apportionment by ratios, multivariate statistical techniques and scanning electron microscopy. *Chemosphere*, 67, 312-321.
- Mottl, M. J., Komor, S. C., Fryer, P., Moyer, C. L. (2003). Deep-slab fluids fuel extremophilic Archaea on a Mariana forearc serpentinite mud volcano: Ocean Drilling Program Leg 195. *Geochemistry, Geophysics, Geosystems*, 4, 1525-2027.
- Muehlenbachs, K. (1986). Alteration of the oceanic crust and the 18 O history of seawater. *Reviews in mineralogy and geochemistry*, 16, 425-444.
- Müller, P. (1977). CN ratios in Pacific deep-sea sediments: Effect of inorganic ammonium and organic nitrogen compounds sorbed by clays. *Geochimica et Cosmochimica Acta*, 41, 765-776.
- Müller, P. J., Kirst, G., Ruhland, G., Von Storch, I., Rosell-Melé, A. (1998). Calibration of the alkenone paleotemperature index U<sub>37</sub>K' based on core-tops from the eastern South Atlantic and the global ocean (60 N-60 S). *Geochimica et Cosmochimica Acta*, 62, 1757-1772.
- Müller, R. D., Roest, W. R., Royer, J. Y., Gahagan, L. M., Sclater, J. G. (1997). Digital isochrons of the world's ocean floor. *Journal of Geophysical Research: Solid Earth*, 102, 3211-3214.
- Müntener, O., Pettke, T., Desmurs, L., Meier, M., Schaltegger, U. (2004). Refertilization of mantle peridotite in embryonic ocean basins: trace element and Nd isotopic evidence and implications for crust–mantle relationships. *Earth and Planetary Science Letters*, 221, 293-308.
- Müntener, O., & Manatschal, G. (2006). High degrees of melt extraction recorded by spinel harzburgite of the Newfoundland margin: The role of inheritance and consequences for the evolution of the southern North Atlantic. *Earth and Planetary Science Letters*, 252, 437-452.
- Müntener, O., Manatschal, G., Desmurs, L., Pettke, T. (2010). Plagioclase peridotites in ocean–continent transitions: refertilized mantle domains generated by melt stagnation in the shallow mantle lithosphere. *Journal of Petrology*, 51, 255-294.
- Nakashima, S., & Hayashi, Y. (2016). Determination of Detection Limits and Quantitation Limits for Compounds in a Database of GC/MS by FUMI Theory. *Mass Spectrometry*, 5, A0043-A0043.
- Naslund, H., Hughes, J., Birnie, R. (1983). Ilvaite, an alteration product replacing olivine in the Skaergaard intrusion. *American Mineralogist*, 68, 1004-1008.

- Neal, C., & Stanger, G. (1983). Hydrogen generation from mantle source rocks in Oman. *Earth and Planetary Science Letters*, 66, 315-320.
- Neff, J. M., Stout, S. A., Gunster, D. G. (2005). Ecological risk assessment of polycyclic aromatic hydrocarbons in sediments: identifying sources and ecological hazard. *Integrated Environmental Assessment and Management*, 1, 22-33.
- Nichols, P. D., Palmisano, A. C., Rayner, M. S., Smith, G. A., White, D. C. (1990). Occurrence of novel C30 sterols in Antarctic sea-ice diatom communities during a spring bloom. *Organic geochemistry*, 15, 503-508.
- Nicol, S., & Endo, Y., (1997), Krill fisheries of the world pp.). v. 367: Food & Agriculture Org.
- Niemann, H., Duarte, J., Hensen, C., Omoregie, E., Magalhães, V., Elvert, M., Pinheiro, L., Kopf, A., Boetius, A. (2006). Microbial methane turnover at mud volcanoes of the Gulf of Cadiz. *Geochimica et Cosmochimica Acta*, 70, 5336-5355.
- Nitschke, W., & Russell, M. J. (2013). Beating the acetyl coenzyme A-pathway to the origin of life. *Phil. Trans. R. Soc. B*, 368, 20120258.
- O'hanley, D. S. (1991). Fault-related phenomena associated with hydration and serpentine recrystallization during serpentinization. *The Canadian Mineralogist*, 29, 21-35.
- O'Neil, J. R., Clayton, R. N., Mayeda, T. K. (1969). Oxygen isotope fractionation in divalent metal carbonates. *The Journal of Chemical Physics*, 51, 5547-5558.
- Onstott, T., McGown, D., Kessler, J., Lollar, B. S., Lehmann, K., Clifford, S. (2006). Martian CH<sub>4</sub>: sources, flux, and detection. *Astrobiology*, 6, 377-395.
- Orem, W. H., Spiker, E. C., Kotra, R. K. (1990). Organic matter in hydrothermal metal ores and hydrothermal fluids. *Applied Geochemistry*, 5, 125-134.
- Orphan, V. J., House, C. H., Hinrichs, K.-U., McKeegan, K. D., DeLong, E. F. (2001). Methane-consuming archaea revealed by directly coupled isotopic and phylogenetic analysis. *Science*, 293, 484-487.
- Oufi, O., Cannat, M., Horen, H. (2002). Magnetic properties of variably serpentinized abyssal peridotites. *Journal of Geophysical Research: Solid Earth*, 107.
- Owen, T., Cess, R. D., Ramanathan, V. (1979). Enhanced CO<sub>2</sub> greenhouse to compensate for reduced solar luminosity on early Earth. *Nature*, 277, 640-642.
- Pan, A., Yang, Q., Zhou, H., Ji, F., Wang, H., Pancost, R. D. (2016). A diagnostic GDGT signature for the impact of hydrothermal activity on surface deposits at the Southwest Indian Ridge. *Organic geochemistry*, 99, 90-101.
- Pancost, R. D., Damsté, J. S. S., de Lint, S., van der Maarel, M. J., Gottschal, J. C. (2000). Biomarker evidence for widespread anaerobic methane oxidation in Mediterranean sediments by a consortium of methanogenic archaea and bacteria. *Applied and environmental microbiology*, 66, 1126-1132.

- Pancost, R. D., Bouloubassi, I., Aloisi, G., Damsté, J. S. S. (2001). Three series of non-isoprenoidal dialkyl glycerol diethers in cold-seep carbonate crusts. *Organic geochemistry*, 32, 695-707.
- Paulick, H., Bach, W., Godard, M., De Hoog, J., Suhr, G., Harvey, J. (2006). Geochemistry of abyssal peridotites (Mid-Atlantic Ridge, 15 20' N, ODP Leg 209): implications for fluid/rock interaction in slow spreading environments. *Chemical Geology*, 234, 179-210.
- Pearce, B. K., Pudritz, R. E., Semenov, D. A., Henning, T. K. (2017). Origin of the RNA world: The fate of nucleobases in warm little ponds. *Proceedings of the National Academy of Sciences*, 201710339.
- Pearson, A., Huang, Z., Ingalls, A., Romanek, C., Wiegel, J., Freeman, K., Smittenberg, R., Zhang, C. (2004). Nonmarine crenarchaeol in Nevada hot springs. *Applied and environmental microbiology*, 70, 5229-5237.
- Pedersen, R. B., Rapp, H. T., Thorseth, I. H., Lilley, M. D., Barriga, F. J., Baumberger, T., Flesland, K., Fonseca, R., Früh-Green, G. L., Jorgensen, S. L. (2010). Discovery of a black smoker vent field and vent fauna at the Arctic Mid-Ocean Ridge. *Nature communications*, 1, 126.
- Peltzer, E., & Gagosian, R. (1989). Organic geochemistry of aerosols over the Pacific Ocean. *Chemical oceanography*, 10, 281-338.
- Pérez-Gussinyé, M., & Reston, T. J. (2001). Rheological evolution during extension at nonvolcanic rifted margins: onset of serpentinization and development of detachments leading to continental breakup. *Journal of Geophysical Research: Solid Earth*, 106, 3961-3975.
- Perner, M., Seifert, R., Weber, S., Koschinsky, A., Schmidt, K., Strauss, H., Peters, M., Haase, K., Imhoff, J. F. (2007). Microbial CO<sub>2</sub> fixation and sulfur cycling associated with low-temperature emissions at the Lilliput hydrothermal field, southern Mid-Atlantic Ridge (9 S). *Environmental Microbiology*, 9, 1186-1201.
- Peron-Pinvidic, G., Shillington, D. J., Tucholke, B. E. (2010). Characterization of sills associated with the U reflection on the Newfoundland margin: evidence for widespread early post-rift magmatism on a magma-poor rifted margin. *Geophysical Journal International*, 182, 113-136.
- Peron-Pinvidic, G., Manatschal, G., Osmundsen, P. T. (2013). Structural comparison of archetypal Atlantic rifted margins: A review of observations and concepts. *Marine and Petroleum Geology*, 43, 21-47.
- Péron-Pinvidic, G., & Manatschal, G. (2008). The final rifting evolution at deep magma-poor passive margins from Iberia-Newfoundland: a new point of view. *International Journal of Earth Sciences*, 98, 1581-1597.
- Péron-Pinvidic, G., Manatschal, G., Minshull, T. A., Sawyer, D. S. (2007). Tectonosedimentary evolution of the deep Iberia-Newfoundland margins: Evidence for a complex breakup history. *Tectonics*, 26.

- Peters, K., Walters, C., Moldowan, J., (2005a), *The Biomarker Guide: 2, Biomarkers and Isotopes in Petroleum Systems and Earth History*. (700 pp.). Cambridge University Press.
- Peters, K. E., & Moldowan, J. M., (1993), *The biomarker guide: interpreting molecular fossils in petroleum and ancient sediments* pp.). Prentice Hall.
- Peters, K. E., Fraser, T. H., Amris, W., Rustanto, B., Hermanto, E. (1999). Geochemistry of crude oils from eastern Indonesia. *The American Association of Petroleum Geologists* 83, 1927-1942.
- Peters, K. E., Walters, C. C., Moldowan, J. M., (2005b), *The biomarker guide: 1, Biomarkers and isotopes in the environment and human history* (490 pp.). Cambridge University Press.
- Peters, T. (1968). Distribution of Mg, Fe, Al, Ca and Na in Coexisting Olivine, Orthopyroxene and Clinopyroxene in the Totalp Serpentinite (Davos, Switzerland) and in the Alpine Metamorphosed Malenco Serpentinite (N. Italy). *Contributions to Mineralogy and Petrology*, 18, 65-75.
- Peters, T., & Stettler, A. (1987). Radiometric age, thermobarometry and mode of emplacement of the Totalp peridotite in the Eastern Swiss Alps. . *Schweizerische Mineralogische und Petrographische Mitteilungen*, 67, 285-294.
- Phillips, J. D., Thompson, G., Von Herzen, R. P., Bowen, V. T. (1969). Mid-Atlantic ridge near 43° N latitude. *Journal of Geophysical Research*, 74, 3069-3081.
- Picazo, S., Manatschal, G., Cannat, M., Andréani, M. (2013). Deformation associated to exhumation of serpentinitized mantle rocks in a fossil Ocean Continent Transition: The Totalp unit in SE Switzerland. *Lithos*, 175-176, 255-271.
- Pinto, V. H. 2014. "Linking tectonic evolution with fluid history in hyperextended rifted margins: examples from the fossil Alpine and Pyrenean rift systems, and the present-day Iberia rifted margin." 45, Geological Society of America Abstracts with Programs (7).
- Pond, D. W., Bell, M. V., Dixon, D. R., Fallick, A. E., Segonzac, M., Sargent, J. R. (1998). Stable-carbon-isotope composition of fatty acids in hydrothermal vent mussels containing methanotrophic and thiotrophic bacterial endosymbionts. *Applied and environmental microbiology*, 64, 370-375.
- Pons, M.-L. 2011. "La Terre à l'Archéen. Apport des isotopes de métaux de transition (Zn, Fe)." Lyon, École normale supérieure.
- Pons, M.-L., Quitté, G., Fujii, T., Rosing, M. T., Reynard, B., Moynier, F., Douchet, C., Albarède, F. (2011). Early Archean serpentine mud volcanoes at Isua, Greenland, as a niche for early life. *Proceedings of the National Academy of Sciences*, 108, 17639-17643.
- Powell, T., & McKirdy, D. (1973). Relationship between ratio of pristane to phytane, crude oil composition and geological environment in Australia. *Nature*, 243, 37-39.
- Powell, T. (1988). Pristane/phytane ratio as environmental indicator. *Nature*, 333, 604-604.

- Power, I. M., Wilson, S. A., Dipple, G. M. (2013). Serpentinite carbonation for CO<sub>2</sub> sequestration. *Elements*, 9, 115-121.
- Prahl, F. G., & Wakeham, S. G. (1987). Calibration of unsaturation patterns in long-chain ketone compositions for palaeotemperature assessment. *Nature*, 330, 367-369.
- Proskurowski, G., Lilley, M. D., Kelley, D. S., Olson, E. J. (2006). Low temperature volatile production at the Lost City Hydrothermal Field, evidence from a hydrogen stable isotope geothermometer. *Chemical Geology*, 229, 331-343.
- Proskurowski, G., Lilley, M. D., Seewald, J. S., Früh-Green, G. L., Olson, E. J., Lupton, J. E., Sylva, S. P., Kelley, D. S. (2008). Abiogenic hydrocarbon production at Lost City hydrothermal field. *Science*, 319, 604-607.
- Pusztaszeri, L. 1966. "Etude pétrographique du massif du Chenaillet (Hautes-Alpes, France)." University of Geneva.
- Raghoebarsing, A. A., Pol, A., Van de Pas-Schoonen, K. T., Smolders, A. J., Ettwig, K. F., Rijpstra, W. I. C., Schouten, S., Damsté, J. S. S., den Camp, H. J. O., Jetten, M. S. (2006). A microbial consortium couples anaerobic methane oxidation to denitrification. *Nature*, 440, 918-921.
- Rajendran, S., & Nasir, S. (2014). Hydrothermal altered serpentinitized zone and a study of Ni-magnesioferrite-magnetite-awaruite occurrences in Wadi Hibi, Northern Oman Mountain: Discrimination through ASTER mapping. *Ore Geology Reviews*, 62, 211-226.
- Raleigh, C., & Paterson, M. (1965). Experimental deformation of serpentinite and its tectonic implications. *Journal of Geophysical Research*, 70, 3965-3985.
- Ranero, C. R., Morgan, J. P., McIntosh, K., Reichert, C. (2003). Bending-related faulting and mantle serpentinization at the Middle America trench. *Nature*, 425, 367.
- Rasmussen, B. (2000). Filamentous microfossils in a 3,235-million-year-old volcanogenic massive sulphide deposit. *Nature*, 405, 676-679.
- Reeburgh, W., Whalen, S., Alperin, M., Murrell, J., Kelly, D., (1996), Microbial growth on C1 compounds pp.). Kluwer Academic Publishers, Dordrecht, The Netherlands.
- Reeburgh, W. S. (2007). Oceanic methane biogeochemistry. *Chemical Reviews*, 107, 486-513.
- Reed, A. J., Dorn, R., Van Dover, C. L., Lutz, R. A., Vetriani, C. (2009). Phylogenetic diversity of methanogenic, sulfate-reducing and methanotrophic prokaryotes from deep-sea hydrothermal vents and cold seeps. *Deep Sea Research Part II: Topical Studies in Oceanography*, 56, 1665-1674.
- Reeves, E. P., McDermott, J. M., Seewald, J. S. (2014). The origin of methanethiol in midocean ridge hydrothermal fluids. *Proceedings of the National Academy of Sciences of the United States of America*, 111, 5474-5479.

- Reinen, L. A., Weeks, J. D., Tullis, T. E. (1991). The frictional behavior of serpentinite: Implications for aseismic creep on shallow crustal faults. *Geophysical Research Letters*, 18, 1921-1924.
- Reston, T. J., & Manatschal, G. (2011). Rifted Margins: Building Blocks of Later Collision. 3-18.
- Reston, T. J., & McDermott, K. G. (2011). Successive detachment faults and mantle unroofing at magma-poor rifted margins. *Geology*, 39, 1071-1074.
- Reveillaud, J., Reddington, E., McDermott, J., Algar, C., Meyer, J. L., Sylva, S., Seewald, J., German, C. R., Huber, J. A. (2016). Subseafloor microbial communities in hydrogen-rich vent fluids from hydrothermal systems along the Mid-Cayman Rise. *Environmental Microbiology*, 18, 1970-1987.
- Rickard, D., Mussmann, M., Steadman, J. A. (2017). Sedimentary sulfides. *Elements*, 13, 117-122.
- Ridgwell, A. J., Marshall, S. J., Gregson, K. (1999). Consumption of atmospheric methane by soils: A process-based model. *Global Biogeochemical Cycles*, 13, 59-70.
- Roehrig, E. E., Laó-Dávila, D. A., Wolfe, A. L. (2015). Serpentinization history of the Río Guanajibo serpentinite body, Puerto Rico. *Journal of South American Earth Sciences*, 62, 195-217.
- Rona, P., Widenfalk, L., Boström, K. (1987). Serpentinized ultramafics and hydrothermal activity at the Mid-Atlantic Ridge crest near 15 N. *Journal of Geophysical Research: Solid Earth*, 92, 1417-1427.
- Rona, P., Bougault, H., Charlou, J., Appriou, P., Nelsen, T., Trefry, J., Eberhart, G., Barone, A., Needham, H. (1992). Hydrothermal circulation, serpentinization, and degassing at a rift valley-fracture zone intersection: Mid-Atlantic Ridge near 15 N, 45 W. *Geology*, 20, 783-786.
- Rona, P. A. (1978). Criteria for recognition of hydrothermal mineral deposits in oceanic crust. *economic geology*, 73, 135-160.
- Rona, P. A. (1984). Hydrothermal mineralization at seafloor spreading centers. *Earth-Science Reviews*, 20, 1-104.
- Rontani, J.-F., Bonin, P., Vaultier, F., Guasco, S., Volkman, J. K. (2013). Anaerobic bacterial degradation of pristenes and phytanes in marine sediments does not lead to pristane and phytane during early diagenesis. *Organic geochemistry*, 58, 43-55.
- Rossel, P. E., Lipp, J. S., Fredricks, H. F., Arnds, J., Boetius, A., Elvert, M., Hinrichs, K.-U. (2008). Intact polar lipids of anaerobic methanotrophic archaea and associated bacteria. *Organic geochemistry*, 39, 992-999.
- Roussel, E. G., Konn, C., Charlou, J.-L., Donval, J.-P., Fouquet, Y., Querellou, J., Prieur, D., Cambon Bonavita, M.-A. (2011). Comparison of microbial communities associated with three Atlantic ultramafic hydrothermal systems. *FEMS microbiology ecology*, 77, 647-665.

- Rowland, S. (1990). Production of acyclic isoprenoid hydrocarbons by laboratory maturation of methanogenic bacteria. *Organic geochemistry*, 15, 9-16.
- Russell, M. J., Hall, A. J., Turner, D. (1989). In vitro growth of iron sulphide chimneys: possible culture chambers for origin-of-life experiments. *terra nova*, 1, 238-241.
- Russell, M. J., Daniel, R. M., Hall, A. J., Sherringham, J. A. (1994). A hydrothermally precipitated catalytic iron sulphide membrane as a first step toward life. *Journal of Molecular Evolution*, 39, 231-243.
- Russell, M. J., Hall, A. J., Martin, W. (2010). Serpentinization as a source of energy at the origin of life. *Geobiology*, 8, 355-371.
- Russell, S., & Whitmarsh, R. (2003). Magmatism at the west Iberia non-volcanic rifted continental margin: evidence from analyses of magnetic anomalies. *Geophysical Journal International*, 154, 706-730.
- Sachse, V., Littke, R., Jabour, H., Schümann, T., Kluth, O. (2012). Late Cretaceous (late Turonian, Coniacian and Santonian) petroleum source rocks as part of an OAE, Tarfaya Basin, Morocco. *Marine and Petroleum Geology*, 29, 35-49.
- Saha, M., Togo, A., Mizukawa, K., Murakami, M., Takada, H., Zakaria, M. P., Chiem, N. H., Tuyen, B. C., Prudente, M., Boonyatumanond, R. (2009). Sources of sedimentary PAHs in tropical Asian waters: differentiation between pyrogenic and petrogenic sources by alkyl homolog abundance. *Marine pollution bulletin*, 58, 189-200.
- Saha, M., Takada, H., Bhattacharya, B. (2012). Establishing criteria of relative abundance of alkyl polycyclic aromatic hydrocarbons (PAHs) for differentiation of pyrogenic and petrogenic PAHs: An application to Indian sediment. *Environmental Forensics*, 13, 312-331.
- Saunio, M., Bousquet, P., Poulter, B., Peregon, A., Ciais, P., Canadell, J. G., Dlugokencky, E. J., Etiope, G., Bastviken, D., Houweling, S. (2016). The global methane budget 2000–2012. *Earth System Science Data (Online)*, 8.
- Sawyer, D., Whitmarsh, R., Klaus, A., Party, S. S. (1994). Sites 897–901. *Proc. Ocean Drill. Prog. Initial Rep*, 149, 41-268.
- Scambelluri, M., Müntener, O., Ottolini, L., Pettke, T. T., Vannucci, R. (2004). The fate of B, Cl and Li in the subducted oceanic mantle and in the antigorite breakdown fluids. *Earth and Planetary Science Letters*, 222, 217-234.
- Schaltegger, U., Desmurs, L., Manatschal, G., Müntener, O., Meier, M., Frank, M., Bernoulli, D. (2002). The transition from rifting to sea-floor spreading within a magma-poor rifted margin: field and isotopic constraints. *terra nova*, 14, 156-162.
- Schidlowski, M. (1988). A 3,800-million-year isotopic record of life from carbon in sedimentary rocks. *Nature*, 333, 313-318.
- Schidlowski, M. (2001). Carbon isotopes as biogeochemical recorders of life over 3.8 Ga of Earth history: evolution of a concept. *Precambrian Research*, 106, 117-134.

- Schmid, S. M., Fügenschuh, B., Kissling, E., Schuster, R. (2004). Tectonic map and overall architecture of the Alpine orogen. *Eclogae Geologicae Helvetiae*, 97, 93-117.
- Schmidt, K., Koschinsky, A., Garbe-Schönberg, D., de Carvalho, L. M., Seifert, R. (2007). Geochemistry of hydrothermal fluids from the ultramafic-hosted Logatchev hydrothermal field, 15 N on the Mid-Atlantic Ridge: temporal and spatial investigation. *Chemical Geology*, 242, 1-21.
- Schouten, S., Hopmans, E. C., Pancost, R. D., Damsté, J. S. S. (2000). Widespread occurrence of structurally diverse tetraether membrane lipids: evidence for the ubiquitous presence of low-temperature relatives of hyperthermophiles. *Proceedings of the National Academy of Sciences*, 97, 14421-14426.
- Schouten, S., Hopmans, E. C., Schefuß, E., Damste, J. S. S. (2002). Distributional variations in marine crenarchaeotal membrane lipids: a new tool for reconstructing ancient sea water temperatures? *Earth and Planetary Science Letters*, 204, 265-274.
- Schouten, S., Hopmans, E. C., Damsté, J. S. S. (2013). The organic geochemistry of glycerol dialkyl glycerol tetraether lipids: a review. *Organic geochemistry*, 54, 19-61.
- Schrenk, M. O., Brazelton, W. J., Lang, S. Q. (2013). Serpentinization, carbon, and deep life. *Rev Mineral Geochem*, 75, 575-606.
- Schulte, M., Blake, D., Hoehler, T., McCollom, T. (2006). Serpentinization and Its Implications for Life on the Early Earth and Mars. *Astrobiology*, 6.
- Schwarzenbach, E. 2011. "Serpentinization, fluids and life: comparing carbon and sulfur cycles in modern and ancient environments." Diss., Eidgenössische Technische Hochschule ETH Zürich, Nr. 19588, 2011.
- Schwarzenbach, E. M., Früh-Green, G. L., Bernasconi, S. M., Alt, J. C., Shanks III, W. C., Gaggero, L., Crispini, L. (2012). Sulfur geochemistry of peridotite-hosted hydrothermal systems: comparing the Ligurian ophiolites with oceanic serpentinites. *Geochimica et Cosmochimica Acta*, 91, 283-305.
- Schwarzenbach, E. M., Früh-Green, G. L., Bernasconi, S. M., Alt, J. C., Plas, A. (2013). Serpentinization and carbon sequestration: A study of two ancient peridotite-hosted hydrothermal systems. *Chemical Geology*, 351, 115-133.
- Seewald, J. S., Zolotov, M. Y., McCollom, T. (2006). Experimental investigation of single carbon compounds under hydrothermal conditions. *Geochimica et Cosmochimica Acta*, 70, 446-460.
- Seifert, W. K., & Moldowan, J. M. (1980). The effect of thermal stress on source-rock quality as measured by hopane stereochemistry. *Physics and Chemistry of the Earth*, 12, 229-237.
- Shanks, W. (2001). Stable isotopes in seafloor hydrothermal systems: vent fluids, hydrothermal deposits, hydrothermal alteration, and microbial processes. *Reviews in mineralogy and geochemistry*, 43, 469-525.

- Sharp, Z. (2009). Application of Stable Isotope Geochemistry to Low-Grade Metamorphic Rocks. *Low-Grade Metamorphism*, 227-260.
- Sharp, Z. (2017). Principles of stable isotope geochemistry.
- Shiller, A. M., & Joung, D. (2012). Nutrient depletion as a proxy for microbial growth in Deepwater Horizon subsurface oil/gas plumes. *Environmental Research Letters*, 7, 045301.
- Shock, E. L. (1992). Chemical environments of submarine hydrothermal systems. In (ed.), *Marine hydrothermal systems and the origin of life*, (pp.67-107): Springer.
- Shock, E. L., McCollom, T., Schulte, M. D. (2002). The emergence of metabolism from within hydrothermal systems. In Juergen Wiegel&Adams W.W. Michael (ed.), *Thermophiles: the keys to molecular evolution and the origin of life*, (pp.59-76): CRC Press.
- Sibson, R., Moore, J. M. M., Rankin, A. (1975). Seismic pumping—a hydrothermal fluid transport mechanism. *Journal of the Geological Society*, 131, 653-659.
- Simoneit, B., & Philp, R. (1982). Organic geochemistry of lipids and karogen and the effects of basalt intrusions in unconsolidated oceanic sediments site 477, site 478 and site 481, Guaymas basin, Gulf of California. In J.R. Curray&D.G.Moore (ed.), *Initial Reports of the Deep Sea Drilling Project*, (pp.883-904) Washington: U.S. Government Printing office.
- Simoneit, B. R., Brenner, S., Peters, K., Kaplan, I. (1978). Thermal alteration of Cretaceous black shale by basaltic intrusions in the Eastern Atlantic. *Nature*, 273, 501-504.
- Skelton, A., Whitmarsh, R., Arghe, F., Crill, P., Koyi, H. (2005). Constraining the rate and extent of mantle serpentinization from seismic and petrological data: implications for chemosynthesis and tectonic processes. *Geofluids*, 5, 153-164.
- Slotznick, S. P., & Fischer, W. W. (2016). Examining Archean methanotrophy. *Earth and Planetary Science Letters*, 441, 52-59.
- Smith, D. C., Spivack, A. J., Fisk, M. R., Haveman, S. A., Staudigel, H. (2000a). Tracer-based estimates of drilling-induced microbial contamination of deep sea crust. *Geomicrobiology Journal*, 17, 207-219.
- Smith, D. C., Spivack, A. J., Fisk, M. R., Haveman, S. A., Staudigel, H., Party, L. (2000b). Methods for quantifying potential microbial contamination during deep ocean coring. *Ocean Drilling Program Technical Note*.
- Sofer, Z. (1980). Preparation of carbon dioxide for stable carbon isotope analysis of petroleum fractions. *Analytical chemistry*, 52, 1389-1391.
- Sofer, Z. (1984). Stable carbon isotope compositions of crude oils: application to source depositional environments and petroleum alteration. *AAPG Bulletin*, 68, 31-49.

- Spear, J. R., Walker, J. J., McCollom, T. M., Pace, N. R. (2005). Hydrogen and bioenergetics in the Yellowstone geothermal ecosystem. *Proceedings of the National Academy of Sciences of the United States of America*, 102, 2555-2560.
- Stadnitskaia, A., Bouloubassi, I., Elvert, M., Hinrichs, K.-U., Damsté, J. S. (2008). Extended hydroxyarchaeol, a novel lipid biomarker for anaerobic methanotrophy in cold seepage habitats. *Organic geochemistry*, 39, 1007-1014.
- Steinmann, G., (1905), Geologische beobachtungen in den Alpen: Scharfsteinsche Ueberfaltungstheorie und die geologische Bedeutung der Tiefseeabsätze un der ophiolithischen Massengestein. II pp.). publisher not identified.
- Styr, M., Brackmann, A., Holland, H., Clark, B., Pisutha-Arnond, V., Eldridge, C., Ohmoto, H. (1981). The mineralogy and the isotopic composition of sulfur in hydrothermal sulfide/sulfate deposits on the East Pacific Rise, 21 N latitude. *Earth and Planetary Science Letters*, 53, 382-390.
- Suess, E. (1980). Particulate organic carbon flux in the oceans—surface. *Nature*, 288, 261.
- Sugisaki, R., Ido, M., Takeda, H., Isobe, Y., Hayashi, Y., Nakamura, N., Satake, H., Mizutani, Y. (1983). Origin of hydrogen and carbon dioxide in fault gases and its relation to fault activity. *The Journal of Geology*, 239-258.
- Summons, R. E., Jahnke, L. L., Roksandic, Z. (1994). Carbon isotopic fractionation in lipids from methanotrophic bacteria: relevance for interpretation of the geochemical record of biomarkers. *Geochimica et Cosmochimica Acta*, 58, 2853-2863.
- Sutra, E., Manatschal, G., Mohn, G., Unternehr, P. (2013). Quantification and restoration of extensional deformation along the Western Iberia and Newfoundland rifted margins. *Geochemistry, Geophysics, Geosystems*, 14, 2575-2597.
- Swan, M., Keith, S., Hovland, M., Rueslatten, H., Johnsen, H., Page, N. 2010. "The Serpentsphere." *Geochimica et Cosmochimica Acta*.
- Swart, P. K., Burns, S., Leder, J. (1991). Fractionation of the stable isotopes of oxygen and carbon in carbon dioxide during the reaction of calcite with phosphoric acid as a function of temperature and technique. *Chemical Geology: Isotope Geoscience section*, 86, 89-96.
- Takai, K., Gamo, T., Tsunogai, U., Nakayama, N., Hirayama, H., Nealson, K. H., Horikoshi, K. (2004). Geochemical and microbiological evidence for a hydrogen-based, hyperthermophilic subsurface lithoautotrophic microbial ecosystem (HyperSLiME) beneath an active deep-sea hydrothermal field. *Extremophiles*, 8, 269-282.
- Takishita, K., Chikaraishi, Y., Leger, M. M., Kim, E., Yabuki, A., Ohkouchi, N., Roger, A. J. (2012). Lateral transfer of tetrahymanol-synthesizing genes has allowed multiple diverse eukaryote lineages to independently adapt to environments without oxygen. *Biology direct*, 7, 5.
- Tanner, J., 1948. Shape and size of bacterial cells. Wiley New York,, USA.

- Taylor, C. D., Zierenberg, R. A., Goldfarb, R. J., Kilburn, J. E., Seal, I., Kleinkopf, M. (1995). Volcanic-associated massive sulfide deposits. *Preliminary compilation of descriptive geoenvironmental mineral deposit models. US Geological Survey Open-File Report*, 95, 137-144.
- Templeton, A. S., Chu, K.-H., Alvarez-Cohen, L., Conrad, M. E. (2006). Variable carbon isotope fractionation expressed by aerobic CH<sub>4</sub>-oxidizing bacteria. *Geochimica et Cosmochimica Acta*, 70, 1739-1752.
- Ten Haven, H., De Leeuw, J., Rullkötter, J., Damsté, J. S. (1987). Restricted utility of the pristane/phytane ratio as a palaeoenvironmental indicator. *Nature*, 330, 641-643.
- Teske, A., Hinrichs, K.-U., Edgcomb, V., de Vera Gomez, A., Kysela, D., Sylva, S. P., Sogin, M. L., Jannasch, H. W. (2002). Microbial diversity of hydrothermal sediments in the Guaymas Basin: evidence for anaerobic methanotrophic communities. *Applied and environmental microbiology*, 68, 1994-2007.
- Thiel, V., Peckmann, J., Seifert, R., Wehrung, P., Reitner, J., Michaelis, W. (1999). Highly isotopically depleted isoprenoids: molecular markers for ancient methane venting. *Geochimica et Cosmochimica Acta*, 63, 3959-3966.
- Tobiszewski, M., & Namieśnik, J. (2012). PAH diagnostic ratios for the identification of pollution emission sources. *Environmental Pollution*, 162, 110-119.
- Toft, P. B., Arkani-Hamed, J., Haggerty, S. E. (1990). The effects of serpentization on density and magnetic susceptibility: a petrophysical model. *Physics of the Earth and Planetary Interiors*, 65, 137-157.
- Trommsdorff, V., & Evans, B. (1974). Alpine metamorphism of peridotitic rocks. *Schweiz Mineral Petrogr Mitt*, 54, 333-352.
- Trommsdorff, V. (1983). Metamorphose magnesiumreicher Gesteine: Kritischer Vergleich von Natur, Experiment und thermodynamischer Datenbasis. *Fortschr Mineral*, 61, 283-308.
- Tucholke, B., Sibuet, J., Klaus, A. (2004). Leg 210 summary. *Proceedings of the Ocean Drilling Program, Initial reports, Volume 210*, 1-78.
- Tucholke, B. E., & Sibuet, J.-C. 2007a. "Leg 210 synthesis: tectonic, magmatic, and sedimentary evolution of the Newfoundland-Iberia rift." *Proceedings of the Ocean Drilling Program, Scientific Results*.
- Tucholke, B. E., & Sibuet, J.-C. (2007b). LEG 210 SYNTHESIS: TECTONIC, MAGMATIC, AND SEDIMENTARY EVOLUTION OF THE NEWFOUNDLAND-IBERIA RIFT. *Proceedings of the Ocean Drilling Program, Scientific Results*, 210.
- Turetsky, M. R., Kotowska, A., Bubier, J., Dise, N. B., Crill, P., Hornibrook, E. R., Minkinen, K., Moore, T. R., Myers-Smith, I. H., Nykänen, H. (2014). A synthesis of methane

- emissions from 71 northern, temperate, and subtropical wetlands. *Global change biology*, 20, 2183-2197.
- Ulmer, P., & Trommsdorff, V. (1995). Serpentine Stability to Mantle Depths and Subduction-Related Magmatism. *Science*, 268, 858-861.
- Unternehr, P., Péron-Pinvidic, G., Manatschal, G., Sutra, E. (2010). Hyper-extended crust in the South Atlantic: in search of a model. *Petroleum Geoscience*, 16, 207-215.
- Valley, J. W. (1986). Stable isotope geochemistry of metamorphic rocks. *Reviews in mineralogy and geochemistry*, 16, 445-489.
- van Acken, D., Becker, H., Walker, R. J., McDonough, W. F., Wombacher, F., Ash, R. D., Piccoli, P. M. (2010). Formation of pyroxenite layers in the Totalp ultramafic massif (Swiss Alps) – Insights from highly siderophile elements and Os isotopes. *Geochimica et Cosmochimica Acta*, 74, 661-683.
- Van Dover, C. L. (1995). Ecology of mid-Atlantic ridge hydrothermal vents. *Geological Society, London, Special Publications*, 87, 257-294.
- Vaughan, D. J., & Corkhill, C. L. (2017). Mineralogy of Sulfides. *Elements*, 13, 81-87.
- Vents, I. 07.2017. "InterRidge Vents database ver.3.4." <https://vents-data.interridge.org/>.
- Villanueva, J., Grimalt, J. O., Cortijo, E., Vidal, L., Labeyrie, L. (1997). A biomarker approach to the organic matter deposited in the North Atlantic during the last climatic cycle. *Geochimica et Cosmochimica Acta*, 61, 4633-4646.
- Vils, F., Pelletier, L., Kalt, A., Müntener, O., Ludwig, T. (2008). The lithium, boron and beryllium content of serpentinized peridotites from ODP Leg 209 (Sites 1272A and 1274A): implications for lithium and boron budgets of oceanic lithosphere. *Geochimica et Cosmochimica Acta*, 72, 5475-5504.
- Vils, F., Müntener, O., Kalt, A., Ludwig, T. (2011). Implications of the serpentine phase transition on the behaviour of beryllium and lithium–boron of subducted ultramafic rocks. *Geochimica et Cosmochimica Acta*, 75, 1249-1271.
- Volkman, J. (1988). Biological marker compounds as indicators of the depositional environments of petroleum source rocks. *Geological Society, London, Special Publications*, 40, 103-122.
- Volkman, J. K. (2005). Sterols and other triterpenoids: source specificity and evolution of biosynthetic pathways. *Organic geochemistry*, 36, 139-159.
- Von Damm, K. (1990). Seafloor hydrothermal activity: black smoker chemistry and chimneys. *Annual Review of Earth and Planetary Sciences*, 18, 173-204.
- Vu, T., Zink, K.-G., Mangelsdorf, K., Sykes, R., Wilkes, H., Horsfield, B. (2009). Changes in bulk properties and molecular compositions within New Zealand Coal Band solvent extracts from early diagenetic to catagenetic maturity levels. *Organic geochemistry*, 40, 963-977.

- Watanabe, T., Kasami, H., Ohshima, S. (2007). Compressional and shear wave velocities of serpentinized peridotites up to 200 MPa. *Earth, planets and space*, 59, 233-244.
- Webster, C. R., Mahaffy, P. R., Atreya, S. K., Flesch, G. J., Mischna, M. A., Meslin, P.-Y., Farley, K. A., Conrad, P. G., Christensen, L. E., Pavlov, A. A. (2015). Mars methane detection and variability at Gale crater. *Science*, 347, 415-417.
- Webster, G., Sass, H., Cragg, B. A., Gorra, R., Knab, N. J., Green, C. J., Mathes, F., Fry, J. C., Weightman, A. J., Parkes, R. J. (2011). Enrichment and cultivation of prokaryotes associated with the sulphate–methane transition zone of diffusion-controlled sediments of Aarhus Bay, Denmark, under heterotrophic conditions. *FEMS microbiology ecology*, 77, 248-263.
- Wegener, G., Niemann, H., Elvert, M., Hinrichs, K. U., Boetius, A. (2008). Assimilation of methane and inorganic carbon by microbial communities mediating the anaerobic oxidation of methane. *Environmental Microbiology*, 10, 2287-2298.
- Weissert, H., McKenzie, J., Channell, J. (1985). Natural variations in the carbon cycle during the Early Cretaceous. In E.T. Sundquist and W.S. Broecker (ed.), *The Carbon Cycle and Atmospheric CO: Natural Variations Archean to Present*, (pp.531-545) Washington D.C.: American Geophysical Union Geophysical Monograph.
- Weissert, H. J., & Bernoulli, D. (1985). A transform margin in the Mesozoic Tethys: evidence from the Swiss Alps. *Geologische Rundschau*, 74, 665-679.
- Wellsbury, P., Goodman, K., Cragg, B. A., Parkes, R. J. 2000. "The geomicrobiology of deep marine sediments from Blake Ridge containing methane hydrate (Sites 994, 995 and 997)." *Proceedings of the Ocean Drilling Program, Scientific Results*.
- Whitman, W. B., Coleman, D. C., Wiebe, W. J. (1998). Prokaryotes: the unseen majority. *Proceedings of the National Academy of Sciences*, 95, 6578-6583.
- Whitmarsh, B., Manatschal, G., Minshull, T. A. (2001a). Evolution of magma-poor continental margins from rifting to seafloor spreading. *Nature*, 413, 150-154.
- Whitmarsh, R., Beslier, M.-O., Wallace, P. (1998a). 1. LEG 173 INTRODUCTION1. *Proceedings of the Ocean Drilling Program, Initial reports*, 173.
- Whitmarsh, R., Beslier, M.-O., Wallace, P. 1998b. "Return to Iberia." *Proceedings of the Ocean Drilling Program, Initial reports*.
- Whitmarsh, R., Manatschal, G., Minshull, T. (2001b). Evolution of magma-poor continental margins from rifting to seafloor spreading. *Nature*, 413, 150-154.
- Whitmarsh, R., & Wallace, P. (2001). The rift-to-drift development of the West Iberia non-volcanic continental margin; a review of the contribution of Ocean Drilling Program Leg 173.
- Whitmarsh, R. B., Beslier, M.-O., Wallace, P. J. 1998c. "Site 1068." Whitmarsh, RB, Beslier, M.-O., Wallace, PJ, et al., *Proc. ODP, Init. Repts*.

- Whitmarsh, R. B., Beslier, M.-O., Wallace, P. J., Party, S. S. (1998d). Shipboard Scientific Party, 1998. Site 1070. *Proc. ODP, Init. Repts., 173: College Station, TX (Ocean Drilling Program)*, 265–294.
- Wicks, F., & Whittaker, E. (1977). SERPENTINE TEXTURES AND SERPENTINIZATION.
- Wicks, F., & O'Hanley, D. S. (1988). Serpentine minerals; structures and petrology. *Reviews in mineralogy and geochemistry*, 19, 91-167.
- Williams, L. A., Parks, G. A., Crerar, D. A. (1985). Silica diagenesis, I. Solubility controls. *Journal of Sedimentary Research*, 55, 301-311.
- Wójcik-Tabol, P., & Ślącza, A. (2015). Are Early Cretaceous environmental changes recorded in deposits of the Western part of the Silesian Nappe? A geochemical approach. *Palaeogeography, Palaeoclimatology, Palaeoecology*, 417, 293-308.
- Wolff, G. A., Boardman, D., Horsfall, I., Sutton, I., Davis, N., Chester, R., Ripley, M., Lewis, C. A., Rowland, S. J., Patching, J. (1995). The biogeochemistry of sediments from the Madeira Abyssal Plain—preliminary results. *Internationale Revue der gesamten Hydrobiologie und Hydrographie*, 80, 333-349.
- Wolin, M. (1982). Hydrogen transfer in microbial communities. *Microbial interactions and communities*, 1, 323-356.
- Yunker, M. B., Macdonald, R. W., Vingarzan, R., Mitchell, R. H., Goyette, D., Sylvestre, S. (2002). PAHs in the Fraser River basin: a critical appraisal of PAH ratios as indicators of PAH source and composition. *Organic geochemistry*, 33, 489-515.
- Zehnder, A., & Brock, T. (1979). Methane formation and methane oxidation by methanogenic bacteria. *Journal of Bacteriology*, 137, 420-432.
- Zeng, Z., Niedermann, S., Chen, S., Wang, X., Li, Z. (2015). Noble gases in sulfide deposits of modern deep-sea hydrothermal systems: Implications for heat fluxes and hydrothermal fluid processes. *Chemical Geology*, 409, 1-11.
- Zhang, Y. G., Zhang, C. L., Liu, X.-L., Li, L., Hinrichs, K.-U., Noakes, J. E. (2011). Methane Index: a tetraether archaeal lipid biomarker indicator for detecting the instability of marine gas hydrates. *Earth and Planetary Science Letters*, 307, 525-534.